IPC2024

International Conference on Innovative Production and Construction

Conference Proceedings

11-12 July 2024
Perth Convention and Exhibition Centre
Perth, Australia
ISBN: 978-0-9873918-9-6

Preface

We are pleased to present you the proceedings of the 10th International Conference on Innovative Production and Construction (IPC2024). The conference will be held in Perth, Australia, on July 11-12, 2024. It is co-organized by Curtin University and East China Jiaotong University. IPC2024 is a continuation of the previous nine very successful IPC conference series — Information Technology in Construction (ITC2012, Wuhan), ITC2014 (Shenyang), Innovative Construction and Production (IPC2015, Perth), IPC2016 (Melbourne), IPC2017 (Perth), IPC2018 (Perth), IPC2020 (Hong Kong), IPC2022 (Melbourne), aiming to provide an excellent academic platform for relevant practitioners, scholars, scientists, and engineers from all over the world to share and discuss issues in the field of sustainable production and construction. The latest developments and provide an excellent opportunity to interact with outstanding researchers so that production and construction practitioners can learn about future directions and developments in related fields.

Following peer review, this conference proceeding includes 25 conference papers and 28 abstracts. We thank the authors for their outstanding contributions and dedication, as well as the reviewers for providing valuable feedback on all papers. We would also like to thank the members of our organising committee for the success of IPC2024.

On behalf of the organising committee, we hope you enjoy the IPC2024 proceedings and your stay in Perth.

A/Professor Honglei Xu
General Chair, IPC2024

Professor Xiangyu Wang
Honorary Chair, IPC2024

Organisation

General Chair

Honglei Xu, Curtin University

Honorary Chair

Xiangyu Wang, East China Jiaotong University

Secretary

Lois Paffett, Curtin University

Chongyi Liu, Curtin University

Organising Committee

Tele Tan, Curtin University

Guanglu Zhou, Curtin University

Jun Li, Curtin University

Jun Wang, Western Sydney University

Junbo Sun, Chongqing University

Shengping Li, Curtin University

Tao Fang, East China Jiaotong University

Danqi Li, Curtin University

Lei Hou, RMIT University

International Scientific Committee

Professor Ning Gu, University of South Australia

Dr. Benson Lim, University of New South Wales

Professor Farzad Pour-Rahimian, Teesside University

Professor Lucio Soibelman, University of South California

Professor Makarand Hastak, Purdue University

Professor Roger Flanagan, Reading University

Professor Mani Golparvar Fard, University of Illinois, Urbana-Champion

Professor Rahinah Ibrahhim, Universiti Putra Malaysia

Professor Raymond Issa, University of Florida

Professor Robert Amor, University of Auckland

Professor Po-Han Chen, National Taiwan University

Professor Shang-Hsien Hsieh, National Taiwan University

Associate Professor Tomohiro Fukuda, Osaka University

Professor Nobuyoshi Yabuki, Osaka University

Associate Professor Hyun Woo Lee, University of Washington

Professor Nuria Forcada, Universitat Politècnica de Catalunya

Professor Ghang Lee, Younsei University

Professor Inhan Kim, Korea Kyung Hee University

Professor Chan-Sik Park, Chung-Ang University

Professor Huajun Li, Ocean University of China

Professor Dongping Fang, Tsinghua University

Associate Professor Nan Li, Tsinghua University

Professor Albert Chan, Hong Kong Polytecnical University

Professor Yu Bai, Monash University

Professor Jack C.P. Cheng, The Hong Kong University of Science and Technology

Sponsorships

Destination Sponsor

Business Events Perth - Acknowledge the support of the Government of Western Australia and Tourism WA through Business Events Perth, the City of Perth and relevant stakeholders.

Other Sponsors

Alpha Solar Technologies Pty Ltd
MDPI Buildings Best Paper Award
Hunan University of Science and Technology
Hunan City University
Nanjing Institute of Technology
Yangzhou University
Xiamen Zhichuangcheng Technology Co., Ltd.
Lianyungang Langheng Intelligent Manufacturing Technology Co.

Special thanks to

School of Electrical Engineering, Computing and Mathematical Sciences, Curtin University
Faculty of Science and Engineering, Curtin University

Contents

Part I: Conference Papers

Part II: Abstracts

Proceeding of the 10th International Conference on Innovative Production and Construction, Perth, Australia, July 11-12, 2024

A Simulation-based Genetic Algorithm Schedule Optimization Method for Multi-line Precast Production

Yuan Yao[1], Vivian WY Tam[1 *], Jun Wang[1], Khoa N Le[1], Anthony Butera[1], Tao Sheng[2]

1. Western Sydney University, School of Engineering, Design and Built Environment, Locked Bag 1797, Penrith, NSW 2751, Australia
2. Chongqing Liang Jiang Construction Company, Chongqing 400000, China

ABSTRACT: With the increasing utilization of precast concrete elements in off-site construction, improving precast production scheduling becomes a growing focus to enhance construction efficiency. Although research has been made in production optimization, studies addressing precast production with multiple production lines are still scarce. This paper aims at developing simulation-based Genetic Algorithm (S-GA) for scheduling optimization. By implementing simulation environment, the parallel production problem is addressed. Compared with traditional dispatching rules method, proposed method shows superiority in shortening production makespan and total weighted penalty. This research fills the gap in real-world production concerns and theoretical method in multiple production lines.

KEYWORDS: genetic algorithm; simulation; multiple production line; scheduling optimization

1 INTRODUCTION

Precast concrete (PC) is a construction material that is manufactured off-site and then transported to the building site for assembly. PC offers several advantages over traditional cast-in-place concrete, including high quality, fast erection, and on-site time saving[1-3]. For a precast concrete project, the production of prefabricated components is a critical factor constraining the project's completion timeline. Therefore, precast concrete production scheduling (PCPS) is crucial for the precast component factory.

Recently, the shift towards prefabricated buildings has been at the forefront of innovation and modernization in China's construction industry, representing a major change in building methods[4]. The demand of precast and off-site construction rises as Chinese government proposed their Green Building Action Plan in 2013[5]. The precast market has grown up to 533.2 billion yuan with 150 million square meters area in 2017[6] and that market is expected to reach higher in future. Many studies have been made to propose optimal precast production scheduling methods. Among these studies, heuristic algorithm especially Genetic Algorithm (GA) is the most popular baseline algorithm. Leu and Hwang[7] first used GA with RUX3 crossover and RUM3 mutation strategy to solve the resource-constrained production scheduling problem (RCPSP) in PCPS. GA showed flexibility in generating near-optimal solutions for the proposed flow shop model. After their work, GA was improved to further solve multi-objective schedule optimizations such as minimizing total makespan, penalties for earliness, and penalties for tardiness. Those improved GA outperformed the traditional DP methods in multi-objective task[8-15]. However, the majority of research has centred on the idealized setting of a single production line, while actual factory environments typically allow multiple parallel production lines to execute order manufacturing concurrently. Studies on optimization in parallel production are scarce.

To address the practical needs in real-world factories and the current research gaps, this study proposes a S-GA method for multi-line PCPS. The proposed method is designed to generate optimal production schedules with minimized earliness and tardiness penalties as well as shortened makespan.

Resources constraint, working hour constraint, and production precedence constraint are considered in modelling the PC production.

2 METHOD

2.1 Problem Definition

Lin and Liao [16] indicated that production scheduling aligns with the flow shop scheduling problem. In this study, the PC production process identified in this research comprises six distinct processes: mould assembling (P1), reinforcement setting (P2), concrete casting (P3), curing (P4), mould stripping (P5), and finishing (P6). The six processes can be divided into interruptible and non-interruptible ones. The necessity to define interruptible processes stems from the restriction that crews can only work a certain number of hours per day. Once their allotted work hours (H_W) are used up, no new tasks are given to them. Interruptible processes can be halted after regular work hours and continued the next day. Conversely, non-interruptible processes must be finished during overtime hours (H_O) and cannot be postponed.

The objectives of this research consist of two parts: minimizing total makespan and the total weighted penalties. The total weighted penalties include earliness and tardiness penalty, which in fact are two conflicting indicators. The constraints of the optimization include limited working hour, limited quantity of labours, and limited quantity of moulds.

Objectives:

$$\min f_1 = Max\left(C_{i,6}\right) \quad \text{Eq.1}$$

$$\min f_2 = \sum_{i=1}^{n}\left(\alpha \cdot \max\left(0, D_i - C_{i,6}\right) + \beta \cdot \max\left(0, C_{i,6} - D_i\right)\right) \quad \text{Eq.2}$$

Subject to:

$$C_{i,k} \geq \begin{cases} T_{i,k} \\ T_{i,k} + H_N \end{cases}, \begin{matrix} if\ T_{i,k} \leq 24d + H_W\ and\ j = 1,2,5,6 \\ if\ T_{i,k} > 24d + H_W\ and\ j = 1,2,5,6 \end{matrix} \quad \text{Eq.3}$$

$$C_{i,k} \geq \begin{cases} T_{i,k} \\ 24(d+1) + P_{i,k} \end{cases}, \begin{matrix} if\ T_{i,k} \leq 24d + H_W\ and\ j = 3 \\ if\ T_{i,k} > 24d + H_W\ and\ j = 3 \end{matrix} \quad \text{Eq.4}$$

$$C_{i,k} \geq \begin{cases} 24(d+1) \\ T_{i,k} \end{cases}, \begin{matrix} if\ 24d + H_W \leq T_{i,k} \leq 24(d+1)\ and\ j = 4 \\ if\ T_{i,k} < 24d + H_W\ or\ T_{i,k} > 24(d+1)\ and\ j = 4 \end{matrix} \quad \text{Eq.5}$$

$$\sum_{n=1}^{m} L_{n,k} \leq \mathcal{L}_k \quad \text{Eq.6}$$

$$m \leq M \quad \text{Eq.7}$$

Where: $C_{i,k}$: completion time of the k^{th} process of i^{th} production jobs; D_i: due date of the i^{th} production jobs; α, β: the penalty factors of earliness and tardiness respectively; $T_{i,k}$: the estimated job completion time without interruption; d: current day count; H_W, H_N: work hour and non-work hour; $P_{i,k}$: process time of the k^{th} process of i^{th} production jobs; $\mathcal{L}_k$: Total number of crews responsible for k^{th} process; L_n: current working crew executing the k^{th} process on the n^{th} mould plate; m, M: current occupied mould plates and the total quantity of mould plates.

2.2 S-GA Design

Because of the varied cases and assumptions in current research, existing PCPS algorithms cannot be directly applied to this study. To bridge this gap, a new approach involving a simulation-based GA is introduced. This approach combines a modified GA with a simulation framework. In this model, each gene corresponds to a specific PC element, and their sequence dictates the order in which these elements are arranged on the mould plates for production. Focusing on parallel production issues, the simulation environment serves as the decoder for the GA's chromosomes, ensuring that resources and mould plates are utilized efficiently at all times. To generate the initial population, the algorithm uses regret-based biased random sampling (RBRS) and a serial schedule generation scheme (SSGS). The evolutionary process includes selecting top-performing individuals, applying two-point crossover, swapping genes (swap mutation), and a mutation method that adjusts its probability linearly over time (parameters present in Table 1). The study's results were evaluated against conventional scheduling techniques, including two traditional dispatching rules. The dispatching rules examined are Earliest Due Date (EDD) and Shortest Process Time (SPT). EDD prioritizes tasks based on their due dates, scheduling those with the earliest deadlines first. In contrast, SPT prioritizes tasks according to their processing times, scheduling those that require the least time to complete before others.

Table 1: S-GA parameters

Population Size	200
Crossover Rate	0.8
Mutation Rate	0.2
TOP	0.15

2.3 Case Study

The cases in this research are derived from field studies in China, as the use of PCs is considered an environmentally friendly construction practice[17]. Scheduling tasks in this study are based on the real PC orders that provided by Meiruisi Construction Industrialization Co., Ltd. The number of fixed mould plates in their facility is established at 6, with 3 distinct types of PC components (namely wall panel A, window panel B, and roof panel C) in various quantities and due dates. The daily working hour is set at 8 hours, leaving 16 non-working hours. The penalty factors for earliness and tardiness are set to -0.5 and -10 respectively. The PC details are presented in following table (Table 2):

Table 2:Case study details

PC Code	Quantity	Due date	P1	P2	P3	P4	P5	P6
A	15	240	4/2	4/3	1/2	8/0	1/2	1/2
B	20	360	3/4	3/3	1/2	8/0	1/3	1/2
C	17	168	3/2	1/1	1/2	8/0	1/1	1/1

2.4 Results and Discussion

Table 3 presents the scheduling and rescheduling outcomes of both traditional methods and the proposed S-GA. The results clearly shows that the proposed S-GA generates better schedules compared with traditional heuristic rules. The total weighted penalties are reduced by 11.62% and the

makespan is reduced by 6%. The S-GA incurs the lowest total penalty at $2893.5, compared to $3274 for EDD and a substantial $19579 for SPT. It effectively minimizes tardiness costs to $890, far below those of EDD and SPT, while maintaining a competitive earliness cost of $2003.5. Additionally, S-GA achieves a shorter makespan of 386 hours, compared to 410 hours for both EDD and SPT, showcasing its efficiency in reducing overall completion time. These results demonstrate that S-GA provides a more balanced and optimized scheduling approach, making it a better choice for minimizing penalties and improving operational efficiency.

The results also indicate that Genetic Algorithms are inherently flexible and adaptive, capable of evolving over time to find optimal solutions even in complex and dynamic environments. This adaptability often makes GAs superior in handling a wide range of scheduling scenarios compared to static dispatching rules like EDD and SPT.

Table 3: Results comparison

	EDD	SPT	S-GA
Earliness ($)	**1944**	2469	2003.5
Tardiness ($)	1330	17110	**890**
Total Penalty ($)	3274	19579	**2893.5**
Penalty Gap	/	-498.01%	**11.62%**
Makespan (h)	410	410	**386**
Makespan Gap	/	0%	**6%**

3 CONCLUSION

This study proposed an automatic multi-line precast production scheduling method using S-GA to minimize production makespan and total weighted penalties. Real-world constraints such as limited working hours and limited quantities of resources are considered. A multi-line simulation for PCPS is designed and integrated with a GA algorithm. Through real-world cases, the proposed S-GA outperformed traditional dispatching rules with less total weighted penalties and makespan. This work extends the GA methods' application in production operations. The optimized production schedules are optimal and feasible than tradition rules. Future work should explore the method's generalization ability for more types of PC elements. Another direction is to discuss the rescheduling ability of GA-based method when uncertainties occur.

REFERENCES

[1]. Jang S, Lee G. Process, productivity, and economic analyses of BIM–based multi-trade prefabrication—A case study. translator. Automation in Construction. 2018;89:86-98.
[2]. Anvari B, Angeloudis P, Ochieng WY. A multi-objective GA-based optimisation for holistic Manufacturing, transportation and Assembly of precast construction. translator. Automation in Construction. 2016;71:226-41.
[3]. Tam VW, Fung IW, Sing MC, Ogunlana SO. Best practice of prefabrication implementation in the Hong Kong public and private sectors. translator. Journal of cleaner production. 2015;109:216-31.
[4]. Lou N, Guo J. Study on Key Cost Drivers of Prefabricated Buildings Based on System Dynamics. translator. Advances in Civil Engineering. 2020;2020:8896435.
[5]. Shi XM, Zhang D, editors. Proceedings of the Research on the appropriate technology of green residences design in eastern Henan; 2014: Research on the appropriate technology of green residences design in eastern Henan: p. 845-9. 6. Zhou J, Ren D. A hybrid model of external environmental benefits

compensation to practitioners for the application of prefabricated construction. translator. Environmental Impact Assessment Review. 2020;81.
[6]. Leu SS, Hwang ST. A Ga-based model for maximizing precast plant production under resource constraints. translator. Engineering Optimization. 2001;33(5):619-42.
[7]. Chan WT, Hu H. Production scheduling for precast plants using a flow shop sequencing model. translator. Journal of Computing in Civil Engineering. 2002;16(3):165-74.
[8]. Ko CH, Wang SF. GA-based decision support systems for precast production planning. translator. Automation in Construction. 2010;19(7):907-16.
[9]. Ko CH, Wang SF. Precast production scheduling using multi-objective genetic algorithms. translator. Expert Systems with Applications. 2011;38(7):8293-302.
[10]. Du J, Dong P, Sugumaran V, Castro-Lacouture D. Dynamic decision support framework for production scheduling using a combined genetic algorithm and multiagent model. translator. Expert Systems. 2021;38(1).
[11]. Du J, Dong P, Sugumaran V. Dynamic Production Scheduling for Prefabricated Components Considering the Demand Fluctuation. translator. Intelligent Automation and Soft Computing. 2020;26(4):715-23.
[12]. Dan YR, Liu GW, Mao C, Li KJ, Xu PP. Flowshop scheduling optimization for multi-shift precast production with on-time delivery. translator. Engineering Applications of Artificial Intelligence. 2024;127.
[13]. Dan YR, Liu GW, Fu Y. Optimized flowshop scheduling for precast production considering process connection and blocking. translator. Automation in Construction. 2021;125.
[14]. Benjaoran V, Dawood N. Intelligence approach to production planning system for bespoke precast concrete products. translator. Automation in Construction. 2006;15(6):737-45.
[15]. Lin R, Liao C-J. Batch scheduling problem for a machinery factory with fixed-position layout. translator. International Journal of Production Research. 2013;51(3):910-26.
[16]. Ma ZL, Li SY, Wang Y, Yang ZQ. Component-level construction schedule optimization for hybrid concrete structures. translator. Automation in Construction. 2021;125.

Fire Recognition on Construction Sites Based on the SE-DSOD

Jie Fu, Yifan Wang, Mingxing Liu, Peng Jian

School of Civil Engineering and Architecture, East China Jiaotong University, Nanchang 330013, China

ABSTRACT: To address the critical need for enhanced fire safety at construction sites, this study proposed a novel method utilizing the SE-DSOD algorithm for efficient real-time fire detection. The selection of the DSOD algorithm was predicated on its compact nature and the obviation of pre-training, thereby expediting the detection of potential incidents. Furthermore, the integration of a Compression-Excitation attention mechanism was innovatively employed to enrich the model with a broader spectrum of input features, enhancing its detection capabilities. The algorithm's performance was rigorously evaluated using a dedicated dataset comprising construction site fire incidents. Comparative analysis indicated that the SE-DSOD algorithm conferred a notable improvement over the baseline model, with increments of 0.6% in accuracy, 1.4% in recall rate, and 1.9% in Mean Average Precision (mAP). However, this was counterbalanced by a decrement in processing efficiency to 9.35 milliseconds per image and a reduction in the frame rate to 106 FPS. The findings underscore the SE-DSOD algorithm's proficiency and precision in fire detection, offering a significant contribution to the domain of construction site safety management.

KEYWORDS: construction site safety management; fire detection; SE (squeeze-and-excitation) attention block; object detection

1 INTRODUCTION

Against the backdrop of sustained global economic development, the construction industry has emerged as a pivotal force driving societal advancement. It epitomizes a sector characterized by intensive labor involvement. Yet, this growth trajectory is marred by significant safety management challenges, particularly the recurrent incidence of fire accidents. These incidents not only culminate in substantial human casualties but also erect significant barriers to the industry's progression. The intricate milieu of construction sites, coupled with the workers' limited safety awareness and the inadequacies in safety management protocols, contribute markedly to the construction sector's disproportionate share of industrial accidents[1].

Empirical evidence, as cataloged by the United States Fire Administration (USFA)[2], delineates that, within the span of 2018 to 2020, the United States witnessed an annual average of approximately 376,000 residential building fire incidents. These incidents accounted for roughly 2,775 fatalities, 12,075 injuries, and direct economic repercussions amounting to an estimated $8.3 billion. These statistics not only illuminate the profound ramifications of fire accidents on the residential construction sector but also underscore the grave implications for non-residential constructions, with an average annual occurrence of 114,300 incidents, resulting in 100 fatalities, 1,125 injuries, and financial losses approximating $3.5 billion.

A growing corpus of scholarly work advocates for the fortification of behavioral safety management practices as a strategic measure to mitigate errors among construction personnel, thereby substantially reducing the likelihood of accident occurrences[3-5]. Complementary to this discourse, data from the Emergency Management Department's Fire Rescue Bureau in China underscores the severe consequences of fire incidents at construction sites within the 18,000 factory fire incidents reported in 2022, thereby accentuating the critical need for augmented fire prevention and mitigation strategies at construction sites.

This study introduces a novel paradigm for the real-time management of fire safety at construction sites, anchored in the application of advanced computer vision technology. At the heart of this

methodology is the Squeeze-and-Excitation Deeply Supervised Object Detection (SE-DSOD) algorithm, embellished with an attention mechanism. This algorithm demonstrates remarkable proficiency in the precise identification and localization of fire sources, thereby significantly enhancing the detection accuracy and operational efficiency. Furthermore, this research has culminated in the development of an expansive dataset, comprising 3,000 images that encapsulate a broad spectrum of fire scenarios. These images were meticulously curated through manual extraction from extant surveillance systems and augmented via web crawling techniques. Through rigorous training and validation processes, the efficacy of the proposed method in enhancing fire detection capabilities at construction sites has been affirmed, thereby not only facilitating real-time fire safety monitoring but also contributing a novel solution and a rich dataset to the pertinent academic and professional discourse.

By leveraging this technological innovation, we anticipate a substantial diminution in both human casualties and property losses attributable to fires, thereby providing a robust foundation for the advancement of safety management practices within the construction industry. The insights gleaned from this investigation hold the potential to catalyze the modernization of safety protocols in the construction domain and proffer invaluable lessons for the integration of cutting-edge technologies in addressing conventional industry challenges.

2 RELATED WORK

The utilization of deep learning within the realm of fire detection prominently encompasses two domains: image classification and object detection. In the sphere of image classification, Muhammad refined the output of deep convolutional network AlexNet from a thousand target categories down to two—smoke and non-smoke—for smoke detection endeavors[6]. Furthermore, by adjusting the architectural nuances of convolutional networks, scholars have enhanced the precision of algorithms. Notably, Frizzi amplified the detection capabilities for fire, smoke, and safe conditions by repositioning the pooling layer within the convolutional neural network[7]. Ko formulated a technique to eliminate background disturbances leveraging the contrast between flame color and background brightness, thus pinpointing the fire zone with high accuracy[8]. Although these methodologies have registered achievements in tackling fire detection challenges, their efficacy is hampered by the limitations in feature extraction and classification precision.

The evolution of deep learning-based object detection strategies has progressively supplanted the conventional approach of preliminary feature extraction followed by classification. These cutting-edge object detection paradigms bifurcate into two principal classifications: the two-step and the single-step detection algorithms. The former, exemplified by Faster R-CNN, R-CNN, and Faster R-CNN, is characterized by superior detection accuracy and refined outcomes, albeit at the cost of extended training durations and decelerated detection velocities. Conversely, the single-step detection frameworks, including YOLO and SSD, abbreviate the detection timeline, albeit at the expense of diminished accuracy, thereby constraining their applicability in fire detection scenarios[9-13].

The task of object detection necessitates the precise localization of flames. Shen enhanced the YOLOv1 network's detection speed; however, the intricate nature of fire scenes mildly compromised its accuracy[14]. In response to the challenges posed by background noise, various methodological enhancements were proposed. H T, for instance, ingeniously classified the fire dataset and refined the Faster R-CNN algorithm, culminating in commendable detection outcomes[15]. Additionally, attempts to boost detection precision through model fusion and architectural modifications have been made. Xu synergized the YOLOv5 and EfficientNet models for fire detection tasks, heralding a substantial leap in performance[16].

Within the domain of fire detection, a plethora of fusion-based or architecture-specific attention mechanisms have been integrated into detection algorithms[17-19], showcasing distinct advantages for

particular fire scene classifications or imagery data. Nevertheless, when juxtaposed with the Squeeze-and-Excitation (SE) attention mechanism, these alternative approaches reveal discernible limitations on several critical fronts. The SE mechanism distinguishes itself through a streamlined and efficacious design, enabling precise recalibration and enhancement of feature channels sans a substantial augmentation in computational demands. This endows it with unparalleled adaptability and superior generalization capacity across a wide array of scenarios. Conversely, other attention mechanisms might falter in terms of their universal applicability, computational efficiency, simplicity of the model, and the ability to generalize effectively. Hence, although fusion or specific attention mechanisms possess their unique merits within niche application contexts, the SE attention mechanism retains an unparalleled stature within the fire detection landscape, attributed to its broad applicability, operational efficiency, and its capability to directly and efficaciously recalibrate features amidst complex settings.

Surpassing both traditional and contemporary methodologies, the SE-DSOD (Self-Exciting Deeply Supervised Object Detection) algorithm unfurls considerable superiority. It synergizes the SE attention mechanism with DSOD's deep supervision strategy to ensure meticulous detection of diminutive targets in intricate scenes, especially notable in fire scenarios marked by complex backdrops and occlusions. SE-DSOD not only elevates recognition accuracy and stability over conventional techniques but also, in comparison to existing methodologies, adeptly balances a commendable detection pace with high accuracy. This convergence of enhanced accuracy, adaptability, and robust performance earmarks SE-DSOD as a pivotal breakthrough in fire detection technology.

3 METHOD

The above-mentioned study indicates that general object detection algorithms can be applied to the detection of fire incidents. However, in the unique and complex environmental conditions of construction sites, fire targets are susceptible to interference from disorderly accumulated materials. Distant smoke and low flame resolution contribute to limited feature information, rendering traditional fire detection methods inadequate for the requirements of fire detection under such conditions. In light of these challenges, this paper adopts the DSOD (deeply supervised object detectors) detection algorithm, a multi-scale detection model based on the SSD[13] algorithm.
Compared to the SSD[13] object detection algorithm, the DSOD[20] algorithm's network model is more compact. Additionally, it can be directly trained on existing datasets, reducing the time required for parameter adjustments during the pre-training process. Simultaneously, a Squeeze-and-Excitation attention mechanism (hereinafter referred to as SE attention mechanism) is incorporated after the DSOD model's backbone network to enhance model performance.

3.1 DSOD

The network architecture of DSOD[20] consists of a front-end backbone network for extracting image features and a multi-scale feature layer prediction subnetwork. The DSOD algorithm model framework is illustrated in Fig.1. The former is derived from the concept of the DenseNet network, comprising Stem blocks, dense blocks, transition layers, and transition layers without pooling. The incorporation of the Stem module in the main structure significantly improves model accuracy and reduces the loss of image information. Within the four dense blocks, output information can be transmitted to adjacent layers, and each subsequent layer can receive supervised information from the preceding network layers. The inter-layer information exchange ensures that each layer receives information fused from other layers, enhancing the flow and utilization of feature information and, to some extent, streamlining model parameters. To mitigate the impact of resolution changes induced by the depth of the model on the cascaded architecture, transition layers are introduced. Simultaneously, to maintain feature map resolution without reducing it while increasing the number of dense blocks, transition layers with unpooled layers are introduced.

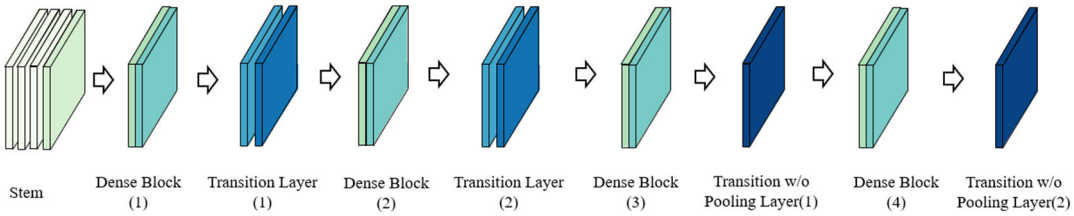

Figure 1. DSOD model framework

The prediction subnetwork of the DSOD detection algorithm is similarly inspired by the DenseNet densely connected concept, incorporating multi-scale information fusion for predicting feature layers. The DSOD network, processing input images, can extract predictions from six different scales of feature maps. Except for the first feature map, each size of the feature prediction layer includes results learned from the pre-convolution layer, while the remaining half of the features are obtained through downsampling continuous high-resolution feature maps. The feature fusion and reuse after multi-scale prediction layers contain richer information, simplifying model parameters and enhancing detection accuracy.

3.2 Squeeze-and-Excitation Block

Due to the unique environmental conditions on construction sites, such as weather, lighting, and obstructions, the features of targets are often not distinctly manifested. To address this issue, this paper introduces a channel attention mechanism into the backbone network to enhance the feature extraction capability of the front-end subnetwork. The attention mechanism is inspired by the human tendency to focus on the object itself when observing something, disregarding the visual characteristics of surrounding objects. As shown in Fig.2, by incorporating the SE (Squeeze-and-Excitation) module into the Stem module of the backbone network, a new feature extraction module, SE-Stem, is constructed.

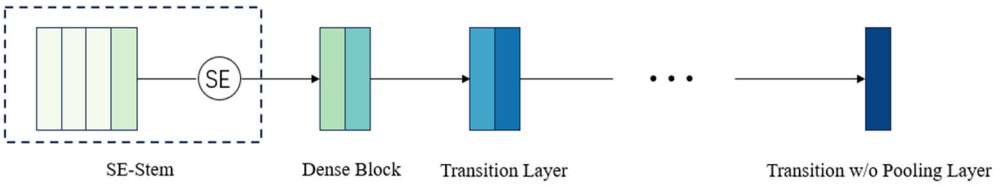

Figure 2. SE-DSOD fire detection model frame

The SE attention mechanism operates on the channel of the input feature maps. After introducing the SE module, the model automatically focuses on channel dimensions with more informative content while suppressing less important channel dimensions in the feature map. The process of the SE attention mechanism is illustrated in Fig.3. Initially, the target image undergoes convolution and pooling in a multi-layer convolutional network, resulting in multiple feature maps. Subsequently, each feature map is compressed to a single channel through global average pooling. The compressed channels are then concatenated and fused through a two-layer fully connected neural network. The output values from the fully connected neural network are normalized by an activation function, obtaining weights for each channel. Ultimately, these weight values are applied to each channel of the initial feature map, introducing attention into the channel.

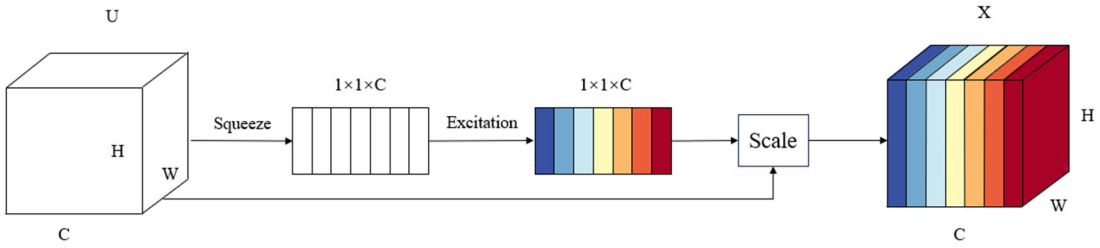

Figure 3. Squeeze-and-Excitation block

During the compression phase, spatial information $U \in \mathbb{R}^{H \times W \times C}$ on a channel is compressed into a real number $Z \in \mathbb{R}^{1 \times 1 \times C}$ through global average pooling, where the information is fused from features extracted across various channels.

$$Z_c = F_{sq}(U_c) = \frac{1}{H \times W} \sum_{i=1}^{H} \sum_{j=1}^{W} U_c(i, j) \tag{1}$$

In the excitation phase, the relationships between channels are captured through two fully connected layers, denoted as $W_1 \in \mathbb{R}^{\frac{c}{r} \times C}$ and $W_2 \in \mathbb{R}^{C \times \frac{c}{r}}$, which then output the weight values for different channels. Here, 'δ' corresponds to the Relu activation function, and 'σ' to the sigmoid activation function.

$$s = F_{ex}(z, W) = \sigma(g(z, W) = \sigma(W_2 \delta(W_1 z)) \tag{2}$$

To reduce the complexity of the model, this module employs two fully connected layers to construct a Bottleneck structure. In this process, the role of the first fully connected layer W1 is to reduce the dimensionality of the input feature map by a reduction ratio r. Specifically, W_1 reduces the feature dimensionality of each channel to 1/r of its original size, thereby compressing spatial information into a real number value u_c. This dimensionality reduction operation helps to decrease the model's complexity while ensuring that crucial feature information is retained. Subsequently, the second fully connected layerW_2 uses the ReLU activation function to remap the reduced features back to their original dimensionality. During this process, the weights of each channel are normalized through the Sigmoid activation function, ensuring that each channel's weight s lies between 0 and 1, representing its importance in the attention mechanism. Finally, the normalized channel weights s_c are multiplied by the original input x_c to obtain $\tilde{x}_c$, implementing the process of introducing attention mechanism on the channel, thereby enabling the model to automatically focus on channels with greater information content and suppress information from less important channel dimensions.

$$\tilde{x}_c = F_{scale}(u_c, s_c) = s_c \times u_c \tag{3}$$

4 EXPERIMENTAL RESULTS AND ANALYSIS

4.1 Datasets

Due to the limited application of deep learning in the detection of fire incidents on construction sites and the absence of open datasets specifically dedicated to construction site fires, this study takes full advantage of online resources and employs web crawling techniques to collect a portion of experimental data. By utilizing several key terms such as "fire," "construction site fire," "workers smoking," etc., over 7000 relevant images were gathered online. However, the existing images on the internet exhibit significant variations in quality, and in some instances, the size of fire targets in the images is too small. Therefore, in addition to online images, a portion of the data in this study was obtained from the actual shooting at a construction site in Nanchang. Images without fire incidents, duplicate images, and those not in the RGB three-channel format were excluded, resulting in a curated dataset of 3000 images depicting construction site fires, as depicted in Fig.4.

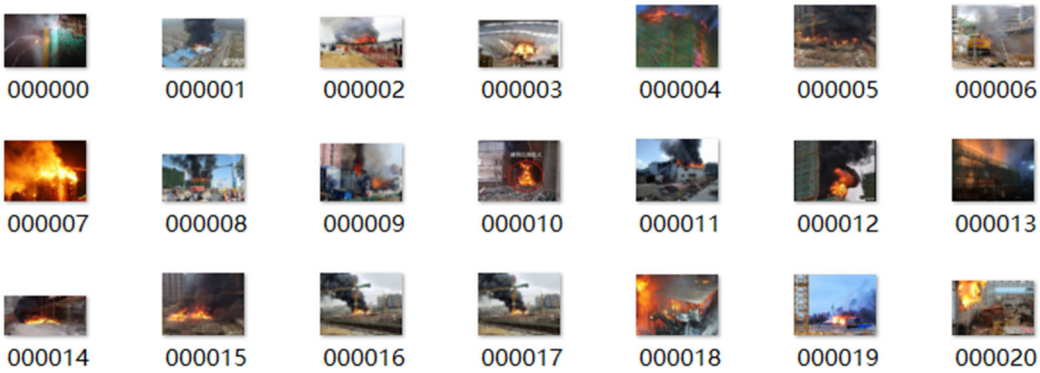

Figure 4. Partial dataset of fire incidents on construction sites

4.2 Implementation Details

The dataset is generated in VOC (Visual Object Classes) format and is randomly divided into three parts: a training set, a validation set, and a test set, with a ratio of 8:1:1. The training set is utilized to train the model and initially determine model parameters. The validation set is employed to assess the model's performance during runtime and adjust suitable hyperparameters, while the test set is used to evaluate the model's generalization performance[21]. To ensure the accuracy of detection results, it is essential to differentiate the test set from the training and validation sets.

All experiments were conducted on an Intel(R) Xeon(R) Platinum 8350 CPU@2.50 GHz, with 42.00 GB RAM, and Nvidia GeForce RTX 3090 GPU, utilizing the PyTorch framework. Stochastic Gradient Descent (SGD) is employed as the training optimizer, with an initial learning rate set at 0.0001, subject to change at each iteration. The momentum coefficient is 0.9, L2 weight decay coefficient is 0.0005, batch normalization decay coefficient is 0.9, and the batch size is set to 32. The training process comprises 100,000 iterations, with model weights saved at the iteration with the minimum loss value on the validation set.

4.3 Performance Comparison of Different Models

The changes in Mean Average Precision (mAP) and the loss function were recorded during the training process. Figure 5 illustrates the loss function graph of the SE-DSOS model over 100,000 iterations, with intervals of 5000 iterations. The value of the loss function represents the difference between real data and predicted results. As depicted in Fig.5, the loss function initially experiences a rapid decline, and as the number of iterations increases to 20,000, the rate of decrease becomes more gradual. Beyond 80,000 iterations, the loss function graph tends to flatten, indicating that the model has begun to converge, signifying the completion of training. Ultimately, after 100,000 iterations, the loss value for the SE-DSOD model converges to 0.73.

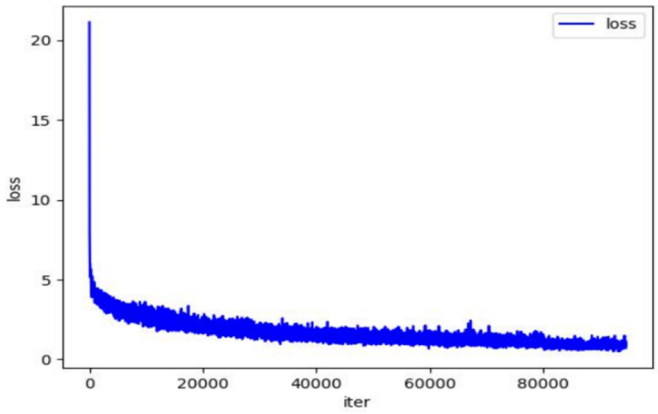

Figure 5. SE-DSOD loss function curve

To further validate the robustness of the improved model, this paper compares the training process curves of two sets of experiments. The key performance metric is the Mean Average Precision (mAP), and the curves of mAP for both models are illustrated in Figure 6. The horizontal axis represents the number of iterations, while the vertical axis represents the values of mAP. Figure 6 demonstrates the overall upward trend of Mean Average Precision (mAP) with iterations, with some fluctuations during the process, indicating that the upward trend is not consistently stable.

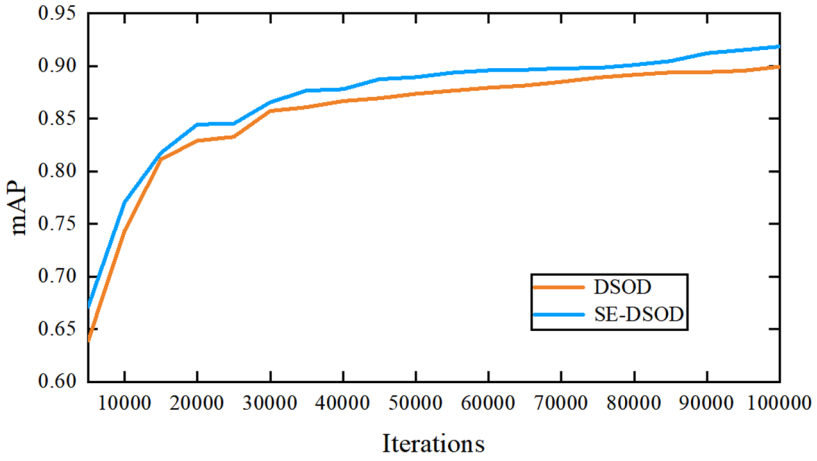

Figure 6. The curves of mAP in the different models

As shown in Table 1, the improved SE-DSOD model, with the addition of the SE attention module, experienced an increase of 0.6% in detection accuracy, a 1.4% improvement in recall rate, and an overall Mean Average Precision (mAP) enhancement of 1.9%, reaching 91.8%. However, the Frames Per Second (FPS) decreased to 106, still meeting the real-time detection requirements for daily use, with a processing speed of 9.35 milliseconds per image. This indicates an elevation in model accuracy with a minimal sacrifice in computational speed, making it more adaptable to meeting the accuracy requirements of detection. Due to the introduction of the attention mechanism, the model's volume and computational load did not experience a significant increase. Moreover, it maintained the original DSOD model's detection performance and outstanding speed during the detection process, aligning with the requirements for improving DSOD.

In Table 1, we compared the experimental performance of our method with existing approaches across three metrics: mAP, FPS, and detection time. We utilized the results from their papers for comparison; however, verifying the accuracy of these values is challenging due to the variations in datasets used across different studies. Nevertheless, our method demonstrates superior accuracy in early fire detection and reduced computational time.

Table 1. Quantitative evaluation results of different fire recognition methods

Approach	mAP/%	FPS	Detection Time/ms
G C et al[19]	87.7	36.6	27.2
C C et al[20]	93.39	-	25.62
C Y et al[21]	97.7	19	-
DSOD	89.9	114	9.35
SE-DSOD	91.8	106	9.14

After the completion of model training, the test set of 300 images was fed into the model. The model outputs predictions based on the images along with confidence scores. Partial verification results are depicted in Fig.7.

Figure 7. The detection results of some test images

As depicted in the above figure, the probability of recognizing a fire on a construction site as "fire" exceeds 80%. However, the output images from the model exhibit some errors in the detection process. For instance, the model struggles to detect small-sized or distant flames. It encounters difficulty identifying safety helmets when there are multiple obstructions in front of flames on the construction site. Additionally, under poor lighting conditions, the model is prone to misidentifying regions with similar colors as flames.

In Fig.8(a), even in the presence of complex background interference and limitations on the proportion of flames in the image, the improved SE-DSOD algorithm can still detect fire targets comprehensively. However, there is room for improvement in the detection confidence. The situation in Fig.8(b) is similar to the first case. In Fig.8(c), the model predicts a probability of 38%, but the probability of identifying the sky as a fire is 81%.

To enhance the model's performance, it is advisable to increase the quantity of the image dataset and perform preprocessing operations on the images. Besides these measures, improvements can be achieved by continually refining the algorithm, adjusting parameters and weights, among other approaches, to reduce false positives.

(a) (b) (c)

Figure 8. The detection results of some test images

4 CONCLUSION

The DSOD, incorporating the Squeeze-and-Excitation (SE) attention block, was employed for model training to investigate real-time management of fire incidents at construction sites, yielding the following conclusions:

(1) The DSOD model with the SE attention block (SE-DSOD) exhibited higher precision and recall rates in detecting construction site fires. The detection precision (P) increased from 88.6% to 89.2%,

recall rate (R) increased from 89.3% to 90.7%, and overall mean average precision (mAP) improved from 89.9% to 91.8%, validating the effectiveness of the attention mechanism. Furthermore, the processing speed per image was 9.35 ms, demonstrating the model's efficiency.

(2) Despite the excellent performance of the SE-DSOD model in real-time and detection accuracy, certain challenges persisted under specific conditions (such as small or distant flames, poor lighting, and obstructed environments). In such scenarios, the model may experience detection difficulties, leading to false positives or false negatives, such as struggles in identifying small flames or misidentifying regions with similar colors as flames.

(3) To further enhance model performance, it is recommended to diversify and increase the dataset size, preprocess data to improve model generalization, and continuously optimize algorithm structures, parameter adjustments, and weight tuning to reduce false alarms and missed detections, thereby better adapting to complex and dynamic real-world detection environments. Additionally, considering the diversity of practical application scenarios, future research may explore more variants of attention mechanisms and deep learning models to further improve detection efficiency and accuracy.

REFERENCES

[1]. Pinto A,Nunes I L, Ribeiro R A.Occupational risk assessment in construction industry - Overview and reflection[J].Safety Science,2011,49(5):616-24.
[2]. U.S. Fire Administration. Data Sources and National Estimation Methodology (Vol. 22) [N]. 2022-05.
[3]. Zhou, G., Cheng, W., Zhuge, F., et al. Analysis and Exploration on Correlative Theories of Man-made Errors and Human Unsafe Behaviors[J].China Safety Science Journal, 2008(03), 10-14+176.
[4]. Han, Y., Mei, Q., Liu, S., et al. Strategies and Methods of Early Intervention of Unsafe Behaviors for Construction Workers: Based on Vulnerability[J].Journal of Engineering Management, 2015, 29(05), 97-102.
[5]. Haslam R A,Hide S A, Gibb A,et al.Contributing factors in construction accidents[J].Applied Ergonomics,2005,36(4):401-415.
[6]. Muhammad K, Ahmad J, Baik S W. Early fire detection using convolutional neural networks during surveillance for effective disaster management[J]. Neurocomputing, 2018, 288(3): 30-42.
[7]. Frizzi S, Kaabi R, Bouchouicha M, et al. Convolutional neural network for video fire and smoke detection[C]. Conference of the IEEE Industrial Electronics Society. IEEE, 2016:877-882.
[8]. Byoung Chul Ko;;Kwang-Ho Cheong;;Jae-Yeal Nam.Fire detection based on vision sensor and support vector machines[J].Fire Safety Journal,2008(3).
[9]. GIRSHICK R. Fast R-CNN(Conference Paper)[C]// IEEE International Conference on Computer Vision, December 11-18, 2015, Santiago, CHILE. New York: IEEE, c2015:1440-1448.
[10]. GIRSHICK R, DONAHUE J, DARRELL T, et al. Rich Feature Hierarchies for Accurate Object Detection and Semantic Segmentation [C]// IEEE Conference on Computer Vision and Pattern Recognition, June 23-28, 2014, Columbus, OH. New York: IEEE, c2014: 580–587.
[11]. REN S, HE K, GIRSHICK R, et al. Faster R-CNN: Towards Real-Time Object Detection with Region Proposal Networks[J]. IEEE Transactions on Pattern Analysis and Machine Intelligence, 2017, 39(6): 1137-1149.
[12]. REDMON J, DIVVALA S K, GIRSHICK R B, et al. You only look once: Unified, real-time object detection[C]// IEEE Conference on Computer Vision and Pattern Recognition. June 27-30, 2016, Seattle, WA. New York: IEEE, c2016: 779-788.
[13]. LIU W, ANGUELOV D, ERHAN D, et al. SSD: Single Shot MultiBox Detector[C]// 14th European Conference on Computer Vision, October 08-16, 2016, Amsterdam, The Netherlands. Berlin: Springer International Publishing, c2016: 21-37.
[14]. Shen D, Chen X, Nguyen M et al. Flame Detection Using Deep Learning. in: 2018 4th International conference on control, automation and robotics (ICCAR): IEEE, 2018. 416-420.
[15]. Hui, T., Halidan·A, Du, H. Multi-type flame detection combined with Faster R-CNN[J]. Journal of Image and Graphics,2019, 24(01), 73-83.
[16]. Xu R, Lin H, Lu K, Cao L, Liu Y. A Forest Fire Detection System Based on Ensemble Learning[J]. Forests. 2021,12(2):217.
[17]. Cao K, Jiao S. Lightweight Fire Detection Model with Fusion Attention Mechanism. Fire Science and Technology. 2024;(03):378-383.
[18]. Li X, Li B, Zhang X, Yu C. YOLOv5 Image Fire Detection Algorithm Based on CA-Res Attention Mechanism. Fire Science and Technology. 2023;(08):1113-1116.

[19]. Lu Y, Chen B. Anchorless Forest Fire Detection Algorithm with Fusion Attention Mechanism. Computer and Modernization. 2021,(11):61-66+76.
[20]. SHEN Z,LIU Z,LI J,et al. DSOD: learning deeply supervised object detectors from scratch[C]/ / IEEE International Conference on Computer Vision. Venice, Italy,2017.
[21]. J. Grum. Book review: pattern recognition and neural net-works by B.D. Ripley. [J] International Journal of Microstructureand Materials Properties.2009, 4(1):146.
[22]. Chen G, Zhou H, Li Z, Gao Y, Bai D, Xu R, Lin H. Multi-Scale Forest Fire Recognition Model Based on Improved YOLOv5s[J].Forests. 2023; 14(2):315.
[23]. Chen, C., Yu, J., Lin, Y. et al. Fire detection based on improved PP-YOLO[J]. Signal, Image and Video Processing.2023,17, 1061–1067.
[24]. Conghan Yue, Jun Ye. Research on Improved YOLOv3 Fire Detection Based on Enlarged Feature Map Resolution and Cluster Analysis[J]. Journal of Physics.2020,1757:012094.

A Review on Knowledge Representation Technology in AEC Industry

Zhekai Xia, Shuyuan Xu

School of Civil Engineering and Architecture, Zhejiang Sci-Tech University, Hangzhou, 310018, China

ABSTRACT: In recent years, knowledge representation technology has sparked significant interest across various industries, including the Architecture, Engineering, and Construction (AEC) sector. Literature related to knowledge representation in this field has shown a rapid growth trend over the past decade. This research aims to provide insightful guidance for researchers in the AEC domain through in-depth literature analysis and summary. This paper conducts a systematic review of literature related to knowledge representation over the last 17 years. The study further explores the application of knowledge representation across three key phases of the project lifecycle, thereby outlining future industry trends. This review has sparked new research approaches and methodologies, driving ongoing innovation within the industry.

KEYWORDS: AEC; knowledge representation; entire lifecycle

1 INTRODUCTION

Knowledge, a collection encompassing all facts, concepts, rules, or principles [1], serves as the foundation for human understanding and interaction with the world. In the field of knowledge engineering, such knowledge not only needs to be effectively extracted, integrated, and processed[2], but also made available for intelligent systems to simulate human decision-making processes. However, a major challenge in knowledge engineering is to deal with the large amounts of fragmented data, including heterogeneous and unstructured data [3]. The sources of data for Knowledge Representation (KR) in knowledge engineering are diverse, ranging from texts and images to database records and social media posts. KR, a key component in knowledge engineering[4], is dedicated to converting these complex, dispersed pieces of knowledge into a structured and standardized form that computer systems can understand and process. It involves not only the structured storage of knowledge but also providing a set of rules and models that describe the complex relationships and logic among pieces of knowledge. In the Architecture, Engineering, and Construction (AEC) sector, knowledge representation refers to how industry-specific knowledge is symbolized, formalized, and modeled within computational frameworks[1]. These frameworks, tailored to meet the constraints of computer systems, are crucial for accurately reflecting real-world scenarios. Essentially, knowledge representation in AEC defines the fundamental concepts and semantic relationships within the industry, enabling the efficient management and processing of construction-related information to support enhanced decision-making and automation. Through effective knowledge representation, computers can not only store and organize a vast and diverse amount of knowledge, making it easy to retrieve, share, and reuse [5], but can also make effective decisions on complex issues through reasoning and other methods.

Over the past decade, with the growing demand for digital technologies in the AEC sector, a substantial number of knowledge representation models have been proposed to advance the management, decision-making, and operational automation of this field. These models have played a crucial role in enhancing design standards[6], optimizing resource allocation[7], and improving project information communication[8]. However, given the diversity of knowledge representation methods and the complexity of application scenarios within the AEC domain, a systematic review of these models has become particularly necessary. Therefore, this paper aims to provide a comprehensive review and analysis of knowledge representation models within the AEC domain, revealing current research trends as well as future development directions and challenges of the industry.

Through an extensive literature search, it has been found that although knowledge representation has been widely studied and applied across many domains, review articles specifically addressing

knowledge representation methods for the AEC sector are relatively scarce. Existing literature reviews[9-11] often focus on discussing a single knowledge representation technology or method, without systematically organizing and analyzing the various knowledge representation methods adopted within the AEC domain. This paper provides a detailed review and analysis of knowledge representation methods used in the AEC sector, discussing their theoretical underpinnings, benefits, and use cases. It evaluates how these methods apply at various project lifecycle stages, highlights associated challenges, and future trends. This analysis aims to offer AEC researchers and practitioners a comprehensive overview of effective knowledge management strategies within the industry.

2 RESEARCH METHODS

To comprehensively explore the development and application of knowledge representation in the AEC domain, this paper employs a systematic literature review approach. It aims to delve into the knowledge representation methods within the AEC field, identifying current research trends, challenges, and future directions. For this purpose, the Web of Science database was chosen as the primary source of literature to ensure coverage of high-quality research findings within the domain. A keyword-based method was adopted to retrieve relevant studies. The main search keywords used in this paper are “knowledge representation” “NLP” “ontology” “Expert system” and “semantic web”. These keywords aim to capture advanced research and applications related to knowledge representation technology. In addition, “construction building technology” was selected as the specific “Research Areas,” along with “AEC,” “Architecture,” “Engineering,” and “Construction” as domain-specific keywords to obtain more precise search results relevant to the AEC industry. The AND Boolean operator was used to precisely combine these thematic keywords and domain-specific keywords. Titles, abstracts and keywords of the literature were targeted for keyword searching, thus maximizing the coverage of relevant academic articles. Although an effective retrieval method can minimize the possibility of retrieving irrelevant articles, it cannot completely eliminate the occurrence of erroneous literature. Therefore, an initial large set of literature obtained through preliminary screening was further filtered to exclude papers that contain matching keywords but are not relevant to the actual expectations of this paper. The filtering was achieved using manual inspection, involving a cursory review of the titles, abstracts, and keywords of the papers to eliminate irrelevant studies. As a result, from an initial screening of 1386 articles, 221 were obtained after further selection and analysed subsequently. This paper utilizes intuitive data from Web of Science and processes it with Excel to achieve data visualization. This method effectively highlights research hotspots and trends within the domain, aiding in the identification of emerging trends[12].

3 BIBLIOMETRIC ANALYSIS

This section utilizes the built-in data analysis feature of Web of Sciences to analyze the direct data from the collected 221 articles, mainly divided into three parts: the number of publications per year, the number of publications by different countries/regions, and the number of publications by different journals.

3.1 Publication Count by Year

Through searching and filtering in Web of Science, a total of 221 documents were obtained. These 221 documents were imported into a newly created marked list in Web of Science, and data on the number of publications for each year were obtained through Web of Science's "Analyze Results". The year of publications span from 2007 to 2023, covering a total of 17 years. Figure 1 presents the annual publication counts in the past 17 years, allowing for a more intuitive identification of trends in publication counts.

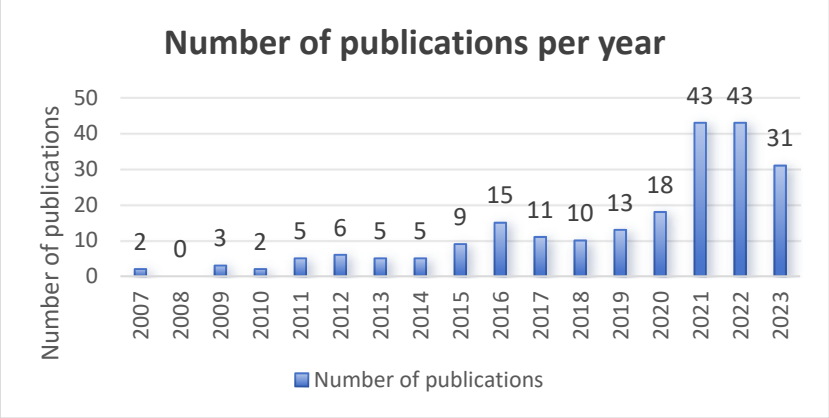

Figure 1 Number of publications per year (bar chart)

It is shown that during the period from 2007 to 2010, there were fewer publications related to knowledge representation in the AEC field. Starting from 2010, except for individual years, the overall number of publications has shown a growth trend, especially reaching its peak in 2021 and 2022, with 43 publications each year, accounting for 19.457% of the total. Although the number of publications experiences fluctuations during the years 2020 to 2023, peaking at 43 in 2021 after a rise from 18 in 2020, and then declining to 31 in 2023, it remains considerably higher compared to previous years (i.e., before 2020), signifying an escalation in research activities and increasing scholarly focus in this domain.

The long-term growth trend and high publication rate in recent years may reflect the increasing maturity of the research domain, a shift in the research focus within the field, and a diversification of research topics and methods.It is evident that knowledge representation in the AEC field is becoming a focal point of research. The overall trend indicates that this research direction is in a phase of vigorous development and possesses great potential for growth.

3.2 Publication by Country and Region

Similarly, using the "Analyze Results" feature in Web of Science, data on the number of publications by different countries/regions can be obtained. Table 1 lists the number of publications by different countries/regions. The data reveals that literature related to knowledge representation in the AEC field spans multiple countries and regions globally. Among the selected 221 articles, a total of 42 countries/regions are represented, with Table 1 only showcasing the top 5. The data shows that CHINA leads with 77 publications, accounting for 34.842% of the total, followed by the USA with 50 publications, representing 22.624%. Together, these two countries contribute more than half of the publications. Additionally, countries like ENGLAND, AUSTRALIA, and GERMANY also have a high number of publications, indicating strong research activity in Europe and Australia regarding this field. Researchers from various countries and regions have made active contributions, albeit to varying degrees.

Table 1 Number of publications in different countries(Showing 5 out of 42 entries)

Countries/Regions	Record Count	% of 221
PEOPLES R CHINA	77	34.820
USA	50	22.624
ENGLAND	20	9.050
AUSTRALIA	15	6.787
GERMANY	14	6.335

3.3 Publication Types and Titles

According to the data provided in Web of Science, it can be observed that among the 221 articles collected in this paper, there are 192 journal articles, 16 review articles, and 14 conference papers.

Applying the same method, the number of publications by different journals can be obtained, with Table 2 displaying the publication count by different journals. this paper selects the top 5 journals with the most publications among the total 72 journals. Data from Table 2 reveals a high concentration of publications in certain journals. AUTOMATION IN CONSTRUCTION leads significantly with 62 publications, accounting for 28.054% of the total and far exceeding other journals. The second position is shared by ADVANCED ENGINEERING INFORMATICS and JOURNAL OF COMPUTING IN CIVIL ENGINEERING, each with 16 publications, representing 7.24%. The top three journals, i.e., "AUTOMATION IN CONSTRUCTION", "ADVANCED ENGINEERING INFORMATICS", and "JOURNAL OF COMPUTING IN CIVIL ENGINEERING", together account for 42.534% of the total. These specialized journals play a crucial role in the research of knowledge representation in the AEC domain, reflecting the focus areas within the field of knowledge representation research. Although publications are concentrated in certain journals, overall, research outcomes are distributed across multiple journals, showcasing the breadth and diversity of knowledge representation research in the AEC domain.

Table 2 Number of publications in different journals(Showing 5 out of 72 entries)

Publication Titles	Record Count	% of 221
AUTOMATION IN CONSTRUCTION	62	28.054
ADVANCED ENGINEERING INFORMATICS	16	7.240
JOURNAL OF COMPUTING IN CIVIL ENGINEERING	16	7.240
BUILDINGS	13	5.882
JOURNAL OF CONSTRUCTION ENGINEERING AND MANAGEMENT	12	5.430

Data from the Web of Science database indicates that knowledge representation in the AEC domain is rapidly advancing and widely relevant globally. Research is primarily published in several high-impact journals, showing both focus and diversity, highlighting significant potential for future growth in this area.

4 APPLICATION OF KNOWLEDGE REPRESENTATION TECHNIQUES THROUGHOUT THE ENTIRE LIFECYCLE

Following the above visual analysis, we can identify several commonly used knowledge representation techniques, such as ontology, natural language processing, semantic web, and knowledge graphs. With the rapid advancement of deep learning, methods of deep learning for supporting knowledge representation have become a research focus in the industry. Hence, this section provides an overview of some developed models applied throughout the project lifecycle, mainly discussing the design, construction, and operation and maintenance phases.

4.1 Design Phase

The success of the design phase directly affects the project's feasibility, cost, quality, and risk. It is the foundation for the smooth progression of the project, specifically providing a grand and detailed blueprint. Based on this blueprint, the project team can refine and implement each step to ensure the achievement of project objectives. Existing knowledge representation methods primarily build models to handle project modeling, contract management, and cost management. In terms of model optimization and information data sharing, knowledge representation technology offers strong support[13-15]. For example Xu, Z, and Wang, JL leverage IFC standards and ontology to optimize prefabricated building designs, significantly enhancing design efficiency and resource reuse through the strategic use of extensible ontologies and IfcDoc for model delivery. For compliance checks, scholars mostly opt for a method that combines BIM with knowledge representation technology to achieve automatic compliance checks[6, 16-18]. For example, Jiang, L, and Shi, JY proposed a method for automated code compliance checking based on BIM and ontology, introducing four ontologies along with a set of mapping and checking rules. Through these rules, compliance reports are generated, leading to reduced document processing time and improved inspection efficiency. Zhou,

YC, and Zheng, Z proposed an automated rule interpretation method that converts regulatory texts into computable checking rules through semantic tagging and syntactic parsing, thus achieving automated compliance checks. In terms of contract management, it is often necessary to deal with a large number of texts, so the optimization of contract management is relatively complex. But researchers combine knowledge representation methods to achieve effective management of contracts[19-24]. Lee, J, and Yi, JS developed an NLP-based method to effectively identify "toxic clauses" in international construction contracts, addressing the challenge contractors face in swiftly reviewing numerous contracts during the bidding phase to pinpoint risk clauses potentially adverse to their interests. In terms of cost management, most literature focuses on optimizing cost management to achieve precise control and effective savings of project budgets. By integrating advanced knowledge representation technology and data analysis methods, researchers have explored various strategies and tools to improve the accuracy of cost estimation[25-28]. Niknam, M, and Karshenas, S integrated a new method for construction cost estimation by combining semantic web and ontology with BIM knowledge bases, estimation knowledge bases, and supplier semantic webs, effectively saving manual input time and improving cost estimation efficiency. By integrating design, compliance, contract management and cost management in a construction project, this paper demonstrates the key role of knowledge representation technology, which significantly improves the efficiency of the entire design phase.

4.2 Construction Phase

The construction phase is a relatively complex stage in the project's entire lifecycle, characterized by the complexity and diversity of the construction process, potentially facing various uncertainties. During this phase, not only is the smooth completion of the implementation process required, but also the proactive prevention and response to many risks encountered. Risk management is crucial for the successful completion of the project, thus many publications focus on risk management strategies. For safety management on construction sites, Chen, QH, and Long, DB[29] utilized a knowledge graph construction method to analyze dynamic risks, proposing a behavior-based safety (BBS) management approach. By conducting graph topology analysis on historical data, they effectively classified risks and reduced BBS risks at construction sites.In addition to the analysis by Chen, QH, and Long, DB on the risks at construction sites, Lee, SK, and Yu, JH[30] utilized artificial intelligence technology to recognize images of objects at construction sites, using predefined ontology rules to infer the current work environment and hazardous conditions. The combination of AI technology and ontology not only significantly reduces the amount of training data (compared to using AI image recognition alone) but also enables effective reasoning.Shen, QY, and Wu, SF [31] also proposed a preventive mechanism for the automatic identification of safety risks, combining BIM and ontology to devise a method for inspecting safety rules during the dynamic process of construction. They employed natural language processing technology to provide an intelligent presentation mechanism, facilitating convenient access to safety information for construction safety management personnel. Similarly, employing ontology, Guo, BHW, and Goh, YM [32] constructed an ontology model (AFPS-Onto) to formalize the knowledge domain of Active Fall Protection Systems (AFPS) design in the construction and building industry. In addition to combining BIM, ontology, and natural language processing to address risks arising during the construction process, there is also accident analysis at construction sites integrating text mining and natural language processing. Zhang, F, and Fleyeh, H[33] used an ensemble model of five basic classifiers to analyze the causes of accidents reported, and employed a rule-based chunk extraction method to identify common objects causing accidents, effectively enhancing construction site safety and accident prevention.Extracting and analyzing the content of accident texts is an important means of achieving hazard control. Tixier, AJP, and Hallowell, MR[34] used NLP for word segmentation and frequency analysis of injury reports, constructed a keyword dictionary, and combined grammatical rules for coding to transform unstructured reports into structured datasets, effectively improving safety management in construction. Unlike traditional construction methods, prefabricated construction has its specific safety risks. Shen, Y, and Xu, M[35] managed safety risks in prefabricated construction by integrating BIM technology with ontology to develop a safety risk management system and a safety risk ontology library. This enables intelligent identification and

precautionary measures for identified risks through BIM software (Revit), effectively reducing the hazards of prefabricated construction. These knowledge representation methods are employed not only in conventional construction projects but also extend to various construction methodologies, including the construction of subways, tunnels, bridges, roads, and more[36-38]. Construction scheduling, resource management, and safety are key research areas in the AEC field, focusing on protecting workers and preventing economic losses. By integrating knowledge extraction with advanced data processing technologies, the accuracy and efficiency of managing construction risks can be enhanced. This improves site safety and supports the successful execution of projects.

4.3 Operation and Maintenance Phase

In the project's entire lifecycle, the operation and maintenance (O&M) phase is indeed a critical stage. It is responsible not only for the stable operation and maximization of efficiency in buildings or other facilities but also for playing a key role in ensuring user safety and comfort. During this phase, the most fundamental tasks involve the maintenance and inspection of the building itself, along with systematic management of the building, energy consumption, and so forth. Consequently, many scholars have a broad range of research objectives during the operation and maintenance phase, aiming to enhance the efficiency of O&M management and optimize the use of resources, among other goals. Regarding maintenance, researchers approach from diverse perspectives [39, 40]. For example, recognizing the inefficiency in allocating personnel for building maintenance, D'Orazio, M, and Bernardini, G have integrated three machine learning and NLP techniques. This innovative approach enables the automatic prediction and prioritization of staff allocation and maintenance tasks by analyzing the textual content of building maintenance requests. In the field of building management, researchers have developed a variety of models by integrating knowledge representation technology to deal with the overall planning and management of buildings, and carry out building optimization, energy management, space utilization efficiency improvement, and environmental impact assessment, so as to realize more intelligent and efficient building operations[41-44]. Schneider, GF, and Kontes, GD developed a system called Automatically enabled Building Management Services (ABMS), which uses a knowledge-based approach to automate the deployment of building management services, enhancing energy efficiency and other operational aspects, thereby advancing the adoption of BMServ. In terms of building performance[7, 45, 46], for example, Hu, S, and Corry, E utilized a hybrid framework aimed at integrating building performance data with its relevant contextual information for a comprehensive evaluation of building performance. This method employed RDF and SQL query languages, using linking and mapping modules to merge contextual information with time series data in relational databases, significantly improving the accuracy of building performance assessments. The literature indicates that knowledge representation technologies significantly boost efficiency during the operation and maintenance phase of buildings. These technologies enhance decision-making and diagnostic processes, enabling quicker and more precise responses to maintenance needs and adjustments. They also support the formalized management of complex data, aiding thorough assessments of building health and performance.

5 DISCUSSION AND FUTURE TRENDS

The analysis provides a comprehensive understanding of knowledge representation in the AEC sector, highlighting the use of technologies such as ontologies, natural language processing, and the semantic web to tackle field-specific challenges. The development of models has enriched AEC knowledge significantly. Moreover, integrating knowledge representation with AI technologies like machine learning has spurred major innovations in the sector. AI is notably transforming industries including AEC, enhancing aspects like project design, construction, and maintenance. Recent advances in AI, especially large language models like ChatGPT and BERT, have optimized model performance, increased data processing efficiency, minimized risks, and fostered industry growth[47]. For example, Baek, S, and Han, SH used ChatGPT to extract key phrases from long news texts, benefiting from its larger context window and broader domain knowledge coverage. However, referring to such sophisticated applications as merely data processing might not fully capture the extensive capabilities and innovative contributions of large language models. Looking further ahead, a large language

model dedicated to the AEC field seems promising, which can facilitate the development of knowledge representation in a more abstract direction. For example, it could include question-and-answer systems for specific domains and more[48]. In the current AEC field, knowledge often needs to be derived from certain types of textual content, represented through defined semantic rules. This method typically requires precise manual definitions and systematic encoding, relying on highly accurate logic rules, thus facing certain limitations when dealing with ambiguous semantic expressions. Traditional knowledge representation also requires manual updates to the knowledge base, making this approach not only labor-intensive but also lacking the ability to update and learn information promptly. Although the introduction of machine learning has improved this to some extent, it still faces issues such as limited learning of tacit knowledge and inaccurate outputs. Therefore, large language models hold tremendous potential for future development in the AEC field. They can directly understand natural language texts without explicit encoding, handle ambiguous information queries, and provide interpretive texts with their inherent flexibility and generalization capabilities, allowing for the timely learning of new information and knowledge. In the field of computer science, numerous scholars are beginning to explore the use of LLM for tasks related to knowledge representation [49-53], or combining LLM with technologies such asNLP , ontology and knowledge graphs to extract knowledge from data and further realize its representation[54-57]. For example, Kommineni, VK; König-Ries, B employ LLM to develop a semi-automated pipeline for ontology and knowledge graph construction. In the AEC field, some scholars have also engaged in exploratory attempts using LLM[58, 59]. For example, Wong, S, and Zheng, C proposed a method using language models for identifying risks in construction contracts. Thus, the future development of knowledge representation in the AEC field should involve a combination of traditional methods and advanced computing technologies. The emergence of AEC-specific large language models like ChatGPT could greatly enhance the deep analysis and intelligent application of industry knowledge, opening up endless possibilities for the industry's future development.

6 CONCLUSION

Knowledge representation technology in the AEC field has become an indispensable core part of industry development. Therefore, this paper primarily conducts a comprehensive analysis of 211 articles published over the past 17 years, focusing on how knowledge is represented and utilized. Initially, the publication numbers, journals, and countries/regions of the literature in different periods were processed and analyzed. The research hotspots and growth dynamics were retrieved and visualized, showcasing global interest in knowledge representation technology. The paper then analyzes examples applied in the three stages of a project's entire life cycle to gain insight into the current development situation. Finally, combining the aforementioned analysis, the future research development trends have been illuminated. The integration of knowledge representation methods with machine learning and the incorporation of large language models will become key factors in the industry's future development. Technological advancements not only optimize the entire life cycle management of projects but also improve the quality and efficiency of problem-solving solutions.

REFERENCE

[1]. Lin, J.J., et al., Domain knowledge graph-based research progress of knowledge representation. Neural Computing & Applications, 2021. 33(2): p. 681-690.
[2]. Zhu, D., et al., A Survey of Advanced Information Fusion System: from Model-Driven to Knowledge-Enabled. Data Science and Engineering, 2023. 8(2): p. 85-97.
[3]. Wu, X., et al., Knowledge Engineering with Big Data. Ieee Intelligent Systems, 2015. 30(5): p. 46-55.
[4]. El-Diraby, T.E., Domain Ontology for Construction Knowledge. Journal of Construction Engineering and Management, 2013. 139(7): p. 768-784.
[5]. Jia, L., et al., Ontological Method for the Modeling and Management of Building Component Construction Process Information. Buildings, 2023. 13(8): p. 20.
[6]. Malsane, S., et al., Development of an object model for automated compliance checking. Automation in Construction, 2015. 49: p. 51-58.
[7]. Hu, S.S., et al., Building energy performance assessment using linked data and cross-domain semantic reasoning. Automation in Construction, 2021. 124: p. 13.

[8]. Zhang, J.S. and N.M. El-Gohary, Automated Information Transformation for Automated Regulatory Compliance Checking in Construction. Journal of Computing in Civil Engineering, 2015. 29(4): p. 16.
[9]. Ding, Y.X., J. Ma, and X.W. Luo, Applications of natural language processing in construction. Automation in Construction, 2022. 136: p. 19.
[10]. Pauwels, P., S.J. Zhang, and Y.C. Lee, Semantic web technologies in AEC industry: A literature overview. Automation in Construction, 2017. 73: p. 145-165.
[11]. Wu, C.K., et al., Natural language processing for smart construction: Current status and future directions. Automation in Construction, 2022. 134: p. 22.
[12]. Song, J., H. Zhang, and W. Dong, A review of emerging trends in global PPP research: analysis and visualization. Scientometrics, 2016. 107(3): p. 1111-1147.
[13]. Xu, Z., J.L. Wang, and H.X. Zhu, A Semantic-Based Methodology to Deliver Model Views of Forward Design for Prefabricated Buildings. Buildings, 2022. 12(8): p. 30.
[14]. Werbrouck, J., et al., Scan-to-graph: Semantic enrichment of existing building geometry. Automation in Construction, 2020. 119: p. 15.
[15]. Gómez-Romero, J., et al., A fuzzy extension of the semantic Building Information Model. Automation in Construction, 2015. 57: p. 202-212.
[16]. Jiang, L., J.Y. Shi, and C.Y. Wang, Multi-ontology fusion and rule development to facilitate automated code compliance checking using BIM and rule-based reasoning. Advanced Engineering Informatics, 2022. 51: p. 15.
[17]. Guo, D.M., E. Onstein, and A.D. la Rosa, A Semantic Approach for Automated Rule Compliance Checking in Construction Industry. Ieee Access, 2021. 9: p. 129648-129660.
[18]. Zhou, Y.C., et al., Integrating NLP and context-free grammar for complex rule interpretation towards automated compliance checking. Computers in Industry, 2022. 142: p. 16.
[19]. Hassan, F., T.Y. Le, and X. Lv, Addressing Legal and Contractual Matters in Construction Using Natural Language Processing: A Critical Review. Journal of Construction Engineering and Management, 2021. 147(9): p. 17.
[20]. Hassan, F.U. and T. Le, Automated Requirements Identification from Construction Contract Documents Using Natural Language Processing. Journal of Legal Affairs and Dispute Resolution in Engineering and Construction, 2020. 12(2): p. 12.
[21]. Lee, J., J.S. Yi, and J. Son, Development of Automatic-Extraction Model of Poisonous Clauses in International Construction Contracts Using Rule-Based NLP. Journal of Computing in Civil Engineering, 2019. 33(3): p. 13.
[22]. Al Qady, M. and A. Kandil, Concept Relation Extraction from Construction Documents Using Natural Language Processing. Journal of Construction Engineering and Management, 2010. 136(3): p. 294-302.
[23]. Candas, A.B. and O.B. Tokdemir, Automated Identification of Vagueness in the FIDIC Silver Book Conditions of Contract. Journal of Construction Engineering and Management, 2022. 148(4): p. 13.
[24]. Candas, A.B. and O.B. Tokdemir, Automating Coordination Efforts for Reviewing Construction Contracts with Multilabel Text Classification. Journal of Construction Engineering and Management, 2022. 148(6): p. 9.
[25]. Niknam, M. and S. Karshenas, Integrating distributed sources of information for construction cost estimating using Semantic Web and Semantic Web Service technologies. Automation in Construction, 2015. 57: p. 222-238.
[26]. Liu, Z. and Z.L. Ma. Establishing formalized representation of standards for construction cost estimation by using ontology learning. in Creative Construction Conference 2015, Selected Papers. 2015. Krakow, POLAND: Elsevier Science Bv.
[27]. Ma, Z.L., Z. Liu, and Z.H. Wei, Formalized Representation of Specifications for Construction Cost Estimation by Using Ontology. Computer-Aided Civil and Infrastructure Engineering, 2016. 31(1): p. 4-17.
[28]. Im, H., et al., Development of an Ontological Cost Estimating Knowledge Framework for EPC Projects. Ksce Journal of Civil Engineering, 2021. 25(5): p. 1578-1591.
[29]. Chen, Q.H., et al., Knowledge Graph Improved Dynamic Risk Analysis Method for Behavior-Based Safety Management on a Construction Site. Journal of Management in Engineering, 2023. 39(4): p. 15.
[30]. Lee, S.K. and J.H. Yu, Ontological inference process using AI-based object recognition for hazard awareness in construction sites. Automation in Construction, 2023. 153: p. 13.
[31]. Shen, Q.Y., et al., BIM-Based Dynamic Construction Safety Rule Checking Using Ontology and Natural Language Processing. Buildings, 2022. 12(5): p. 26.
[32]. Guo, B.H.W. and Y.M. Goh, Ontology for design of active fall protection systems. Automation in Construction, 2017. 82: p. 138-153.

[33]. Zhang, F., et al., Construction site accident analysis using text mining and natural language processing techniques. Automation in Construction, 2019. 99: p. 238-248.
[34]. Tixier, A.J.P., et al., Automated content analysis for construction safety: A natural language processing system to extract precursors and outcomes from unstructured injury reports. Automation in Construction, 2016. 62: p. 45-56.
[35]. Shen, Y., et al., Safety Risk Management of Prefabricated Building Construction Based on Ontology Technology in the BIM Environment. Buildings, 2022. 12(6): p. 20.
[36]. Xu, N., et al., Relation Extraction of Domain Knowledge Entities for Safety Risk Management in Metro Construction Projects. Buildings, 2022. 12(10): p. 16.
[37]. Dong, C., et al., Knowledge dynamics-integrated map as a blueprint for system development: Applications to safety risk management in Wuhan metro project. Automation in Construction, 2018. 93: p. 112-122.
[38]. Jeong, S., et al., An information modeling framework for bridge monitoring. Advances in Engineering Software, 2017. 114: p. 11-31.
[39]. Matthews, J., et al., Smart data and business analytics: A theoretical framework for managing rework risks in mega-projects. International Journal of Information Management, 2022. 65: p. 12.
[40]. D'Orazio, M., G. Bernardini, and E. Di Giuseppe, Automated Priority Assignment of Building Maintenance Tasks Using Natural Language Processing and Machine Learning. Journal of Architectural Engineering, 2023. 29(3): p. 13.
[41]. Schneider, G.F., et al., Design of knowledge-based systems for automated deployment of building management services. Automation in Construction, 2020. 119: p. 23.
[42]. Mahdavi, A. and M. Taheri, An ontology for building monitoring. Journal of Building Performance Simulation, 2017. 10(5-6): p. 499-508.
[43]. Chen, X.B., et al., Ontology-Based Representations of User Activity and Flexible Space Information: Towards an Automated Space-Use Analysis in Buildings. Advances in Civil Engineering, 2019. 2019: p. 15.
[44]. Gao, S., G.Q. Ren, and H.J. Li, Knowledge Management in Construction Health and Safety Based on Ontology Modeling. Applied Sciences-Basel, 2022. 12(17): p. 19.
[45]. Pauwels, P., et al., A performance benchmark over semantic rule checking approaches in construction industry. Advanced Engineering Informatics, 2017. 33: p. 68-88.
[46]. Hu, S., et al., Building performance optimisation: A hybrid architecture for the integration of contextual information and time-series data. Automation in Construction, 2016. 70: p. 51-61.
[47]. Baek, S., S.H. Han, and W.Y. Jung, Automated Identification of Active Players for International Construction Market Entry Using Natural Language Processing. Journal of Management in Engineering, 2023. 39(5): p. 11.
[48]. Tang, H., et al. ChatSOS: LLM-based knowledge Q&A system for safety engineering. 2023. arXiv:2312.08629 DOI: 10.48550/arXiv.2312.08629.
[49]. Li, Z., et al. KnowCoder: Coding Structured Knowledge into LLMs for Universal Information Extraction. 2024. arXiv:2403.07969 DOI: 10.48550/arXiv.2403.07969.
[50]. Yang, S., et al. Sequential Recommendation with Latent Relations based on Large Language Model. 2024. arXiv:2403.18348 DOI: 10.48550/arXiv.2403.18348.
[51]. Cui, H., et al. Multimodal Fusion of EHR in Structures and Semantics: Integrating Clinical Records and Notes with Hypergraph and LLM. 2024. arXiv:2403.08818 DOI: 10.48550/arXiv.2403.08818.
[52]. Whittaker, E. and I. Kitagishi Large Language Models for Simultaneous Named Entity Extraction and Spelling Correction. 2024. arXiv:2403.00528 DOI: 10.48550/arXiv.2403.00528.
[53]. Meyuhas, B., A. Bremler-Barr, and T. Shapira IoT Device Labeling Using Large Language Models. 2024. arXiv:2403.01586 DOI: 10.48550/arXiv.2403.01586.
[54]. Krishna Kommineni, V., B. König-Ries, and S. Samuel From human experts to machines: An LLM supported approach to ontology and knowledge graph construction. 2024. arXiv:2403.08345 DOI: 10.48550/arXiv.2403.08345.
[55]. Gouidis, F., et al. Fusing Domain-Specific Content from Large Language Models into Knowledge Graphs for Enhanced Zero Shot Object State Classification. 2024. arXiv:2403.12151 DOI: 10.48550/arXiv.2403.12151.
[56]. Oruganti, S., et al. Automating Knowledge Acquisition for Content-Centric Cognitive Agents Using LLMs. 2023. arXiv:2312.16378 DOI: 10.48550/arXiv.2312.16378.
[57]. Rula, A. and J. D'Souza Procedural Text Mining with Large Language Models. 2023. arXiv:2310.03376 DOI: 10.48550/arXiv.2310.03376.
[58]. Wong, S., et al. Construction contract risk identification based on knowledge-augmented language model. 2023. arXiv:2309.12626 DOI: 10.48550/arXiv.2309.12626.

[59]. Zheng, C., et al. A knowledge representation approach for construction contract knowledge modeling. 2023. arXiv:2309.12132 DOI: 10.48550/arXiv.2309.12132.

High-rise Modular Buildings Design Guidelines: A Literature Review

Yanhui Sun[1], Jeremy Wu[1], Xiangyu Wang[2]

1. School of Design and Built Environment, Curtin University, Perth, WA 6102, Australia;
2. School of Civil Engineering and Architecture, East China Jiao Tong University, Nanchang 330013, Chin[a]

ABSTRACT: The Australian construction industry contributes over $150 billion to the gross domestic product, which is around 10% of the total output of goods and services. However, the off-site construction sector (OSC) amounts to just $4.6 billion (i.e. 3% of the construction industry's output). In recent years, OSC has increased because of its advantages such as improved quality control, reduced skilled labour, faster construction time, decreased material wastage, and a friendly working environment. Modular buildings, as the most cutting-edge technology in OSC, have been used for residential buildings, student accommodation, and hotel projects because they comprise massive repetitive units. However, as a result of existing and underlying constraints, the adoption of modular buildings, especially the application of high-rise modular buildings, remains relatively low. Derived from the manufacturing industry, the concept of Design for Manufacture and Assembly (DfMA) has provided innovations and opportunities for solving the imbalance between the growing housing demand and inefficient construction productivity. However, according to previous studies, the implementation of DfMA focusing on high-rise modular buildings remains limited in empirical projects. Therefore, this paper presents a holistic literature review related to high-rise modular building design guidelines. DfMA concept, which is the foundation of the guidelines, is to investigate. The outcomes and conclusion are presented at last
.

KEYWORDS: modular building; high-rise; DfMA; design guidelines.

1 INTRODUCTION

The number of households in Australia is projected to increase from 9.2 million in 2016 to 13.2 million in 2041 [1]. According to the National Housing Finance and Investment Corporation[2], more than 1.7 million new households are expected to form between 2022 and 2032. The growing housing demand is stimulating a historically high level of housing supply, with more than 550,000 net new dwellings expected from 2023 to 2035. Furthermore, construction, as a labour-intensive industry, has been subjected to a shortage of skilled labour. There is a critical need for an additional skilled workforce to address skills shortages in the Australian construction industry [3]. As a result of the COVID-19 pandemic, the industry has been suffering a severe labour shortage. A survey undertaken at the end of 2021 found that over 70% of construction firms have been affected by the skilled labour shortage, which is the highest among all industries in Australia [4]. In recent decades, modular buildings have been used in both the public and private sectors to bridge the gap between the capacity of housing supply and the explosion of housing demand while mitigating the influence caused by the labour shortage. The construction industry has increasingly employed off-site construction (OSC) because of its advantages such as improved quality control, reduced skilled labour, faster construction time, decreased material wastage, and a friendly working environment [5].

Modular buildings, as the most cutting-edge technology in OSC, are preferred in structures with massive repetitive units such as hotels, apartments, dormitories, offices, and hospitals [6]. Therefore, high-rise buildings with an increased number of repeated rooms can fully exploit the benefits of modular buildings [7]. However, the implementation of modular buildings for high-rise buildings is limited, in contrast to the booming market in low-rise buildings [8]. Modular building design, which is not as mature as traditional building design, has experienced difficulty because of a lack of designers with experience and knowledge [9]. To guarantee error-free drawings delivered to manufacturers, designers have to devote excessive time to modular design, which results in a long lead-in time for the adoption of modular buildings. Furthermore, although modular buildings present high-level modularisation and standardisation, they are disputed for underdeveloped design flexibility [10]. In

addition, the capacity of suppliers and manufacturers cannot keep pace with demand from the growing utilisation of modular construction. Blismas et al. identified that the domestic supply chain of prefabrication cannot keep up with the progress of modular buildings [11]. Developers and designers are reluctant to adopt modular buildings because of the incompetence of suppliers and manufacturers. Moreover, considering the market size of modular construction, prefabrication manufacturing barely achieves economies of scale to advance its development. Despite reduced labour at the construction site, modular construction requires a vast amount of skilled labour for the manufacture of prefabricated modules, which increases the construction cost [12]. In addition, transportation is an indispensable part of modular construction, with the delivery of modules from factories to construction sites accounting for approximately 10% of overall costs [13]. W. Lu and Yuan indicated that transportation costs can increase to over 18% of the total cost when taking into account long-distance transport resulting from offshore manufacture [14]. Moreover, the weight and dimensions of modules restrict the transportation route and increase the cost as a result of specific vehicle requirements [15]. Regardless of the method of transport used (cargo, rail, road), damage to modules during transit must be considered. Transportation teams that supply transportation services should spend considerable time and money on extra protection to avoid severe damage to modules, which may trigger construction delays [16]. In the process of on-site assembly, a substantial amount of equipment—especially cranes—is required to install prefabricated modules, which increases the overall cost [17]. Contractors should pick up competent mobile cranes or fixed cranes based on the crane capacity of radius, load, and height. Moreover, Salama et al. revealed that numerous complex connections of modular buildings are a critical issue during the installation of modules [18]. As a result of the lack of corresponding inspection criteria, contractors must spend a significant amount of time on connection installation to reduce underlying quality issues such as water leakages [19]. Therefore, this paper presents a holistic literature review related to high-rise modular building design guidelines. DfMA concept, which is the foundation of the guidelines, is to investigate. The outcomes and conclusion are presented at last.

2 METHOD

Design for Manufacture and Assembly

Derived from the manufacturing enterprise, the concept of DfMA is a combination of DfM (Design for Manufacture) and DfA (Design for Assembly). The DfMA method and principles provide a methodological approach to quantify potential shortages and improve product design for both economic manufacturing and assembly [20]. Having witnessed the successful application of DfMA in the manufacturing industry, the construction industry has attempted to embrace DfMA in recent years. With the development of OSC, DfMA has provided innovations and opportunities for solving the imbalance between the growing housing demand and inefficient construction productivity. The implementation of DfMA in OSC has been explored in previous empirical projects. Trinder demonstrated that DfMA-focused management delivers cost, time, and quality improvements in water construction projects [21]. Safaa et al. showed that implementing DfMA in bridge construction projects achieves significant outcomes, including around 28% simplification of design, 8% saving in component materials, 25% ease of handling, 51% assembly time, 23% cost of work, and 18% duration [22]. Compared with infrastructure construction, building construction has raised the application of DfMA to a higher standard. K. Chen and Lu revealed the benefits of a DfMA-oriented curtain wall system in terms of reduced material cost and waste, decreased assembly time on site, and improved quality and performance of the curtain wall system [23]. According to Gerth et al., the use of DfMA theory can facilitate the identification of potential problems, optimise wall joint design and minimise assembly operation [24]. Banks et al. embraced the principles of DfMA in the design stage of a high-rise residential building that delivered optimal solutions involving precast components, prefabricated bathroom pods, and modular MEP services [25]. Conversely, high-rise modular buildings can reap the full benefits of DfMA because of the large number of modules with high repetition and low variation in types [19]. Banks et al. applied DfMA principles to a 40-storey modular building, which led to a reduced program and improved safety, quality, and reliability throughout the design, manufacture, and transportation stages [25].

To improve construction productivity and address labour shortage, the construction industry is seeking innovative construction methods. Modular construction, which reduces traditional on-site construction activities, adopts prefabricated components produced at off-site factories. Unlike traditional construction, modular construction must consider downstream processes (i.e. manufacture, transportation, and assembly) in advance. This design philosophy refers to DfMA, which has been widely implemented in the construction industry.Table 1 shows the current DfMA guides and roadmaps published in different countries and regions, including the United Kingdom, Singapore, Hong Kong SAR, the United States, and Australia.

United Kingdom

Since the 1960s, the number of households in the UK has rapidly increased, and the traditional construction method has not been able to meet the housing demand and quality standards [26]. As a result, OSC has attracted extensive attention from the construction industry [27]. For example, Laing O'Rourke developed a successful approach to DfMA to improve the quality of construction while reducing construction time and waste [28]. In 2013, the British government published a policy paper, Construction 2025: Strategy, which noted that OSC will be the key factor in the future construction industry [29]. Furthermore, RIBA issued a Plan of Work 2013: DfMA to explore how the design team can promote performance and productivity in OSC based on the DfMA concept [30]. This publication, which provided a detailed description of DfMA, also pointed out the benefits and typical processes of DfMA using associated case studies. In 2021, RIBA updated the new DfMA, Overlay to the Plan of Work 2020, highlighting the widespread application of DfMA in construction, which emphasises actions and feedback from the perspectives of the industry as well as the market [31]. Additionally, the publication summarised the best option for implementing DfMA in OSC given the critical data and project management, critical design considerations, and critical logistical issues.

Singapore

Singapore's government has a clear view of the significance of OSC given its limited land resources and labour shortages [32]. OSC has been regarded as the most effective solution for reaching the national target of construction productivity growth, which was set in the first Construction Productivity Roadmap in 2011 [33]. Subsequently, in 2015, the Second Construction Productivity Roadmap indicated that the move towards DfMA is a key driver to improve construction productivity [34]. Therefore, the construction industry has embarked on the OSC method instead of traditional construction with the adoption of PPVC for high-rise modular buildings increasing gradually [19]. In 2017, BCA published Design for Manufacturing and Assembly—Prefabricated Prefinished Volumetric Construction Guidebook, which demonstrates key aspects of PPVC integrated with the DfMA concept and related success practices [35]. The guidebook provides a holistic understanding of PPVC and DfMA for practitioners, including the entire life cycle of modular construction, such as design considerations, installation, inspection and quality checks, maintenance, and replacement and renovation.

Hong Kong SAR

The construction industry in Hong Kong SAR (HKSAR) has paid attention to OSC since the 1980s because of its scarce developable land and strong housing demand. As a result of the large economies of scale and relatively cheap labour and material costs in mainland China, HKSAR has used a large number of precast components such as staircases, walls and bathrooms [36]. In recent years, MiC, which refers to the highest level of prefabrication, has been promoted widely by the HKSAR government [37]. It has been identified as an effective approach to address the shortage of labour and manufacturing capability while enhancing the life cycle quality of buildings in line with the greater number of applications of MiC in the city of high-density high-rise buildings [38]. Moreover, HKSAR developed Construction 2.0, which discusses the direction for the future of the construction industry [39]. It emphasises the significance of innovation and new technologies, including DfMA and MiC, in the industry. Codes and references related to MiC were issued by the HKSAR Building Department to clarify the relevant design considerations and requirements for all stakeholders, which is aligned with the DfMA concept [40].

United States

The OSC in the United States is not dominant in the industry; however, an increasing number of practitioners have embarked on this innovative approach to enhance productivity and quality [41]. The International Code Council (ICC), coupled with the Modular Building Institute (MBI), issued two joint standards—ICC/MBI 1200-2021 Standard for Off-site Construction: Planning, Design, Fabrication and Assembly and ICC/MBI 1205-2021 Standard for Off-site Construction: Inspection and Regulatory Compliance—outlining the entire process of modular construction from the perspectives of different stakeholders (i.e. design team, manufacturer, logistical team and contractor). These publications also take into consideration the downstream processes in relation to the DfMA concept [42].

Australia

As a result of strong housing demand as well as soaring labour and material costs, the industry has employed various new approaches, including OSC, to improve construction productivity. However, compared with the abovementioned countries and regions, Australia has a relatively low adoption of OSC [43]. To promote the widespread application of OSC, several associated guidebooks and reports have been published. In 2004, the Australian Cooperative Research Centre (CRC) for Construction Innovation issued Construction 2020 to disclose the future directions of the industry, with OSC indicated as one key vision to enable more efficient construction processes and improved quality control [44]. With the increased uptake of OSC in the Australian industry, more publications have focused on modular construction, such as Off-site Manufacture in Australia: Current State and Future Directions, which was published by the CRC for Construction Innovation in 2007 [45]. This publication, according to seven case studies in Australia, identified numerous benefits and challenges of OSC. It stated that design considerations need to meet the requirements of manufacturing, transportation, and installation, despite not directly discussing DfMA philosophy. Moreover, in 2017, the Modular Construction Codes Board (MCCB) developed the Handbook for the Design of Modular Structures, which was the first holistic guidebook concerning modular structures for the Australian industry [46]. This document integrated the DfMA concept and shared the experience and knowledge related to modular design to the industry based on the aspects of structure, building services, façades, architecture, materials and manufacturing, durability, safety, and transportation.

3 CONCLUSION

The abovementioned guides, based on the regional development of OSC, presented a holistic view of modular construction, with a focus on design considerations for meeting the requirements of downstream processes, which follows the DfMA philosophy. However, the majority of guides emphasised the benefits and significance of implementing DfMA in modular construction using several practices. It is still relatively difficult for practitioners to adopt this innovative approach in future projects without specific guidelines and quantitative criteria. For instance, two publications issued by RIBA introduced the drives and advantages of using DfMA in OSC while providing detailed adoption strategies for each step of the modular construction. However, it is difficult to exploit these qualitative recommendations to generate a standard or code for modular design. Furthermore, there are few guides related to high-rise modular buildings. There are significant differences between the requirements of various types of OSC. Compared with precast components of OSC, high-rise modular buildings, representing the highest level of prefabrication, have entirely different manufacturing and assembly processes that require distinct design considerations as well as specific DfMA guidelines.

REFERENCES

[1]. Australian Bureau of Statistics. (2019). Household and family projections, Australia, 2016 to 2041. https://www.abs.gov.au/statistics/people/population/household-and-family-projections-australia/latest-release

[2]. National Housing Finance and Investment Corporation. (2022). State of the nation's housing 2021–2022. https://www.nhfic.gov.au/research/state-nations-housing-2021-22

[3]. Oo, B. L., Liu, X., & Lim, B. T. H. (2020). The experiences of tradeswomen in the Australian construction industry. International Journal of Construction Management, 22(8), 1408–1419. https://doi.org/10.1080/15623599.2020.1717106
[4]. National Australia Bank. (2021). NAB business insight report. https://business.nab.com.au/
[5]. Sun, Y., Wu, J., Fan, J., Wang, J., & Wang, X. (2019). Rule-based automated design check for modular building [Paper presentation]. 43rd AUBEA: Australasian Universities Building Education Association Conference, Noosa, Qld, Australia.
[6]. Lawson, M., Ogden, R., & Goodier, C. (2014). Design in modular construction. Taylor and Francis Group.
[7]. Liew, J. Y. R., Chua, Y. S., & Dai, Z. (2019). Steel concrete composite systems for modular construction of high-rise buildings. Structures, 21, 135–149. https://doi.org/10.1016/j.istruc.2019.02.010
[8]. Pan, W., Yang, Y., & Yang, L. (2018). High-rise modular building: Ten-year journey and future development. In Construction Research Congress 2018, American Society of Civil Engineers (ASCE), 523-532. https://doi.org/10.1061/9780784481301.052
[9]. Kamar, K., Azman, M., & Nawi, M. (2014). IBS survey 2010: Drivers, barriers and critical success factors in adopting industrialised building system (IBS) construction by G7 contractors in Malaysia. Journal of Engineering Science and Technology, 9(4), 490–501.
[10]. Zhang, X., Skitmore, M., & Peng, Y. (2014). Exploring the challenges to industrialized residential building in China. Habitat International, 41, 176–184. https://doi.org/10.1016/j.habitatint.2013.08.005
[11]. Blismas, N., Arif, M., & Wakefield, R. (2009). Drivers, constraints and the future of offsite manufacture in Australia. Construction Innovation, 9(1), 72–83. https://doi.org/10.1108/14714170910931552
[12]. Choi, J. O., Chen, X. B., & Kim, T. W. (2017). Opportunities and challenges of modular methods in dense urban environment. International Journal of Construction Management, 19(2), 93–105. https://doi.org/10.1080/15623599.2017.1382093
[13]. Hong, J., Shen, G. Q., Li, Z., Zhang, B., & Zhang, W. (2018). Barriers to promoting prefabricated construction in China: A cost–benefit analysis. Journal of Cleaner Production, 172, 649–660. https://doi.org/10.1016/j.jclepro.2017.10.171
[14]. Lu, W., & Yuan, H. (2013). Investigating waste reduction potential in the upstream processes of offshore prefabrication construction. Renewable and Sustainable Energy Reviews, 28, 804–811. https://doi.org/10.1016/j.rser.2013.08.048
[15]. Navaratnam, S., Ngo, T., Gunawardena, T., & Henderson, D. (2019). Performance review of prefabricated building systems and future research in Australia. Buildings, 9(2), Article 38. https://doi.org/10.3390/buildings9020038
[16]. Liu, Z., Gu, Z., Bai, Y., & Zhong, N. (2018). Intermodal transportation of modular structure units. World Review of Intermodal Transportation Research, 7(2), 99–123.
[17]. Mao, C., Xie, F., Hou, L., Wu, P., Wang, J., & Wang, X. (2016). Cost analysis for sustainable off-site construction based on a multiple-case study in China. Habitat International, 57, 215–222. https://doi.org/10.1016/j.habitatint.2016.08.002
[18]. Salama, T., Salah, A., Moselhi, O., & Al-Hussein, M. (2017). Near optimum selection of module configuration for efficient modular construction. Automation in Construction, 83, 316–329. https://doi.org/10.1016/j.autcon.2017.03.008
[19]. Xu, Z., Zayed, T., & Niu, Y. (2020). Comparative analysis of modular construction practices in mainland China, Hong Kong and Singapore. Journal of Cleaner Production, 245, Article 118861. https://doi.org/10.1016/j.jclepro.2019.118861
[20]. Boothroyd, G. (2005). Assembly automation and product design (Vol. 66). CRC Press. https://doi.org/10.1201/9781420027358
[21]. Trinder, L. (2018). Design for manufacture and assembly: Its benefits and risks in the UK water industry. Proceedings of the Institution of Civil Engineers—Management, Procurement and Law, 171(4), 152–163. https://doi.org/10.1680/jmapl.17.00021
[22]. Safaa, Y. P., Hatmoko, J. U. D., & Purwanggono, B. (2019). Evaluation of the use of prefabricated bridge elements with Design for Manufacture and Assembly (DfMA) criteria. MATEC Web of Conferences, 270, Article 05006. https://doi.org/10.1051/matecconf/201927005006
[23]. Chen, K., & Lu, W. (2018). Design for manufacture and assembly oriented design approach to a curtain wall system: A case study of a commercial building in Wuhan, China. Sustainability, 10(7), Article 2211. https://doi.org/10.3390/su10072211
[24]. Gerth, R., Boqvist, A., Bjelkemyr, M., & Lindberg, B. (2013). Design for construction: Utilizing production experiences in development. Construction Management and Economics, 31(2), 135–150. https://doi.org/10.1080/01446193.2012.756142

[25]. Banks, C., Kotecha, R., Curtis, J., Dee, C., Pitt, N., & Papworth, R. (2018). Enhancing high-rise residential construction through design for manufacture and assembly—A UK case study. Proceedings of the Institution of Civil Engineers—Management, Procurement and Law, 171(4), 164–175. https://doi.org/10.1680/jmapl.17.00027
[26]. Office of the Deputy Prime Minister. (2005). Sustainable communities: Homes for all. https://assets.publishing.service.gov.uk/government/uploads/system/uploads/attachment_data/file/272227/6722.pdf
[27]. Pan, W., & Sidwell, R. (2011). Demystifying the cost barriers to offsite construction in the UK. Construction Management and Economics, 29(11), 1081–1099. https://doi.org/10.1080/01446193.2011.637938
[28]. Laing O'Rourke. (2013). The future of DFMA is the future of construction. Engineering Excellence Journal, 2013. http://www.laingorourke.com/~/media/lor/files/lor-engineering-excellence-journal-2013.pdf
[29]. Her Majesty's Government. (2013). Construction 2025—Industrial strategy: Government and industry in partnership. HM Government.
[30]. Royal Institute of British Architects. (2013). RIBA plan of work 2013: Designing for manufacture and assembly. http://consig.org/wp-content/uploads/2018/10/RIBAPlanofWorkDfMAOverlaypdf.pdf
[31]. Royal Institute of British Architects. (2021). DfMA overlay to the plan of work. https://www.architecture.com/knowledge-and-resources/resources-landing-page/dfma-overlay-to-the-riba-plan-of-work
[32]. Hwang, K.-E., & Kim, I. (2022). Post-COVID-19 modular building review on problem-seeking framework: Function, form, economy, and time. Journal of Computational Design and Engineering, 9(4), 1369–1387. https://doi.org/10.1093/jcde/qwac057
[33]. Building and Construction Authority. (2011). Construction productivity roadmap.
[34]. Building and Construction Authority. (2015). The second construction productivity roadmap. https://www.bca.gov.sg/emailsender/BuildSmart-062015/microsite/others/bca-newsletter.pdf
[35]. Building and Construction Authority. (2017). Design for Manufacturing and Assembly (DfMA) prefabricated prefinished volumetric construction.
[36]. Tam, V. W. Y., Fung, I. W. H., Sing, M. C. P., & Ogunlana, S. O. (2015). Best practice of prefabrication implementation in the Hong Kong public and private sectors. Journal of Cleaner Production, 109(1), 216–231. https://doi.org/10.1016/j.jclepro.2014.09.045
[37]. Hong Kong Special Administrative Region. (2017a). The 2017 policy address. https://www.policyaddress.gov.hk/2017/eng/
[38]. Pan, W., & Hon, C. K. (2020). Modular integrated construction for high-rise buildings. Proceedings of the Institution of Civil Engineers—Municipal Engineer, 173(2), 64–68. https://doi.org/10.1680/jmuen.18.00028
[39]. Hong Kong Special Administrative Region. (2018). Construction 2.0: Time to change. https://www.psgo.gov.hk/assets/pdf/Construction-2-0-en.pdf
[40]. Hong Kong Special Administrative Region. (2017b). Codes and references for modular integrated construction. https://www.bd.gov.hk/en/resources/codes-and-references/modular-integrated-construction/index.html
[41]. Razkenari, M., Fenner, A., Shojaei, A., Hakim, H., & Kibert, C. (2020). Perceptions of offsite construction in the United States: An investigation of current practices. Journal of Building Engineering, 29, Article 101138. https://doi.org/10.1016/j.jobe.2019.101138
[42]. Jung, S., & Yu, J. (2022). Design for Manufacturing and Assembly (DfMA) checklists for Off-Site Construction (OSC) projects. Sustainability, 14(19), Article 11988. https://doi.org/10.3390/su141911988
[43]. Khalfan, M. M. A., & Maqsood, T. (2014). Current state of off-site manufacturing in Australian and Chinese residential construction. Journal of Construction Engineering, 2014, 1–5. https://doi.org/10.1155/2014/164863
[44]. Hampson, K., & Brandon, P. (2004). Construction 2020: A vision for Australia's property and construction industry. Cooperative Research Centre for Construction Innovation.
[45]. Blismas, N. (2007). Off-site manufacture in Australia: Current state and future directions. Cooperative Research Centre for Construction Innovation. http://www.construction-innovation.info/images/pdfs/Publications/Industry_publications/Off-site_manufacture_in_Australia.pdf
[46].Murray Parke.J & Bai, Y. (2017). Handbook for the design of modular structures.Monash Uniersity.

Optimisation and Automatic Modelling of Window Layouts on Façade Walls: A BIM-Based Generative Design Method

Wei Ma[1], Xiangyu Wang[2,3], Wenchi Shou[4] and Jun Wang[4]

1. School of Design and the Built Environment, Curtin University, Bentley, WA 6102, Australia
2. School of Civil Engineering and Architecture, East China JiaoTong University, Nanchang, Jiangxi, 330044, China
3. Australasian Joint Research Centre for Building Information Modelling, Curtin University, Perth, WA, Australia
4. School of Engineering, Design and Built Environment, Western Sydney University, Kingswood, NSW 2745, Australia

ABSTRACT: Window layouts on façade walls can affect daylighting significantly, thus affecting the energy consumption of artificial lighting. Evenly distributing apertures on walls is believed to benefit daylighting. Thus, if there are only window apertures on a façade wall, evenly distributing window apertures can be a rational way to optimise the window layout to improve daylighting. However, there is currently no research on optimising window layout by distributing windows on walls evenly, let alone design visualisation studies that can facilitate frequent interaction, feedback, and layout adjustment. This study proposes, develops, and demonstrates an innovative design method to optimise and automatically model window layouts on a façade wall for early design stages. To optimise window layout, centroid Voronoi tessellation (CVT) is creatively applied to place windows on walls evenly, and maximising daylighting is incorporated as the design objective. A BIM-based generative design program is then developed to enable rapid optimisation and automatic modelling, followed by a case study to demonstrate. This paper concludes by providing innovations, limitations, and future works.

KEYWORDS: window layout optimisation; automatic modelling; BIM; generative design; centroid voronoi tessellation application

1 INTRODUCTION

The façade window system is an important design element of the building envelope, significantly affecting indoor lighting, ventilation, solar radiation, heat conduction, etc[1-3]. Proper design of the façade window system can considerably reduce energy consumption in maintaining a comfortable indoor environment [2]. Therefore, many studies have delved into design parameters of façade windows, such as window materials, insulations, size, window-to-wall ratio (WWR), locations, etc. [4], [5], [6], [7], [8]. These studies intend to optimise

window parameter design to achieve multiple indoor comforts (e.g., thermal comfort, visual comfort, air quality) energy-efficiently [9]. Most current research focuses on thermal comfort, benefiting from the widespread application of simulation technologies in thermal performance [9]. However, studies on visual comfort are relatively deficient and need more attention.

Visual comfort depends on maximum daylight autonomy [10]. Optimising façade window design to maximise natural lighting can improve visual comfort and reduce energy in artificial lighting [11]. Current research in this area mainly focuses on investigating window properties or configurations, such as window materials, layers, size, proportion, etc. [7], [12], [13]. Other factors, such as window layout, can also affect daylighting greatly. However, research on optimising layout is still deficient because the current practices mainly rely on aesthetic judgment or design experience and lack methodological support.

According to industry studies [14], evenly distributed light is crucial to good natural lighting. Thus, evenly distributed apertures on walls benefit daylight autonomy, improving indoor visual comfort. Consequently, placing windows evenly on façade walls is considered a rational way to optimise façade window layout for maximising daylighting. However, there has been no research on design methods for evenly distributing windows on walls, let alone design visualisation studies such as digital modelling that can facilitate frequent interaction, feedback, and layout adjustment in the early stage.

This paper aims to propose, develop, and demonstrate an innovative design method for this research problem to optimise and automatically model window layouts on façade walls at early design stages. Centroid Voronoi tessellation (CVT) is creatively applied to form this design method for distributing windows on walls evenly. Maximising daylighting is incorporated into the method as the design objective. A BIM-based generative design (GD) tool is used to develop this method, enabling the generation and automatic modelling of various layouts for visualisation and interaction.

2 METHOD

Four main steps constitute the research methodology of this study: 1) Propose the innovative idea of applying CVT to distribute windows on walls evenly; 2) Incorporate the maximising daylighting as the objective; 3) Formulate a workflow of the proposed innovative design method and develop it accordingly using the GD tool in Revit to enable layouts generation and automatic modelling; 4) Conduct a case study within the developed program to demonstrate the innovative design method.

2.1 Applying CVT to distribute windows on walls evenly

A Voronoi tessellation (or Voronoi diagram), in two dimensions, is a plane divided into multiple convex polytopes, where "*each partition contains a generator such that every point in the partition is closer to its own generator than any other generator*" [15]. A CVT "*is a special type of Voronoi tessellation in which the generating points are the centroids (centres of mass) of the corresponding Voronoi cells*" [16]. See Figure 1 [17].

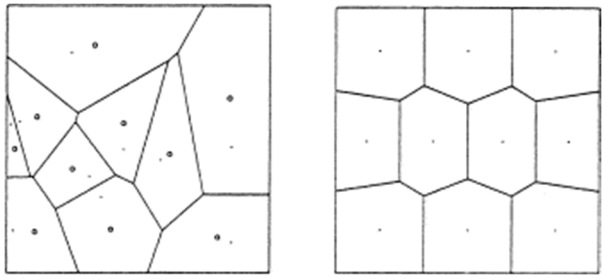

Figure 1. A Voronoi tessellation (left) and CVT.

Therefore, CVT algorithms can find optimal distributions of generating points, such as evenly distributed in a domain based on a given density function [18]. In this study, a wall is viewed as a vertical domain. A CVT algorithm developed based on Lloyd's method [19], [20] is applied to the vertical domain to find evenly distributed generating points (i.e., centroids), which will serve as the geometric centres for windows generated and placed, as indicated in Figure 2.

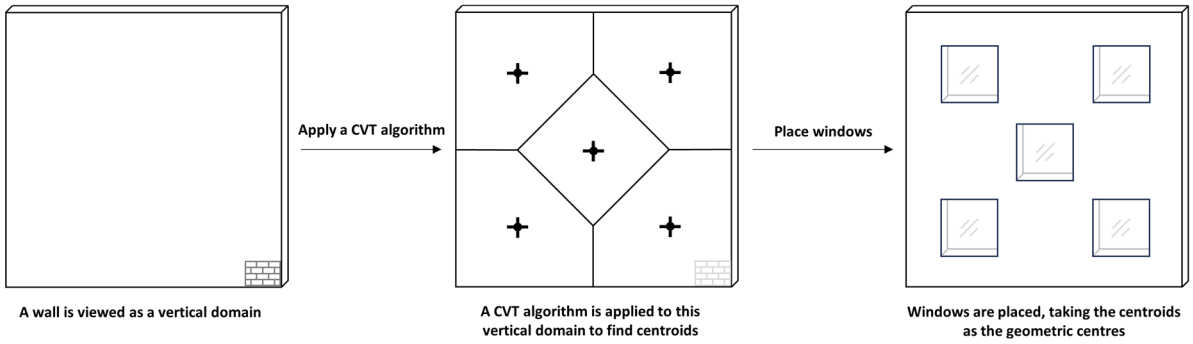

Figure 2. Diagram of the method utilising a CVT algorithm for window evenly placement.

For convenience, we employ the same type of window. Also, we restrict the window shape to square and maintain consistent window sizes within the same window group, ranging from 500mm to 2300mm with 100mm intervals, considering the regular height of the Australian house façade is 2400mm (from floor to eave). Meanwhile, the generating points of CVTs are limited to 1 to 10. Since the generating points are randomly picked between 1 to 10, the CVT generation process would be time-consuming if uncontrolled. To improve efficiency, we establish a logic for moving the generating points to support the finding of centroids, as indicated in Figure 3. This logic will be written in Dynamo nodes in GD during development.

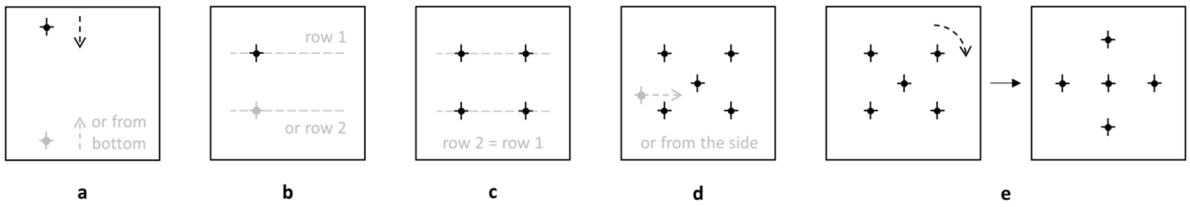

Figure 3. Diagram of the logic for moving the generating points to support the finding of CVT centroids.

The logic in Figure 3 is explained as follows:

a) The generating points begin to find the positions of the corresponding centroids from either the top or the bottom edge of a wall surface.
b) For convenience, the initial rows of the generating points are defined as the maximum of two, i.e., one or two rows of the generating points begin the search.
c) If the initial rows are two, each row is set to have the same number of generating points.
d) When the number of the generating points needs to be odd, and the initial rows are two, an additional point needs to be added (to make the generated points an odd number). The point can be added to the centre directly or moved from the side.
e) The obtained centroids can be rotated to a certain angle until a new pattern of CVT is formed.

2.2 Incorporate daylighting requirement

The objective of optimising window layouts is to maximise daylighting in this study. Therefore, daylighting requirements must be incorporated to form the innovative design method. The parameter *effective aperture (EA)* has been employed in related studies to assess the impact of fenestration characteristics on building lighting and energy consumption [6], [21]. The findings reveal that an increase in *EA* leads to an increase in daylighting and a decrease in lighting energy usage [21]. Therefore, we adopt the objective of maximising *EA* when navigating the window evenly placement.

EA was initially proposed in the study of John et al. [21], and the calculation method is:

$$EA = WWR \times VLT \quad (1)$$

Where *WWR* denotes the *Window-to-Wall Ratio*, i.e., the proportion of the window surface (including framing) to the gross wall area [4]. *VLT* represents the *Visible Light Transmittance,* indicating the percentage of visible daylight that the glass allows to pass. *VLT* is a window property parameter, and the value can be found in the window product information. Note that the *VLT* value is the intrinsic property of a window and may impact results if an energy simulation is conducted. Since the simulation method is not employed in this study, and the *VLT* value is consistent for all windows, the generating result will not be affected by the *VLT* values. Therefore, we pre-set the *VLT* value as 0.5 (a common actual value) for the convenience of this study.

2.3 Development

The GD function in Revit 2024 (a BIM software) is adopted in this study as the research and development tool. Dynamo in Revit is used as the programming language. Revit 2024 is employed for model generation and visualisation. The Revit-based GD enables the rule-based iterative design processes utilising algorithmic and parametric modelling [22] while enhancing the constructability of GD solutions through BIM's powerful building data functions [23], [24], [25].The convenience of using Revit-based GD for development also lies in the simplification of programming: easy-to-use visual programming language Dynamo [23] and the direct use of the acclaimed genetic algorithm "NSGA-II" [25], [26].

To guide development, a workflow of the proposed method is drawn as per Figure 4. The presentation of this workflow synthesises factors such as the regular user interface of GD, the application and programming environment, and the visualisation of design outcomes. Noted, window objects (ranging from 500mm to 2300mm with 100mm intervals) were pre-created in Revit 2024 (as these windows are not basic objects built into Revit) to form an object library so the model generation stage can automatically take from.

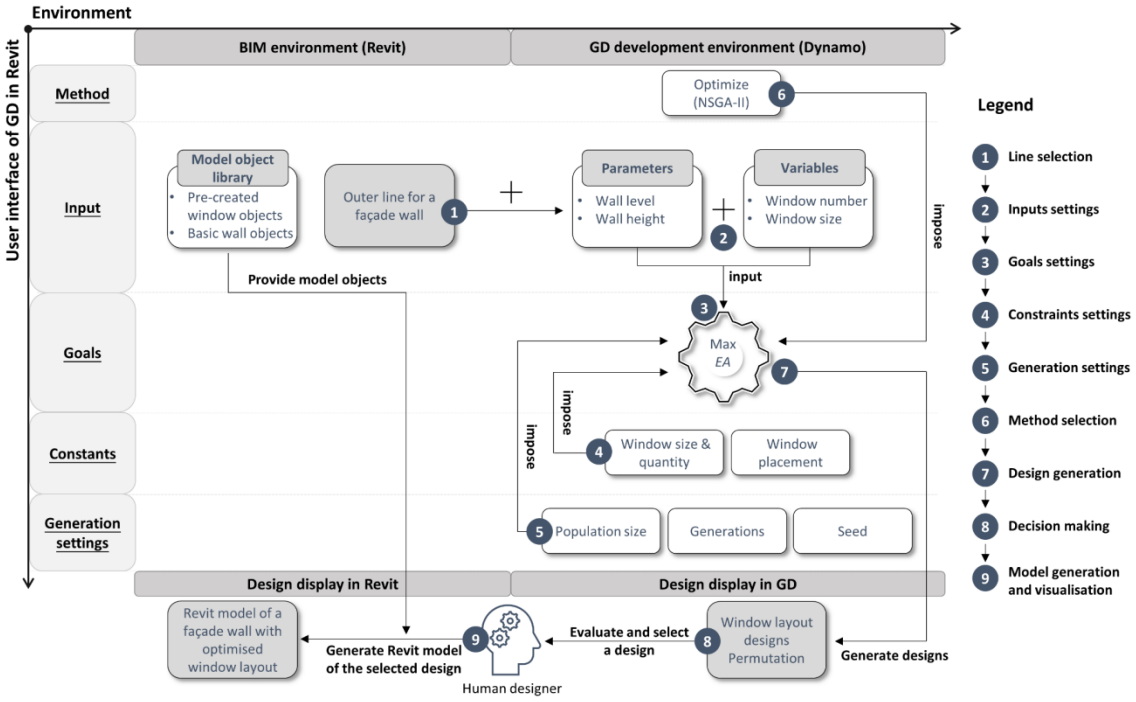

Figure 4. Workflow of the proposed innovative BIM-based GD method.

Nine steps are involved in this workflow:

- **Step 1: Line selection.** Select the pre-drawn wall outer line on the corresponding level in Revit, where the façade wall with optimised window layout is to be generated.
- **Step 2: Inputs settings.** Set the parameter values and the variable ranges. Parameter values are inputs to define the design background and remain unchanged during the GD process. In contrast, design variables are manipulated automatically within the pre-set ranges until the optimal values are found.
- **Step 3: Goals settings.** To maximise *EA*.
- **Step 4: Constraints settings**. To control window size & quantity as mentioned above and to use CVT to find evenly distributed centroids to place windows.
- **Step 5: Generation Settings.** Three settings need to be determined: population size, generations, seed.
- **Step 6: Method selection.** The "Optimize" method needs to be selected for this study, in which the NSGA-II algorithm is incorporated.

- **Step 7: Design generation.** Generate designs once all settings are completed. Multiple designs will be generated accordingly and permuted based on certain criteria.
- **Step 8: Decision making.** Human designers evaluate designs and interact with the program interfaces to filter out the optimal one from the permutation.
- **Step 9: Model generation and visualisation**. By operation, a 3D Revit model of the selected design will be automatically generated on the line selected in Step 1. The pre-created window objects and a basic wall object will be used together to generate the model. The optimised window layout on a façade wall is completed at this point.

Based on this workflow, Dynamo in Revit is used for development. Figure 5 presents the partial Dynamo script and the corresponding program interface.

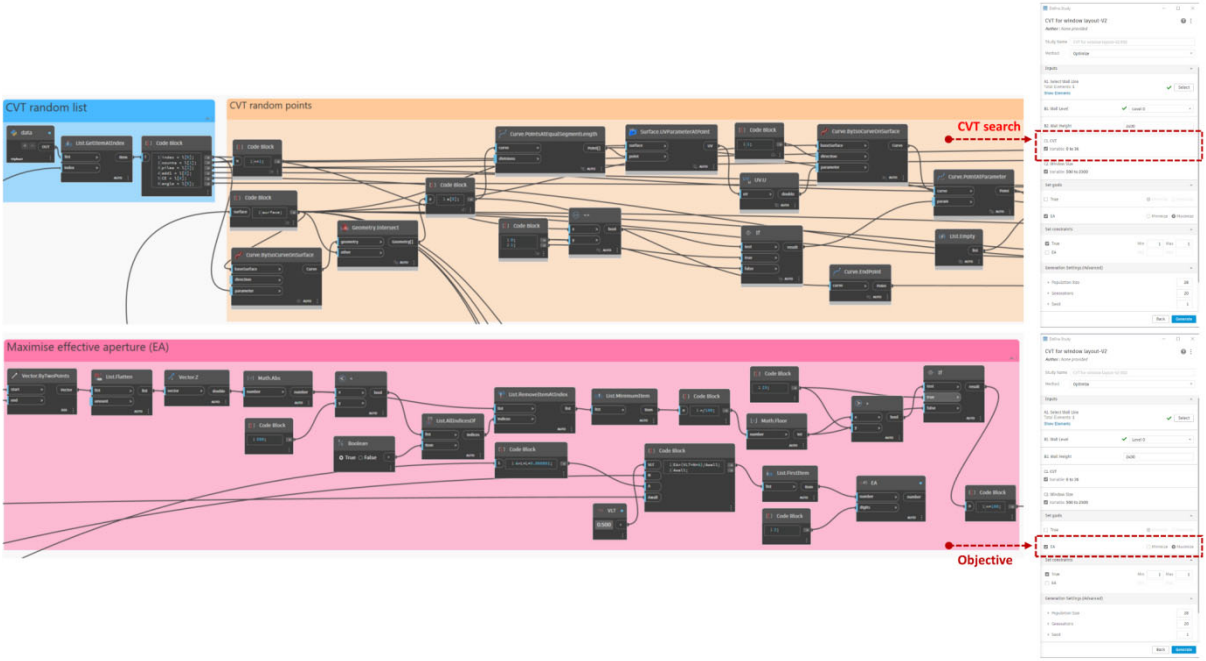

Figure 5. Screen captures of the partial Dynamo script and the corresponding program interface.

2.4 Case study

After development, a case study is conducted within the developed program for demonstration. The program is operated on a laptop with a Windows 10 system. The processor is Intel(R) Core(TM) i7-6700K CPU @ 4.00GHz, and the RAM is 16 GB. Figure 6 shows this case study:

Fig 6a illustrates the pre-drawn wall line. A 9-meter (9000mm) line was drawn in the Revit 2024 workplace for selection as the baseline to generate a façade wall with an optimised window layout. The line length was determined arbitrarily as it is close to the house wall length.

Fig 6b shows the next step operations in the developed GD study interface, which can be accessed by clicking “Create Study” of “Generative Design” under the “Manage” ribbon:

- Under *Inputs*, select *Wall line* and *Wall level* (Level 0), enter "2400" (mm) in *Wall height*, and tick *CVT* and *Window size*.
- Under *Set goals*, tick *Maximize EA* as the goal and leave *True* blank.
- Under *Set constraints*, tick *Ture* and enter "1" in *Min* and *Max* of *True*. Leave *EA* blank. *Ture* controls whether all generated designs are valid. For instance, if "1" is not entered, the windows generated may overlap each other or exceed the wall boundary.
- Under *Generation Settings*, enter 28 for *Population Size*, 20 for *Generations*, and 1 for *Seed*. These configurations control the number of design iterations and generations.
- Lastly, click *Generate* to start the generation process.

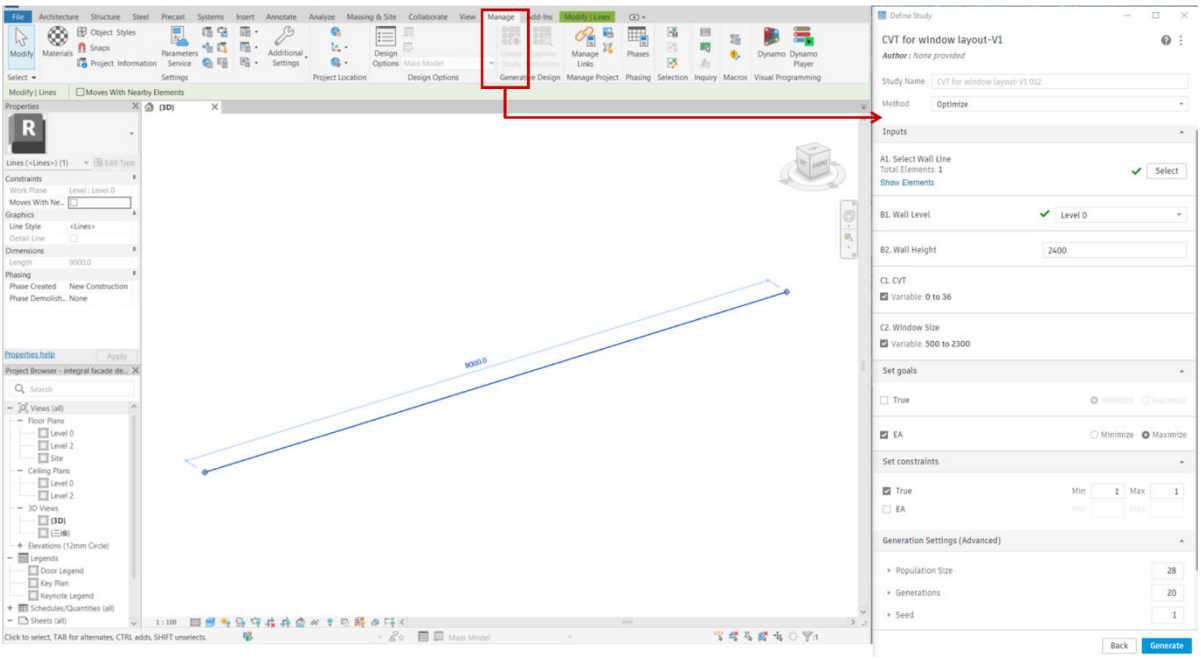

(a) A 9000 mm pre-drawn wall line in the Revit 2024 workplace. (b) The GD study interface.

Figure 6. Case study settings within the developed Revit-based GD program.

3 RESULTS

Window layouts are then generated. Here are the results:

- The generation process is fast, taking 73 seconds.
- Two window layouts are generated accordingly and permuted in the GD outcome interface for designers to evaluate and make decisions, as per Fig 7a. Designers can click on any permuted option to view design details and drag in the Parallel Coordinates interface to filter out the best option based on personal or specific preference.
- The *EA* for both layouts is maximised as 19% (0.19). Ten centroids (the maximum number of the presetting) are found for both layouts, so ten windows are placed

accordingly. The window size for both layouts is generated as 900 mm, which is the lower middle size of the presetting. These results are within the preset range, and the windows do not overlap each other or extend beyond the walls, so both designs are considered valid.

- By evaluating the two layouts, we believe the second one is more even. Therefore, the second layout is selected for model generation.
- By clicking "*Create Revit Elements*" in the GD outcome interface, the corresponding Revit model is generated automatically in the Revit workplace shortly (on the pre-selected wall line in Fig 6a), as per Fig 7b.
- The generated Revit model is consistent with the selected layout, thus confirming the feasibility of the proposed BIM-based GD method for optimising and automatically modelling window layouts on a façade wall.

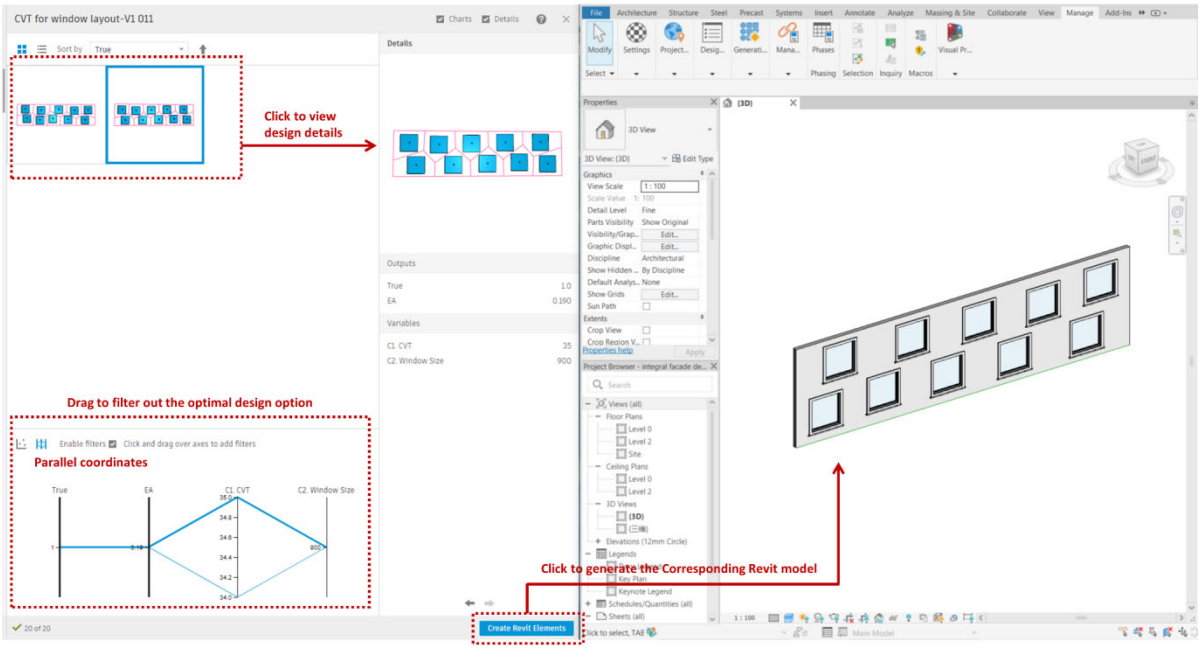

(a) Design generation and permutation in GD. (b) Generate the corresponding 3D model in Revit.

Figure 7. Case study results.

4 CONCLUSION

This paper proposes, develops, and demonstrates an innovative BIM-based GD method to optimise and automatically model window layouts on façade walls for early design stages. To optimise window layout, a CVT algorithm was creatively applied to place windows on walls evenly, and maximising *EA* to maximise daylighting was incorporated as the objective. A workflow of this design method was then formulated. Based on the workflow, a Revit-based GD program was developed using Dynamo, enabling the rapid optimisation and automatic modelling of window layouts on a wall. In the end, a case study was conducted within the developed GD program to demonstrate the feasibility of the innovative method. Compared

with traditional design methods such as aesthetic judgement or experiential design, this innovative method enables efficient and rapid explorations of well-founded designs.

The innovations of this study include:

- An innovative method of applying CVT algorithms to window layout design is proposed, developed, and implemented.
- A practical and instructive GD workflow is formulated, based on which a feasible Revit-based GD program is developed. These constitute a development paradigm of the Revit-based GD methods that can guide more sophisticated and functional GD developments to facilitate more creative and diverse studies.
- Integrating BIM with GD for façade design research is initiated and demonstrated, which can inspire further innovative façade design or building design studies utilising this integration.

However, limitations still exist:

- The CVT search logic was simplified in this study, leading to relatively insufficient CVT findings. Thus, the patterns of window even distribution were not fully explored.
- Constraints on window shape (square only) and size (consistent within the same group) restricted the variety of window solutions.
- Only one objective was set (maximising *EA*), resulting in insufficient designs being generated.

Therefore, further works involve:

- Develop and apply more sophisticated CVT search logic to explore more possibilities for evenly window layouts.
- Regulate window constraints to allow more diverse window scheme generations.
- Incorporate additional objectives to form a multi-objective study that generates more various and practical façade design schemes, such as energy-efficient façade designs that facilitate energy saving in satisfying multiple indoor comforts.

In conclusion, this study has provided valuable insights into integrating BIM with GD for a façade component design optimisation and automatic modelling under a single objective. However, it represents a preliminary investigation. The findings and methodologies presented here will be a foundation for a more comprehensive and multi-objective study into energy-efficient façade design research using the BIM-based GD method. The forthcoming study will provide more extensive investigation, analysis, and discussion and will be submitted for publication in a peer-reviewed journal soon.

REFERENCES

[1]. D. H. W. Li, ‘A review of daylight illuminance determinations and energy implications’, *Applied Energy*, vol. 87, no. 7, pp. 2109–2118, Jul. 2010, doi: 10.1016/j.apenergy.2010.03.004.

[2]. M. Thalfeldt, E. Pikas, J. Kurnitski, and H. Voll, 'Facade design principles for nearly zero energy buildings in a cold climate', *Energy and Buildings*, vol. 67, pp. 309–321, Dec. 2013, doi: 10.1016/j.enbuild.2013.08.027.

[3]. S. B. Sadineni, S. Madala, and R. F. Boehm, 'Passive building energy savings: A review of building envelope components', *Renewable and Sustainable Energy Reviews*, vol. 15, no. 8, pp. 3617–3631, Oct. 2011, doi: 10.1016/j.rser.2011.07.014.

[4]. C. Marino, A. Nucara, and M. Pietrafesa, 'Does window-to-wall ratio have a significant effect on the energy consumption of buildings? A parametric analysis in Italian climate conditions', *Journal of Building Engineering*, vol. 13, pp. 169–183, Sep. 2017, doi: 10.1016/j.jobe.2017.08.001.

[5]. S. Shaik, K. Gorantla, A. Ghosh, C. Arumugam, and V. R. Maduru, 'Energy Savings and Carbon Emission Mitigation Prospective of Building's Glazing Variety, Window-to-Wall Ratio and Wall Thickness', *Energies*, vol. 14, no. 23, p. 8020, Dec. 2021, doi: 10.3390/en14238020.

[6]. Z. Chen, A. W. A. Hammad, I. Kamardeen, and A. Haddad, 'Optimising Window Design on Residential Building Facades by Considering Heat Transfer and Natural Lighting in Nontropical Regions of Australia', *Buildings*, vol. 10, no. 11, Art. no. 11, Nov. 2020, doi: 10.3390/buildings10110206.

[7]. K. A. Al-Sallal, 'Sizing windows to achieve passive cooling, passive heating, and daylighting in hot arid regions', *Renewable Energy*, vol. 14, no. 1, pp. 365–371, May 1998, doi: 10.1016/S0960-1481(98)00091-3.

[8]. Z. Chen, A. W. A. Hammad, I. Kamardeen, and A. Akbarnezhad, 'Optimising Embodied Energy and Thermal Performance of Thermal Insulation in Building Envelopes via an Automated Building Information Modelling (BIM) Tool', *Buildings*, vol. 10, no. 12, Art. no. 12, Dec. 2020, doi: 10.3390/buildings10120218.

[9]. W. Ma, X. Wang, W. Shou, and J. Wang, 'Energy-efficient façade design of residential buildings: A critical review', *Developments in the Built Environment*, vol. 18, p. 100393, Apr. 2024, doi: 10.1016/j.dibe.2024.100393.

[10]. I. Acosta, M. Á. Campano, and J. F. Molina, 'Window design in architecture: Analysis of energy savings for lighting and visual comfort in residential spaces', *Applied Energy*, vol. 168, pp. 493–506, Apr. 2016, doi: 10.1016/j.apenergy.2016.02.005.

[11]. I. Acosta, C. Munoz, M. A. Campano, and J. Navarro, 'Analysis of daylight factors and energy saving allowed by windows under overcast sky conditions', *Renewable Energy*, vol. 77, pp. 194–207, May 2015, doi: 10.1016/j.renene.2014.12.017.

[12]. P. Xue, C. M. Mak, and Y. Huang, 'Quantification of luminous comfort with dynamic daylight metrics in residential buildings', *Energy and Buildings*, vol. 117, pp. 99–108, Apr. 2016, doi: 10.1016/j.enbuild.2016.02.026.

[13]. K. Alhagla, A. Mansour, and R. Elbassuoni, 'Optimizing windows for enhancing daylighting performance and energy saving', *Alexandria Engineering Journal*, vol. 58, no. 1, pp. 283–290, Mar. 2019, doi: 10.1016/j.aej.2019.01.004.

[14]. S. Autodesk, 'Apertures for Daylighting', Autodesk. Accessed: Nov. 30, 2023. [Online]. Available: https://www.autodesk.com/support/technical/article/caas/tsarticles/ts/yJWMKir9zcjQLh7oa4ccr.html

[15]. J. Burns, 'CENTROIDAL VORONOI TESSELLATIONS', *Centroidal Voronoi Tessellations*, 2009.

[16]. Q. Du, V. Faber, and M. Gunzburger, 'Centroidal Voronoi Tessellations: Applications and Algorithms', *SIAM Review*, vol. 41, no. 4, pp. 637–676, 1999.

[17]. Q. Du and M. Gunzburger, 'Grid generation and optimization based on centroidal Voronoi tessellations', *Applied Mathematics and Computation*, vol. 133, pp. 91–607, 2002.

[18]. Y. Liu *et al.*, 'On centroidal voronoi tessellation—energy smoothness and fast computation', *ACM Trans. Graph.*, vol. 28, no. 4, pp. 1–17, Aug. 2009, doi: 10.1145/1559755.1559758.

[19]. Q. Du, 'Advances in Studies and Applications of Centroidal Voronoi Tessellations', *NMTMA*, vol. 3, no. 2, pp. 119–142, Jun. 2010, doi: 10.4208/nmtma.2010.32s.1.

[20]. D. Jason, 'Lloyd's Relaxation'. Accessed: Jun. 08, 2023. [Online]. Available: https://www.jasondavies.com/lloyd/

[21]. R. Johnson, R. Sullivan, S. Selkowitz, S. Nozaki, C. Conner, and D. Arasteh, 'Glazing energy performance and design optimization with daylighting', *Energy and Buildings*, vol. 6, no. 4, pp. 305–317, Jan. 1984, doi: 10.1016/0378-7788(84)90014-8.

[22]. M. Deshmukh and C. Mahatme, 'Generative Design: A New Intelligent Design & Manufacturing Approach', *CHEMIK*, pp. 193–198, Sep. 2020.

[23]. W. Ma, X. Wang, J. Wang, X. Xiang, and J. Sun, 'Generative Design in Building Information Modelling (BIM): Approaches and Requirements', *Sensors*, vol. 21, no. 16, Art. no. 16, Jan. 2021, doi: 10.3390/s21165439.

[24]. S. Abrishami, J. Goulding, F. Pour Rahimian, and A. Ganah, 'Integration of BIM and generative design to exploit AEC conceptual design innovation', *Electronic Journal of Information Technology in Construction*, vol. 19, pp. 350–359, Sep. 2014.

[25]. Autodesk, 'Generative Design Primer', Generative Design Primer. Accessed: Aug. 03, 2021. [Online]. Available: https://www.generativedesign.org/

[26]. S. Karaman, B. Ekici, C. Cubukcuoglu, B. K. Koyunbaba, and I. Kahraman, 'Design of rectangular façade modules through computational intelligence', in *2017 IEEE Congress on Evolutionary Computation (CEC)*, Jun. 2017, pp. 1021–1028. doi: 10.1109/CEC.2017.7969420.

Proceeding of the 10th International Conference on Innovative Production and Construction (IPC 2024), Perth, Australia, July 11-12, 2024

Review of Computational Optimization Techniques in Cement-Based Materials

Jiajie Shang[1], Yuanyuan Yang[2], Yufei Wang[3]

1. School of Accounting, Economics and Finance, Curtin University, Perth, WA 6102, Australia
2. Business School, University of Southampton, Southampton, SO17 1BJ, United Kingdom
3. School of Design and Built Environment, Curtin University, Perth, WA 6102, Australia

ABSTRACT: Concrete plays a pivotal role in the infrastructure and construction industry, attracting extensive research focus. The areas of strength forecasting and mix design optimization are central to this exploration, transitioning from traditional experimental approaches to contemporary machine learning techniques. This paper compiles and summarizes research on three widely used machine learning models: Artificial Neural Networks (ANN), Support Vector Machines (SVM), and Decision Trees. Covering from their fundamental concepts to their adapted versions in the construction domain, this document endeavors to offer a comprehensive review of these prevalent machine learning methods.

KEYWORDS: machine learning; cementitious material; objective optimization; strength prediction; metaheuristic algorithm.

1 INTRODUCTION

Globally, concrete is a widely used building material, with its annual consumption reaching approximately 10 billion tons [1]. There has been a surge in research focusing on its diverse attributes since its inception, highlighting benefits such as cost-effectiveness, formability, and combined strength [2]. In scholarly discussions, two areas—strength forecasting and design optimization—are identified as key research interests due to their critical application value [3]. Traditional approaches to predicting concrete strength often rely on statistical techniques, including linear and non-linear regression models, which now fail to meet the expectations of designers and builders [4]. This inadequacy arises from the practice of adding various substances to ordinary Portland cement (OPC) to meet certain criteria, altering cement's basic microstructure in ways that statistical models cannot account for. For instance, Snell, Van Roekel [5] ever compared the efficiency of the statistical model for compressive strength prediction between OPC and concrete involving superplasticizers. They observed that the determination of coefficient (R^2) for the innovative concrete, which was utilized as a performance measure of the applying model, was unexpectedly low and unreliable with 0.1. Regarding optimization, researchers often employ forward-looking or performance-driven strategies that are iterative or experimental in nature, seeking a satisfactory rather than optimal solution from the final data set [6]. This process is complicated by the numerous variables in concrete mix design, resulting in an exhaustive workload for those preparing

samples [7]. Moreover, the optimized concrete design outcomes are constrained to specific conditions, such as certain temperatures and moisture levels, limiting their applicability to more general scenarios [8].

To address the challenges previously mentioned, researchers have turned to machine learning (ML), a leading subset of artificial intelligence. ML allows computers to identify patterns within datasets. Within the realm of construction and infrastructure, ML is broadly categorized into supervised and unsupervised learning. Unsupervised learning algorithms focus on uncovering patterns in input data, often analyzing the mechanical properties of concrete as reported in various studies [9]. In contrast, supervised learning algorithms differ by incorporating a feedback loop that compares predicted outcomes against actual results, thereby fine-tuning the algorithm's parameters for improved accuracy. This method selects models based on the nature of the output data: classification models for discrete outputs and regression models for continuous outputs. Given the continuous nature of problems such as optimization design and strength prediction in concrete, supervised regression models are commonly chosen. These models include but are not limited to artificial neural networks (ANN), support vector machines (SVM), and decision trees, as illustrated in Figure 1.

Despite the vast research on the application of machine learning models, a limited number of articles have aimed at providing a holistic overview of these models. Hence, this paper aims to critically review and summarize the applications of these three specific models from published articles, offering clear insights to the relevant audience. To this end, approximately 300 articles related to machine learning, concrete mixture optimization, and strength prediction were initially gathered from Google Scholar. Based on this research, studies were organized into three categories according to the different models they focused on. Further analysis led to the selection of topics related to strength predictions and optimizations, which were then sorted into categories of traditional versus evolved models. This methodical approach has enabled the paper to construct a clear framework and derive comprehensive conclusions.

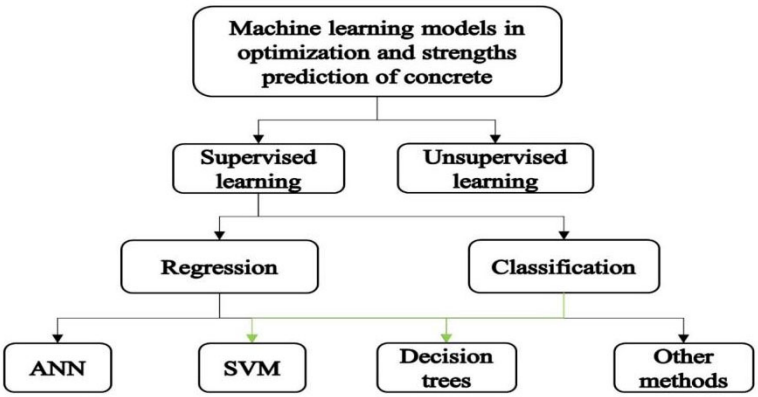

Figure 1. Common mechanical learning models in optimization and strengths prediction of concrete

2 METHOD

This part includes four sections. Section 2.1, 2.2, 2.3 mainly focused on basic theories and evolved applications of ANN, SVM, Decision trees on strengths predictions respectively. As for section 2.4, it referred to their applications of concrete mixture optimization.

2.1 Artificial neural network (ANN)

Artificial Neural Networks (ANN), models inspired by the neural architecture of the human brain, have been deployed to address complex issues across multiple disciplines. A traditional ANN structure comprises three key components: input layers, hidden layers, and output layers. To determine the importance of input variables, different weights are associated with these inputs and transmitted to the neurons in the hidden layers [10]. Although there is no fixed number of hidden layers, the architecture typically includes one or two. Neurons perform computations on the weighted inputs, accounting for bias within this process. The outcome is then determined using an activation function [11]. Among the various activation functions for ANN output layers, the sigmoid function has been popular among researchers. The first application of ANN in predicting the compressive strength of high-performance concrete (HPC) was by Kasperkiewicz, Racz [12] in 1995, who analyzed the impact of six variables, achieving a determination coefficient R^2 of 0.757. Subsequently, ANN has gained widespread recognition for its ability to predict the compressive strength of various types of concrete. For instance, Elsanadedy, Al-Salloum [13] compared the efficacy of ANN with linear regression models in predicting the compressive strength of fibre reinforced concrete. The findings indicated that ANN was superior, evidenced by a higher R^2 of 0.94, compared to linear methods which had an R^2 of 0.73. This trend was consistent across studies on cellular concrete, recycled aggregate concrete (RAC), and ultra-high-performance concrete.

Variants of ANN models were developed to meet higher accuracy demands. As previously discussed, weights and bias are crucial hyperparameters in the ANN approach [14]. Thus, researchers have leveraged the backpropagation algorithm for updating these parameters to diminish the errors between simulated and actual strengths. This refinement led to the popularity of the backpropagation neural network model (BPNN) for analyzing mechanical properties. BPNN has been applied to various concrete types, including HPC [15], RAC [16], self-compacting concrete (SCC) [17], and other innovative types. For example, Shirgir, Mamdoohi [16] compared the BPNN model with the fuzzy logic (FL) model in RAC compressive strength prediction. Through some measuring parameters like R2, MAPE, RMSE, they concluded that BPNN performed better than the FL model. Apart from the compressive aspect, BPNN also worked well at predicting the tensile and shear performances. Wang, Wu [18] integrated compressive strength as a variable in BPNN to assess its influence on the tensile behaviors of steel fiber concrete, noting higher accuracy with BPNN compared to SVM outcomes. In shear performance research, multiple studies have focused on beams made with innovative concrete [19] , using geometric and mechanical properties as input variables.

Beyond BPNN, recent research has also introduced hybrid ANN models. These hybrid approaches possess additional benefits over the traditional ANN technique [20]. For example,

the Adaptive Neuro-Fuzzy Inference System (ANFIS) integrates the capacity for human-like qualitative reasoning through FL's IF-Then rules [11]. Vickers [21] applied ANFIS to geopolymer concrete experiments, achieving greater accuracy than with BPNN. Metaheuristic algorithms offer another hybrid strategy, utilized for their flexibility in meeting diverse objectives and overcoming dataset limitations. These algorithms include the Genetic Algorithm (GA), firefly algorithm (FA), and multi-objective grey wolves optimization (MOGWO). Despite the emergence of these advanced models, ANN remains highly favored due to its self-adaptation, precision in predictions, and non-linear mapping capabilities. It stands as the recommended choice for researchers with access to extensive datasets, outperforming other models in versatility and effectiveness.

2.2 Support vector machine (SVM)

Distinct from the biologically inspired ANN model, the Support Vector Machine (SVM) operates on a more computational basis. Introduced by Smola, Schölkopf [22] in 1964 and further developed by 1992 [23] , SVM is a supervised learning model adept at handling both regression and classification tasks. In regression contexts, it is referred to as Support Vector Regression (SVR). To tackle complex challenges, SVM initially employs a hyperplane to bifurcate the dataset into two categories. The aim is to maximize the margin between the hyperplane and the nearest data points of each category, thereby identifying the optimal hyperplane for enhanced clustering of test data. Support vectors are the data points located along the margins, and the solution to the problem emerges from the combination of these vector points. Depending on the nature of class separation, the optimal hyperplane can be either linear or non-linear. For non-linear classification, SVM utilizes a higher-dimensional space for data mapping to facilitate as linear a separation as possible. The outcomes of non-linear mapping through the hyperplane are determined using kernel functions, including sigmoid, polynomial, linear, radial, and exponential radial basis functions. The radial basis function (RDF) is often chosen for concrete experiments, as highlighted by Nunez, Marani [11]. Ashrafian, Shokri [24] ever modeled the compressive performances of cellular concrete by SVR. In this study, two kernel functions comprising RDF and polynomial were adopted in the SVR model and compared their estimation accuracy. Results showed that the former SVR model had a better performance based on higher R^2 (0.922) and lower RMSE (4.65) than that of polynomial supported one (R^2 0.749; RMSE 7.88). SVM has been applied in the prediction of the strength of various concrete. For example, Gupta and Technology [25] applied the original SVM model to predict the compressive strength in HPC, acquiring R^2 as high as 0.9913 and therefore validating its great efficiency. Wang, Wu [18] applied SVM to assess the tensile performance of steel fibre reinforced concrete (SFRC), concluding that SVM surpassed non-linear regression methods in effectiveness.

Similar to ANN, SVM has undergone modifications to improve its predictive accuracy. Enhanced SVM variants include the Least Square Support Vector Machine (LSSVM) [26] , SVM augmented with Enhanced Cat Swarm Optimization (ECSO-SVM) [27], and weighted support vector machine (WSVM) [28]. LSSVM and other LS-supported SVM/SVR variants have been applied to predicting concrete strengths, such as compressive strength in foamed concrete, tensile strength in concrete with recycled aggregates, and shear strength in

fiber-reinforced concrete. The ECSO-SVM model leverages a swarm-based algorithm to fine-tune SVM's hyperparameters, demonstrating superior predictive capabilities through statistical metrics. WSVM, on the other hand, incorporates Fuzzy Logic (FL) in a hybrid approach, achieving an accuracy improvement of 10.15% over traditional SVM models due to FL's pre-processing filter role before SVM execution. Compared to ANN, SVM is less dependent on the size of the dataset, making it suitable for smaller data sets. Moreover, it avoids the pitfall of getting trapped in local minima, a significant limitation faced by models like ANN [29].

2.3 Decision trees

Among machine learning techniques, tree-based models are recognized as the third most universal approach [11]. Unlike ANNs, which operate as a "black box" due to the opaque processing within hidden layers, decision trees are favored for their transparency and ease of result interpretation. Decision trees, a form of supervised learning, are divided into classification trees for discrete outcomes and regression trees for continuous data, known collectively as CART. This approach begins with tests on the input dataset before executing partitioning steps, aiming to minimize the variance within partitions, measured by the squared differences between values and their mean. The process is repeated until branches terminate in nodes that predict output values. However, basic decision tree models have seen limited use in construction due to challenges in model suitability [9]. Consequently, enhanced tree models like Multiple Additive Regression Trees (MART), M5P-tree, and Random Forest (RF) have been developed for predicting concrete mechanical strengths.

MART, integrating CART with boosting techniques for error reduction, exhibits superior performance [21]. Kaveh and Zolghadr [30] previously conducted experiments on HPC and predicted its compressive strength by MART. Results for R2 showed that this model behaved better than ANN and SVM. Another tree variant model, M5P-tree, was improved by the utilization of linear regression function at nodes. Details for CART to become M5P-tree were not fully explained here, and researchers who have interests are recommended to read the paper from Zhan, Gan [31]. This evolved model was applied to predict strengths in creative concrete by inputting multiple variables like w/c, concrete age, etc. For instance, Melanie [32] predicted the compressive performance of HPC through the M5P-tree model and obtained high accuracy (R2 0.9505). Tensile strength simulation on the basis of this model was also conducted by Behnood, Golafshani [33], who conducted tests on concrete involving waste sand. As for the RF, it was one of the most superior machine learning models for mechanical performances forecast. Instances like compressive strength of HPC, shear strength of RC, their results validated the reliability of this model. For the merits of tree-based models, it could avoid the phenomenon of overfitting, while may not accurate as other models.

2.4 Applications on optimization

The discussion thus far has primarily highlighted the application of machine learning models and their adaptations to predicting mechanical strengths. When it comes to mixture optimization, the focus has shifted from merely satisfying a singular mechanical performance

criterion set by designers to addressing a range of requirements including strength, environmental impact, and production costs [9]. Researchers are tasked with finding a balance among these objectives, where machine learning has demonstrated its effectiveness through extensive computational capabilities and resource efficiency. This section delves into the use of the discussed models in optimizing concrete mix proportions. For instance, an SVM model enhanced with an evolutionary algorithm was applied by Cheng, Prayogo [34] for optimizing the mix ratios to achieve optimal compressive strength in high-performance concrete. Similarly, an ANN model augmented with a harmony search algorithm showed remarkable results in reducing the production cost of reactive powder concrete. This study considered slump, alongside compressive and tensile strengths, as constraints within the optimization framework.

3 CONCLUSION

This review synthesized the findings from articles focusing on strength prediction and mixture optimization through machine learning models, particularly examining ANN, SVM, and tree-based models in terms of their core principles, initial implementations, and subsequent enhancements. The analysis led to several key insights:

1. Machine learning models have shown significant effectiveness in predicting material strengths, notably in assessing compressive strength.
2. ANN stands out as the most favored model among researchers due to its adaptability, though its performance is contingent upon the availability of large datasets.
3. For smaller datasets, SVM emerges as a viable option, offering capabilities for global minimum searches.
4. Tree-based models, known for their resistance to overfitting, are recommended for use in combination with other models to leverage their strengths.
5. The integration of metaheuristic algorithms and the development of hybrid models represent promising approaches to augment the capabilities of machine learning models, meriting further investigation.
6. The field of multi-objective optimization presents a largely untapped area of research within the context of machine learning, offering a frontier for future exploration.

REFERENCES

[1]. ZHAO XIAOBO, LU YIYAN, LIANG HONGJUN, WANG YUHU and YAN YUHONG %J ENGINEERING STRUCTURES, *Optimal design of reinforced concrete columns strengthened with square steel tubes and sandwiched concrete.* 2021. **244**: p. 112723.

[2]. SUN JUNBO, ASLANI FARHAD, LU JENNY, WANG LINING, HUANG YIMIAO and MA GUOWEI %J CERAMICS INTERNATIONAL, *Fibre-reinforced lightweight engineered cementitious composites for 3D concrete printing.* 2021. **47**(19): p. 27107-27121.

[3]. FENG WANHUI, WANG YUFEI, SUN JUNBO, TANG YUNCHAO, WU DONGXIAO, JIANG ZHIWEI, WANG JIANQUN, WANG XIANGYU %J CONSTRUCTION, and

MATERIALS BUILDING, *Prediction of thermo-mechanical properties of rubber-modified recycled aggregate concrete.* 2022. **318**: p. 125970.

[4]. SUN JUNBO, MA YONGZHI, LI JIANXIN, ZHANG JUNFEI, REN ZHENHUA and WANG XIANGYU %J JOURNAL OF BUILDING ENGINEERING, *Machine learning-aided design and prediction of cementitious composites containing graphite and slag powder.* 2021. **43**: p. 102544.

[5]. SNELL LUKE M, VAN ROEKEL JACOB and WALLACE NORVAL D %J CONCRETE INTERNATIONAL, *Predicting early concrete strength.* 1989. **11**(12): p. 43-47.

[6]. ASLANI FARHAD, SUN JUNBO and HUANG GUANQI %J JOURNAL OF MATERIALS IN CIVIL ENGINEERING, *Mechanical behavior of fiber-reinforced self-compacting rubberized concrete exposed to elevated temperatures.* 2019. **31**(12): p. 04019302.

[7]. SUN JUNBO, LIN SEN, ZHANG GENBAO, SUN YUANTIAN, ZHANG JUNFEI, CHEN CHANGFU, MORSY AMR M, WANG XIANGYU %J CONSTRUCTION, and MATERIALS BUILDING, *The effect of graphite and slag on electrical and mechanical properties of electrically conductive cementitious composites.* 2021. **281**: p. 122606.

[8]. SUN JUNBO, TANG YUNCHAO, WANG JIANQUN, WANG XIANGYU, WANG JIAQING, YU ZIMEI, CHENG QIAN, WANG YUFEI %J JOURNAL OF MATERIALS RESEARCH, and TECHNOLOGY, *A multi-objective optimisation approach for activity excitation of waste glass mortar.* 2022. **17**: p. 2280-2304.

[9]. DEROUSSEAU MA, KASPRZYK JR, SRUBAR III WV %J CEMENT and RESEARCH CONCRETE, *Computational design optimization of concrete mixtures: A review.* 2018. **109**: p. 42-53.

[10]. FADAEI NILOUFAR, YAN WEI-MON, TAFARROJ MOHAMMAD MAHDI, KASAEIAN ALIBAKHSH %J ENERGY CONVERSION and MANAGEMENT, *The application of artificial neural networks to predict the performance of solar chimney filled with phase change materials.* 2018. **171**: p. 1255-1262.

[11]. NUNEZ ITZEL, MARANI AFSHIN, FLAH MAJDI, NEHDI MONCEF L %J CONSTRUCTION and MATERIALS BUILDING, *Estimating compressive strength of modern concrete mixtures using computational intelligence: A systematic review.* 2021. **310**: p. 125279.

[12]. KASPERKIEWICZ JANUSZ, RACZ JANUSZ and DUBRAWSKI ARTUR %J JOURNAL OF COMPUTING IN CIVIL ENGINEERING, *HPC strength prediction using artificial neural network.* 1995. **9**(4): p. 279-284.

[13]. ELSANADEDY HM, AL-SALLOUM YA, ABBAS H and ALSAYED SH %J COMPOSITES PART B: ENGINEERING, *Prediction of strength parameters of FRP-confined concrete.* 2012. **43**(2): p. 228-239.

[14]. CHOPRA PALIKA, SHARMA RAJENDRA KUMAR, KUMAR MANEEK %J INTERNATIONAL JOURNAL OF APPLIED SCIENCE and ENGINEERING, *Artificial neural networks for the prediction of compressive strength of concrete.* 2015. **13**(3): p. 187-204.

[15]. CHITHRA SARANGAPANI, KUMAR SRR SENTHIL, CHINNARAJU K, ASHMITA F ALFIN %J CONSTRUCTION and MATERIALS BUILDING, *A comparative study on the compressive strength prediction models for High Performance Concrete containing nano silica and copper slag using regression analysis and Artificial Neural Networks.* 2016. **114**: p. 528-535.

[16]. SHIRGIR BEHROOZ, MAMDOOHI AMIR REZA and HASSANI ABOLFAZL %J INTERNATIONAL JOURNAL OF TRANSPORTATION ENGINEERING, *Prediction of*

pervious concrete permeability and compressive strength using artificial neural networks. 2015. **2**(4): p. 307-316.

[17]. ASTERIS PANAGIOTIS G, KOLOVOS KONSTANTINOS G %J NEURAL COMPUTING and APPLICATIONS, *Self-compacting concrete strength prediction using surrogate models.* 2019. **31**(1): p. 409-424.

[18]. WANG DONGPO, WU DONGSHENG, HE SIMING, ZHOU JUN, OUYANG CHAOJUN %J CONSTRUCTION and MATERIALS BUILDING, *Behavior of post-installed large-diameter anchors in concrete foundations.* 2015. **95**: p. 124-132.

[19]. TANARSLAN HM, SECER M, KUMANLIOGLU A %J CONSTRUCTION and MATERIALS BUILDING, *An approach for estimating the capacity of RC beams strengthened in shear with FRP reinforcements using artificial neural networks.* 2012. **30**: p. 556-568.

[20]. CHAABENE WASSIM BEN, FLAH MAJDI, NEHDI MONCEF L %J CONSTRUCTION and MATERIALS BUILDING, *Machine learning prediction of mechanical properties of concrete: Critical review.* 2020. **260**: p. 119889.

[21]. VICKERS NEIL J %J CURRENT BIOLOGY, *Animal communication: when i'm calling you, will you answer too?* 2017. **27**(14): p. R713-R715.

[22]. SMOLA ALEX J, SCHöLKOPF BERNHARD %J STATISTICS and COMPUTING, *A tutorial on support vector regression.* 2004. **14**(3): p. 199-222.

[23]. BOSER BERNHARD E, GUYON ISABELLE M and VAPNIK VLADIMIR N. *A training algorithm for optimal margin classifiers*. in *Proceedings of the fifth annual workshop on Computational learning theory*. 1992.

[24]. ASHRAFIAN ALI, SHOKRI FARANAK, AMIRI MOHAMMAD JAVAD TAHERI, YASEEN ZAHER MUNDHER, REZAIE-BALF MOHAMMAD %J CONSTRUCTION and MATERIALS BUILDING, *Compressive strength of Foamed Cellular Lightweight Concrete simulation: New development of hybrid artificial intelligence model.* 2020. **230**: p. 117048.

[25]. GUPTA SM %J WORLD ACADEMY OF SCIENCE, ENGINEERING and TECHNOLOGY, *Support vector machines based modelling of concrete strength.* 2007. **36**(1): p. 305-311.

[26]. KUKI ÁKOS, NAGY LAJOS, ZSUGA MIKLóS and KéKI SáNDOR %J INTERNATIONAL JOURNAL OF MASS SPECTROMETRY, *Fast identification of phthalic acid esters in poly (vinyl chloride) samples by direct analysis in real time (DART) tandem mass spectrometry.* 2011. **303**(2-3): p. 225-228.

[27]. YU YANG, LI WENGUI, LI JIANCHUN, NGUYEN THUC N %J CONSTRUCTION and MATERIALS BUILDING, *A novel optimised self-learning method for compressive strength prediction of high performance concrete.* 2018. **184**: p. 229-247.

[28]. MUSTAPHA RGUIG, MOHAMED EA %J INTERNATIONAL JOURNAL OF ENGINEERING RESEARCH and APPLICATIONS, *High-performance concrete compressive strength prediction based weighted support vector machines.* 2017. **7**(1): p. 68-75.

[29]. TSOCHANTARIDIS IOANNIS, HOFMANN THOMAS, JOACHIMS THORSTEN and ALTUN YASEMIN. *Support vector machine learning for interdependent and structured output spaces*. in *Proceedings of the twenty-first international conference on Machine learning*. 2004.

[30]. KAVEH A and ZOLGHADR A %J JOURNAL OF COMPUTING IN CIVIL ENGINEERING, *Guided modal strain energy-based approach for structural damage identification using tug-of-war optimization algorithm.* 2017. **31**(4): p. 04017016.

[31]. ZHAN CHENGJUN, GAN ALBERT and HADI MOHAMMED %J IEEE TRANSACTIONS ON INTELLIGENT TRANSPORTATION SYSTEMS, *Prediction of lane clearance time of freeway incidents using the M5P tree algorithm.* 2011. **12**(4): p. 1549-1557.

[32]. MELANIE MITCHELL %J CAMBRIDGE, MASSACHUSETTS LONDON, ENGLAND, FIFTH PRINTING, *An introduction to genetic algorithms.* 1999. **3**: p. 62-75.

[33]. BEHNOOD ALI, GOLAFSHANI EMADALDIN MOHAMMADI %J CONSTRUCTION and MATERIALS BUILDING, *Machine learning study of the mechanical properties of concretes containing waste foundry sand.* 2020. **243**: p. 118152.

[34]. CHENG MIN-YUAN, PRAYOGO DODDY and WU YU-WEI %J JOURNAL OF COMPUTING IN CIVIL ENGINEERING, *Novel genetic algorithm-based evolutionary support vector machine for optimizing high-performance concrete mixture.* 2014. **28**(4): p. 06014003.

Proceeding of the 10th International Conference on Innovative Production and Construction (IPC 2024), Perth, Australia, July 11-12, 2024

Predicting Sustainable High-Strength Concrete's Mechanical Performance with a Bio-Inspired Neural Network

Yuanyuan Yang[1], Jiajie Shang[2], Junbo Sun[3]

1. Business School, University of Southampton, Southampton, SO17 1BJ, United Kingdom
2. School of Accounting, Economics and Finance, Curtin University, Perth, WA 6102, Australia
3. Institute for Smart City of Chongqing University In Liyang, Chongqing University, Jiangsu 213300, China

ABSTRACT: This study introduces an efficient approach for predicting the Unconfined Compressive Strength (UCS) of High-Strength Concrete (HSC), leveraging a machine learning model optimized by a bio-inspired algorithm. Utilizing a back-propagation neural network (BPNN) model, whose hyperparameters are fine-tuned with a beetle antennae search (BAS) algorithm, we predict UCS with notable reliability and accuracy, evidenced by a high correlation coefficient (R=0.9893) and a low Root-mean-square error (RMSE=1.5158MPa). This methodology, based on data from 324 HSC samples from existing literature, enhances the mix design process for HSC by making it more efficient and less dependent on costly and time-consuming laboratory tests. The BAS-BPNN model automates the prediction process, achieving optimal hyperparameter settings without manual trial and error. A sensitivity analysis within the study highlights cement content as a critical factor influencing UCS, whereas superplasticizer content has minimal impact. Nonetheless, to improve prediction accuracy further, ongoing data collection and model refinement are necessary.

KEYWORDS: high-strength concrete; unconfined compressive strength; beetle antennae search; backpropagation neural network; sensitivity analysis.

1 INTRODUCTION

High-strength concrete (HSC), characterized by a uniaxial compressive strength (UCS) greater than 40 MPa [1], demonstrates superior mechanical attributes, enhanced durability, reduced permeability, and increased density over conventional concrete [2]. HSC's exceptional qualities have led to its widespread application in long-span bridges, offering the advantages of sustaining higher loads with fewer supports, thereby extending service longevity [3]. Moreover, HSC's utility in high-rise construction allows for the design of larger column spans and increased usable floor space without compromising structural integrity on lower levels [4]. Research into HSC has explored the performance of embedded connectors, focusing on aspects such as shear resistance and ductility [5], and the general behavior of HSC beams, including mid-span deflection, failure patterns, and crack propagation [6]. The material's compatibility with cutting-edge construction technologies, like building information modeling and 3D printing, further amplifies its relevance in modern construction practices [7, 8].

Additionally, the integration of solid waste materials like waste glass and recycled aggregate into HSC addresses the limitations of these materials while enhancing strength and promoting sustainability [9, 10], thus presenting a dual advantage of bolstering mechanical performance and advancing environmental sustainability [11].

To address these complexities, machine learning (ML) algorithms have seen rapid development for predicting the UCS of concrete materials. ML models, which derive mathematical models from sample data for making predictions and decisions without explicit programming, are being extensively employed [12]. Several ML models, such as neural networks, support vector regression (SVR), and tree-based models, have been utilized for this purpose [13]. For instance, Huynh, et al. (2020) [14] applied artificial neural network (ANN), deep neural network (DNN), and deep residual network (ResNet) to forecast the compressive strength of fly ash-based geopolymer concrete. The performance of backpropagation neural network (BPNN) models is largely influenced by two critical parameters: the number of hidden layers and the optimal number of neurons in each layer. Meta-heuristic algorithms, including Genetic Algorithm (GA) and Particle Swarm Optimization (PSO), have been developed to optimize ML models, particularly in tuning ANN for property prediction [15]. Another promising meta-heuristic, the Beetle Antennae Search (BAS), has been effective in adjusting BPNN architecture, offering advantages such as quick convergence, stability in local optimization, and ease of implementation [16].

This research concentrates on forecasting the Unconfined Compressive Strength (UCS) of High-Strength Concrete (HSC) utilizing a novel machine learning (ML) model that integrates backpropagation neural network (BPNN) with Beetle Antennae Search (BAS) algorithms, referred to as BAS-BPNN. Distinguishing itself from conventional ML approaches, this innovative model is constructed upon an extensive dataset comprising 324 experimental results sourced from existing literature. The BAS algorithm, known for its rapid convergence, proves especially advantageous for analyses leveraging sizable datasets. This groundbreaking study introduces a unique methodology for estimating the mechanical strength of HSC, offering significant contributions to the field of advanced engineering construction and its applications.

2 METHOD

2.1 Materials

This study has compiled a comprehensive dataset of 324 HSC samples from existing research [17]. Type 1 ordinary Portland cement (OPC) is utilized as the binding material, with silica sand acting as the fine aggregate (FA) and gravel, sized below 20 mm, functioning as the coarse gravel aggregate (CA). To enhance the mix's workability and segregation properties, a polycarboxylate-based superplasticizer (SP) with a density of 1.06 g/cm^3 is incorporated. A detailed statistical analysis of both input and output variables, drawing from this dataset, is presented in Table 1. The dataset encompasses five critical variables affecting HSC's mechanical performance: cement content, fine and coarse aggregate proportions, water, and SP content.

Table 1. Chart of input and output statistics.

ID	Data	Unit	Minimum	Maximum	Mean Value
Cement	Input	kg/m3	284	600	417
Water	Input	kg/m3	160	180	170
Coarse Aggregate	Input	kg/m3	845	989	899
Fine Aggregate	Input	kg/m3	552	951	768
SP	Input	kg/m3	0	2	0.95
UCS	Output	MPa	37.5	73.6	52

2.2 BPNN

The artificial neural network (ANN) stands as a widely adopted model in machine learning, encompassing various types like recurrent neural networks (RNN) and feedforward neural network (FFNN). Among them, the Back-propagation neural network (BPNN), a subtype of FFNN, is frequently utilized in the realm of building materials and construction [18]. Back propagation (BP) serves as a common method for fine-tuning the model's weights and biases, consisting of an input layer, several hidden layers, and an output layer. This BP mechanism involves comparing actual and predicted outputs to determine the network's optimal weights and threshold values. The output (O) of a neuron is calculated as follows:

$$O = f\left(\sum_{j=1}^{n}\left(w_j x_j\right) + b\right), \mathrm{UCS(MPa)} \qquad (1)$$

where w_j represents the weight value of the jth input neuron (x_j) in the previous layer; b is the bias value of the output neuron; f denotes the activation function. In this study, the following active function was used mainly due to its superior performance[18]:

$$f(x) = \frac{2}{1+\exp(-x)} - 1 \qquad (2)$$

During the backpropagation process, the technique calculates the gradient of the error function relative to the weights within the neural network. Training iterations conclude once the mean square error (MSE) between actual and predicted outputs falls below a predetermined threshold. The structure of the backpropagation process is depicted in Figure 1.

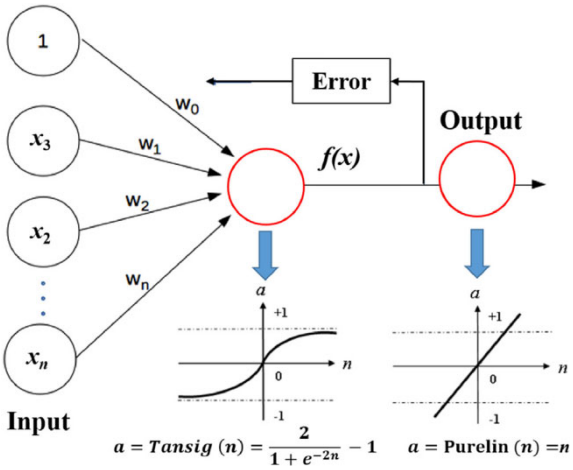

Figure 1. Backpropagation in the BPNN.

2.3 BAS

The Beetle Antennae Search (BAS) algorithm is a metaheuristic optimization technique introduced recently [19]. Its design draws inspiration from the foraging behavior exhibited by longhorn beetles, which use their elongated antennae to navigate toward a food source (representing the global optimum). Thus, the odor concentration, guiding the beetle to the food, is analogized by the objective function at a given position x. Within a multi-dimensional space, the global optimum, or the source point, is identified at the position with the most favorable objective value. The searching behavior of the beetle is described as follows:

$$\mathbf{x}_r = \mathbf{x}^i + d^i\mathbf{b} \qquad (3)$$

$$\mathbf{x}_l = \mathbf{x}^i - d^i\mathbf{b} \qquad (4)$$

where x_r and x_l represent the areas in the right-hand side and left-hand side, respectively; x^i is the position at an ith time instant. d^i denotes the length of the beetle's antennae at ith iteration. b denotes a unit vector that is randomly normalized, which is expressed as

$$\mathrm{b} = \frac{\mathrm{rnd(k,1)}}{\|\mathrm{rnd(k,1)}\|} \qquad (5)$$

where k denotes the dimensionality of the position; rnd(·) is a random function. The beetle's detecting behaviour is determined using the following equation:

$$\mathbf{x}^{i+1} = \mathbf{x}^i + \delta^i\mathbf{b} \cdot \mathrm{sign}(f(\mathbf{x}_r) - f(\mathbf{x}_l) \qquad (6)$$

where sign(·) is the sign function; δ^i represents the step size at the ith iteration, which is updated using the following formula:

$$\delta^{i+1} = \eta\delta^i \qquad (7)$$

where η is the attenuation coefficient of the step size.

2.4 Performance evaluation

In this study, Root-mean-square error (RMSE) and Correlation coefficient (R) are used to evaluate the performance of the proposed model. RMSE and R are calculated as follows

$$\text{RMSE} = \sqrt{\frac{1}{n}\sum_{i=1}^{n}\left(y_i^* - y_i\right)^2}, \text{MPa} \qquad (8)$$

where n denotes the number of data samples; y_i^* is the predicted value; y_i represents the actual value;

$$R = \frac{\sum_{i=1}^{n}(y_i^* - \overline{y^*})(y_i - \bar{y})}{\sqrt{\sum_{i=1}^{n}(y_i^* - \overline{y^*})^2}\sqrt{\sum_{i=1}^{n}(y_i - \bar{y})^2}}, dimensionless \qquad (9)$$

where and are the mean value of predicted and observed values, respectively.

3 RESULTS AND DISCUSSION

In our research, we employed the Beetle Antennae Search (BAS) algorithm to fine-tune the number of neurons within each layer. For every fold, we computed the Root Mean Square Error (RMSE) using the Back-propagation Neural Network (BPNN) configured with the fold's optimal neuron count. Figure 2 showcases the smallest RMSE values across iterations for different hidden layer configurations, illustrating the neuron number tuning process. The data indicates a reduction in RMSE to its lowest point within just 40 iterations, underscoring BAS's effectiveness in identifying the optimal neuron count. The process concludes with the determination that a single hidden layer, containing 24 neurons, is optimal.

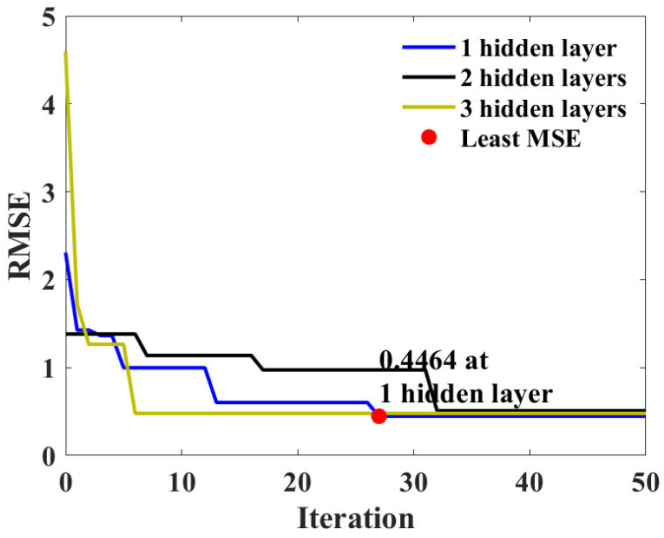

Figure 2. The lowest RMSE versus iteration corresponding to different hidden layers.

Figure 3 delineates the actual UCS values (depicted by a blue line), alongside the predicted UCS values (marked by red points), and the discrepancies between the actual and predicted UCS (illustrated by yellow bars). Notwithstanding the presence of some significant deviations, the majority of discrepancies remain minimal across both the training set (shown in Figure 8a) and the test set (displayed in Figure 3b). These observations underscore the high accuracy of

the BAS-BPNN model. The relationship between the actual and predicted UCS is further detailed in Figure 4, where a remarkable prediction precision is evident in both the training set (Figure 4a) and the test set (Figure 4b), highlighted by elevated R values (0.9971 and 0.9893 for the training and test sets, respectively) and diminished RMSE values (0.7167 MPa and 1.5158 MPa for the training and test sets, respectively). When juxtaposed with findings from prior studies [20], this model demonstrates significantly enhanced accuracy (R approximately 0.99), potentially owing to either model performance or the database's quality and volume. Moreover, the consistency of RMSE (and R) values between the test and training sets indicates the absence of overfitting issues. The robustness of the BAS-BPNN model is further validated by statistical analysis of an additional 20 runs, as summarized in Table 2, reflecting the BAS algorithm's inherent stochastic nature.

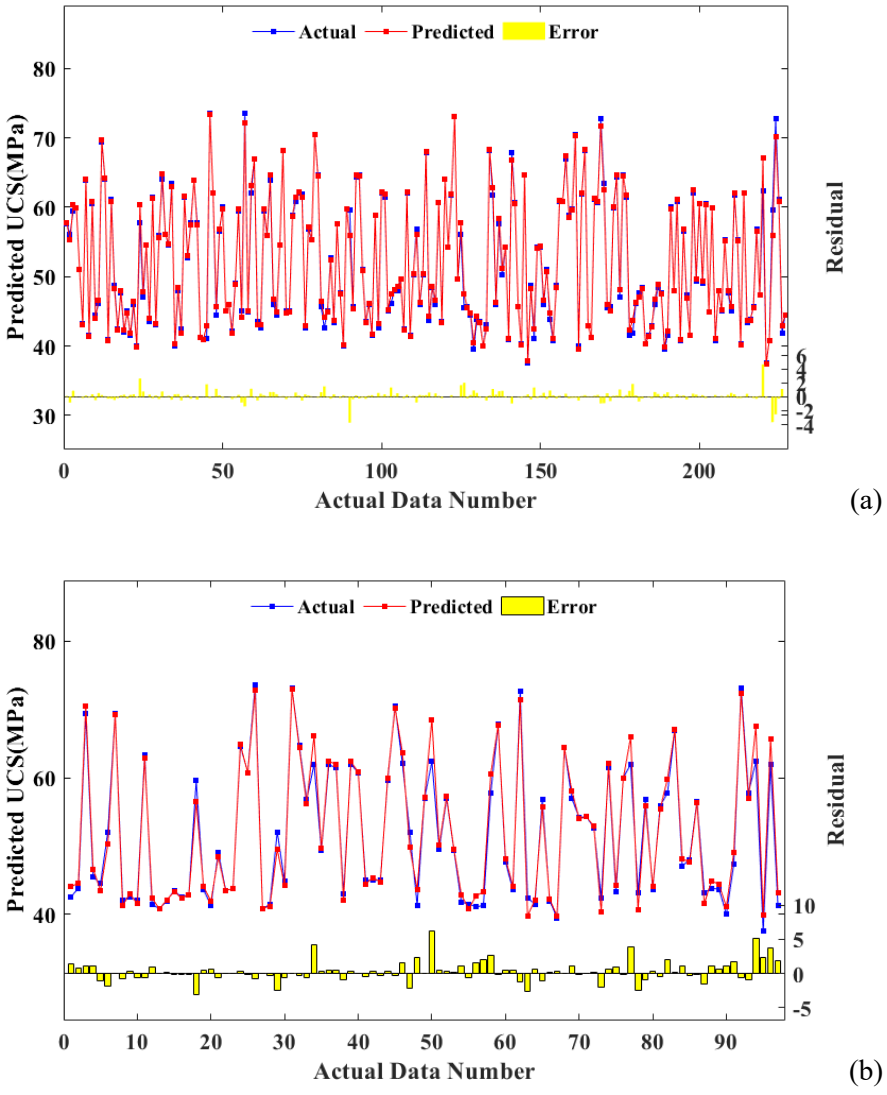

Figure 3. The error between actual and predicted UCS values on the training set (a) and test set (b).

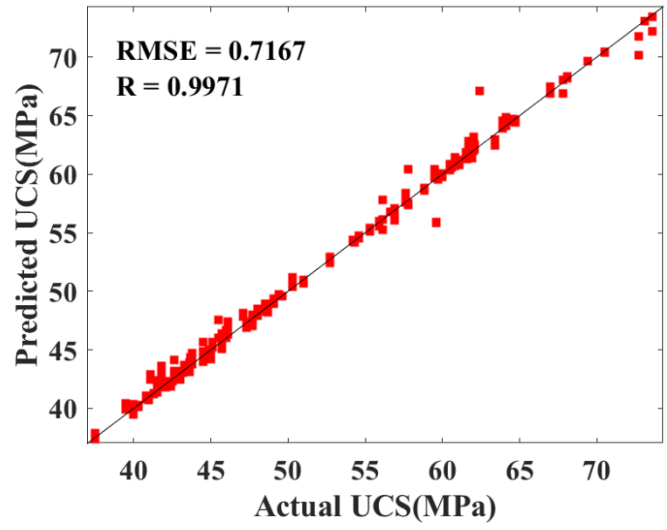

(a)

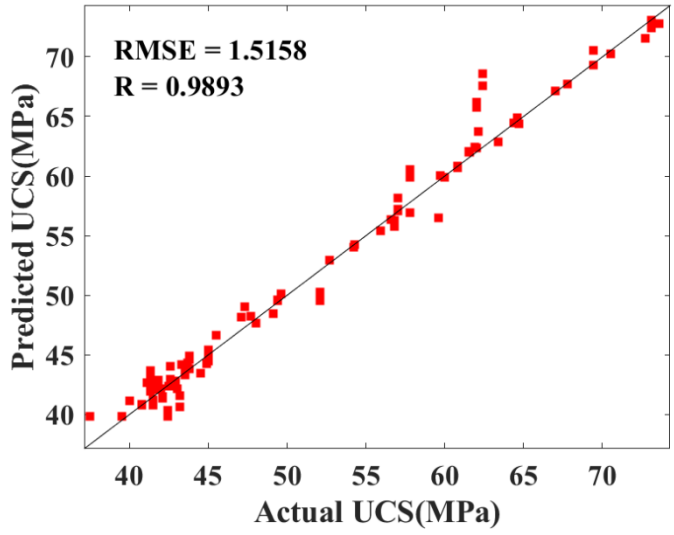

(b)

Figure 4. Predicted UCS versus actual UCS on the training set (a) and test set (b).

Table 2. Statistical outcomes (RMSE, R) of the BAS-BPNN for the extra 20 run times.

Run time	RMSE of training and test sets (MPa)	R of training and test sets	Run time	RMSE of training and test sets (MPa)	R of training and test sets
1	1.0036, 1.1543	0.9945, 0.9922	11	1.3392, 1.1305	0.9893, 0.9942
2	1.0879, 1.3876	0.9933, 0.9894	12	0.9725, 1.0086	0.9949, 0.9937
3	0.8851, 1.2874	0.9956, 0.9906	13	1.1523, 1.1125	0.9929, 0.9919
4	1.0482, 1.0455	0.9935, 0.9945	14	1.1654, 1.3617	0.9925, 0.9898
5	1.3044, 1.6762	0.9914, 0.9844	15	0.9353, 1.0637	0.9951, 0.9940
6	0.8887, 1.1730	0.9955, 0.9927	16	1.1210, 1.3923	0.9929, 0.9891
7	1.0657, 1.2421	0.9940, 0.9919	17	1.1539, 1.3263	0.9928, 0.9896
8	0.9304, 1.8270	0.9953, 0.9804	18	1.2006, 1.2839	0.9925, 0.9901
9	0.9678, 1.3371	0.9948, 0.9898	19	0.9878, 1.2744	0.9945, 0.9913
10	1.2053, 1.5601	0.9921, 0.9875	20	0.8121, 1.1521	0.9960, 0.9945

4 CONCLUSION

In this research, the integration of the Beetle Antennae Search (BAS) algorithm for hyperparameter optimization within a Back-propagation Neural Network (BPNN) model was implemented to forecast the Unconfined Compressive Strength (UCS) of High-Strength Concrete (HSC). The BAS-BPNN model was constructed using a dataset of over 300 HSC samples, each characterized by distinct mix compositions. BPNN configurations, varying by one, two, and three hidden layers, were evaluated to determine the most effective structure, which was found to be a single hidden layer equipped with 24 neurons. The outcomes highlight BAS's capability in efficiently optimizing BPNN's hyperparameters, resulting in a highly precise BAS-BPNN model, as evidenced by its performance metrics (R=0.9893 and RMSE=1.5158MPa) on the test dataset.

REFERENCES

[1]. ZHANG WEI, TANG ZHANZHAN, YANG YAN, WEI JIANGANG and STANISLAV POSPíŠIL, *Mixed-Mode Debonding Behavior between CFRP Plates and Concrete under Fatigue Loading.* Journal of Structural Engineering, 2021. **147**(5): p. 04021055 doi: 10.1061/(ASCE)ST.1943-541X.0003032.

[2]. ZHANG WEI and TANG ZHANZHAN, *Numerical Modeling of Response of CFRP–Concrete Interfaces Subjected to Fatigue Loading.* Journal of Composites for Construction, 2021. **25**(5): p. 04021043 doi: 10.1061/(ASCE)CC.1943-5614.0001154.

[3]. DEHGHANI AYOUB, MOZAFARI ALI REZA and ASLANI FARHAD. *Evaluation of the efficacy of using engineered cementitious composites in RC beam-column joints*. in *Structures*. 2020. Elsevier.

[4]. DEHGHANI AYOUB and ASLANI FARHAD, *Fatigue performance and design of concrete-filled steel tubular joints: A critical review.* Journal of Constructional Steel Research, 2019. **162**: p. 105749.

[5]. SHARIATI ALI, SHARIATI MAHDI, SULONG NH RAMLI, SUHATRIL MELDI, KHANOUKI MM ARABNEJAD and MAHOUTIAN MEHRDAD, *Experimental assessment of angle shear connectors under monotonic and fully reversed cyclic loading in high strength concrete.* Construction and Building Materials, 2014. **52**: p. 276-283.

[6]. MOHAMMADHASSANI MOHAMMAD, AKIB SHATIRAH, SHARIATI MAHDI, SUHATRIL MELDI and KHANOUKI MM ARABNEJAD, *An experimental study on the failure modes of high strength concrete beams with particular references to variation of the tensile reinforcement ratio.* Engineering Failure Analysis, 2014. **41**: p. 73-80.

[7]. SUN JUNBO, ASLANI FARHAD, LU JENNY, WANG LINING, HUANG YIMIAO and MA GUOWEI, *Fresh and mechanical behaviour of developed fibre-reinforced lightweight engineered cementitious composites for 3D concrete printing containing hollow glass microspheres.* Ceramics International, 2021.

[8]. SUN JUNBO, HUANG YIMIAO, ASLANI FARHAD and MA GUOWEI, *Electromagnetic wave absorbing performance of 3D printed wave-shape copper solid cementitious element.* Cement and Concrete Composites, 2020: p. 103789.

[9]. LI JIANWEI, QIN QIRONG, SUN JUNBO, MA YONGZHI and LI QIA, *Mechanical and conductive performance of electrically conductive cementitious composite using graphite, steel slag, and GGBS.* Structural Concrete, 2020.

[10]. ASLANI FARHAD, HOU LIJUN, NEJADI SHAMI, SUN JUNBO and ABBASI SAMER, *Experimental analysis of fiber-reinforced recycled aggregate self-compacting concrete using waste recycled concrete aggregates, polypropylene, and steel fibers.* Structural Concrete, 2019. **20**(5): p. 1670-1683.

[11]. SUN JUNBO, LIN SEN, ZHANG GENBAO, SUN YUANTIAN, ZHANG JUNFEI, CHEN CHANGFU, MORSY AMR M, and WANG XIANGYU, *The effect of graphite and slag on electrical and mechanical properties of electrically conductive cementitious composites.* Construction and Building Materials, 2021. **281**: p. 122606.

[12]. ZHANG JUNFEI, SUN YUANTIAN, LI GUICHEN, WANG YUHANG, SUN JUNBO and LI JIANXIN, *Machine-learning-assisted shear strength prediction of reinforced concrete beams with and without stirrups.* Engineering with Computers, 2020: p. 1-15.

[13]. SUN YUANTIAN, ZHANG JUNFEI, LI GUICHEN, WANG YUHANG, SUN JUNBO and JIANG CHAO, *Optimized neural network using beetle antennae search for predicting the unconfined compressive strength of jet grouting coalcretes.* International Journal for Numerical and Analytical Methods in Geomechanics, 2019.

[14]. HUYNH AN THAO, NGUYEN QUANG DANG, XUAN QUI LIEU, MAGEE BRYAN, CHUNG TAECHOONG, TRAN KIET TUAN, and NGUYEN KHOA TAN, *A machine learning-assisted numerical predictor for compressive strength of geopolymer concrete based on experimental data and sensitivity analysis.* Applied Sciences, 2020. **10**(21): p. 7726.

[15]. SHARIATI MAHDI, MAFIPOUR MOHAMMAD SAEED, MEHRABI PEYMAN, BAHADORI ALIREZA, ZANDI YOUSEF, SALIH MUSAB NA, NGUYEN HOANG, DOU JIE, SONG XUAN, and POI-NGIAN SHEK, *Application of a hybrid artificial neural network-particle swarm optimization (ANN-PSO) model in behavior prediction of channel shear connectors embedded in normal and high-strength concrete.* Applied Sciences, 2019. **9**(24): p. 5534.

[16]. SUN YUANTIAN, ZHANG JUNFEI, LI GUICHEN, MA GUOWEI, HUANG YIMIAO, SUN JUNBO, WANG YUHANG, and NENER BRETT, *Determination of Young's modulus of jet grouted coalcretes using an intelligent model.* Engineering Geology, 2019. **252**: p. 43-53.

[17]. AL-SHAMIRI ABOBAKR KHALIL, KIM JOONG HOON, YUAN TIAN-FENG and YOON YOUNG SOO, *Modeling the compressive strength of high-strength concrete: An extreme learning approach.* Construction and Building Materials, 2019. **208**: p. 204-219.

[18]. ZHANG JUNFEI, HUANG YIMIAO, WANG YUHANG and MA GUOWEI, *Multi-objective optimization of concrete mixture proportions using machine learning and metaheuristic algorithms.* Construction and Building Materials, 2020. **253**: p. 119208.

[19]. WANG JIANGYU and CHEN HUANXIN, *BSAS: Beetle swarm antennae search algorithm for optimization problems.* arXiv preprint arXiv:1807.10470, 2018.

[20]. FENG WANHUI, WANG YUFEI, SUN JUNBO, TANG YUNCHAO, WU DONGXIAO, JIANG ZHIWEI, WANG JIANQUN, and WANG XIANGYU, *Prediction of thermo-mechanical properties of rubber-modified recycled aggregate concrete.* Construction and Building Materials, 2022. **318**: p. 125970.

Proceeding of the 10th International Conference on Innovative Production and Construction (IPC 2024), Perth, Australia, July 11-12, 2024

Prediction of Mechanical Performance of 3D Printed Concrete in Steam Curing Condition

Yufei Wang[1], Hamad AI Jassmi[2], Junbo Sun[3], Shengping Li[1], Zimo Li[4], Haicheng Li[5], Xiangyu Wang[4]

1. School of Design and Built Environment, Curtin University, Perth, WA 6102, Australia
2. Department of Civil Engineering, College of Engineering, UAEU, Al Ain 15551, United Arab Emirates
3. Institute for Smart City of Chongqing University in Liyang, Chongqing University, Jiangsu 213300, China
4. School of Civil Engineering and Architecture, East China Jiao Tong University, Nanchang 330013, China
5. Faculty of Construction and Environment, Hong Kong Polytechnic University

ABSTRACT: The exploration of 3D concrete printing (3DCP) techniques has attracted significant attention among researchers and businesses, yet systematic studies on the impact of curing conditions on 3DCP's mechanical performance are sparse. This research examines the influence of varied steam curing parameters—specifically, temperature rise rate, retention capacity, and sustained temperature—on the mechanical properties of 3D printed concrete materials at different curing ages. Through both macroscopic and microscopic analyses, the investigation identifies optimal steam curing conditions for enhancing compressive characteristics in multiple directions. These findings advance the theoretical understanding of how steam curing conditions affect printed components. Additionally, experimental data informed the development of two machine learning models, utilizing the beetle antennae search (BAS) algorithm for hyperparameter optimization. This approach ensures the models' efficient construction and accuracy in predicting the mechanical performance of steam-cured concrete.

KEYWORDS: 3D printed concrete; steam curing; anisotropy; compressive strength; machine learning; beetle antennae search.

1 INTRODUCTION

3D concrete printing (3DCP) is gaining global traction for its formless builds, design freedom, less waste, and quicker construction [1, 2]. Its ability to utilize recycled materials like construction waste makes it eco-friendly, reducing waste and dust compared to traditional methods [3]. By incorporating industrial by-products such as fly ash (FA), silica fume (SF), and ground granulated blast furnace slag (GGBS), 3DCP enhances sustainability, mitigates shrinkage, and improves printing quality, offsetting the high disposal costs associated with these materials [4-7].

Steam curing, a method where the concrete's surface directly contacts hot, moist air, requires heat to conduct through the mold and into the concrete for uniform heating. This process leads to higher surface temperatures in steam-cured concrete, increasing surface porosity and the presence of harmful pores compared to the interior. Surface porosity in steam-cured concrete is higher than internal porosity but can be controlled by using a geotextile cover. Furthermore, higher treatment temperatures widen the temperature gradient between the concrete's surface and interior, resulting in lower compactness and higher permeability. However, few researchers have been conducted on 3DCP.

Machine learning (ML) models, which have gained significant attention in recent years, hold considerable potential in predicting material characteristics [8]. Their ability to analyze unstructured data from datasets and generate precise, reliable predictions underpins their value [9, 10]. Among the most prominent ML models in the concrete industry are Artificial Neural Network (ANN), Support Vector Regression (SVR), and Random Forest (RF), noted for their widespread application [11]. This research introduces various ML methods to forecast the performance of 3D printed concrete under steam curing conditions.

2 METHOD

2.1 Materials and test setup

The materials include Portland cement (42.5R), FA (Class F), GGBS, SF, and quartz sand with particle sizes from 40 to 70 mesh. Quartz sand, preferred for its simplicity and low impurity content, enhances printability. A polycarboxylic acid type water-reducing agent is used to improve print quality. The cellulose in this study is hydroxypropyl methyl cellulose with a viscosity of 4W, and the fiber is polyethylene fiber. As illustrated in Figure 1, a three-dimensional coordinate system with perpendicular X, Y, and Z axes is established to analyze the load orientation and anisotropy of the 3D printing material, with each axis perpendicular to the central point of the printing layer cross-section, the outline surface, and the plane cross-section, respectively.

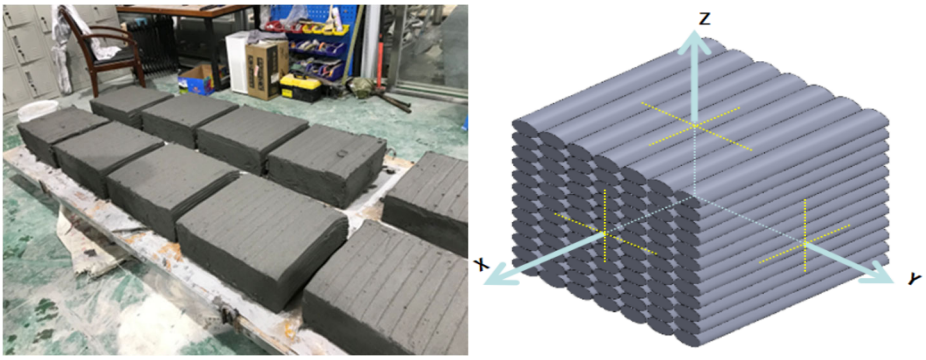

Figure 1. Coordinate system

For 3D printed concrete to meet fluidity, extrudability, and support requirements, the aggregate distribution and additive proportions are critical. This experiment utilized a 0.36 water to binder ratio for fluidity and support, and a sand to binder ratio of 1.3 for extrudability and cost efficiency. Key admixtures included fiber, cellulose, and water reducer. According to

Table 1, the proportions of FA, SF, and GGBS in cementitious materials were 20wt%, 15wt%, and 10wt%, respectively, assuming a total binder content of 100wt%. PVA fiber, hydroxypropyl methylcellulose, and water reducer were added at 0.21wt%, 0.016wt%, and 0.23wt%, respectively, to improve flowability and water retention. The mix ratio was established through research. The printing nozzle had a rectangular section of 38mm by 14mm, moving at 12cm/s. Each layer was printed using 12 round-trip routes to create a 20-layer vertical sedimentary structure, with a printing path interval of 40mm and a layer height of 13mm. Cube samples with 100mm sides were mechanically cut for testing after 8 hours of curing.

Table 1. Control mix proportion of this test.

Components (wt.%)								
Cement	FA	SF	GGBS	Sand	Water	Water reducer	PVA fibre	Hydroxypropyl methylcellulose
56	9	15	20	130	36	0.23	0.21	0.016

The goal of the orthogonal test was to analyze the impact of steam curing conditions on the mechanical strength of 3D printed concrete, adhering to Chinese standards [12] and previous research [13], Table 2 shows an orthogonal experiment with variables including temperature rise rate (e), sustained temperature time (E), and sustained temperature (f) across three levels. Additionally, 18 experimental groups were incorporated for the training of machine learning (ML) models. The study utilized range analysis for its simplicity and clarity. This method identifies the dominant factors affecting the outcome by calculating the range values from the averages of the highest and lowest levels. The chosen resting time of 8 hours aligns with the initial setting phase of conventional concrete, which acquires enough structural strength in 4-7 hours to withstand internal phase expansion. A cooling rate fixed at 10°C/h and post-curing conditions maintained at 20°C ± 5 with 70% ± 10 humidity were selected to prevent damage to the print transition zone.

Table 2. The curing conditions of samples in this test.

Test group	Curing conditions		
	e （℃/h）	E （h）	f （℃）
1	10	6	50
2	10	8	70
3	10	10	60
4	15	6	70
5	15	8	60
6	15	10	50
7	20	6	60
8	20	8	50
9	20	10	70

C_c	Curing in natural condition
C_p	

2.2 Machine learning

The Beetle Antennae Search (BAS) method is utilized for hyperparameter optimization in machine learning models like back propagation neural network (BPNN) and Random Forest (RF) to fine-tune settings automatically for peak performance across various problems [14, 15]. Inspired by the behavior of the longhorn beetle, which moves in the direction of its longer antenna to find food, adjusting its course based on the sensory input, the BAS algorithm mimics this by exploring in any given dimension. In this context, x_l and x_r represent different orientations of the left and right antennas respectively, and the following equation represents the position of the i^{th} time:

$$\begin{aligned} x_l^i &= x^i + d^i b \\ x_r^i &= x^i - d^i b \end{aligned} \tag{1}$$

where b is a random vector, which is determined by the equation Eq (2).

$$b = \frac{rand(k,1)}{\|rand(k,1)\|} \tag{2}$$

where rand (k, 1) denotes a random function that generates random vectors in a specified dimension, and k is the dimensionality of the search space. The next three equations depict the position vector of the beetle and the step size after the antenna length is updated.

$$x^i = x^{i-1} + \delta^i b sign(f(x_r^i) - f(x_l^i)) \tag{3}$$

$$d^i = 0.95 d^{i-1} + 0.01 \tag{4}$$

$$\delta^i = 0.95 \delta^{i-1} \tag{5}$$

where $sign()$ is the sign function, δ is the step length, $f(x)$ is the fitness function.

To evaluate ML model performance, the Root Mean Square Error (RMSE) and correlation coefficient (R) are used.

$$RMSE = \sqrt{\frac{1}{n}\sum_{i=1}^{n}(y_i^* - y_i)^2} \tag{6}$$

$$R = \frac{\sum_{i-1}^{N}(y_i^* - \overline{y^*})(y_i - \bar{y})}{\sqrt{\sum_{i-1}^{N}(y_i^* - \overline{y^*})^2}\sqrt{\sum_{i-1}^{N}(y_i - \bar{y})^2}} \tag{7}$$

where n is the number of observations, y_i^* is the anticipated output, and y_i is the final output, and the average of the predicted and the average of the actual results are expressed in$\overline{y^*}$ and $\bar{y}$ respectively.

3 RESULTS AND ANALYSIS

Figure 2 shows the variation in 28-day compressive strengths across different directions, indicating the end of the hydration phase for the specimen. The impact of varying steam curing conditions on compressive properties becomes evident under consistent material and printing parameters [16]. Orthogonal experiments and subsequent calculations provide average values for compressive strengths in the X (CS_x), Y (CS_y), and Z (CS_z) directions. The influence of steam curing conditions on CS_x is ranked as: temperature rise rate (6 MPa) > sustained temperature (4 MPa) > sustained temperature time (2 MPa). For CS_y, the order of influence is: sustained temperature time (5 MPa) > temperature rise rate (4 MPa) > sustained temperature (2 MPa). The impact on CS_z follows a similar trend: sustained temperature time (5 MPa) > temperature rise rate (3 MPa) > sustained temperature (2 MPa).

Figure 2(a) shows CS_x's negative correlation with temperature rise rate, positive correlation with sustained temperature time, and a parabolic correlation with sustained temperature. Figure 2(b) illustrates CS_y's negative correlation with temperature rise rate and parabolic relationships with both sustained temperature time and sustained temperature. Figure 2(c) indicates that CS_z has a parabolic correlation with all three curing conditions. The rapid heating and high sustained temperatures lead to volume expansion of free water and air within the specimen, causing micro-cracks and affecting mechanical properties post-steaming. Optimal conditions for late-stage curing in the X and Y directions include a 10°C/h temperature rise rate, 10h of sustained temperature time, and a sustained temperature of 70°C. For CS_z, the best parameters are a 20°C/h temperature rise rate, 8h sustained temperature time, and 60°C sustained temperature. The negative correlation of CS_x and CS_y with the temperature rise rate may be due to rapid curing creating a nonuniform pore distribution and a coarser pore structure, as rapid hydration does not allow even spread of hydration products [17]. With increasing maintenance temperature, the hydration rate of cement and the calcium-silica ratio of C-S-H, its main hydration product, increase, leading to C-S-H crystallization, reduced specific surface area, decreased bonding among hydration products, and increased brittleness. This results in a parabolic correlation between CS_z and the temperature rise rate [18, 19].

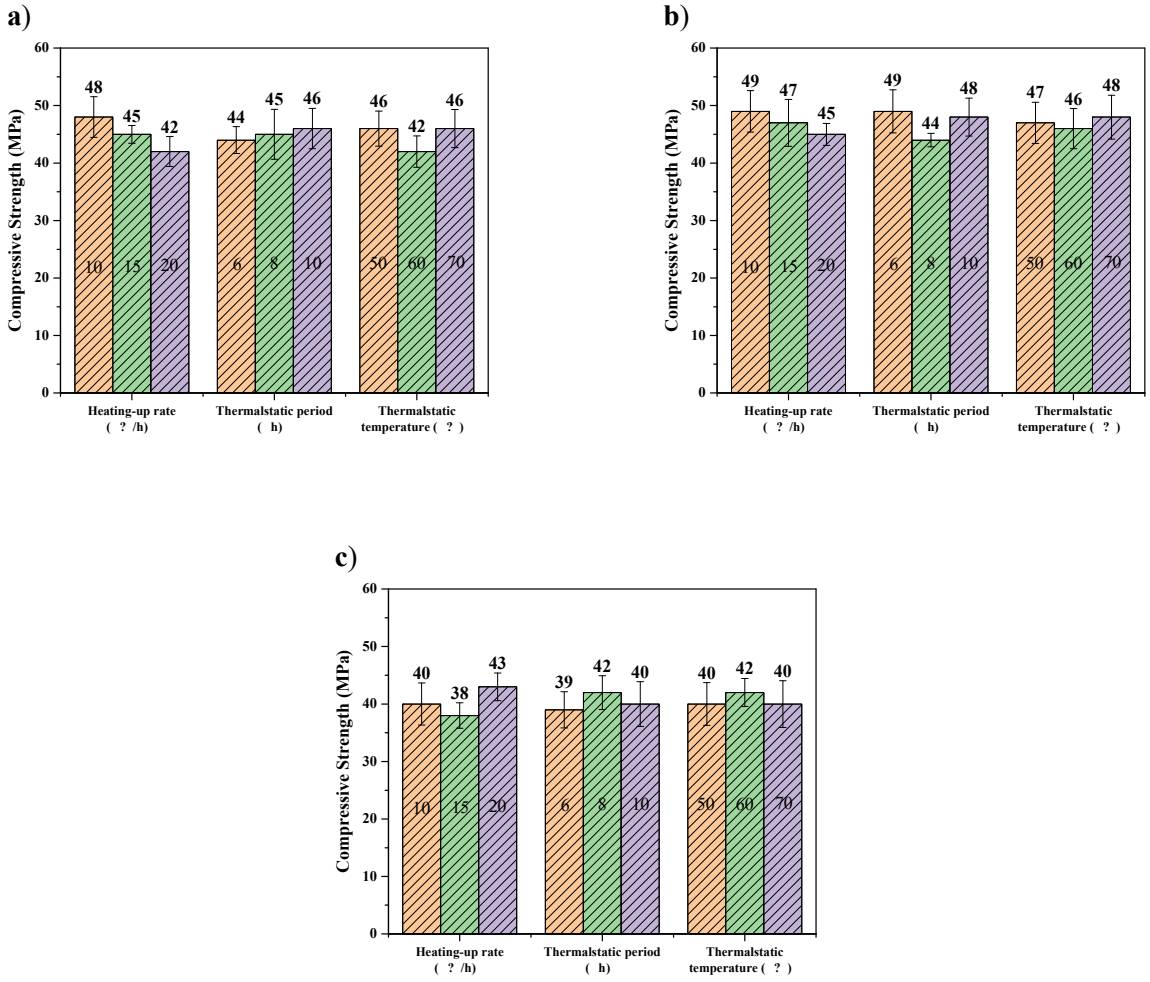

Figure 2. Effect of curing conditions on CS_x, CS_y, CS_z (sustained temperatures at 28 days).

A 30% test set was used to evaluate the performance of the RF model, which was optimized using the BAS method. Figures 3a and 3b depict the actual vs. predicted values of CS and strain, respectively, showcasing the model's accuracy on the dataset. The minimal discrepancy between the predicted and actual values demonstrates the precision of the BPNN in estimating UCS and strain. Further, a scatterplot illustrating both actual and estimated CS values across the training and test sets, along with their correlation and RMSE, is presented in Figure 4. The data for CS prediction showed a prediction value of 0.9565, a dataset correlation coefficient of 0.9108, and RMSE values of 2.0621 and 2.85. This indicates that the RF model's prediction of CS is both accurate and reliable, evidenced by a high correlation coefficient and low RMSE. Moreover, the consistency between the training and test set evaluations suggests that the model fits the data well, meeting the necessary accuracy requirements.

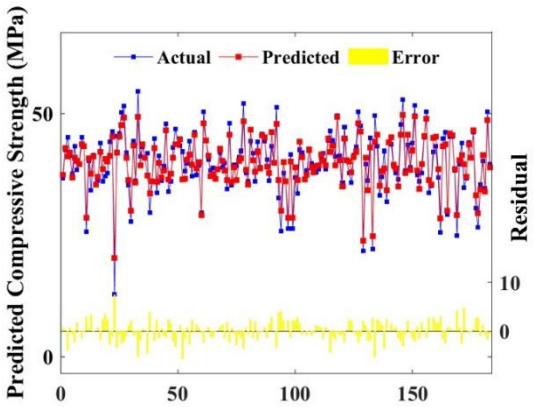

(a)

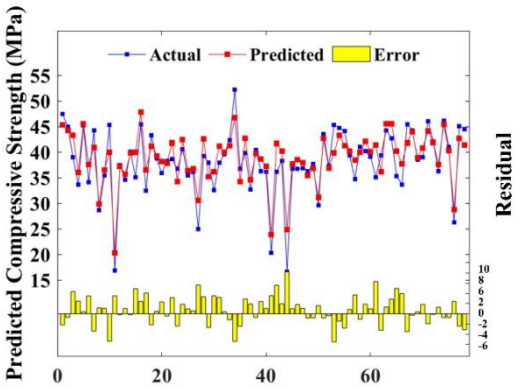

(b)

Figure 3. Scatter plot of simulated and actual CS for (a) training and (b) test sets

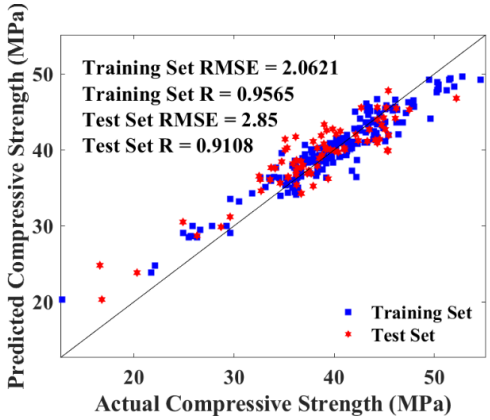

Figure 4. Scatter plot of simulated and actual CS for training and test sets

Figure 5(a) displays a box plot comparing the discrepancy between predicted and actual values of CS by the BPNN and RF models. The RF model's interquartile range is narrower (between the upper and lower black lines), and it has a lower median (indicated by the red line), signifying a smaller prediction error. In terms of CS prediction, the maximum error limit for RF is lower than that for BPNN, showcasing the superior accuracy of the RF model over the BPNN. In addition, Figure 5(b) utilizes a Taylor chart to consolidate three critical model evaluation metrics—maximum correlation coefficient, minimum RMSE, and minimum standard deviation—into polar coordinates. For both CS prediction and overall performance,

the RF model plots closer to the "ideal" position when compared to the BPNN model, further evidencing the enhanced performance and accuracy of RF in predicting CS.

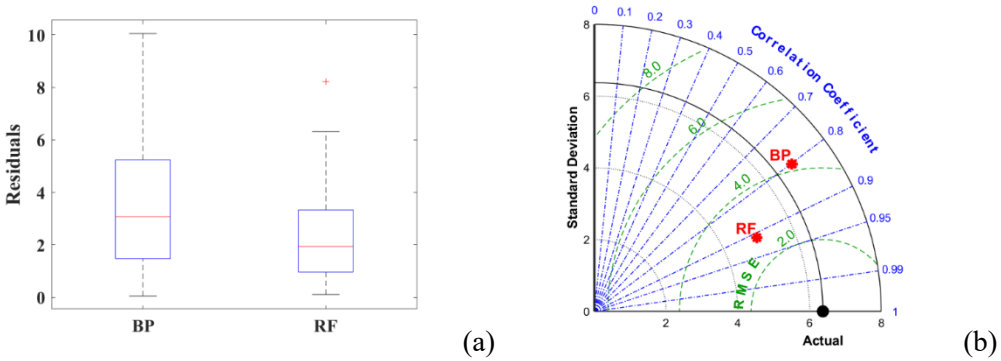

Figure 5. Performance evaluation of four models by CS prediction (a) boxplot and (b) Taylor

4 CONCLUSION

The study highlighted how different curing parameters influence the mechanical anisotropy of printed concrete, as evidenced by uniaxial compression test data. An accurate BAS-RF prediction model was developed to optimize maintenance parameters for various engineering demands. Key findings include:

7. Steam curing markedly improves the early strength of concrete, necessitating a balance between early strength growth and ultimate strength in the selection of curing conditions.

8. A temperature rise rate of 10°C/h and a sustained temperature of 50°C are advised for late strength growth. The duration of thermal-static conditions appears to have a minimal impact on strength development.

9. The BAS method effectively identified the hyperparameters for the ML model. With an R value of 0.9108 for CS, the BAS-RF model proved to be highly accurate.

10. Box and Taylor plot comparisons underscore the RF model's superiority over BPNN models, evidenced by higher R values and lower RMSE, showcasing its better prediction capabilities and generalizability.

REFERENCES

[1]. SUN JUNBO, WANG XIANGYU, ZHANG JUNFEI, XIAO FAN, SUN YUANTIAN, REN ZHENHUA, ZHANG GENBAO, LIU SHUKUI, and WANG YUFEI, *Multi-objective optimisation of a graphite-slag conductive composite applying a BAS-SVR based model.* Journal of Building Engineering, 2021. **44**: p. 103223.

[2]. ZHAO TIANJIE, SHI JIANCHENG, LV LIQING, XU HONGXIN, CHEN DEQING, CUI QIAN, JACKSON THOMAS J, YAN GUANGJIAN, JIA LI, and CHEN LIANGFU %J REMOTE SENSING OF ENVIRONMENT, *Soil moisture experiment in the Luan River supporting new satellite mission opportunities.* 2020. **240**: p. 111680. doi: 10.1016/j.rse.2020.111680.

[3]. SUN JUNBO, ASLANI FARHAD, WEI JIANJUN and WANG XIANGYU, *Electromagnetic absorption of copper fiber oriented composite using 3D printing.* Construction and Building Materials, 2021. **300**: p. 124026.

[4]. ZHANG JUNFEI, SUN YUANTIAN, LI GUICHEN, WANG YUHANG, SUN JUNBO and LI JIANXIN, *Machine-learning-assisted shear strength prediction of reinforced concrete beams with and without stirrups.* Engineering with Computers, 2020: p. 1-15.

[5]. SUN JUNBO, WANG JIAQING, ZHU ZHAOYUE, HE RUI, PENG CHENG, ZHANG CHAO, HUANG JIZHUO, WANG YUFEI, and WANG XIANGYU, *Mechanical performance prediction for sustainable high-strength concrete using bio-inspired neural network.* Buildings, 2022. **12**(1): p. 65.

[6]. ASPRONE DOMENICO, AURICCHIO FERDINANDO, MENNA COSTANTINO and MERCURI VALENTINA, *3D printing of reinforced concrete elements: Technology and design approach.* Construction and Building Materials, 2018. **165**: p. 218-231.

[7]. SUN JUNBO, WANG YUFEI, LI KEFEI, YAO XUPEI, ZHU BINRONG, WANG JIAQING, DONG QIANQIAN, and WANG XIANGYU, *Molecular interfacial properties and engineering performance of conductive fillers in cementitious composites.* Journal of Materials Research and Technology, 2022.

[8]. QI BOWEN, XU PEILONG and WU CHENGZHAO %J WATER, *Analysis of the Infiltration and Water Storage Performance of Recycled Brick Mix Aggregates in Sponge City Construction.* 2023. **15**(2): p. 363. doi: 10.3390/w15020363.

[9]. HAN LIANG, WANG LIN and ZHANG WENGANG. *Quantification of statistical uncertainties of rock strength parameters using Bayesian-based Markov Chain Monte Carlo method*. in *IOP Conference Series: Earth and Environmental Science*. 2020. IOP Publishing.

[10]. ZHANG HAIPING, OUYANG ZHIGUO, LI LI, MA WEI, LIU YANG, CHEN FANGHUAI, and XIAO XINHUI %J METALS, *Numerical study on welding residual stress distribution of corrugated steel webs.* 2022. **12**(11): p. 1831. doi: 10.3390/met12111831.

[11]. DONG ZEJIAO, QUAN WEIWEN, MA XIANYONG, LI XINKAI, ZHOU JIE %J COMPUTERS and STRUCTURES, *Asymptotic homogenization of effective thermal-elastic properties of concrete considering its three-dimensional mesostructure.* 2023. **279**: p. 106970. doi: 10.1016/j.compstruc.2022.106970.

[12]. GB/T 51231-2016 Technical standard for assembled buildings with concrete structure.

[13]. SHI JINYAN, LIU BAOJU, HE ZHIHAI, WU XIANG, TAN JINXIA, CHEN JIAZHUO, and JIANG JUNYI, *Properties evolution of high-early-strength cement paste and interfacial transition zone during steam curing process.* Construction and Building Materials, 2020. **252**: p. 119095.

[14]. SCHAPIRE ROBERT E., *The Boosting Approach to Machine Learning: An Overview*, in *Nonlinear Estimation and Classification*. 2003, Springer New York: New York, NY. p. 149-171.

[15]. WANG JIANGYU and CHEN HUANXIN, *BSAS: Beetle swarm antennae search algorithm for optimization problems.* arXiv preprint arXiv:1807.10470, 2018.

[16]. ODLER IVAN and GASSER MICHAEL, *Mechanism of Sulfate Expansion in Hydrated Portland Cement.* Journal of the American Ceramic Society, 1988. **71**(11): p. 1015-1020 DOI: 10.1111/j.1151-2916.1988.tb07573.x.

[17]. IGARASHI SHIN-ICHI, WATANABE AKIO and KAWAMURA MITSUNORI, *Evaluation of capillary pore size characteristics in high-strength concrete at early ages.* Cement and Concrete Research, 2005. **35**(3): p. 513-519 DOI: 10.1016/j.cemconres.2004.06.036.

[18]. GIRãO A. V., RICHARDSON I. G., PORTENEUVE C. B. and BRYDSON R. M. D., *Composition, morphology and nanostructure of C–S–H in white Portland cement pastes hydrated at 55 °C.* Cement and Concrete Research, 2007. **37**(12): p. 1571-1582 DOI: 10.1016/j.cemconres.2007.09.001.

[19]. LACHOWSKI E. E. *CRYSTALLINITY IN CSH GELS: INFLUENCE OF PREPARATION AND CURE CONDITIONS EE LACHOWSKI, SY HONG AND FP GLASSER*. in *PRO 13: 2nd International RILEM Symposium on Hydration and Setting-Why does cement set? An interdisciplinary approach*. 2000. RILEM Publications.

Proceeding of the 10th International Conference on Innovative Production and Construction (IPC 2024), Perth, Australia, July 11-12, 2024

Generating A Dataset of 3D BIM Models of Condominium Units Using Deep Learning

Xing Liang, Nobuyoshi Yabuki, Tomohiro Fukuda

Graduate School of Engineering, Osaka University, Japan

ABSTRACT: Within the architecture, engineering, and construction (AEC) industry, there is a growing research interest in the integration of artificial intelligence (AI) technology to create 3D building information modeling (BIM) for existing buildings based on 2D documentation. However, the number of available datasets for AI training is insufficient. Further, the datasets are mostly in 2D format, lacking height information, and the annotation styles in different datasets vary. These pose significant challenges for training AI to assist engineers in creating 3D BIM models for existing buildings. This paper proposes a two-step method based on deep learning to generate a dataset consisting of 3D BIM models of condominium units. The advantage of BIM datasets lies in their 3D nature, providing height information, and the editability of BIM models, allowing researchers to create various dimensions and annotations according to their research preferences. We have created a dataset containing 327 sets of 3D BIM models of condominium units. To the best of the authors' knowledge, our results provide the first dataset of 3D BIM models of condominium units.

KEYWORDS: AEC, 3D BIM models, dataset, condominium units, deep learning

1 INTRODUCTION

In the architecture, engineering, and construction (AEC) industry, computer-aided design (CAD) drawings represent detailed 2D or 3D designs of structures. It allows architects and engineers to create precise representations of physical objects or systems, typically focusing on geometrical representation. Building information modeling (BIM) refers to the 3D representation of a building, which is a more comprehensive approach to designing, constructing, and managing buildings and infrastructure projects. A 3D BIM model incorporates not only geometric information but also data about materials and performance characteristics, as well as it can support engineers in carrying out real-time tasks [1], such as building upgrades, asset management, and life cycle assessment.

2D drawings have long served as primary tools for design and planning [2]. Although 2D drawings are simple and easy to understand for engineers, they have some limitations. Firstly, it is often difficult for 2D drawings to accurately reflect the 3D form of a building or structure, leading to potential ambiguity and misunderstandings in the design phase. Secondly, when design changes or adjustments need to be made, modifications are relatively error-prone and

require a lot of manual operations. This can extend the project design cycle and increase costs.

In contrast, 3D models encompass most of the advantages of 2D drawings and can more comprehensively present the 3D structure of a project. This comprehensive visual presentation can also be used for collision detection and real-time simulation, helping engineers discover potential problems during the design stage and make timely adjustments, thereby reducing changes and corrections in later construction, and thus, improving construction efficiency and quality. In recent years, the adoption of 3D models in engineering has become a trend, resulting in a 21% to 61% increase in efficiency [3] in the AEC industry compared to using 2D drawings. However, most existing buildings still only have 2D documentation, as their design and construction process were often completed in an earlier period, when 3D modeling technology may not have been widely applied.

Integrating AI and 2D engineering documentation to create 3D models for existing buildings has attracted growing research interest. Despite the rapid development of AI and its applications in AEC, the availability of openly accessible datasets remains limited. Further, the available datasets primarily exist in 2D formats, lacking height information [4]. There is also not a standard drawing style in different datasets [5]. These limitations pose a significant challenge to the application of AI in AEC [6].

To solve these problems, this paper proposed a two-step method based on deep learning (DL) for generating a dataset of 3D BIM models of condominium units. Firstly, we develop a DL model and train it with a dataset of floorplan drawings of condominium units. The trained model can generate a detailed floorplan drawing based on the inputs of external walls of condominium units. The second step involves the development of two programs. The first Python program can denoise the generated floorplan, extract the geometric information and the coordinates of all the elements in the floorplan, and finally save them in an Excel file. Based on the Excel file, the second C# program can generate 3D BIM models within the BIM software combined with the BIM software API. Our approach can create datasets containing a large number of 3D BIM models. The advantage of BIM datasets lies in their 3D nature, providing height information, and the editability of BIM models, allowing researchers to create various dimensions and annotations according to their research preferences. Each element within BIM can also be assigned material properties, facilitating research into the diversity of construction materials. We have created a dataset containing 327 sets of 3D BIM models of condominium units within one hour.

2 RELATED WORK

The creation of accurate 3D models for existing buildings is crucial in AEC industries for various purposes, such as historical building preservation, reducing energy consumption, operation, and maintenance, as well as enhancing the efficiency of design, planning, and construction. Datasets play an important role since recent advancements have introduced the integration of AI into the process. This paper reviews the methods of BIM creation for existing buildings and the AI models for generating data.

2.1 On-site surveying

On-site surveying plays a pivotal role in the process of creating accurate 3D models for existing buildings. This method involves conducting detailed assessments and measurements directly at the building's location to capture its physical attributes and spatial characteristics. One or more methods among manual measurements, full station surveying, photogrammetry, and laser scanning are used to obtain spatial information about the targeted building. Laser scanning and photogrammetry are often used since they can quickly acquire spatial information to accurately create a detailed point cloud representation of the structure [7]. This point cloud data serves as the foundation for generating the 3D model [8], providing an accurate digital representation of the building's exterior and interior geometry.

The integration of AI algorithms into the modeling pipeline has emerged as a promising approach to streamline and automate the process of 3D model generation from point cloud data. Machine learning techniques, such as DL, have demonstrated remarkable capabilities in tasks such as feature extraction, object recognition, and semantic segmentation, which are crucial for processing point cloud data and reconstructing 3D geometry [9].

While the integration of on-site surveying data clouds with AI holds immense potential for creating accurate 3D BIM models for the targeted building, challenges and limitations persist. These include issues related to noise removal, data quality and consistency [10], and most importantly, time-consuming. Therefore, on-site surveying is primarily used for projects that require accurate field data to create 3D BIM models, especially those involving complex structures, historical buildings, or large-scale projects [11].

2.2 Manual creation based on 2D documentation

Traditionally, engineers reconstruct 3D BIM models manually for existing buildings based on 2D documentation [12]. Typically, this process requires the assistance of CAD software or specialized modeling tools. This approach is error-prone, time-consuming, and labor-intensive, particularly for complex architectural structures and details.

The integration of AI technology into the manual creation process has attracted growing research interest. In recent years, with the advancement of DL and computer vision technologies, an increasing number of AI algorithms have been applied in the field of 3D modeling. By inputting 2D blueprints into corresponding AI models, the model can automatically recognize the structures and features within the blueprints and generate the corresponding 3D model [13]. The advantage of this method is that it can significantly improve the efficiency and speed of reconstruction, reduce manual intervention, and be applicable to large-scale reconstruction tasks. However, AI models may be limited by the training data and algorithm constraints [14], resulting in generated models that may not be precise enough or require further manual adjustments.

2.3 AI models for generating data

DL models can learn the structure and layout of rooms from real room images and then generate new room data with diversity and authenticity. Many interdisciplinary studies at the intersection of computer science and AEC indicate that using DL models is a promising approach to automatically generate a large amount of data for AI training purposes.

House-GAN++ [15] is an integrated generative adversarial network for the automatic generation of floorplans. This model uses the semantics and topology of the bubble diagram as input aimed at generating and refining architectural layout designs. BubbleFormer [16] is a novel approach for generating bubble diagrams using dual transformer models. This approach showed the potential applications in architectural design, which can directly drive the existing floorplan generation method to obtain high-quality floorplans. WallPlan [17] introduces a novel approach for synthesizing floorplans by learning to generate wall graphs, providing a promising solution for automating the floorplan design process in architectural design.

However, the datasets of floorplans generated by these models, as well as processed floorplans from real estate companies, such as RPLAN [18] and R-FP [19], have the following drawbacks:

(a) Most of them are 2D floorplan drawing without height information [5].
(b) The styles of dimensions and texts vary in different datasets.
(c) The total number of datasets is limited.

As a result, many studies only focus on the aspect of geometrical accuracy in the floorplan, while setting the floor elevation and height of openings as default or entered manually [20].

3 METHODOLOGY

3.1 Training dataset and neural network

RPLAN dataset [18] is used. This dataset provides more than 80k vectorized images of floorplans based on the Asian real estate market. All the vectorized floorplan images in the dataset meet the following rules:

(a) Each of the vectorized images is 256 × 256 × 4 (256 pixels × 256 pixels × 4 channels).
(b) One vectorized image represents a squared region of 18m x 18m.
(c) The total area of each floorplan ranges from 60m^2 to 120m^2.
(d) The number of rooms in the floorplan ranges from 3 to 9, and the area of each single room is between 10m^2 to 20m^2.
(e) There must be a living room on the floorplan.
(f) The ratio of the living room's area to the whole area is between 0.25 to 0.55.

The 4 channels in the input data are external walls, internal walls, midpoints of spatial semantics (the function of the room), and inside areas, respectively, as shown in Figure 1. Using this dataset to train our neural network ensures that the resulting 3D BIM models are closely aligned with real-world design.

A modified Resnet-34 [21] is used to extract the features in the input images. The Resnet-34 network is modified so that it can use 256 × 256 × 4 images as inputs. Then these extracted features are used to train an encoder-decoder network which can learn the relations among spatial semantics, internal walls, and external walls.

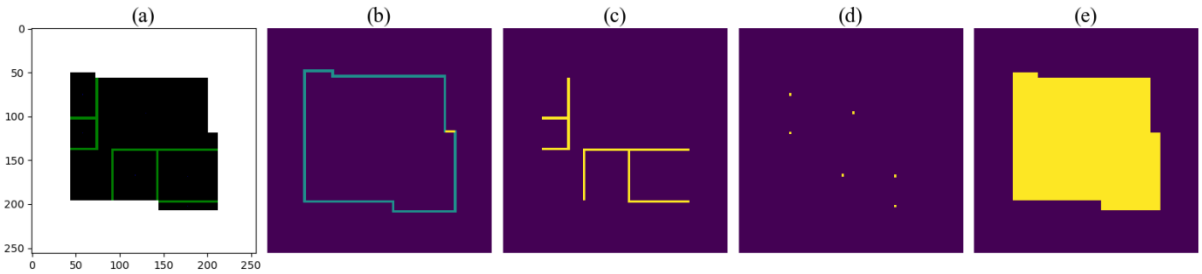

Figure 1. An image (a) in the training dataset and its 4 channels (b) ~ (e). They are namely (b) external walls, (c) internal walls, (d) midpoints of spatial semantics, and (e) inside areas, where the yellow area within (b) is the main entrance of the condominium

3.2 Trained model

After training, the generative model can generate floorplans that meet architectural design requirements. When an image of external walls, shown as (a) in Figure 2, is passed to the generative model, it will generate a new image corresponding to the input that represents possible internal floorplans with noises, as shown in (a') in Figure 2. Both the input and output images are 256 × 256 × 4, having the same shape as the training data. Specifically, in the input image, the first channel is the enclosed external walls, and the fourth channel is the inside areas shown as (b) and (e), while the second channel and the third channel are empty, shown as (c) and (d) in Figure 2. In the output image, the first and fourth channels are the same as the input image, shown as (b') and (e'), while the trained model generates internal walls (with noises) in the second channel and spatial semantics in the third channel, shown as (c') and (d') in Figure 2.

3.3 Coordinate extraction and 3D BIM model generation

Two programs are developed to generate 3D BIM models of condominium units from the DL-generated floorplans. The first Python program can denoise the output floorplan image generated in Section 3.2, and then compress the image from 4 channels to 1 channel (256 × 256 × 1). Then it can extract the geometric information and coordinates of all the elements in the denoised 256 × 256 × 1 image. All the information will be separately saved in 5 sheets in an Excel file, namely external walls, internal walls, windows, doors, and midpoints of spatial semantics, as shown in Figure 3.

The second C# program incorporates Autodesk Revit API, which can retrieve the data saved in the Excel file and generate a BIM model within Autodesk Revit, as shown in Figure 4. Because each vectorized image represents a squared region of 18m x 18m, therefore, each pixel in the resulting image should represent the real distance of 70.3125cm. The generated BIM models are based on this data, ensuring precision in elements such as walls, doors, and windows within the BIM.

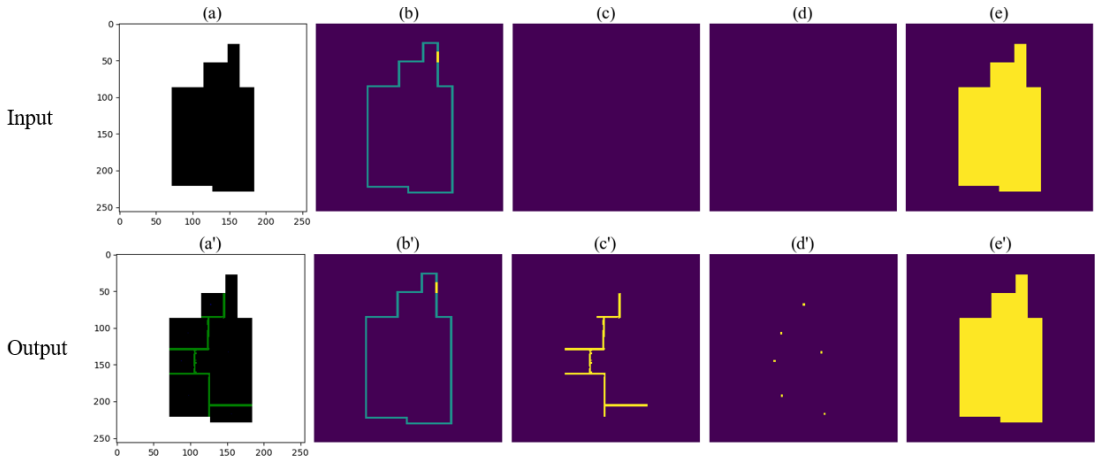

Figure 2. Input data (a) and its 4 channels (b) ~ (e). Output data (a') and its 4 channels (b') ~ (e').

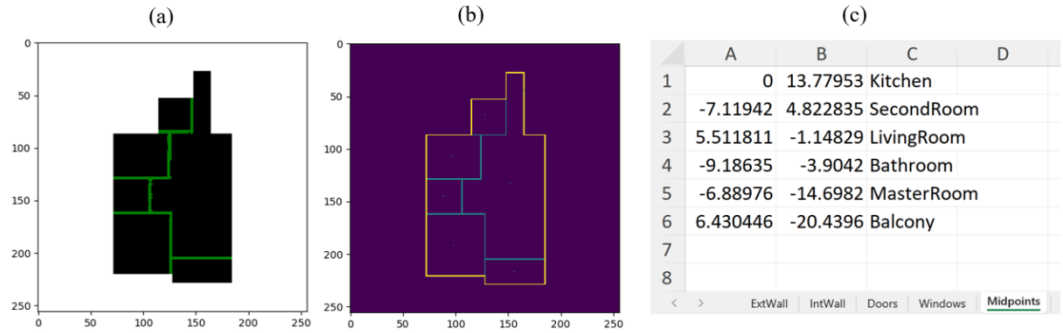

Figure 3. (a) Output data with noises, (b) denoised and compressed image, and (c) geometric data and coordinates within an Excel file.

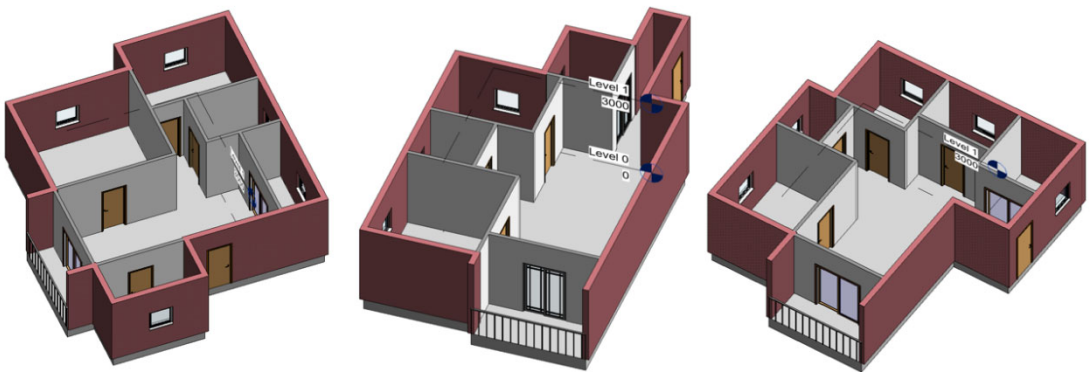

Figure 4. Three samples of generated 3D BIM models

4 RESULTS

Our proposed two-step method can generate 3D BIM models with precise dimension in elements within the BIM based on the 2D floorplans generated by the DL model. We also utilized 350 different external walls of condominium units as inputs for our model, generating 350 sets of BIM models within half an hour. After screening, 327 models were found to comply with the design rules and were compiled into a dataset. Our 3D BIM dataset has the following benefits:

(a) It not only provides floorplans but also offers elevation views in the four cardinal directions (north, south, east, and west), addressing the issue of height information absence in existing datasets.
(b) Our DL model was trained using the dataset RPLAN [18], which consists of vectorized floorplans modified from real estate companies. Therefore, the generated BIM models exhibit high authenticity, with some models even comparable to those designed by human architects.
(c) Each BIM model in the dataset is editable, allowing researchers to create annotations, text, scale, and other operations according to their research preferences, thus avoiding the problem of inconsistent annotation standards in varied datasets.
(d) All the elements within every BIM model in the dataset, such as doors, windows, walls, etc., were assigned material properties, which can support research on the object recognition of building material.

5 DISCUSSION AND LIMITATIONS

AI technology will play a more important role in helping engineers create 3D BIM models for existing buildings in the future, implying that datasets will also become increasingly important. Currently, due to the absence of datasets containing height information, many studies focusing on generating 3D BIM models from 2D documents only address geometric accuracy in floorplan views, neglecting floor elevations and opening heights. Our work can support the recognition of heights in research for creating 3D BIM models from existing buildings, and it can also address issues related to variations in annotation styles across different datasets.

The lack of diversity in datasets (such as floorplans with complex elements, electrical, and plumbing drawings, infrastructure drawings, etc.), the inconsistency among different datasets, and the limited quantity of datasets will be a long-term and open challenge in the AEC field.

This work mainly has 3 limitations. Firstly, our DL model can only generate 3D BIM for condominium units, which is a relatively simple category within the AEC industry. Each BIM model only contains up to 7 categories of elements: external walls, internal walls, flooring, ceiling, doors, windows, and railing. This is because the performance of the DL model and the quality of the results largely depend on the quality and diversity of the training data used. Currently, there is still a lack of large quantities of high-quality, complex design blueprints available for DL models to learn from in the AEC field.

Secondly, these BIM models are not representations of real existing condominium units but conceptual designs, although some designs can rival those of human designers. Furthermore, our 3D BIM dataset is generated based on 2D floorplans produced by DL models. Therefore,

the heights of all elements within the BIM, such as floor heights and window offsets, are determined by us based on our engineering design experience.

Finally, there are some unreasonable designs in the 2D floorplans generated by the DL model, though the model was trained using architectural design blueprints that adhere to real-world principles. A total of 350 different external wall images were utilized as input. Out of the 350 results generated by the DL model, only 327 complied with the design rules and could be further transformed into 3D BIM models.

6 CONCLUSION

The main contribution of this work is that providing a method for generating 3D BIM models of condominium units in Autodesk Revit, and creating a dataset containing 327 sets of 3D BIM models using this method.

Firstly, we utilized a vectorized dataset comprising over 80k floorplans from the real estate sector as our training set for the DL model. This enabled our model to generate well-designed floorplans by inputting external wall images. Subsequently, two programs were developed. The first Python program can eliminate noises from the floorplans generated by the DL model and then compress them from a size of 256 x 256 x 4 to 256 x 256 x 1. This program then extracts the geometric data and coordinates of all elements from the denoised floorplans and saves them into an Excel file. Then, the second C# program, integrated with the Autodesk Revit API, can create 3D BIM models within Autodesk Revit based on the data provided in the Excel file.

Despite the limitations, this 3D BIM dataset can address the existing dataset issues in the AEC field.

REFERENCE

[1]. L. Chen, Q. Lu, and X. Zhao, “A semi-automatic image-based object recognition system for constructing as-is IFC BIM objects based on fuzzy-MAUT,” International Journal of Construction Management, vol. 22, no. 1, pp. 51–65, 2022, doi: 10.1080/15623599.2019.1615754.

[2]. R. Sacks and R. Barak, “QUANTITATIVE ASSESSMENT OF THE IMPACT OF 3D MODELLING OF BUILDING STRUCTURES ON ENGINEERING PRODUCTIVITY,” 2006.

[3]. G. B. Dadi, P. M. Goodrum, T. R. B. Taylor, and C. M. Carswell, “Cognitive Workload Demands Using 2D and 3D Spatial Engineering Information Formats,” J Constr Eng Manag, vol. 140, no. 5, May 2014, doi: 10.1061/(asce)co.1943-7862.0000827.

[4]. V. Badenko et al., “Scan-to-bim methodology adapted for different application,” in International Archives of the Photogrammetry, Remote Sensing and Spatial Information Sciences - ISPRS Archives, International Society for Photogrammetry and Remote Sensing, Sep. 2019, pp. 1–7. doi: 10.5194/isprs-archives-XLII-5-W2-1-2019.

[5]. P. N. Pizarro, N. Hitschfeld, I. Sipiran, and J. M. Saavedra, “Automatic floor plan analysis and recognition,” Automation in Construction, vol. 140. Elsevier B.V., Aug. 01, 2022. doi: 10.1016/j.autcon.2022.104348.

[6]. M. Urbieta, M. Urbieta, T. Laborde, G. Villarreal, and G. Rossi, “Generating BIM model from structural and architectural plans using Artificial Intelligence,” Journal of Building Engineering, vol. 78, p. 107672, Nov. 2023, doi: 10.1016/j.jobe.2023.107672.

[7]. J. Liu, D. Xu, J. Hyyppa, and Y. Liang, "A Survey of Applications with Combined BIM and 3D Laser Scanning in the Life Cycle of Buildings," IEEE Journal of Selected Topics in Applied Earth Observations and Remote Sensing, vol. 14. Institute of Electrical and Electronics Engineers Inc., pp. 5627–5637, 2021. doi: 10.1109/JSTARS.2021.3068796.

[8]. M. Lo Brutto, E. Iuculano, and P. Lo Giudice, "Integrating topographic, photogrammetric and laser scanning techniques for a scan-to-bim process," in International Archives of the Photogrammetry, Remote Sensing and Spatial Information Sciences - ISPRS Archives, International Society for Photogrammetry and Remote Sensing, Jun. 2021, pp. 883–890. doi: 10.5194/isprs-archives-XLIII-B2-2021-883-2021.

[9]. H. Fathi, F. Dai, and M. Lourakis, "Automated as-built 3D reconstruction of civil infrastructure using computer vision: Achievements, opportunities, and challenges," Advanced Engineering Informatics, vol. 29, no. 2, pp. 149–161, Apr. 2015, doi: 10.1016/j.aei.2015.01.012.

[10]. M. E. Esfahani, C. Rausch, M. M. Sharif, Q. Chen, C. Haas, and B. T. Adey, "Quantitative investigation on the accuracy and precision of Scan-to-BIM under different modelling scenarios," Autom Constr, vol. 126, Jun. 2021, doi: 10.1016/j.autcon.2021.103686.

[11]. L. Sanhudo et al., "A framework for in-situ geometric data acquisition using laser scanning for BIM modelling," Journal of Building Engineering, vol. 28, Mar. 2020, doi: 10.1016/j.jobe.2019.101073.

[12]. Q. Lu, L. Chen, S. Li, and M. Pitt, "Semi-automatic geometric digital twinning for existing buildings based on images and CAD drawings," Autom Constr, vol. 115, Jul. 2020, doi: 10.1016/j.autcon.2020.103183.

[13]. B. Yang, B. Liu, D. Zhu, B. Zhang, Z. Wang, and K. Lei, "Semiautomatic Structural BIM-Model Generation Methodology Using CAD Construction Drawings," Journal of Computing in Civil Engineering, vol. 34, no. 3, May 2020, doi: 10.1061/(asce)cp.1943-5487.0000885.

[14]. A. Zabin, V. A. González, Y. Zou, and R. Amor, "Applications of machine learning to BIM: A systematic literature review," Advanced Engineering Informatics, vol. 51, Jan. 2022, doi: 10.1016/j.aei.2021.101474.

[15]. N. Nauata, S. Hosseini, K.-H. Chang, H. Chu, C.-Y. Cheng, and Y. Furukawa, "House-GAN++: Generative Adversarial Layout Refinement Network towards Intelligent Computational Agent for Professional Architects," 2021. [Online]. Available: https://ennauata.github.io/houseganpp/page.html.

[16]. J. Sun, L. Zheng, G. Zhang, and W. Wu, "BubbleFormer: Bubble Diagram Generation via Dual Transformer Models," Computer Graphics Forum, vol. 42, no. 7, Oct. 2023, doi: 10.1111/cgf.14984.

[17]. J. Sun, W. Wu, L. Liu, W. Min, G. Zhang, and L. Zheng, "WallPlan: Synthesizing Floorplans by Learning to Generate Wall Graphs," ACM Trans Graph, vol. 41, no. 4, Jul. 2022, doi: 10.1145/3528223.3530135.

[18]. W. Wu, X. M. Fu, R. Tang, Y. Wang, Y. H. Qi, and L. Liu, "Data-driven interior plan generation for residential buildings," ACM Trans Graph, vol. 38, no. 6, Nov. 2019, doi: 10.1145/3355089.3356556.

[19]. S. Dodge, J. Xu, and B. Stenger, "Parsing floor plan images," in 2017 Fifteenth IAPR International Conference on Machine Vision Applications (MVA), 2017, pp. 358–361. doi: 10.23919/MVA.2017.7986875.

[20]. C. Zhang, Y. Zou, and J. Dimyadi, "A Systematic Review of Automated BIM Modelling for Existing Buildings from 2D Documentation," 2021.

[21]. K. He, X. Zhang, S. Ren, and J. Sun, "Deep Residual Learning for Image Recognition," 2021. [Online]. Available: http://image-net.org/challenges/LSVRC/2015/

Performance Investigation of Rubberized Concrete Reinforced with Fibres for 3D Printing

Anqing Wang[1], Wenfu Zhang[1], Zhaoyue Zhu[1], Jin Peng[2], Cheng Yang[1], Xianda Liu[3], Weichen Tang[3*]

1. School of Architectural Engineering, Nanjing Institute of Technology, Nanjing, China
2. Hunan Provincial Key Laboratory of Structures for Wind Resistance and Vibration Control, Hunan University of Science and Technology, Xiangtan 411201, China
3. School of Civil Engineering and Architecture, East China Jiao Tong University, Nanchang 330013, China

ABSTRACT: The construction industry is developing towards intelligent and green technologies with the Fourth Industrial Revolution. The combination of 3D printing concrete and recycled solid materials is in great demand for intelligent and low-carbon construction. This paper incorporates the crumb rubber (0-1mm) into the printing ink and analyses the fresh and hardened properties. Six sets of mix proportions were designed with fibre content and rubber replacement as variables to analyse the material flowability and mechanical properties. Specifically, the fluidity is positively correlated with the rubber proportion and peaks with 40% rubber content. The anisotropic compressive strength and flexural strength reach the highest and lowest values when rubber content reaches 20%. Moreover, the increased PP fibre content from 1.5% to 2% has a positive effect on the anisotropic compressive strength but a negative effect on flexural strength.

KEYWORDS: 3D printing concrete; PP fibre; crumb rubber; fresh and mechanical properties.

1 INTRODUCTION

3D printing concrete (3DPC) technology is an addictive manufacturing method promoting intelligent and environmental construction [1, 2]. Pegna [3] first used automated construction technology to produce building components and concluded the advantages of saving labour costs, raw materials, and construction efficiency [4, 5]. 3DPC technology eliminates the limitations of moulds and prints various curved and irregular structures to meet personalized needs [6, 7].

Muti-functional and printable mixtures and admixtures incorporated with 3DPC have attracted great attention. Panda et al. [8] studied the flocculation characteristics of clay particles and concluded that the optimal mix proportion of nano clay was 0.5 w% to cement. Pshtiwan et al. [9] researched the fresh and hardened properties of fibre-reinforcement mortar

and concluded the increasing effect of PP fibres on flexural strength. Research on recycled industrial solid waste also attracted great attention for further reducing the environmental impact of printable mixtures. Aslani et al. [10] replaced natural coarse aggregates with 10mm rubber aggregates and generated remained similar slump flow result but only 50% compressive strength compared with the recycled concrete control group. The corresponding research concluded that crumb rubber incorporated in concrete improves the deformability of concrete but negatively affect the compressive strength [12-14]. Sambucci et al. [11] studied the synergy between rubber powders (0-1mm) and rubber granules (2-4mm) and discovered better mixture fluidity and enhanced inter-layer adhesion than the neat mix in 3D printing. There is still limited research on the combined effect of various composite materials, such as PP fibres and rubber.

In this paper, six sets of mix proportions were designed with fibre content and rubber replacement as variables. The material flowability and mechanical properties were analysed to explore the impact mechanism of the variables. Frame-based 3D printers with a 10mm-diameter nozzle were employed to manufacture the samples. The connection of the mechanical properties, fibres, and crumb rubber will be researched for promoting the eco-friendly 3DPC.

2 MATERIALS AND METHODS

2.1 Materials and mix proportion

The experiment used Onoda P.O42.5 cement, 6mm-long PP fibre, and quartz sand with a fineness modulus of 0.59. The Admixtures included 1 wt% of Polycarboxylic acid high-efficiency water-reducing agent, 1 wt% of nano clay, 0.2 wt% of hydroxypropyl methylcellulose, and 0.1 wt% sodium gluconate. The mix proportions are shown in Table 1. The 3D-printed samples and cut specimens with different directions are shown in Figure 1.

Table 1. Mixed proportions of 3D printed fibre reinforcement rubber concrete (unit: kg/m^3)

No.	OPC	FA	SF	Sand	Rubber	Water	Fibre	NC	HPMC	SG	SP
R0F15	765.05	678.18	163.62	583.05	0.00	160.41	6.06	0.01	0.002	0.001	0.01
R0F20	763.36	676.68	163.26	581.75	0.00	160.06	8.07	0.01	0.002	0.001	0.01
R20F15	786.20	696.93	168.15	479.33	17.07	164.85	6.23	0.01	0.002	0.001	0.01
R20F20	784.41	695.34	167.76	478.24	17.03	164.47	8.29	0.01	0.002	0.001	0.01
R40F15	808.56	716.74	172.93	369.72	35.12	169.54	6.41	0.01	0.002	0.001	0.01
R40F20	806.66	715.07	172.52	368.85	35.04	169.14	8.52	0.01	0.002	0.001	0.01

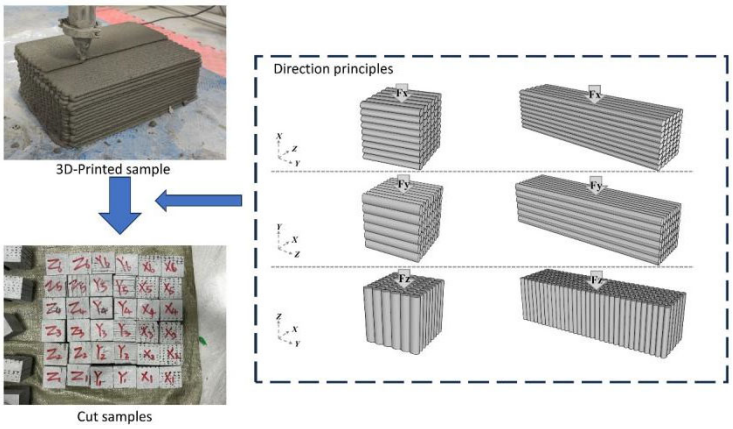

Figure 1. Coordinate system

2.2 Experimental methods

2.2.1 Flowability test

Flowability test reflects the rheological property of the fresh phase and determines the shape stability of 3DPC. Balancing the time-dependent rheological properties of flowability and buildability in 3DCP poses significant challenges that have been widely recognized. The flowability was determined by the slump test and the standing test [12]. The flowability test was conducted by testing fresh mortar through a vibrating table [13]. The test was performed every 15 minutes and measured the two perpendicular spreading diameters.

2.2.2 Mechanical property test

The 3DPC specimens were cured for 28 days in the standard environment and then cut into prismoids with dimensions of 40 mm × 40 mm × 160 mm and cubes with sides of 50 mm for the anisotropic mechanical properties test [14]. The compressive and flexural strength tests were performed in three directions relative to filaments, including two perpendicular directions and one parallel direction named X, Y, and Z, respectively. Specifically, filaments on load surface in X were set to 10% overlap by code and that in Y direction exhibited deposition due to gravity.

3 RESULTS AND DISCUSSION

The flowability is positively correlated with the rubber content but negatively correlated with the fibre content (Figure 2). PP fibres were hydrophobic but increased the viscosity and internal friction of the mortar, leading to flowability reduced. Meanwhile, rubber particles created a soft packing structure in the mortar and filled the voids in fresh mortar, thereby increasing the flowability. The optimal flowability was obtained with 2% PP fibre and 40% rubber considering the silo size, travel speed, and extrusion speed of 3D printing.

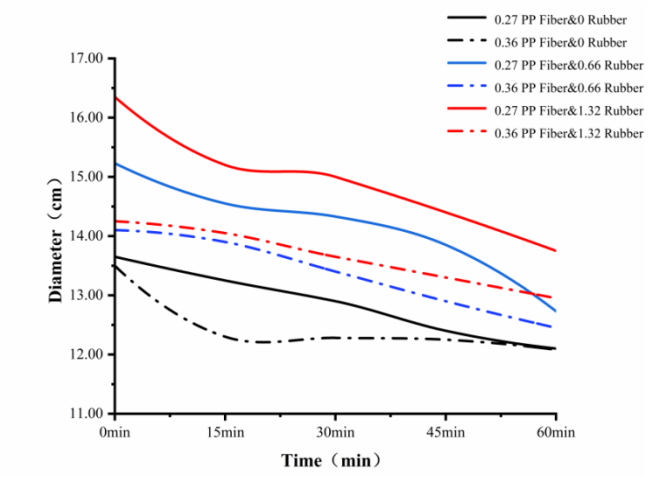

Figure 2. Fluidity test results

The mean compressive strength of the three specimens is depicted in Figure 3(a). X direction (compression load applied along the filaments) obtained the highest strength in the whole anisotropic test, followed by Y and Z. Anisotropic strength is attributed for the structure stacked layer by layer and vibration lacking, which introduces voids and weakness between filaments and layers. X-R20F15 (X direction of R20F15) and X-R20F20 obtained the highest strength of 69.45Mpa and 64.5Mpa respectively in 1.5% and 2.0% fibre content series. According to the result of R20F15, the peak strength of X improved by 48.16% and 68.51% than that of Y and Z. Figures for X-R20F20 were 20.70% and 73.43% respectively. As the fibre content of R20F15 increased from 1.5% to 2.0%, the strength of X that exceed Y and Z were 60.00% and 97.59%, respectively. PP fibre incorporated into 3DPC mitigates the negative effects from CR. However, excessive fibres and fibre orientation in 3D exclusion printing enhanced the fibre agglomeration and then inhibited mortar entrance and cement hydration. In addition to delamination, crumb rubber is considered an artificial internal defect, leading to a decrease in mechanical strength. All test samples reached their highest strength with 20% CR but then decreased with CR further adding. Reduction ratio was 44.15%, 42.35%, 18.93%, 8.91%, 46.74%, and 37.41% corresponding to X-R20F15, X-R20F20, Y-R20F15, Y-R20F20, Z-R20F15, and Z-R20F20. The decrease ratio in the Y direction was less than half of the others. Moreover, high fibre content counteracted this debilitating effect and the reduction ratio of Y-R20F20 was half of that of Y-R20F15.

The flexural strength of all anisotropic tests rises first and then decreases as rubber content increases (Figure 3b). The flexural strength reduced with the CR increasing and validated the effect of CR as artificial internal defect. CR incorporated the poor cohesiveness between aggregates and cement paste and exacerbated the weakness between layers [11]. Excessive rubber particles in the mortar can cause particle build-up and aggregation due to the softness and elastic properties of rubber [15]. The trend of strength with rubber content is consistent with the research from Ye, Cui [16]. These localized stress concentrations resulting from the aggregation decreased the overall strength of the specimen. Consequently, when the CR was added, it caused a decrease in flexural strength. Strength of X-F15 obtains the lowest strength, which decreases by 6.92% and then increases by 2.76% as CR ratio changes from 0 to 20%

and then to 40%. The highest flexural strength was obtained in the Y with a fibre content of 1.5%. The highest value was 6.715Mpa, 5.240Mpa, and 6.213Mpa, corresponding to CR content of 0, 20%, and 40%. Specially, strength of Y-F20 is lower than Y-F15, different from other directions. Thus, fibres are more likely to agglomerate in the Y direction first. The specific surface area of the fibre enhanced the bondability of fibres to mortar, while fibre lap function promotes the synergistic effect when suffering the bending load. However, excessive fibre also led to weak interfaces increasing. Therefore, the flexural strength was reduced when the effect of interlayer weakness exceeded the reinforcement of fibre.

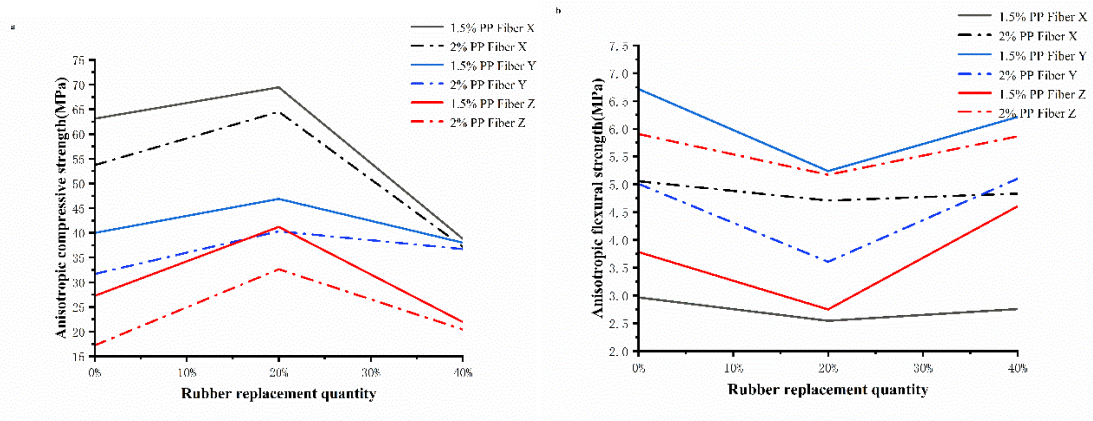

Figure 3. Anisotropic compressive and flexural strength

The strain and fissure development of sample R20F15 were also investigated by Digital Image Correlation (DIC), which were exhibited in Fig. 4. The mid-span deflection of the samples increased with the load increase, where exx represents the horizontal strain. The fissure occurred when the deflection was between 20% and 50% maximum value (x direction). However, the sample would not damage immediately until the 100% u_{max} due to the fiber pull-out effect. The dispersion of fibers occurs parallel to the printing direction, leading to a higher fiber content along the y and z axes. This has been verified in Fig. 4 that the fissures occurred when the deflection was over 50% (y and z directions).

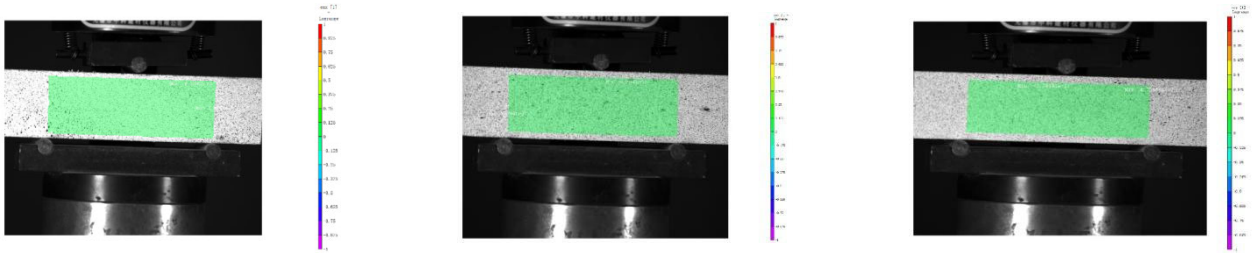

0% u_{max} (X)　　0% u_{max} (Y)　　0% u_{max} (Z)

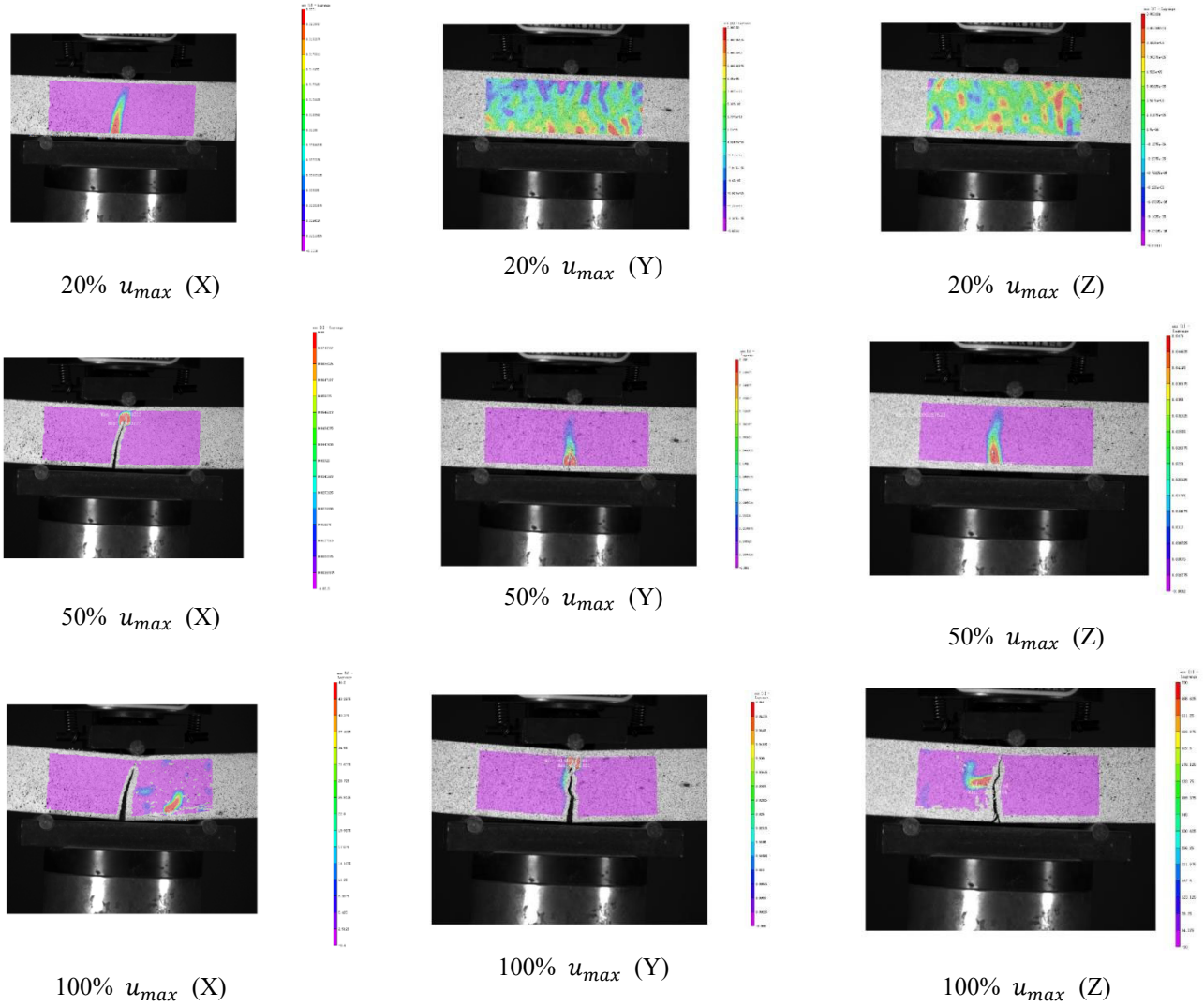

Figure 4. The strain (exx) and fissure development for sample R20F15 in different directions by DIC

4 CONCLUSION

This research set six mix proportions with variables including the rubber ratio and the PP fibre content. The fresh and hardened properties have been analysed considering the variables and effect mechanism, and the following conclusions are drawn:

11. The flowability is positively correlated with the rubber proportion but negatively correlated with the PP fibre content.

12. Fibres are more likely to agglomerate in the Y direction first attributed to the fibre orientation in 3D printing process and excessive fibre incorporation. This phenomenon has been verified by the DIC test.

13. Excessive fibre adds weak interfaces and then decreases the anisotropic compressive strength, while the increasing rubber content reduces the negative effect of fibre agglomeration. The flexural strength reduces when the weak interface effect exceeds the reinforcement of fibre.

REFERENCES

[1]. WOLFS RJM, BOS FP and SALET TAM, *Hardened properties of 3D printed concrete: The influence of process parameters on interlayer adhesion.* Cement and Concrete Research, 2019. **119**: p. 132-140.

[2]. LEE JIAN-YUAN, TAN WEN SEE, AN JIA, CHUA CHEE KAI, TANG CHUYANG Y, FANE ANTHONY G, and CHONG TZYY HAUR, *The potential to enhance membrane module design with 3D printing technology.* Journal of Membrane Science, 2016. **499**: p. 480-490.

[3]. PEGNA JOSEPH, *Exploratory investigation of solid freeform construction.* Automation in construction, 1997. **5**(5): p. 427-437.

[4]. WANGLER TIMOTHY, ROUSSEL NICOLAS, BOS FREEK P, SALET THEO AM and FLATT ROBERT J, *Digital concrete: a review.* Cement and Concrete Research, 2019. **123**: p. 105780.

[5]. PANDA BIRANCHI, RUAN SHAOQIN, UNLUER CISE and TAN MING JEN, *Investigation of the properties of alkali-activated slag mixes involving the use of nanoclay and nucleation seeds for 3D printing.* Composites Part B: Engineering, 2020. **186**: p. 107826.

[6]. ZHANG JINGCHUAN, WANG JIALIANG, DONG SUFEN, YU XUN and HAN BAOGUO, *A review of the current progress and application of 3D printed concrete.* Composites Part A: Applied Science and Manufacturing, 2019. **125**: p. 105533.

[7]. DE SCHUTTER GEERT, LESAGE KAREL, MECHTCHERINE VIKTOR, NERELLA VENKATESH NAIDU, HABERT GUILLAUME and AGUSTI-JUAN ISOLDA, *Vision of 3D printing with concrete—Technical, economic and environmental potentials.* Cement and Concrete Research, 2018. **112**: p. 25-36.

[8]. PANDA BIRANCHI, UNLUER CISE and TAN MING JEN, *Extrusion and rheology characterization of geopolymer nanocomposites used in 3D printing.* Composites Part B: Engineering, 2019. **176**: p. 107290.

[9]. SHAKOR PSHTIWAN, NEJADI SHAMI and PAUL GAVIN, *A study into the effect of different nozzles shapes and fibre-reinforcement in 3D printed mortar.* Materials, 2019. **12**(10): p. 1708.

[10]. ASLANI FARHAD, MA GUOWEI, WAN DOMINIC LAW YIM and MUSELIN GOJKO, *Development of high-performance self-compacting concrete using waste recycled concrete aggregates and rubber granules.* Journal of Cleaner Production, 2018. **182**: p. 553-566.

[11]. SAMBUCCI MATTEO, MARINI DANILO, SIBAI ABBAS and VALENTE MARCO, *Preliminary mechanical analysis of rubber-cement composites suitable for additive process construction.* Journal of Composites Science, 2020. **4**(3): p. 120.

[12]. GENERAL ADMINISTRATION OF QUALITY SUPERVISION INSPECTION AND QUARANTINE OF THE PEOPLE'S REPUBLIC OF CHINA, STANDARDIZATION ADMINISTRATION OF THE PEOPLE'S REPUBLIC OF CHINA., *Test method for fluidity of cement mortar : GB/T 2419-2005 [S] (in Chinese)*. 2005, China Standard Press: Beijing.

[13]. LACHEMI M., HOSSAIN K. M. A., LAMBROS V., NKINAMUBANZI P. C. and BOUZOUBAA N., *Performance of new viscosity modifying admixtures in enhancing the rheological properties of cement paste.* Cement and Concrete Research, 2004. **34**(2): p. 185-193 DOI: https://doi.org/10.1016/s0008-8846(03)00233-3.

[14]. GENERAL ADMINISTRATION OF QUALITY SUPERVISION INSPECTION AND QUARANTINE OF THE PEOPLE'S REPUBLIC OF CHINA, STANDARDIZATION

ADMINISTRATION OF THE PEOPLE'S REPUBLIC OF CHINA., *Standard for test method of mechanical properties on ordinary concrete : GB/T 50081-2019 [S] (in Chinese)*. 2019, China Standard Press: Beijing.

[15]. TURATSINZE A. and GARROS M., *On the modulus of elasticity and strain capacity of Self-Compacting Concrete incorporating rubber aggregates.* Resources Conservation and Recycling, 2008. **52**(10): p. 1209-1215 DOI: 10.1016/j.resconrec.2008.06.012.

[16]. YE J. H., CUI C., YU J. T., YU K. Q. and XIAO J. Z., *Fresh and anisotropic-mechanical properties of 3D printable ultra-high ductile concrete with crumb rubber.* Composites Part B-Engineering, 2021. **211** DOI: 10.1016/j.compositesb.2021.108639.

Proceeding of the 10th International Conference on Innovative Production and Construction (IPC 2024), Perth, Australia, July 11-12, 2024

Research on Defect Detection of Grout Sleeve and Intelligent Grouting Technology

Xiushu Qu and Zexian Du

Beijing University of Civil Engineering and Architecture, Beijing 100044, China

ABSTRACT: Prefabricated concrete structure is a fast, efficient and environmentally friendly construction method, it has become a new trend in the development of the construction industry. Among them, the grout sleeve has been widely used in prefabricated concrete structures as an important rebar connection technology. However, quality defects may occur during the construction process due to insufficient technical skills of construction personnel and difficulty in monitoring the construction process. Moreover, existing detection methods have shortcomings such as poor applicability and low accuracy, which seriously affects the construction quality and safety of the overall structure. In this paper, the defect forms of grout sleeves were studied; The existing detection methods were introduced from two aspects: destructive detection and non-destructive detection; The intelligent grouting technology of grout sleeve was studied, and a new type of intelligent grouting equipment was proposed to solve the problem of frequent grout leakage in the grouting layer due to the subjective judgment of construction personnel during the grouting process; Finally, the future development trend of grout sleeve was analyzed from three aspects: non-destructive, digital and intelligent.

KEYWORDS: prefabricated concrete structure; grout sleeve; defect detection; non-destructive resistance method; intelligent grouting technology;

1 INTRODUCTION

Prefabricated concrete structure is regarded as a highly industrialized form of building structure, which has the advantages of short construction period, low energy consumption, green environmental protection, and good development prospects. However, due to the technical level is uneven, and the quality control is not strict, there are certain quality problems in prefabricated concrete structure[1]. In prefabricated concrete structure, seams and nodes connect the prefabricated components into a whole, so that the entire structure has the necessary load-bearing capacity and earthquake resistance. These connections directly affect the structural safety of prefabricated concrete structures and determine the overall quality of the building.

The most widely used and reliable rebar connection in prefabricated concrete structure is grout sleeve connection[2]. It is a metal sleeve made by foundry technology or machining process. The full grout sleeve connection is shown in Figure 1. As an important construction process in the prefabricated concrete structure[3], the steel sleeve grouting connection technology is commonly used for the connection of rebar in vertical and horizontal

components on the construction site. It has the advantages of wide application range, short anchorage length and high reliability. But there is less research on the current grout sleeve connection construction technology, and there is a lack of strict control of construction quality norms and standards, so it is often difficult to ensure the quality of sleeve grouting connections. Moreover, the grout sleeve connection is a hidden project, if the grouting quality does not meet the requirements, it will seriously affect the strength of the subsequent entities. Thereby endangering the structural safety of the entire building and causing heavy losses. Therefore, how to make the grout sleeve quality detection more simple and effective has always been a problem that people need to be solved urgently. The following will conduct a study on the current grout sleeve defect forms, defect detection methods, intelligent grouting technology, and future development trends.

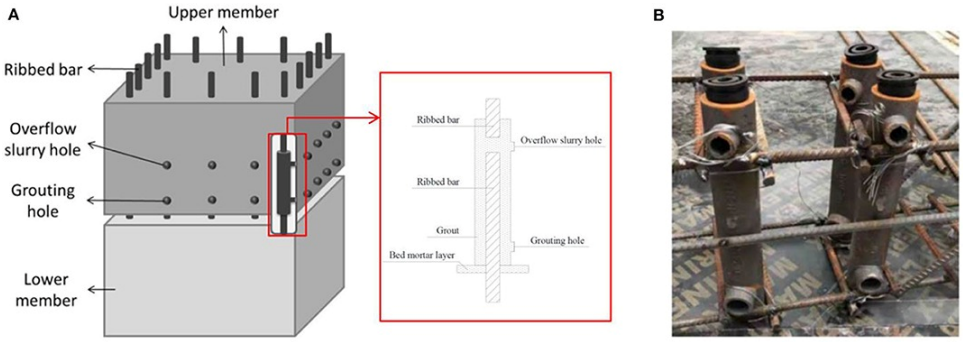

[4]**Fig. 1.** Full grout sleeve connection. (A) Schematic diagram. (B) Physical diagram.

2 RESEARCH ON DEFECT FORMS OF GROUT SLEEVES

In actual projects, various problems such as voids, bubbles, uneven distribution of grouting materials occur in the sleeves due to improper selection of raw materials, and irregular construction operations. The following analyzes the potential hazards and quality issues of different types of grout sleeves.

2.1 Voids and bubbles

In the grouting process, if the construction method is improper or the vibration quality is poor, the bubbles in the grout cannot be effectively excluded resulting to the existence of large voids inside the node. It directly affects the compactness and uniformity of the grout. This will reduce the load-bearing capacity of the sleeve, thereby affecting the mutual coordination and stability of the node and the surrounding structure.

2.2 Quality of grouting materials

When selecting grouting materials, if there is a lack of consideration of factors such as the fluidity and compressive strength of the grout, it will affect the process performance of the grout and the grouting quality of the component nodes. Problems such as poor quality of the selected grouting material, non-compliance with standard requirements, or uneven mixing may lead to insufficient strength and poor compactness of the grout sleeve. Ultimately it will affect the stability and durability of the overall structure.

2.3 Irregular construction technology

Prefabricated concrete structure is a new type of construction mode, but at present there is less research on the construction process of grout sleeve connection, and there is a lack of strict norms and standards for controlling the construction quality, which resulting in the prevalence of uneven levels of construction personnel. During the construction process of the grout sleeve, if there are problems such as irregular operation and equipment failure, it will lead to uneven distribution of grouting material in the node. Some parts are over-grouted, and other parts are under-grouted. This uneven distribution will directly affect the strength and stability of the node, reducing its bearing capacity[5]. Moreover, the uneven thickness of the grouting layer poured inside the grout sleeve may also cause structural instability, which will increase the risk of uneven stress on the structure, and even cause structural damage. Thereby it will affect the use effect and life of the sleeve.

Influenced by the above factors, during the grouting process, the sleeve often suffers from grout level defects, defects in the upper part of the sleeve, defects in the middle part of the sleeve, and eccentricity of the reinforcement. The defect in the upper part of the sleeve is shown in Figure 2. Li Xiangmin et al.[6] determined through tests that under the same circumstances, the length of the upper defect is greater than 30% of the unilateral anchorage length or 15% of the central defects will occur when the joint is brittle. It seems that when the middle defect occurs in the sleeve, it has the most serious effect on the strength of the joint, and at present there are fewer inspection methods that can conveniently detect the middle defect without damaging the sleeve.

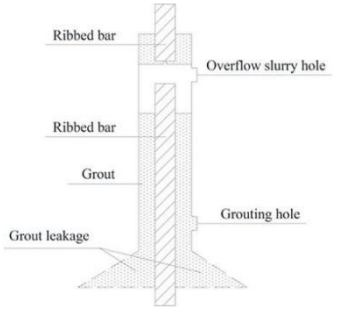

[4]**Fig. 2**. Diagram of defect in the upper part of the sleeve.

3 RESEARCH ON DEFECT DETECTION OF GROUT SLEEVE

The current defect detection methods of grout sleeve in engineering are categorized into destructive testing and non-destructive testing based on whether it causes damage to the detection target. Destructive testing generally causes irreversible damage to the structure itself, such as pre-embedded sensor method, borehole endoscope method and so on; Non-destructive testing mainly includes ultrasonic wave method, preformed hole endoscope method, pre-embedded wire pulling method, resistance method and so on. In actual projects, multiple methods are often combined with each other to improve the accuracy of detection[7]. Through the study of comparisons and examples of various detection methods, the principle of detection and the evaluation of the applicability were obtained as follows.

3.1 Destructive testing method

3.1.1 Pre-embedded sensor method

The pre-embedded sensor method is by pre-embeded sensor at the grout outlet, the sensor generates vibration at a certain frequency under a specific signal, and it receives the vibration wave conduction signal outside the sleeve. Determine the internal defects of the sleeve by analyzing the vibration wave frequency and amplitude curve. The sensor diagram is shown in Figure 3. Existing research has shown that the vibration signal is fed back by the sensor can quickly and intuitively reflect the fullness of the grout sleeve[8]. The pre-embedded sensor method is suitable for detection during the grouting process. This method can more accurately judge the fullness of the grout sleeve. In actual operation, secondary grouting can also be performed based on the test results to ensure construction quality. However, due to problems such as non-standard operation of construction personnel, insufficient standardized procedures, high cost of testing equipment and so on, the application effect is not as good as expected in the test[9].

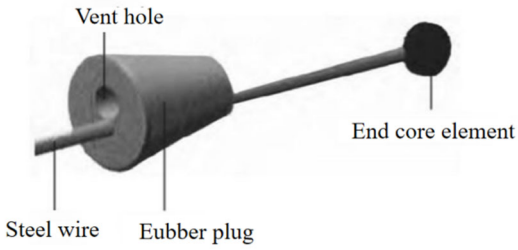

[10]**Fig. 3.** Sleeve grouting detection sensor.

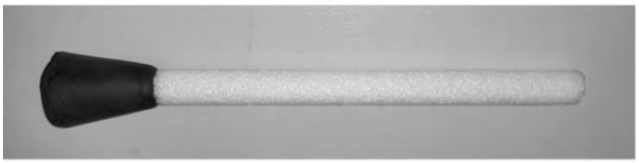

[14]**Fig. 4.** Diagram of preformed hole device

3.1.2 Borehole endoscope method

The borehole endoscope method uses an endoscope in the slurry outlet hole of the sleeve to detect the fullness of the grout sleeve and possible defects. The test results can be presented clearly and intuitively. The borehole endoscope method is easy to operate and suitable for detection of prefabricated concrete structure, but it will cause damage to the sleeve[11].

3.2 Non-destructive testing method

3.2.1 Ultrasonic wave method

The ultrasonic wave method is based on Fermat's principle. When there are defects such as holes in the grouting material, the ultrasonic wave will bypass the defective area and propagate along the shortest path to detect the grout defects[12]. The ultrasonic wave method does not damage the sleeve and can detect the overall defects of the sleeve. However, it cannot accurately determine the size and specific location of defects, and it has high environmental requirements. In addition, when using the ultrasonic wave method, transmitting and receiving transducers must be arranged, and the requirements for detection conditions are relatively high[13].

3.2.2 Preformed hole endoscope method

The preformed hole endoscope method uses rubber plugs and heat shrink components to seal the outlet hole after the slurry flows out, after the operation is completed, the rubber plug is pulled out and the three-dimensional imaging measurement endoscope is inserted to obtain a three-dimensional image of the defect. The diameter of the outlet hole can be controlled by

heating the heat shrink components. Sun Bin et al.[14] designed a preformed hole device, which can be placed into the outlet hole instead of the rubber plug. After the grouting material solidifies, the device can be taken out to form a detection channel. Combined with the data from the three-dimensional imaging digital scan of the endoscope, the size of the grouting hollow area can be accurately calculated. The preformed hole device is shown in Figure 4.

3.2.3 Pre-embedded wire pulling method

The pre-embedded wire pulling method is to extend the special steel wire horizontally from the outlet hole of the sleeve to the surface of the rebar close to the outlet hole before grouting[15]. After the grouting material solidifies, the steel wire is polled out, and the fullness of the grout sleeve is judged by the pulling load value. The pre-embedded wire pulling method is simple to operate and has high detection accuracy, and it can be used for on-site detection. But it is easily affected by factors such as temperature and humidity at the construction site, and the maintenance age cannot be determined uniformly and accurately. The results of the pull-out test are greatly affected by the construction quality of the pre-embedded steel wires, and there is also a disturbance inside the structure when the steel wires are pulled out. The pre-embedded steel wire is as shown in the Figure 5.

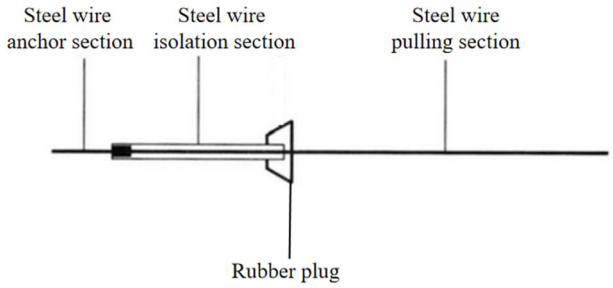

[16]**Fig. 5.** Pre-embedded steel wire.

3.2.4 Resistance method

The resistance method is based on the characteristic that the electrical conductivity of the grouting material decreases with increasing hydration time. A detection device is installed on the top of the sleeve, and the fullness of the grout sleeve is judged by measuring the resistance value between the two probes. The resistance method is simple and intuitive, it can detect fullness to a certain extent. But the scope of use is limited and there is a lack of engineering verification. The detection device is shown in Figure 6.

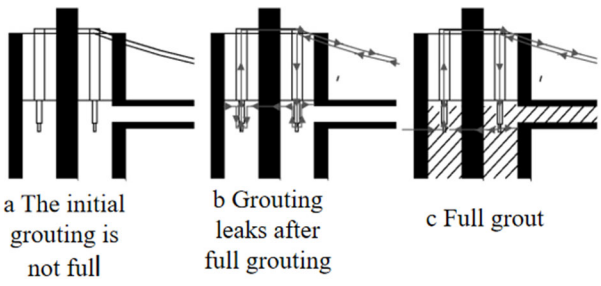

[17]**Fig. 6.** Resistance method current trend.

3.2.5 Non-destructive resistance method

After the grouting material is fully stirred, a large number of conductive ions are suspended in the grout slurry. When electrodes are applied to both ends of the sleeve, the conductive ions in the grout slurry will move directionally to form an electric current. Based on this, non-destructive resistance method is used to detect grouting defects[18].

The device for the non-destructive resistance method is shown in the Figure 7. After the grouting is completed, the grouting hole and the outlet hole of the sleeve are plugged with rubber plugs equipped with metal probes. Afterwards, the DC resistance detector is turned on, and the resistance value displayed on the screen is used to determine the form and volume of defects inside the sleeve. The non-destructive resistance method can better detect various grout sleeve defects with high detection accuracy. The detection process will not cause damage to the sleeve. Therefore, this method has obvious advantages of being convenient, accurate, and non-destructive, and can be extended to construction sites.

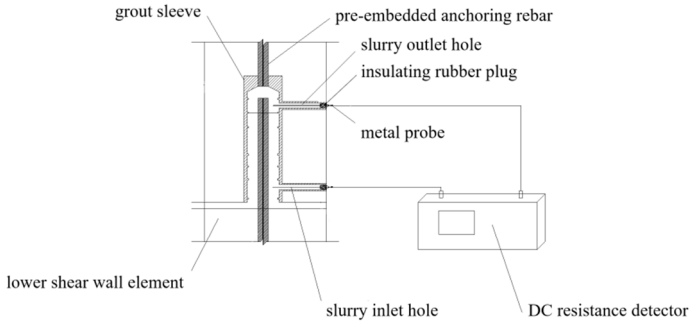

[19]**Fig. 7.** Schematic diagram of non-destructive resistance method.

4 RESEARCH ON INTELLIGENT GROUTING TECHNOLOGY OF GROUT SLEEVE

During the construction process, in order to simplify the grouting process, the duct grouting method is often used. The shear wall and the plane on the shear wall are used to form a sealed grouting layer space, so that multiple sleeves can be grouted at the same time through a single hole. But the grouting operation is mainly subjectively judged by workers, and there is uncertainty. Slurry leakage often occurs due to loose sealing of the grout layer. Moreover, the grout leakage part cannot be monitored, it causing the liquid level in the sleeve to drop and the quality of grouting in the sleeve to be poor. Ultimately, the joint connection strength is insufficient, which affecting the quality and safety of the structure.

An intelligent grouting device for grout sleeve is provided to solve the problem that the sleeve grouting equipment in the prior art relies on manual subjective judgment of grouting, which often causes grout leakage in the grouting layer. The intelligent grouting device is shown in Figures 8 and 9. When using this equipment, the sleeve is grouted through the grouting equipment, and the slurry in the sleeve rises into the cavity of the pressure detection component. Then the slurry drives the piston to move upward, eventually the second cavity becomes a closed space. Real-time pressure is transmitted to the control components. As the height of the slurry in the second chamber increases, the pressure is detected will increase. When the pressure is detected by the pressure detection component exceeds the preset value, the piston can no longer move upward and the slurry can no longer rise. When all the pressure detection components connected to the sleeve detect that the pressure exceeds the preset value,

the slurry levels in all sleeves have reached the preset height. Afterwards, the controller sends corresponding signals to the grouting equipment, and the grouting equipment stops injecting grouting into the sleeve. This device realizes real-time detection of the pressure inside the sleeve. When the pressure inside the sleeve reaches the preset value, it will automatically stop grouting into the sleeve. This realizes the automation of the sleeve grouting process and ensures the quality of the sleeve grouting.

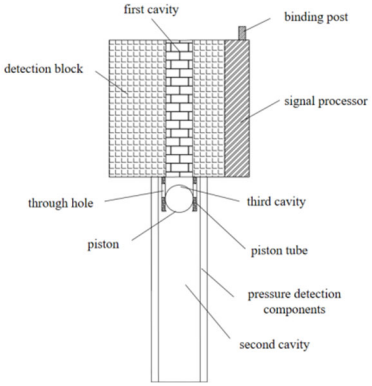

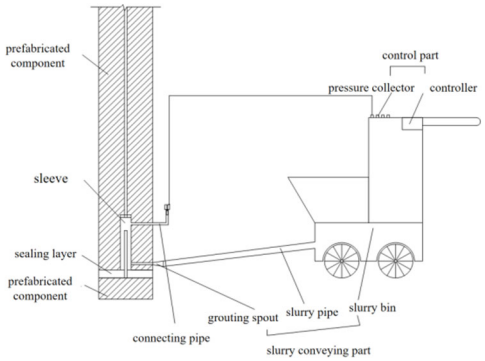

Fig. 8. Cross-sectional view of the grouting pressure detection plug of the grout sleeve. **Fig. 9.** grouting equipment of grout sleeve.

5 DEVELOPMENT TREND OF GROUT SLEEVE DETECTION TECHNOLOGY

The grout sleeve is an important connection node in the prefabricated concrete structure, and its detection method is a key link in structural safety assessment and quality control. With the advancement of science and technology and the improvement of construction level, the development of grout sleeve detection technology is becoming more and more suitable for engineering practice. The following is an analysis and summary of the development trends of grouti sleeve detection technology:

First, non-destructive detection methods will be more widely used. Traditional grout sleeve detection methods often require destroying the sleeve. However, with the continuous improvement of non-destructive detection technologies such as resistance method, ultrasonic wave method, and X-ray method, these technologies can be used to achieve no damage to the sleeve. And the internal structure and performance of the grout sleeve are quickly and accurately evaluated. This ultimately improves inspection efficiency and protects structural integrity. Therefore, we need to verify the accuracy and application methods of different non-destructive detection methods through a large number of experiments, numerical

simulations and theoretical analysis, and promote the widespread application of non-destructive detection methods.

Secondly, the application of digital technology in grout sleeve detection will become more common. With the rapid development of technologies such as artificial intelligence, big data and so on, digital inspection technology has been widely used in the field of structural monitoring. In the future, the deformation and stress of the grout sleeve can be monitored in real time through the sensor network[20,21]. And it combines data analysis and algorithm models to achieve accurate prediction and diagnosis of the safety status of the structure, so that construction workers can perform secondary grouting in a timely manner to improve the reliability and safety of the structure.

Finally, the application of intelligent detection equipment and machine learning algorithms will promote the further development of grout sleeve detection technology. Intelligent detection equipment can automatically identify defects in the sleeve, which improving detection efficiency, accuracy and structural safety. Machine learning algorithms can be trained with large amounts of data to achieve intelligent judgment and prediction of structural health status, which providing a more direct and scientific basis for structural maintenance and management.

In summary, with the continuous advancement and improvement of science and technology, engineering technology, construction methods and various specifications, grout sleeve detection technology will show development trends such as non-destructive, data-based and intelligent. This will provide more effective means and methods for quality monitoring of grout sleeves and structural safety of prefabricated concrete structure, and promote progress and development in the field of structural monitoring.

REFERENCES

[1]. Y. Huan. Quality inspection and control of prefabricated wall panel steel sleeve grouting connections. Sichuan Architecture 41.06(2021):203-204+207. in Chinese.

[2]. G. Zhengxing, Y. Wen. Experimental study on the fullness of grouting material for sleeve grouting connections of prefabricated concrete structures. Jiangsu Architecture. 03(2018):4-8. in Chinese.

[3]. Liu J, Li D, Cui X. Research status and future directions of defect detection in grouted splice sleeves: A review. Construction and Building Materials. 2023 Oct 26;402:133010.(2023)

[4]. Tang, H. , Xie, Y. , Zhao, T. , Xue, S. Identification of grout sleeve joint defect in prefabricated structures using deep learning. Frontiers in Materials, 7, 298. (2020)

[5]. Y. Dai, et al. Research on quality defects analysis and solution measures of sleeve grouting joints in prefabricated buildings. Chongqing Architecture 22.07(2023):55-57. in Chinese.

[6]. L. Xiangmin, et al. Experimental study on the influence of grouting defects on the strength of steel sleeve grouting connection joints. Building Structures 48.07(2018):52-56. in Chinese.

[7]. F. Linfeng, et al. Comparative study on the application status and applicability of on-site detection methods for sleeve grouting fullness. Building Structures 53.S2(2023):1716-1721. in Chinese.

[8]. C. Long, L. Wenzheng, Z. Xiaoling. Research on on-site detection of grouting fullness of precast exterior wall sleeves of a prefabricated concrete structure. Construction Technology 49.S1(2018):169-170 in Chinese.

[9]. L. Chang. Research on the application status of non-destructive testing technology in the detection of grouting density of sleeves in prefabricated buildings. China High-tech. 19(2023):143-146. in Chinese.

[10]. K. Zhengyan, P. Jianhe, H. Gaofeng. Research and application status of sleeve grouting fullness detection method. Sichuan Building Science Research 49.01(2023):62-68+87. in Chinese.

[11]. Li X, Gao R, Xu Q, Wang Z, Zhang F, Liu H. Experimental study on testing grouting plumpness of sleeve by drilling method combined with endoscopy. Constr. Technol (2019);48:6-9.in Chinese.

[12]. Li D L H .Detection of sleeve grouting connection defects in fabricated structural joints based on ultrasonic guided waves.Smart Materials & Structures, (2019), 28(8).

[13]. Xu B , Fan X , Wang H ,et al. Experimental study on grout defects detection for grouted splice sleeve connectors using stress wave measurement. Construction and Building Materials, (2021), 274(3):121755.

[14]. S. Bin, et al. Experimental study on the prefabricated hole method to detect the grouting fullness of the prefabricated structural sleeve. Building Structures 48.23(2018):7-10. in Chinese.

[15]. Rundong G , Xiangmin L I , Zhuolin W ,et al.Research on Testing Technology of Grouting Plumpness of Sleeve Based on Embedded Steel Wire Drawing Method.Construction Technology, (2017).

[16]. Li Hu, et al. Research progress and development trends of sleeve grouting connection quality detection technology for prefabricated concrete structures. Construction Technology (Chinese and English) 52.08(2023):1-9+22. in Chinese.

[17]. G. Hui, et al. Experimental study on monitoring the grouting fullness of steel sleeves by electrical resistance method. Construction Technology 47.22(2018):37-39+95. in Chinese.

[18]. X. Yannan. Research on slurry fullness detection and mechanical properties of steel bar connection grouting sleeves. 2023. Beijing University of Civil Engineering and Architecture, MA thesis.(2023) in Chinese.

[19]. X. Yannan, Q. Xiushu. Research on grouting sleeve fullness detection method and new non-destructive resistance method. Journal of Beijing University of Civil Engineering and Architecture 38.01(2022):79-91. in Chinese.

[20]. Dib, G. , Karpenko, O. , Koricho, E. , Khomenko, A. , Haq, M. , & Udpa, L. Ensembles of novelty detection classifiers for structural health monitoring using guided waves. Smart Materials & Structures(1), 27 (2018). in Chinese.

[21]. Gui, G. , Pan, H. , Lin, Z. , Li, Y. , & Yuan, Z. Data-driven support vector machine with optimization techniques for structural health monitoring and damage detection. KSCE Journal of Civil Engineering, 21(2), 523-534. (2017). in Chinese.

Detection Algorithm for Wearing Safety Helmet in Low Light Scenarios Based on Yolov8

Tao Zeng, Yufeng Wang, Zhiliang Zhu, Guoliang Luo

School of Software, East China Jiaotong University, Nanchang, 330013, China

ABSTRACT: Effective safety supervision at nighttime construction sites is essential to prevent accidents. This study employs the YOLOv8 model to address the challenges posed by poor lighting and complex backgrounds in automated safety helmet detection. We analyze key difficulties such as low contrast and shadow interference and utilize data augmentation techniques to enhance the model's nighttime performance. Our experiments on a specialized dataset demonstrate that YOLOv8 achieves high accuracy and recall in detecting safety helmets, providing robust support for improving nighttime construction safety.

KEYWORDS: YOLOv8, nighttime object detection, safety helmet detection, data augmentation

1 INTRODUCTION

As urbanization accelerates, construction site safety has garnered widespread societal attention. Head injuries, prevalent among various construction accidents, especially under nighttime conditions with limited lighting and visibility, significantly elevate risks for workers. Safety helmets, essential for protecting against head injuries, are critical. However, traditional safety monitoring relying on manual inspections is inefficient and often fails to ensure continuous and comprehensive oversight, particularly at night. This underscores the urgency of developing an automated and effective nighttime safety helmet detection system.

Recent advancements in computer vision and deep learning offer new solutions to these challenges, especially the progress in object detection algorithms. The YOLO (You Only Look Once) series, known for its superior real-time detection capabilities and accuracy, is widely used in industrial and traffic monitoring applications. YOLOv8, the latest iteration, not only inherits the strengths of its predecessors but also significantly improves in accuracy and speed. Nonetheless, applying YOLOv8 directly to nighttime safety helmet detection at construction sites presents several challenges, including poor image quality, small target sizes, and complex backgrounds.

This paper explores a detection scheme based on the YOLOv8 model tailored to the unique requirements of nighttime construction site safety helmet detection. We analyze the challenges in detecting safety helmets in nighttime conditions and enhance the model's recognition capabilities through data augmentation and optimized detection strategies. Our goal is to develop an automated system capable of accurately and swiftly detecting whether workers are wearing safety helmets at night, thereby providing technical support for construction site safety management and reducing safety risks during nighttime operations.

This study aims to offer an effective solution for nighttime safety helmet detection and contribute to the technological advancement in this field.

Detecting safety helmets at nighttime construction sites involves multiple challenges such as dense target distribution, significant scale variations, and complex backgrounds, complicating helmet detection. Recent studies have made strides in this area. Deng et al. [1] developed ML-YOLOv3, a lightweight object detection algorithm designed to address the complex architecture and high computational demands of YOLOv3, integrating CSPNet and GhostNet to create an efficient residual network, CSP-Ghost-Resnet, and a lightweight multi-scale feature extraction network using PAN CSP. Zhou et al. [2] applied YOLOv5 for safety helmet detection, achieving a detection speed of 110 FPS on a dataset of 6,045 annotated images, meeting real-time detection requirements. Chourasia et al. [3] found YOLOv7 to surpass both YOLOv4 and YOLOv5 in accuracy and detection speed for helmet detection. Sun and Wang [4] introduced an improved YOLOv5-based helmet detection algorithm using a residual learning-based feature extraction method to enhance accuracy. Shan et al. [5] integrated an enhanced channel attention mechanism (ECA) with a weighted bidirectional feature pyramid network structure (BiFPN), significantly boosting YOLOv5's performance in helmet detection to an average accuracy of 95.9%. Bochkovskiy et al. [6] contributed YOLOv4, utilizing the PANet path aggregation algorithm and CSPDarknet-53 as its backbone, improving detection precision and balancing speed and accuracy. Jocher et al. [7] introduced an enhanced YOLOv5 in 2020, offering a new solution for real-time object detection tasks. Xu Shoukun et al. [8] proposed a helmet detection method based on an enhanced Faster R-CNN that increased detection accuracy by over 7% and demonstrated improved adaptability to environmental conditions. Silva R et al. [9] identified motorcyclists from surveillance videos using background subtraction and object segmentation techniques, then determining helmet use through visual features and a binary classification method. Zhang et al. [10] designed a system using deep learning to effectively recognize whether workers at substations were correctly wearing helmets and masks, enhancing safety compliance at workplaces. In response to these issues, our study proposes an optimized YOLOv8-based method specifically enhanced for helmet detection under low-light conditions at nighttime construction sites.

Our approach not only incorporates traditional object detection techniques but also integrates advanced image enhancement technologies to boost recognition capabilities in low-light conditions. By refining feature extraction and fusion strategies, our model effectively handles complex backgrounds and dense target distributions typical of nighttime environments, thus reducing false positives and missed detections. Moreover, we explored new loss functions and optimization algorithms to further enhance the accuracy and speed of helmet detection in nighttime construction scenarios. Experimental results show that our improved YOLOv8 model significantly enhances performance in nighttime safety helmet detection tasks, providing an effective automated solution for nighttime construction site safety management.

2 METHOD

As a significant advancement in the YOLO series, YOLOv8 introduces several innovations in the field of object detection aimed at enhancing the model's accuracy and speed, while also

achieving model lightweighting. Compared to its predecessor, YOLOv5, YOLOv8 incorporates the C2f module, a structural enhancement that improves the feature extraction process, allowing the network to handle image features more efficiently. This cross-stage connection facilitated by the C2f module enhances gradient flow, thereby improving feature representation and overall model performance. Another innovation in YOLOv8 is its decoupled head design, which separates classification and localization tasks, reducing interference between the two and allowing the model to focus more on each task, further enhancing detection accuracy. Additionally, YOLOv8 offers various model depths, including YOLOv8n, YOLOv8s, YOLOv8m, YOLOv8l, and YOLOv8x, to accommodate different application needs and computational capacities. This paper utilizes the YOLOv8n model, the structure of which is illustrated in the diagram below:

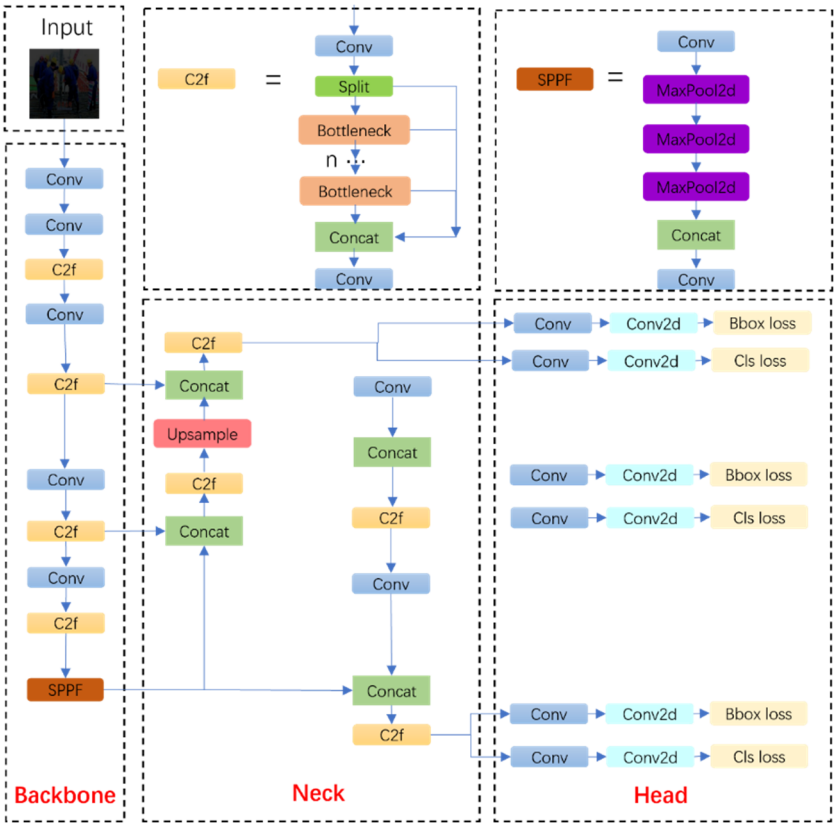

Figure 1: Overall Structure of the YOLOv8 Model

A. C2f Module

The C2f module is one of the core components of YOLOv8 and represents an improvement over the C3 module from YOLOv7. It utilizes deep feature extraction techniques and a series of efficient bottleneck structures to delve deeply into image features while enhancing the network's gradient flow and feature fusion capabilities through cross-layer connections. This design not only improves the model's ability to capture long-range dependencies within images but also enhances detection precision across various scales. The introduction of the C2f module significantly improves the accuracy of object detection while maintaining real-time performance. Additionally, the use of activation functions like SiLU in this module optimizes nonlinear expression, making the model more efficient and robust in complex

scenarios. Overall, the design of the C2f module ensures YOLOv8's powerful detection performance and computational efficiency, making it highly applicable and superior in practical applications.

B. SPPF Module

The SPPF module plays a crucial role in the YOLOv8 architecture, located at the end of the backbone network, where it is responsible for performing spatial pyramid pooling on feature maps to enhance the model's spatial localization accuracy and scale invariance. By pooling feature maps at different scales, the SPPF module captures multi-scale features of the targets, producing outputs of fixed sizes that include global contextual information. These outputs not only contain the local details of the targets but also integrate broader contextual data, enabling the model to better understand the spatial layout of objects. Additionally, the SPPF module enhances the expressiveness of features by merging them across different levels, providing richer and more representative high-level features for subsequent detection tasks. After pyramid pooling, the module employs a series of convolutional layers and nonlinear activation functions to further transform and refine features, which not only optimizes feature representation but also enhances the model's ability to detect targets in complex backgrounds. Overall, the introduction of the SPPF module significantly boosts YOLOv8's accuracy and robustness in object detection, particularly when handling targets that vary in scale and are not fixed in location, showcasing its strong performance advantages.

C. Loss Function

The loss function of the YOLOv8n model integrates classification loss, localization loss, and regularization terms to ensure the model's accuracy and generalization ability in predicting the categories and locations of targets. The classification loss L_{class} is measured by cross-entropy loss, which assesses the accuracy of the model's predictions of target categorie. The calculation formula is:

$$L_{class} = -\sum_{i=1}^{S}\sum_{j=1}^{B}[I_{ij}\log(p_{ij})] \tag{1}$$

In the formula, S represents the grid size, B denotes the number of bounding boxes predicted per grid cell, I_{ij} is an indicator that specifies whether the target j is present in grid cell i. p_{ij} is the probability predicted by the model that target j is present in grid cell i. The localization loss L_{box} ,uses the smooth L1 loss to calculate the difference between the predicted bounding boxes and the actual bounding boxes. The calculation formula is:

$$L_{box} = \sum_{i=1}^{S}\sum_{j=1}^{B}\sum_{k\in\{x,y,w,h\}} I_{ij}\left[t_k - \hat{t}_k\right]^{\mathrm{L1}} \tag{2}$$

Here, t_k represents the parameters of the actual bounding box (center x,中心y,宽度w,高度h),and $\hat{t}_k$ are the corresponding parameters predicted by the model. The regularization term, $L_{regularization}$ uses L2 regularization to prevent the model from overfitting. The calculation formula is:

$$L_{regularization} = \lambda \sum_{l} || \theta_l ||^2 \tag{3}$$

Where θ_l represents the weights of the l-th layer of the model, and λ is the regularization coefficient. Combining these parts, the total loss function of YOLOv8n is expressed as:

$$L_{total} = L_{class} + L_{box} + \lambda \bullet L_{regularization} \tag{4}$$

3 EXPERIMENTAL ENVIRONMENT CONFIGURATION AND DATA PREPARATION

3.1 Experimental Environment Setup

To thoroughly validate the performance of the YOLOv8 model and conduct efficient experimental tests, we established an advanced experimental environment. The operating system is Windows 10, the CPU is an Intel(R) Core(TM) i7-9700K, and the GPU is an NVIDIA RTX 4070 equipped with CUDA 11.0, which significantly enhances the training and inference efficiency of deep learning models. Overall, this experimental environment ensures stable operation and excellent performance of the YOLOv8 model under high-load conditions.

3.2 Dataset

In this experiment, we utilized a dataset of 20,000 nighttime construction site worker images annotated in the PASCAL VOC format, covering three categories: helmets, people, and heads. Each image, precisely marked with bounding boxes, helps the model distinguish between categories. The training set includes 17,248 images with a resolution of 640 x 640 pixels, while the validation set contains 2,438 images for performance assessment.

3.3 Experimental Data Analysis

As shown in Figure 2, we tested the target detection capabilities in a nighttime construction site environment.

Figure 2: Results of Safety Helmet Detection for Construction Workers at Night

We conducted a detailed evaluation of the YOLOv8 model on a nighttime construction worker image dataset. Results, as summarized in Table 1, show the model achieving 86.6% precision and 84.6% recall across 21,032 instances, resulting in an mAP@0.5 of 88.5% and an mAP@0.5-0.95 of 55.7%. This reflects high detection accuracy and robustness. The model excelled in helmet detection with 93% accuracy and an mAP@0.5 of 92.4%, crucial for construction site safety. Vest detection achieved 77.3% accuracy and 83% mAP@0.5, demonstrating effectiveness. Head detection showed the highest accuracy at 89.6%, though with room for improvement in recall and mAP scores, indicating potential areas for model enhancement.

Table 1 Experimental Results

Class	images	R	mAP50	mAP50-95
all	2438	0.8446	0.885	0.557
helmet	2438	0.871	0.924	0.623
vest	2438	0.784	0.83	0.558
head	2438	0.882	0.902	0.489

Overall, the results indicate that the YOLOv8 model demonstrates high accuracy and robustness in detecting images of construction workers at night, particularly excelling in the detection of helmets and heads. However, there is still room for improvement in the detection performance of vests and heads at high confidence levels.

4 CONCLUSION

This study conducted an in-depth analysis and extensive experiments on nighttime construction site safety helmet detection using the YOLOv8 model. The results show that the model achieves high accuracy and high recall rates even in low-light and complex backgrounds. Particularly in safety helmet recognition, the model demonstrated a 93% accuracy rate and an 87.1% recall rate, effectively supporting nighttime construction site safety management. Through data enhancement techniques and optimized experimental environment configurations, the model's recognition capabilities have been significantly improved, providing strong technical support for construction site safety supervision and laying the foundation for the development of related technologies in the future.

REFERENCES

[1]. Deng L, Li H, Liu H, et al. A lightweight YOLOv3 algorithm used for safety helmet detection[J]. Scientific reports, 2022, 12(1): 10981.

[2]. Zhou F, Zhao H, Nie Z. Safety helmet detection based on YOLOv5[C]//2021 IEEE International conference on power electronics, computer applications (ICPECA). IEEE, 2021: 6-11.

[3]. Chourasia S, Bhojane R, Heda L. Safety helmet detection: a comparative analysis using YOLOv4, YOLOv5, and YOLOv7[C]//2023 International Conference for Advancement in Technology (ICONAT). IEEE, 2023: 1-8.

[4]. Sun L, Wang L. An improved YOLO V5-based algorithm of safety helmet wearing detection[C]//2022 34th Chinese Control and Decision Conference (CCDC). IEEE, 2022: 2030-2035.

[5]. Shan C, Liu H M, Yu Y. Research on improved algorithm for helmet detection based on YOLOv5[J]. Scientific reports, 2023, 13(1): 18056.

[6]. Bochkovskiy A, Wang C Y, Liao H Y M. Yolov4: Optimal speed and accuracy of object detection[J]. arXiv preprint arXiv:2004.10934, 2020.

[7]. Jocher G, Nishimura K, Minerva T, et al. YOLOv5 https://github. com/ultralytics/yolov5[J]. Accessed March, 2020, 7: 2021.

[8]. Shoukun X, Yaru W, Yuwan G, et al. Research on helmet wearing detection based on improved Faster RCNN [J][J]. Computer Application Research, 2020, 37(03): 901-905.

[9]. Silva R, Aires K, Santos T, et al. Automatic detection of motorcyclists without helmet[C]//2013 XXXIX Latin american computing conference (CLEI). IEEE, 2013: 1-7.

[10]. Zhang H, Yang N, Chen H, et al. Safety Helmet and Mask Detection in substation Based on Deep Learning[C]//2022 4th International Conference on Electrical Engineering and Control Technologies (CEECT). IEEE, 2022: 145-150.

Proceeding of the 10th International Conference on Innovative Production and Construction (IPC 2024), Perth, Australia, July 11-12, 2024

Integrating Artificial Intelligence with Building Information Modelling: A Novel Approach for Spatial Point Dataset Generation

Sang Du, Lei Hou and Guomin (Kevin) Zhang

School of Engineering, RMIT University, Melbourne, 3000, Victoria, Australia

ABSTRACT: Artificial Intelligence (AI) has begun to integrate with the Architectural, Engineering, and Construction (AEC) industry in recent years. Although the market has seen many applications of AI in rendering, there remains a shortage of AI applications towards the model level. One of the major challenges for integrating AI at the model level is the difficulty AI faces in utilising model data. This research proposes a novel method using Unreal Engine (UE) and the Industry Foundation Classes (IFC) scheme in a Building Information Modelling (BIM) environment to generate spatial point data. This data not only satisfies the accessibility requirements for AI algorithms to train but also offers the flexibility to prepare data for various AI purposes. The further application of this method could significantly facilitate the integration of AI with the AEC industry.

KEYWORDS: BIM; AI; IFC; unreal engine; dataset

1 INTRODUCTION

With the significant advances in Artificial intelligence (AI) in recent years, AI applications are now adopted in many industries including the Architectural, Engineering and Construction (AEC) industry [1,2]. Some commercial AI applications for architectural purposes exist on the market to assist the design process, for example, the application of Stable Diffusion and the Midjourney [3]. Both applications are being used for architectural rendering generation which allows the designer to foresee the final rendered scenes in different design styles. However, most existing AI tools for design stages are limited in AI rendering scenarios, just like the 2 tools mentioned above. AI rendering is a concept derived from image-generative AI where the AI algorithm is trained from actual building renderings to learn the features and styles of architectural design from an image perspective [4,5]. While AI rendering significantly aids in creating visual content, the output images do not offer precise accuracy regarding the dimensions of depicted elements let alone the semantics in between. To bring AI integration a step closer to a more practical application, the desired AI is required to access the complete information of a building design. In the AEC industry, Building Information Modelling (BIM) serves as a comprehensive digital representation that encapsulates all facets of a building project, from geometric details to time schedules, cost estimates, and operational data, thereby facilitating an integrated platform for design, construction, and facility management [6–9]. However, integrating AI with BIM models remains challenging. BIM standards are designed to facilitate the seamless exchange of building information among various software and platforms [10]. Consequently, the model files

are structured primarily for the reconstruction of the building model in different software environments, rather than for direct data access. This structure supports interoperability but complicates the direct extraction of data needed for AI applications. This research proposes a new approach for converting BIM model data into spatial point data, which can be directly utilised by AI algorithms while preserving the spatial relationships among building elements. The outcomes of this approach will serve as the foundational dataset for subsequent advancements in AI applications.

2 LITERATURE REVIEW

BIM standard itself is designed to contain as much information in a building model as possible and become the central data hub of a project. In the research, the open BIM standard Industry Foundation Classes (IFC) is selected for not only its wide adoption around the AEC industry[11–13] but also for its openness to secondary development. For example, in the work of Wu et al. [14] the integration of BIM within geotechnical engineering was discussed and an IFC-based platform was introduced to facilitate the data exchange at the software level. The feature of enriched data also makes the IFC format available option for AI datasets. Emunds et al. [15] proposed IFCnet, which comprises single-entity IFC files spanning a broad range of IFC classes to facilitate IFC entity classification. Xu et al. [16] developed a dataset to facilitate BIM-based quality management processes with IFC models. While in terms of spatial data, many of the related data sets concentrate on the classification and conversion of spatial data into BIM models. For example, in Heritage-BIM (H-BIM), the transformation of point cloud data to a BIM model is a hot topic. The work of Reina Ortiz et al. [17] discussed the integration of various spatial data within a BIM environment including photography, photogrammetry, laser scanning, and reflectance transformation imaging (RTI). Croce et al. [18] proposed a method to utilise point cloud data as an AI database to facilitate Scan-to-BIM in H-BIM. In the construction stage, auto-update of the as-built BIM model is another active research area. For example, Razali et al. [19] utilised a laser scanning dataset to perform as-built reconstruction and validate its accuracy. In the design stage, some research focuses on the individual elements. In the work from Yu et al. [20], The author developed a parametric augmentation approach to create synthetic copies of BIM elements, enriching model instances and generating datasets for further AI applications. On the other hand, there is a lack of spatial-based building datasets available on a project scale. This gap is precisely what this research aims to address. The objective is to fill this void with an approach to generate datasets from existing BIM models.

3 METHOD

The proposed method aims to create customised bridge datasets for each AI application. IFC model files contain the most information and are maintained as the rawest form of all data. AI algorithms interpret data in pure numbers without understanding their representation in the real world. For example, image-related AI algorithms interpret images as data points within a 3-dimensional RGB colour space, where each dimension represents the numerical value associated with one of the three colours: red, green, and blue. The AI algorithm then learns the hidden pattern within the data points and eventually makes predictions. Similarly, for building models, the information will also need to be converted to a unified number-based

format. Traditional building documentation employs drawings to encapsulate the extensive and intricate information contained within a design. However, this approach is built upon the imaginative capacity of the human brain. Humans understand that facades are orthogonal projections of floor plans in different directions, thereby mentally rendering the 3-dimensional building model. In contrast, AI algorithms cannot imagine the model in space. Therefore, the data must be formatted as 3-dimensional data points so that AI algorithms can 'see' the entire model and uncover hidden information within. The idea of the proposed method is derived from the common BIM application of clash detection. As a conceptual strategy, a model space can be partitioned into diminutive cubic volumes, with each cube being systematically tagged with spatial coordinates. When the building model is reconstructed in this model space and naturally overlaps with the cubic volumes. Then a clash detection will be performed on every cubic. For any clash detected, the spatial coordinates from the cubic volume and IFC scheme-based building information from the building element will be extracted. The coordinates and building information are then integrated as one data file. The result of this approach will be a multi-dimensional list of point data with selected information. This clash detection utilises Unreal Engine (UE) and its Application Programming Interface (API) to carry out. UE is a highly popular and advanced game engine developed by Epic Games and provides highly realistic physics simulation, dynamic weather systems, and advanced material responses, enabling environments and objects to interact in lifelike ways. This makes it a powerful tool not only for game development but also for other applications such as film, television, architecture, and automotive design [21,22]. The method is carried out in 4 steps namely data collection, data conversion, clash detection, and visualisation.

Data collection

The initial data for this method is collected from IFC model files. The following rules are applied to the selection of model files. Level of Detail (LoD) refers to the degree of specificity and detail contained in a BIM model at various stages of design, construction, and operation [23]. The model's LoD is highly related to the needs of downstream applications. However, to ensure consistency of information across the models, the LoD of all selected models should remain at the same level. The IFC standard has multiple versions available, with the latest being IFC4. For this research, IFC2x3 has been selected instead of the latest, IFC4. The reason is that some software in the toolchain only accepts the older IFC2x3 format. This is the only obstacle preventing the application of IFC4 and can easily transit to IFC4 in the future. If building modelling is conducted in BIM authoring software like Revit, converting the model from a proprietary format to IFC is necessary. As the final dataset acquires its ground truth tag from IFC properties, it's important to configure the registration of model elements during this conversion to ensure consistency across files.

Data conversion

In this research, the latest version UE 5.3.2 is utilised. UE5 comes with a collection of tools and plugins that bring entire pre-constructed scenes and complex assets created in a variety of industry-standard design applications into UE called Datasmith. This includes the support of IFC file import. However, the imported model in UE by default does not have property for the

physical simulation. Therefore, models must convert first to obtain the property. This process can be done semi-automatically with the tool Dataprep within Datasmith. A dataprep recipe can provide all static mesh in the model with collision complexity as in Fig.1.

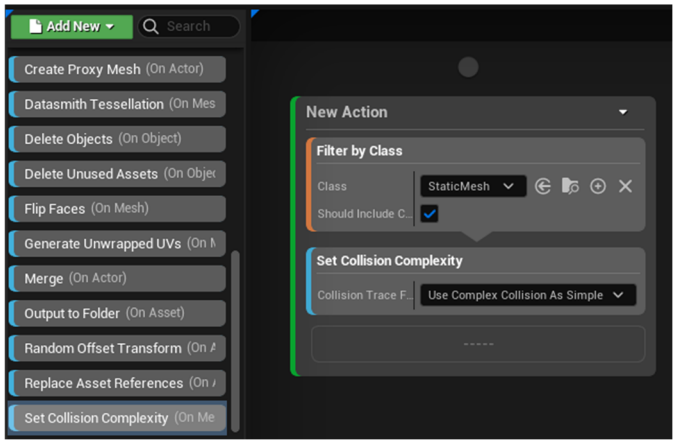

Fig. 2. Dataprep recipe

Clash detection

Clash detection in UE is carried out using a Python script from the UE API. The UE interface offers direct functionality to execute Python scripts within a project. UE, as a game engine, possesses advanced functions for clash or collision detection, widely used in video games. The API method box_overlap_actors plays a crucial role in this process by testing whether a box-shaped space in the model overlaps with 'actors,' a term referring to model elements in the UE context. The model space in UE is organised using internal coordinates, with the default coordinate unit set to 1 cm. This approach divides the model space into small cubic volumes with 5 cm sides, within a predefined spatial range. Each cubic volume is defined by its central point and the distances of its faces from this central point. The Python script iterates through all the central points, performing clash detection for each. If a clash occurs, the script extracts the necessary information from the colliding object and pairs it with the coordinate as a data point. If there is no clash, the coordinate is marked as void. Ultimately, a data array is created to represent the entire space, with each point data representing a cubic model space, tagged with either the extracted information or a void label. The final data is saved in a separate file, utilising the Python library 'NumPy' to manage the data more effectively. This package not only provides a standardised format for accessing the data array but also offers functions to store the data array in a sparse matrix, significantly reducing the file size. The pseudocode of the clash detection is provided as below:

1. Initialise UE API and Python script environment.
2. Define spatial range and partition model space into cubic volumes (5 cm sides).
    a. Each cubic volume is defined by a central point and distances from this point to its faces.
3. For each cubic volume (central point in the predefined spatial range):
    a. Perform clash detection using the 'box_overlap_actors' method.
    b. If a clash is detected:

i. Extract the required information from the colliding object.
ii. Pair this information with the cubic volume's central coordinate.
iii. Tag the paired data as an information point.

c. If no clash is detected:
i. Tag the coordinate as a void point.

4. Aggregate all tagged points (information and void) into a data array representing the whole space.
5. Save the data array as a separate file, with each point representing a cubic model space tagged accordingly.

Visualisation

The output file can be easily visualised using a data visualization library such as 'VisPy'. A demo visualisation is shown in Fig.2, where the different colour of data points represents the IfcClass information from the IFC model file.

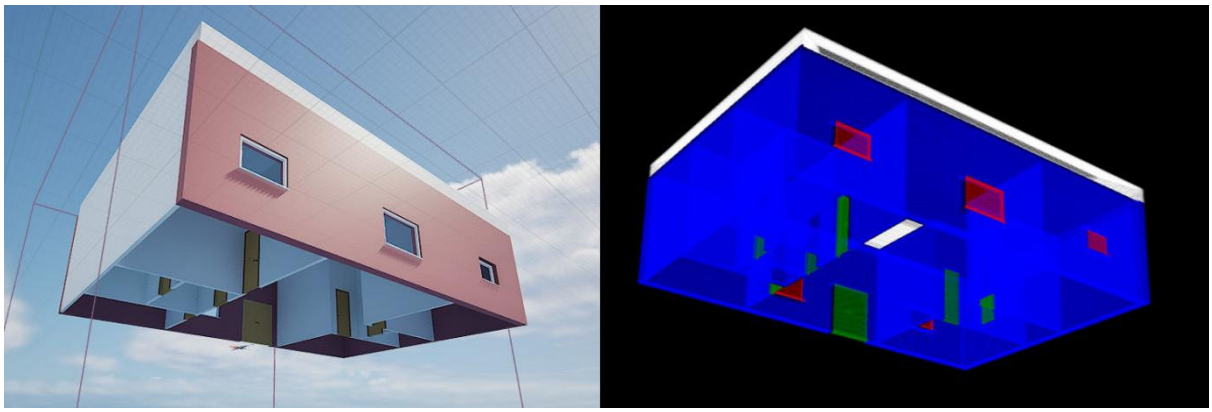

Fig.3. Example of output

4 DISCUSSION

Facilitation of downstream AI applications

The output point data of this method is a high-dimensional data array that reflects the spatial structure of the IFC model and selected information from the IFC scheme. This data structure fits in the current AI algorithms naturally and can be applied in various ways. The spatial features within the model could serve as a data source for AI to learn 3D relationships, like how AI learns from 2D images. Current research on converting point clouds to BIM models has demonstrated that AI can indeed learn spatial features from such data. However, technologies like Light Detection and Ranging (LiDAR) only capture random points on surfaces, resulting in point cloud data that lacks information on the internal structure and does not account for void spaces [24]. This limitation restricts the potential for generating new points outside the dataset's range. The proposed method addresses these issues by providing the algorithm with complete spatial features. It not only reveals the information behind surfaces but also incorporates empty spaces into the algorithm's awareness, enhancing its learning capabilities. Incorporating the IFC schema into this method significantly streamlines data standardisation. Different design software titles building elements uniquely, complicating the aggregation of data for AI applications. The IFC schema enables the transformation of

building information into a unified framework, thereby greatly expanding the dataset range. This, in turn, enhances the training of downstream AI applications.

Computational limitation

Three-dimensional point data significantly increases computational demands throughout the process. On one hand, the data size escalates when transitioning from 2D to 3D. The proposed method samples the entire space to obtain comprehensive spatial data, resulting in a substantial amount of data; for example, even a residential building project occupies a large space. In our setup, a data array of 405x405x105, with each point representing a cubic volume of 5cm, covers only a space of 20.5 meters in length and width and 5.25 meters in height. Such dimensions barely represent a typical residential house in Australia, yet the raw data file is already 500MB in size. On the other hand, the software tools in our pipeline do not support parallel processing for various reasons. This limitation results in a processing time of a couple of minutes, but the computer resource is not fully utilised.

5 CONCLUSION

In conclusion, this study introduces an innovative approach to integrating AI with BIM by converting BIM model data into spatial point data, effectively overcoming the limitations of AI's access to comprehensive building design information. This transformation not only preserves spatial relationships among building elements but also enriches AI datasets, facilitating advancements in AI applications within the AEC industry. Despite facing computational challenges, such as increased data size and processing demands, the methodology represents a significant step forward in bridging the gap between AI capabilities and practical construction needs. Looking forward, the study paves the way for further developments in AI-driven design processes, with a focus on refining techniques, expanding dataset range, and exploring innovative AI applications to enhance design accuracy, efficiency, and innovation in the AEC sector.

REFERENCES

[1]. A. Darko, A.P. Chan, M.A. Adabre, D.J. Edwards, M.R. Hosseini, E.E. Ameyaw, Artificial intelligence in the AEC industry: Scientometric analysis and visualization of research activities, Autom. Constr. 112 (2020) 103081.

[2]. Z. Wang, B. He, Y. Yang, C. Shen, F. Peña-Mora, Building a next generation AI platform for AEC: A review and research challenges, in: Proc 37th CIB W78 Inf. Technol. Constr. Conf. CIB W78 São Paulo Braz., 2020: pp. 27–45.

[3]. J. Ploennigs, M. Berger, AI art in architecture, AI Civ. Eng. 2 (2023) 8. https://doi.org/10.1007/s43503-023-00018-y.

[4]. H. Yan, H. Zhang, L. Liu, D. Zhou, X. Xu, Z. Zhang, S. Yan, Toward intelligent design: An ai-based fashion designer using generative adversarial networks aided by sketch and rendering generators, IEEE Trans. Multimed. (2022).

[5]. H. Jo, J.-K. Lee, Y.-C. Lee, S. Choo, Generative AI and building design: Early photorealistic render visualization of façades using local identity-trained models, J. Comput. Des. Eng. (2024) qwae017.

[6]. S. Matarneh, F. Elghaish, F.P. Rahimian, N. Dawood, D. Edwards, Automated and interconnected facility management system: An open IFC cloud-based BIM solution, Autom. Constr. 143 (2022) 104569. https://doi.org/10.1016/j.autcon.2022.104569.

[7]. M. Li, Y. Liu, B.C.L. Wong, V.J.L. Gan, J.C.P. Cheng, Automated structural design optimization of steel reinforcement using graph neural network and exploratory genetic algorithms, Autom. Constr. 146 (2023) 104677. https://doi.org/10.1016/j.autcon.2022.104677.

[8]. R. Sacks, T. Bloch, M. Katz, R. Yosef, Automating design review with artificial intelligence and BIM: State of the art and research framework, in: ASCE Int. Conf. Comput. Civ. Eng. 2019, American Society of Civil Engineers Reston, VA, 2019: pp. 353–360.

[9]. Q. Shen, S. Wu, Y. Deng, H. Deng, J.C.P. Cheng, BIM-Based Dynamic Construction Safety Rule Checking Using Ontology and Natural Language Processing, Buildings 12 (2022) 564. https://doi.org/10.3390/buildings12050564.

[10].C.M. Eastman, Y.-S. Jeong, R. Sacks, I. Kaner, Exchange model and exchange object concepts for implementation of national BIM standards, J. Comput. Civ. Eng. 24 (2010) 25–34.

[11].Ø. Mejlænder-Larsen, Using a change control system and building information modelling to manage change in design, Archit. Eng. Des. Manag. 13 (2017) 39–51. https://doi.org/10.1080/17452007.2016.1220360.

[12].A. Ahankoob, K. Manley, C. Hon, R. Drogemuller, The influence of building information modelling on the absorptive capacity of project-based organisations, Archit. Eng. Des. Manag. 19 (2023) 1–21. https://doi.org/10.1080/17452007.2021.1881879.

[13].P. Pishdad-Bozorgi, X. Gao, C. Eastman, A.P. Self, Planning and developing facility management-enabled building information model (FM-enabled BIM), Autom. Constr. 87 (2018) 22–38.

[14].J. Wu, J. Chen, G. Chen, Z. Wu, Y. Zhong, B. Chen, W. Ke, J. Huang, Development of Data Integration and Sharing for Geotechnical Engineering Information Modeling Based on IFC, Adv. Civ. Eng. 2021 (2021). https://doi.org/10.1155/2021/8884864.

[15].C. Emunds, N. Pauen, V. Richter, J. Frisch, C. van Treeck, IFCNet: A Benchmark Dataset for IFC Entity Classification, in: Abualdenien J., Borrmann A., Ungureanu L.-C., Hartmann T. (Eds.), EG-ICE Workshop Intell Comput Eng Proc, Technische Universitat Berlin, 2021: pp. 166–175. https://www.scopus.com/inward/record.uri?eid=2-s2.0-85131075535&partnerID=40&md5=5ce560508060650ec61aa31d0dc9cecf.

[16].Z. Xu, T. Huang, B. Li, H. Li, Q. Li, Developing an IFC-Based Database for Construction Quality Evaluation, Adv. Civ. Eng. 2018 (2018) 1–22. https://doi.org/10.1155/2018/3946051.

[17].M. Reina Ortiz, C. Yang, A. Weigert, A. Dhanda, A. Min, M. Gyi, S. Su, S. Fai, M. Santana Quintero, INTEGRATING HETEROGENEOUS DATASETS IN HBIMOF DECORATED SURFACES, Int. Arch. Photogramm. Remote Sens. Spat. Inf. Sci. XLII-2/W15 (2019) 981–988. https://doi.org/10.5194/isprs-archives-XLII-2-W15-981-2019.

[18].V. Croce, G. Caroti, A. Piemonte, L. De Luca, P. Véron, H-BIM and Artificial Intelligence: Classification of Architectural Heritage for Semi-Automatic Scan-to-BIM Reconstruction, Sensors 23 (2023) 2497. https://doi.org/10.3390/s23052497.

[19].A.F. Razali, M.F.M. Ariff, Z. Majid, N. Darwin, A. Aspuri, M.F.M. Salleh, Three-Dimensional (3D) As-Built Reconstruction from Laser Scanning Dataset, in: 2020 IEEE 10th Int. Conf. Syst.

Eng. Technol. ICSET, IEEE, Shah Alam, Malaysia, 2020: pp. 150–155. https://doi.org/10.1109/ICSET51301.2020.9265360.

[20].Y. Yu, D. Ha, K. Lee, J. Choi, B. Koo, ArchShapesNet: a novel dataset for benchmarking architectural building information modeling element classification algorithms, J. Comput. Des. Eng. 9 (2022) 1449–1466. https://doi.org/10.1093/jcde/qwac064.

[21].B. Sanchez, R. Ballinas-Gonzalez, M.X. Rodriguez-Paz, BIM and game engines for engineering online learning, in: 2022 IEEE Glob. Eng. Educ. Conf. EDUCON, IEEE, 2022: pp. 1467–1472.

[22].Y. Wei, B. Akinci, Synthetic Image Data Generation for Semantic Understanding in Everchanging Scenes Using BIM and Unreal Engine, in: Issa R.R.A. (Ed.), Comput Civ Eng - Sel Pap ASCE Int Conf Comput Civ Eng, American Society of Civil Engineers (ASCE), 2021: pp. 934–941. https://doi.org/10.1061/9780784483893.115.

[23].M.L. Trani, M. Cassano, D. Todaro, B. Bossi, BIM level of detail for construction site design, Procedia Eng. 123 (2015) 581–589.

[24].J. Wang, W. Sun, W. Shou, X. Wang, C. Wu, H.-Y. Chong, Y. Liu, C. Sun, Integrating BIM and LiDAR for real-time construction quality control, J. Intell. Robot. Syst. 79 (2015) 417–432.

Proceeding of the 10th International Conference on Innovative Production and Construction (IPC 2024), Perth, Australia, July 11-12, 2024

Research on Prediction and Optimization of Tunneling Parameters for Large-diameter Slurry Balance Shield Machines Using Machine Learning Techniques

Tugen Feng[1,2], Hao Qian[3], Chen Zhang[2], Jian Zhang[2,*], Xusheng Zhang[4]

1. School of Civil Engineering and Surveying & Mapping Engineering, Jiangxi University of Science and Technology, Ganzhou, Jiangxi, 341000, China
2. Key Laboratory of Ministry of Education for Geomechanics and Embankment Engineering, Hohai University, Nanjing, Jiangsu, 210098, China
3. China Railway Construction Urban Development Co., LTD., Hangzhou, Zhejiang, 310000, China
4. Jiangsu Transportation Engineering Construction Bureau, Nanjing, Jiangsu, 210000, China

ABSTRACT: This study presents a hybrid model that combines the extreme learning machine with the sparrow search algorithm to predict and optimize tunneling parameters for large-diameter slurry balance shield machines across different strata. To quantitatively assess the excavation performance of shield machines, a metric termed excavation efficiency is introduced. Utilizing on-site data from the Jiangyin-Jingjiang Yangtze River Tunnel Left Line project, a criterion for high excavation efficiency is established. The proposed model demonstrates superior predictive accuracy for tunneling parameters across different strata, with an average relative error below 3%. Furthermore, the model effectively optimizes tunneling parameters associated with low excavation efficiency, achieving an average improvement of 0.03 m^3/kWh. These results underscore the potential of the model to guide practical engineering projects.

KEYWORDS: large-diameter slurry balance shield machines; tunneling parameter; tunneling efficiency; extreme learning machine; sparrow search algorithm

1 INTRODUCTION

With urbanization rapidly progressing, China has constructed a series of large-diameter shield tunnel projects, such as the Shanghai Yangtze River Tunnel, Jintang Subsea Tunnel, and Shantou Bay Tunnel. Large-diameter shield machines, due to their large excavation area, frequently encounter complex composite strata during construction [1]. In composite strata excavation, slurry balance shield machines are commonly employed [2]. However, the complexity of composite strata increases the variability of tunneling parameters, potentially causing significant changes in the working state of shield machines, thus affecting excavation performance [3]. Therefore, it is vital to predict tunneling parameters across different strata and recommend the optimal parameter combinations suited for the strata.

In recent years, the application of machine learning in the prediction of tunneling parameters has gained significant attention, as evidenced by the numerous studies conducted by scholars [4]. Fan et al. [5] employed a back propagation (BP) neural network to predict

cutterhead torque, energy consumption and grouting pressure using parameters such as total thrust, advance rate and cutterhead speed. Their work demonstrated the potential of neural networks in capturing complex relationships within tunneling data. Relying on the Xinjiang YEGS tunnel project, Lu and Shi [6] used a kernel extreme learning machine optimized through variational modal decomposition and Levy-hunter-prey optimizer to predict advance rate. The results revealed that their model can accurately reflect the actual environmental conditions. Adopting the Songhua River water conveyance project as a case study, Zhang et al. [7] integrated the particle swarm optimization algorithm with a bi-directional long short-term memory model. This hybrid model was designed to predict tunneling parameters under different surrounding rock conditions, as encountered in practical engineering scenarios. Furthermore, Fu et al. [8] made significant strides by applying a hybrid transfer learning framework based on least squares support vector regression. They used 44 shield machine parameters as inputs to achieve dynamic prediction of cutterhead torque. However, whether in homogeneous or composite strata, a common limitation of the studies is the lack of consideration for geological parameters.

The continuous improvement of shield construction technology has indeed highlighted the importance of setting reasonable tunneling parameters to enhance the excavation performance of shield machines [9]. In the field of deformation control optimization, Guo and Zhang [10] proposed a hybrid data-driven approach that aims to mitigate accumulative settlement and building tilt rate by indirectly optimizing some other tunneling parameters. Liu et al. [11] had also contributed to this filed by combining the grey wolf optimizer with the generalized regression neural network and introducing the non-dominated sorting genetic algorithm II. Their work aimed to solve multi-objective optimization problems, focusing on the advance rate and surface settlement as control objectives. By providing decision support for tunneling parameters under conditions of uncertainty, their work has provided a robust tool for engineers to balance the competing demands of efficiency and safety during tunnel construction. In terms of other optimization objectives. Wu et al. [12] used support vector machine to control shield posture. They systematically optimized key parameters such as cutterhead speed and cutterhead torque. Zhou et al. [13], focusing on the reduction of cutterhead energy consumption, employed a hybrid technique integrating least-squares support vector machine and particle swarm optimization to analyze the relative importance of each influencing parameter, such as total thrust, cutterhead torque and advance rate. Furthermore, using on-site data from the Shenzhen Metro Line 13, Yang et al. [14] provided steady-state phase parameters for shield tunneling operations under different geological conditions. It is evident that most existing studies centers on optimization objectives such as surface settlement, shield posture and energy consumption, while studies considering excavation efficiency are relatively less.

To address the problem of low tunneling efficiency of large-diameter slurry balance shield machines across different strata caused by suboptimal setting of tunneling parameters, this study presents a hybrid model integrating the extreme learning machine with the sparrow search algorithm to predict and optimize tunneling parameters based on the Jiangyin-Jingjiang Yangtze River Tunnel Left Line project. First, a metric, excavation efficiency, was introduced.

Second, the proposed model was constructed to predict the tunneling parameters. Lastly, the tunneling parameters associated with low tunneling efficiency were optimized and recommended using data with high excavation efficiency. The results of this study aim to provide decision support for shield tunneling based on information construction and offer guidance for engineering practice.

2 METHOD

2.1 Extreme learning machine (*ELM*)

In the traditional BP neural network model, forward propagation is responsible for generating error signals, while backward propagation serves to transmit these error signals. The core objective is to determine the optimal combination of weights and biases in the network. Despite its advantages of simple structure and high scalability, the BP neural network exhibits low training efficiency, insufficient generalization performance and susceptibility to local minima.

To enhance the training efficiency and prediction accuracy, Huang et al. [15] proposed an innovative architecture for a single-hidden-layer feedforward neural network, ELM. In this model, the connection weights from the input layer to the hidden layer ($\boldsymbol{W}$), as well as the biases of the hidden layer ($\boldsymbol{B}$), are randomly generated. Subsequently, the connection weights from the hidden layer to the output layer ($\boldsymbol{\beta}$) are calculated using Moore-Penrose generalized inverse matrix theory, based on the analysis of hidden layer output ($\boldsymbol{H}$) and actual output ($\boldsymbol{T}$). Notably, ELM does not necessitate traditional BP mechanisms for adjustment, thus simplifying the training process and accelerating the training speed [16][17].

$$\boldsymbol{H} = g\left(\boldsymbol{WX} + \boldsymbol{B}\right) \tag{1}$$

$$\boldsymbol{\beta} = \boldsymbol{H}^{*}\boldsymbol{T} \tag{2}$$

Where $g(.)$ is the activation function; $\boldsymbol{X}$ is the input matrix; and $\boldsymbol{H}^{*}$ is the Moore-Penrose generalized inverse matrix of $\boldsymbol{H}$.

2.2 Sparrow search algorithm (*SSA*)

SSA is a swarm intelligence optimization algorithm, inspired by foraging and anti-predation behaviors of sparrows [18]. It outperforms other optimization algorithms in terms of searching accuracy, convergence speed and stability [19].

In SSA, there are two different roles of sparrows: the producers, who actively seek out food sources; and the scroungers, who rely ono producers to obtain food. Furthermore, SSA introduces a safety threshold to simulate the anti-predation behavior of sparrows when they encounter predators. The detailed behaviors of sparrows are as follows:

(1) The producers typically possess high-level energy reserves and convey food information to scroungers. The fitness value of a producer is positively correlated with its energy reserves.
(2) When a sparrow detects danger, it will emit a alarming signal. If the alarm value exceeds the safety threshold, sparrows collectively fly to a safer area for foraging.
(3) Although any sparrow has the potential to become a producer, the proportion of producers to scroungers remains constant.
(4) The sparrows with high-level energy reserves would be acted as the producers, while others with low-level energy reserves are more likely to fly to other food-rich areas to gain more energy.
(5) The scroungers tend to follow the producer that leads them to optimal foraging areas. Simultaneously, they compete with producers for food to increase their own foraging rates.
(6) Sparrows at the edge quickly move toward a safer area for foraging when aware of danger, while sparrows at the center randomly walk to be close to others.

2.3 SSA-ELM hybrid model

This study employed SSA to optimize the $\boldsymbol{W}$ and $\boldsymbol{B}$ of ELM, aiming to prevent ELM from convergence to local minima. Taking advantage of the global searching ability of SSA, an optimal combination of $\boldsymbol{W}$ and $\boldsymbol{B}$ can be determined, thereby enhancing the performance of ELM. Fig. 1 illustrates the flowchart of SSA-ELM.

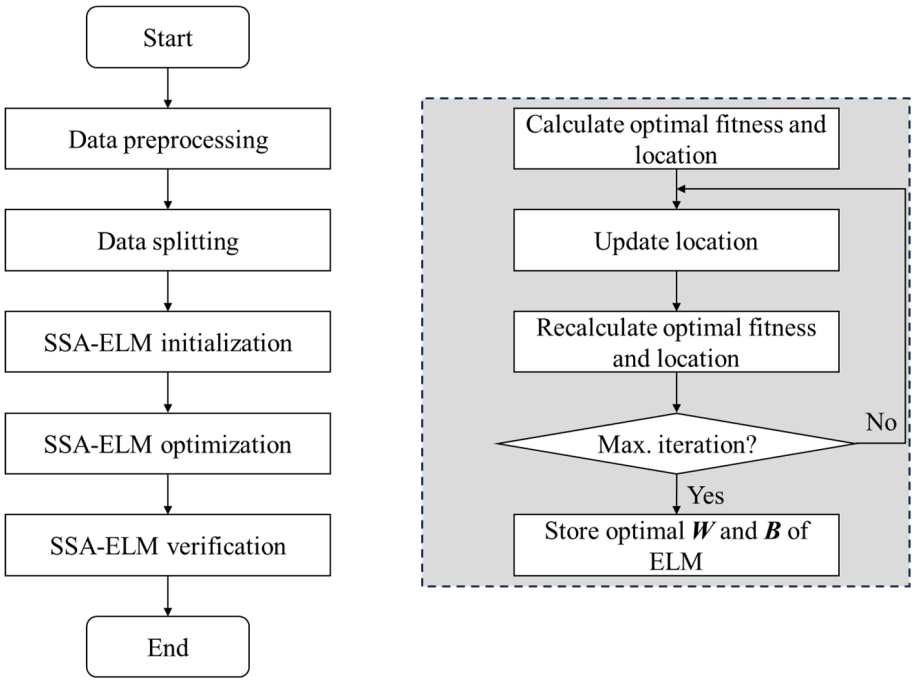

Fig. 1 Flowchart of the *SSA-ELM* hybrid model

3 Database

3.1 Project overview

The Jiangyin-Jingjiang Yangtze River tunnel, which is currently under construction, is the largest in diameter and designed to withstand the highest water pressure among large-diameter tunnels in China. The tunnel initiates at the north bank of the Yangtze River in Jiangyin City and extends southward to reach the south bank in Jingjiang City. The tunnel is 6,450 m in length and constructed by a leading international composite slurry balance shield machine. The outer and inner diameters of the tunnel are 15.5 m and 14.2 m, respectively. Each tunnel segment has a thickness of 0.65 m and a width of 2 m.

The shield machine has completed the land excavation work on the north bank of the Yangtze River and is currently undertaking the subsequent excavation. This study classified the strata into three main types and selected a total of 214 valid datasets for further analysis. The detailed classification of strata is as follows: (1) silt-sand strata (Rings 261-290); (2) sand strata (Rings 374-460); and (3) silty clay-sand strata (Rings 461-557).

3.2 Data preprocessing

The database consisted of tunneling, geological and geometric parameters. Specifically, the tunneling parameters were derived from the data acquisition system of the shield machine, with a recording interval set at every five minutes. The selection of geological and geometric parameters was based on engineering geological survey reports. A summary of all these parameters is presented in Table 1.

Table 1 Details of parameters collected

Type	Item	Unit
Tunneling parameter	Advance rate (*AR*)	mm/min
	Cutterhead torque (*CT*)	MN·m
	Cutterhead speed (*CS*)	rev/min
	Grouting pressure (*GP*)	bar
	Grouting volume (*GV*)	m^3
	Incision pressure (*IP*)	bar
	Slurry inlet density (*SID*)	g/cc
	Slurry inlet flow (*SIF*)	m^3/min
	Slurry inlet pressure (*SIP*)	bar
	Slurry outlet density (*SOD*)	g/cc
	Slurry outlet flow (*SOF*)	m^3/min
	Slurry outlet pressure (*SOP*)	bar

	Total thrust (*TT*)	MN
Geological parameter	Internal friction angle	°
	Cohesion	kPa
	Compression modules	MPa
	Natural unit weight	N/m³
Geometrical parameter	Tunnel depth	m

During the excavation process, numerous parameters were recorded per ring. Consequently, data preprocessing was essential prior to database construction. Missing values were filled by interpolation methods. As for duplicate values, only data from one moment was retained. The treatment of abnormal values was as follows: (1) if there were few abnormal values, they were treated as missing values; and (2) otherwise, abnormal values were directly removed. To mitigate the potential impact of outliers, the Z-score method was employed, as formulated in Eq. (3). Data points that satisfy the condition $|Z| > 3$ were defined as outliers and treated as missing values.

$$Z = \frac{x - \mu}{\sigma} \tag{3}$$

Where x is the raw data; μ is the average value; and σ is the standard deviation (*SD*).

It is necessary to remove the data collected during the shutdown state, as it holds minimal significance for further analysis. The shield machine is in a shutdown state if any of the following conditions are met: (1) the advance speed is zero; (2) the cutterhead torque is zero; (3) the cutterhead speed is zero; and (4) the total thrust is zero.

3.3 Excavation efficiency (*EE*)

This study introduced a new metric, EE, which refers to the excavation capability per unit of energy consumption. The formula is shown in Eqs. (4) and (5):

$$E = T\omega t + Fvt \tag{4}$$

$$\eta = \frac{V}{E} \tag{5}$$

where T is the cutterhead torque; ω is the cutterhead speed; F is the total thrust; v is the advance rate; t is the excavation time per ring; and V is the volume of soil excavated per ring.

From Fig.3 and Table 2, the average EE in sand strata surpasses that in silt-sand and silty clay-sand strata, with values of 0.35, 0.27 and 0.30 m^3/kWh, respectively. The sand strata had more homogeneous geological structure, which allowed for better control over tunneling parameters.

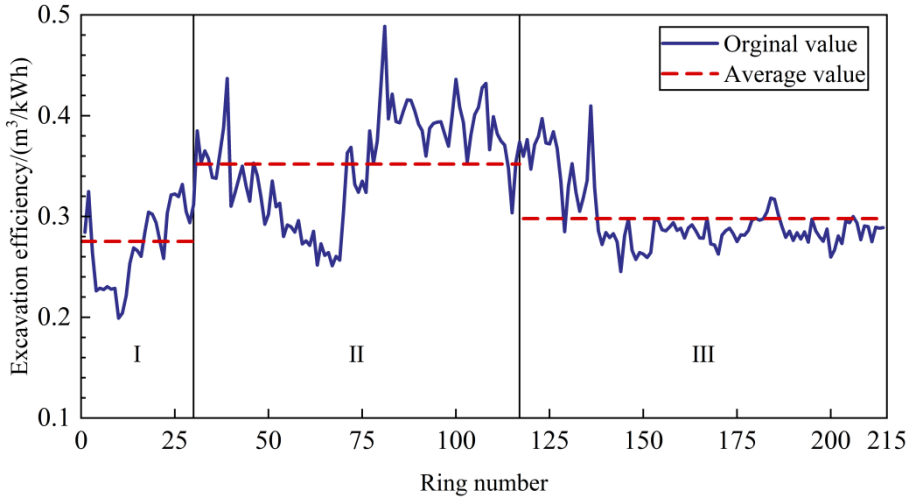

Fig. 3 Calculation result of EE

Table 2 Descriptive statistics of *TEs*

Code	Strata	Min.	Max.	Ave.	SD
I	Silt-sand	0.20	0.33	0.27	0.04
II	Sand	0.25	0.49	0.35	0.05
III	Silty clay-sand	0.25	0.41	0.30	0.03

3.4 Correlation analysis

According to Eq. (4), EE is a function of multiple parameters and most tunneling parameters. Consequently, a correlation analysis between EE and tunneling parameters is necessary [20]. Given the significant differences in dimensions and magnitudes, it is prudent to first normalize each tunneling parameter. Eq. (6) will scale each parameter within the range of [0,1].

$$X_{norm} = \frac{X - X_{\min}}{X_{\max} - X_{\min}} \tag{6}$$

Where X is the original data; $X_{\min}$ is the minimum data; and $X_{\max}$ is the maximum data.

Following normalization, the pearson correlation coefficient (PCC), which ranges from -1 to 1, was employed. Higher absolute values of PCC denote stronger linear correlations. The formula for PCC is given in Eq. (7).

$$\rho(X,Y) = \frac{\operatorname{cov}(X,Y)}{\sqrt{\operatorname{var}(X)\operatorname{var}(Y)}} \tag{7}$$

where cov(X,Y) is the covariance between X and Y; var(X) is the variance of X; and var(Y) is the variance of Y.

However, the PCC is limited to measuring linear correlations. The maximum information coefficient (MIC) is a designed to measure both linear and nonlinear correlations. The MIC yields values ranging from 0 to 1, where higher values denote stronger correlations. Eqs. (8) and (9) demonstrate the calculation process of MIC.

$$I\left[X;Y\right]=\sum_{X,Y}\rho\left(X,Y\right)\log_2\frac{\rho\left(X,Y\right)}{\rho\left(X\right)\rho\left(X\right)} \tag{8}$$

$$MIC\left[X;Y\right]=\max_{|X||Y|<B}\frac{I\left[X;Y\right]}{\log_2\left(\min\left(\left|X\right|,\left|Y\right|\right)\right)} \tag{9}$$

Where $p(X,Y)$ is the joint probability of X and Y; $p(X)$ is the probability of X; $p(Y)$ is the probability of Y; and B is a constant, approximately set to the power of 0.6 of the total amount of data.

In this study, a strong correlation was defined as an absolute PCC value exceeding 0.5. As there is no universally accepted threshold for MIC, the same standard adopted for PCC had been applied to MIC. In Table 3, EE displayed strong linear correlation with AR, CT and SID, with values of 0.55, 0.69 and 0.64, respectively. The MIC values associated with CT, SIP, SOP and IP are 0.90, 0.72, 0.56 and IP, respectively.

Table 3 Correlation analysis result using the PCC and MIC.

Method	AR	CT	CS	GP	GV	SID	SIF	SIP	SOD	SOF	SOP	IP	TT
PCC	**0.55**	**0.69**	0.28	0.03	0.38	**0.64**	0.16	0.11	0.48	0.36	0.09	0.10	0.41
MIC	0.34	**0.90**	0.32	0.30	0.32	0.40	0.35	**0.72**	0.34	0.27	**0.56**	**0.76**	0.40

Boldface indicates a value exceeding 0.5.

4 RESULTS AND DISCUSSION

4.1 Model implementation

This study incorporated not only geological and geometrical parameters as inputs but also incorporated two additional parameters: the composite ratio, which denotes the proportion of sand strata in the excavation face as Eq. (10); and the surrounding environmental conditions, with a value of 1 if infrastructure is adjacent or 0 otherwise.

$$\varphi = \frac{A_s}{A_{ef}} \tag{10}$$

where A_s is the area of sand strata; and A_{ef} is the area of excavation face.

As for outputs, according to correlation analysis result and actual on-site needs, seven tunneling parameters were selected, including AR, CT, CS, GP, GV, IP and TT.

The configurations of ELM were as follows: an input layer with seven nodes; a hidden layer with fifteen nodes; and an output layer with seven nodes. As for SSA, the sparrow population was set to 50, with producers accounting for 20%. The proportion of sparrows aware of danger was 10%. The safety threshold was set to 0.8, and the maximum iteration number was set to 100.

The relative error (*RE*) is used to assess the prediction result of SSA-ELM, with the specific formula as follows:

$$\mathrm{RE} = \sum_{i=1}^{n} \left| \frac{y_i - \hat{y}_i}{y_i} \right| \tag{11}$$

where y_i is the actual value; and $\hat{y}_i$ is the predicted value.

4.2 Prediction result of tunneling parameter

The lower and upper quartiles of EE are 0.28 and 0.36 m^3/kWh, respectively. A high EE is defined as any value exceeding 0.28 m^3/kWh. In the database, 160 datasets met this criterion and have been splitted into 120 training sets and 40 testing sets (20 sets each for sand and silty clay-sand strata).

In Fig. 4, the AR demonstrates greater stability in sand strata compared to that in silty clay-sand strata for actual values. As for predicted values, the performance in sand strata is superior, with only one RE value exceeding 5%. In contrast, there are five data points exceeding 5% in silty clay-sand strata, which account for 25% of the total data points.

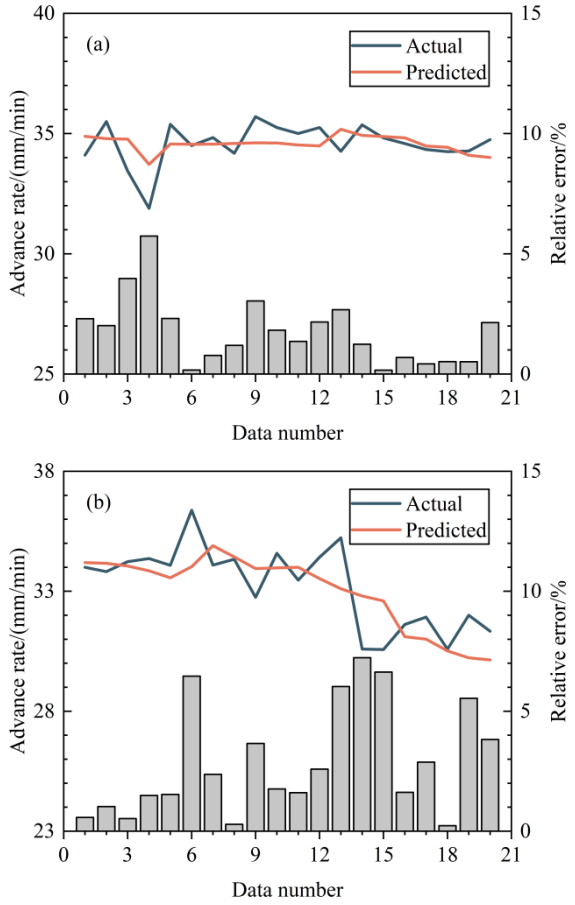

Fig. 4 Prediction result of the AR in: (a) sand strata; and (b) silty clay-sand strata.

In Fig. 6(a), the predicted CS demonstrates a horizontal trend. In Fig. 6(b), it demonstrates a decreasing tend. This difference could be attributed to complexity of the composite strata, where the geological conditions change significantly per ring. Overall, the prediction results in both strata are accurate, with no RE values exceeding 5%.

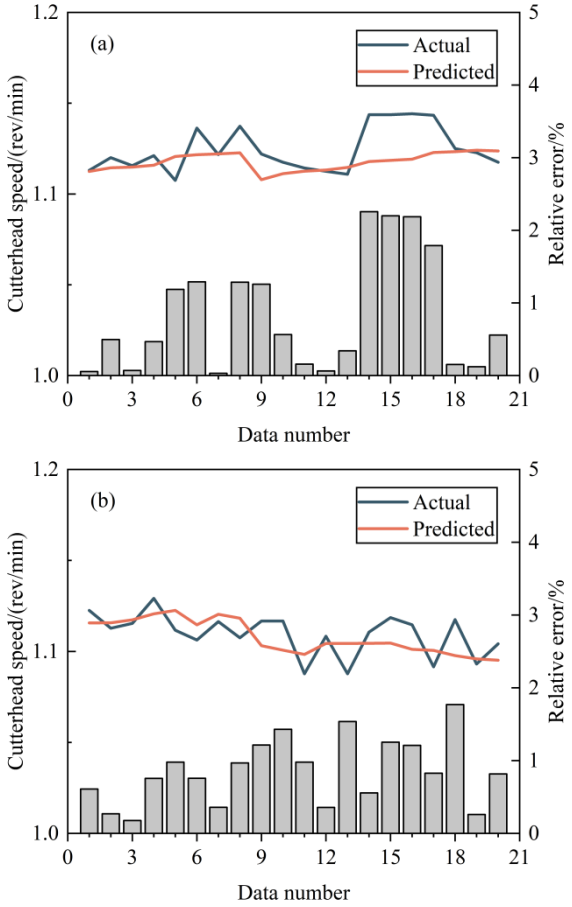

Fig. 5 Prediction result of the CS in: (a) sand strata; and (b) silty clay-sand strata.

The prediction result of the CT is illustrated in Fig. 7. In both strata, the trends of the CT were accurately predicted by SSA-EL. In each stratum, only four data points have a RE value exceeding 5%, accounting for 20%.

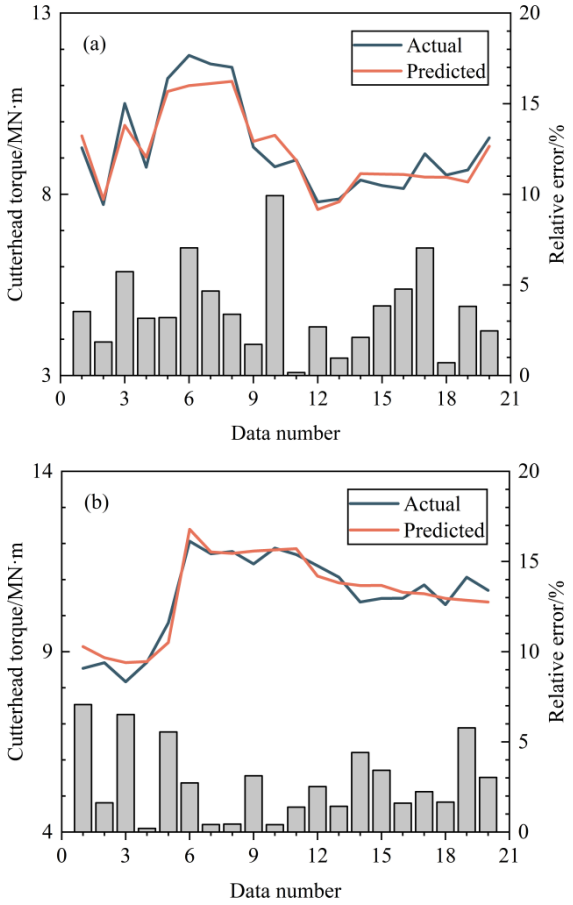

Fig. 6 Prediction result of the CT in: (a) sand strata; and (b) silty clay-sand strata.

In sand strata, there are twelve data points with a RE value exceeding 5%, accounting for 60%. While in silty clay-sand strata, there are only six data points, accounting for 30%. This suggested that SSA-ELM had stronger predictive capabilities for silty clay-sand strata, especially for the "w" trend from point No. 18.

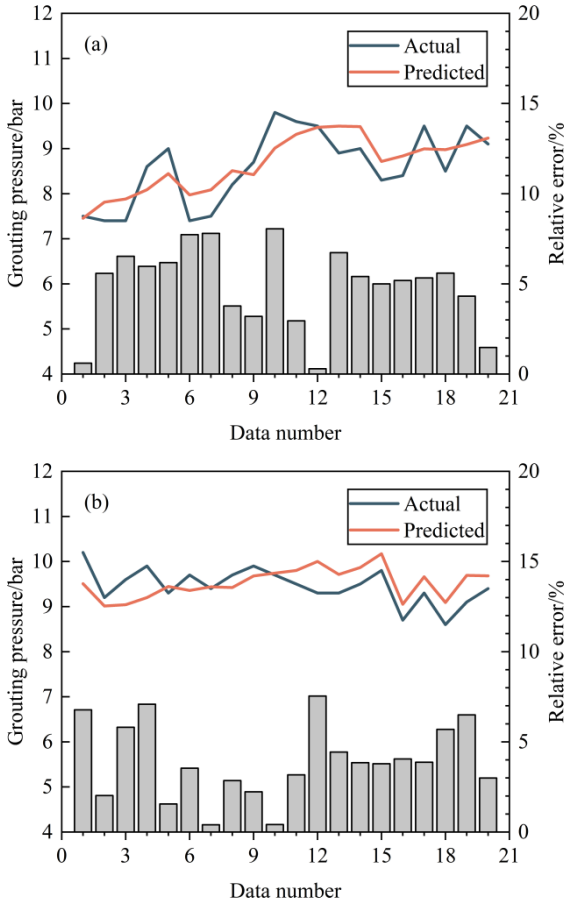

Fig. 7 Prediction result of the GP in: (a) sand strata; and (b) silty clay-sand strata.

The prediction result of the GV (Fig. 8) has a similarity to those of the CS (Fig. 5). Despite all data points exhibited RE values below 5%, the predictive trend deviated from the actual trend. SSA-ELM performs well regarding the overall trend, yet it fails to capture certain fluctuations.

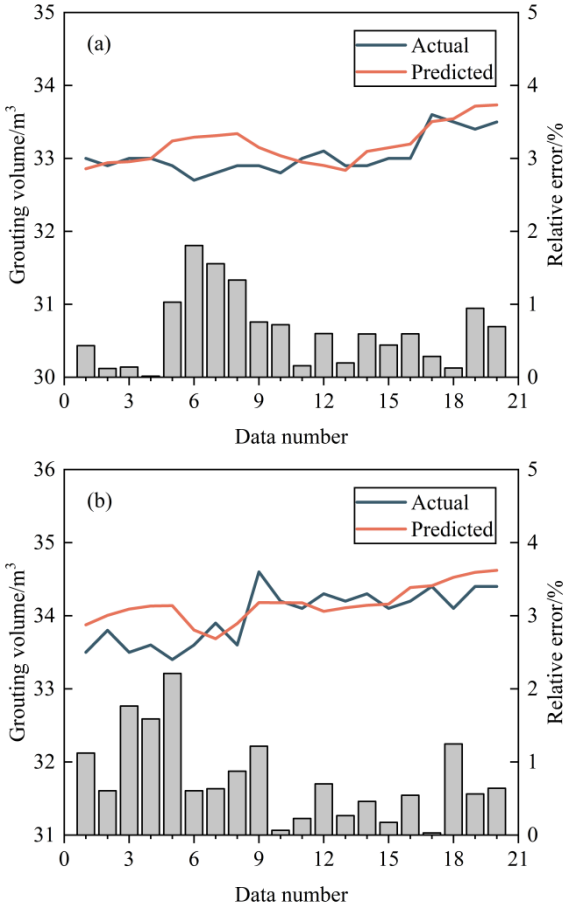

Fig. 8 Prediction result of the GV in: (a) sand strata; and (b) silty clay-sand strata.

Fig. 9(b) reveals a greater range area for the IP compared to that in Fig. 9(a), indicating the complexity of composite strata. In both strata, the RE values are consistently below 5%.

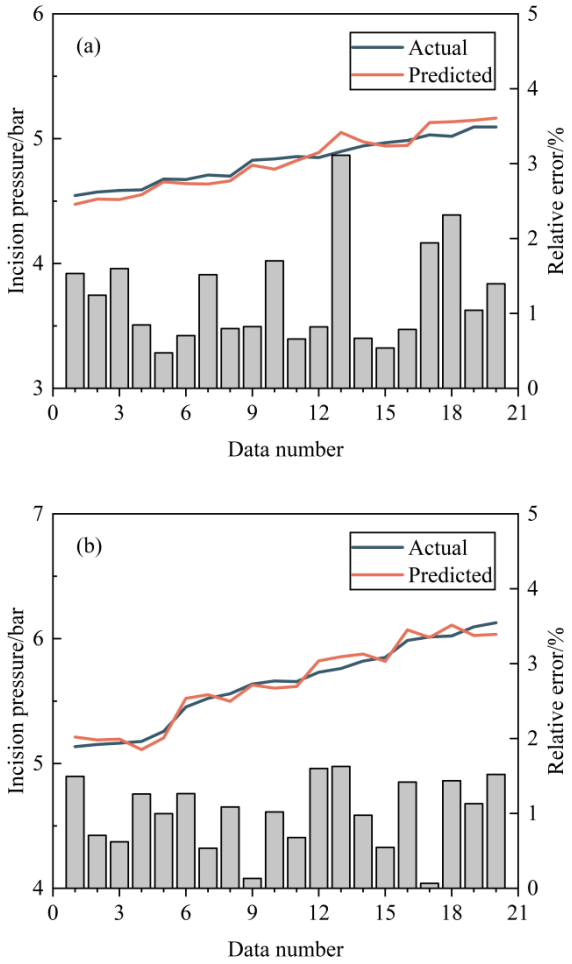

Fig. 9 Prediction result of the IP in: (a) sand strata; and (b) silty clay-sand strata.

The prediction result of the TT is shown in Fig. 10, SSA-ELM predicted better in composite strata than homogenous strata. In each stratum, no data points exceed the 5% RE value.

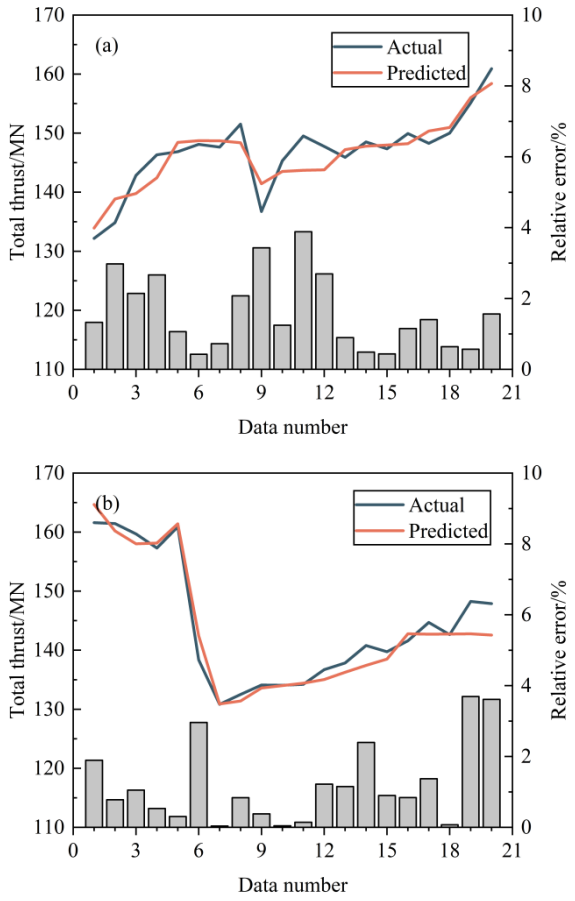

Fig. 10 Prediction result of the TT in: (a) sand strata; and (b) silty clay-sand strata.

The average RE for different tunneling parameter predictions is summarized in Table 3. SSA-ELM demonstrates superior predictive performance for tunneling parameters. The average RE in each stratum is below 5%, with respective values of 2.08% and 1.92%. Among these parameters, the CS and GV exhibit the most predictive performance, with an average RE below 1%.

Table 3 Average RE of tunneling parameter prediction.

Strata	AR	CS	CT	GP	GV	IP	TT	Ave.
Sand	1.76%	0.83%	3.63%	4.88%	0.63%	1.23%	1.59%	2.08%
Silty clay-sand	2.89%	0.85%	2.78%	3.93%	0.78%	1.01%	1.21%	1.92%

4.3 Optimization result of tunneling parameters

The database consisted of 214 datasets, with 160 of them being defined as high EE. The remaining 54 datasets did not meet the high EE criterion. All high EE datasets were used for model training, subsequently providing an optimal combination of tunneling parameters. To assess the optimization effect, a comparison of the EE before and after optimization is depicted in Fig. 11.

There was a notable optimization, with an average improvement of 0.03 m3/kWh. Most of optimized EE met the high EE criterion, but there were still 18.5% of the total data points that did not meet this criterion. For those data points with less significant improvement, it is recommended to adjust other tunneling parameters. This work will be explored in subsequent studies.

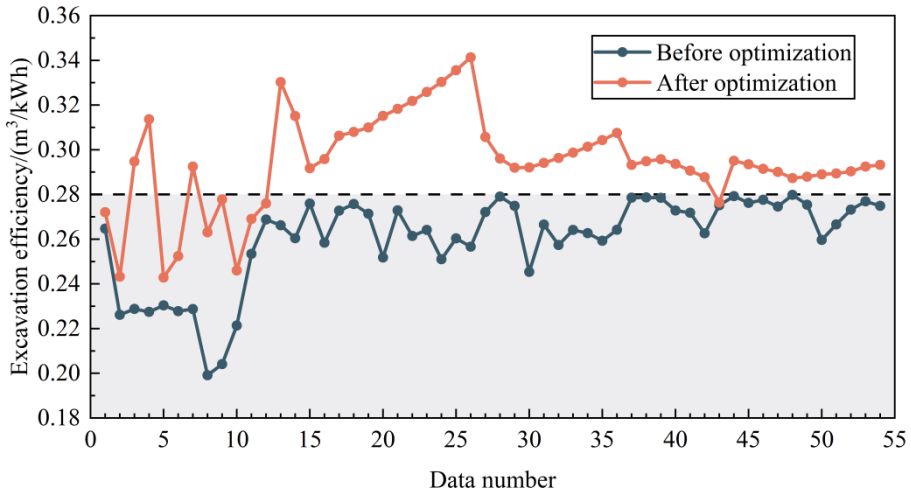

Fig. 11 Comparison of EE before and after optimization.

5 CONCLUSION

Aiming at the problem of low excavation efficiency caused by suboptimal tunneling parameters of large-diameter slurry balance shield machines across different strata, this study presented a hybrid model that combines extreme learning machine with sparrow search algorithm to predict and optimize tunneling parameters. Utilizing data from the Jiangyin-Jingjiang Yangtze River Tunnel Left Line project, this study analyzed excavation efficiencies across different strata and established a crierion for high excavation efficiency. From the results of this study, the following conclusions can be drawn:

(1) The average excavation efficiency in sand strata surpasses that in silt-sand strata and silty clay-sand strata, with values of 0.35, 0.27 and 0.30 m^3/kWh, respectively. Correlation analysis revealed that excavation efficiency is strongly correlated with advance rate, cutterhead torque, incision pressure, slurry inlet density, slurry inlet pressure and slurry outlet pressure, with all values exceeding 0.5.

(2) The lower and upper quartiles of excavation efficiency was 0.28 and 0.36 m^3/kWh, respectively. Any excavation efficiency exceeding lower quartile was considered high, setting a criterion for subsequent study on parameter optimization.

(3) The SSA-ELM hybrid model incorporated geological parameters, geometric parameters, composite ratio and surrounding environmental conditions as inputs. Prediction results showed that the average relative errors associated with different tunneling parameters are below 3%, confirming the accuracy of the proposed model.

(4) The tunneling parameter associated with low excavation efficiency has been optimized, with an average improvement of 0.03 m^3/kWh. This result fully demonstrated the strong potential of SSA-ELM in parameter optimization. However, there are still cases where

the optimization effect is not significant, and these issues will be further explored in subsequent study.

REFERENCES

[1]. D. Xu, Y. Wang, J. Huang, S. Liu, S. Xu, K. Zhou, Prediction of geology condition for slurry pressure balanced shield tunnel with super-large diameter by machine learning algorithms. Tunn. Undergr. Space Technol. 131(2023), 104852, https://doi.org/10.1016/j.tust.2022.104852.

[2]. Y. Zhang, P. Liu, P. Chen, S. Li, F. Ji, Clogging Prevention of Slurry–Earth Pressure Balance Dual-Mode Shield in Composed Strata with Medium–Coarse Sand and Argillaceous Siltstone. Appl. Sci. 13 (2023) (3), 2023, https://doi.org/10.3390/app13032023.

[3]. C. Liu, S. Zhang, D. Zhang, K. Zhang, Z. Wang, Model tests on progressive collapse mechanism of a shallow subway tunnel in soft upper and hard lower composite strata. Tunn. Undergr. Space Technol. 131 (2023), 104824, https://doi.org/10.1016/j.tust.2022.104824.

[4]. Y. Wang, X. Gao, P. Jiang, X. Guo, R. Wang, Z. Guan, L. Chen, C. Xu, An extreme gradient boosting technique to estimate TBM penetration rate and prediction platform. Bull. Eng. Geol. Environ. 81 (2022), 58, https://doi.org/10.1007/s10064-021-02527-5.

[5]. W. Fan, Z. Sun, F. Li, B. Zhang, Q. Chen, F. Wang, K. Wang, Research on Prediction of Tunneling Parameters of Super-large Diameter Slurry Shield in Composite Strata of Shantou Bay Tunnel. Tunn. Constr. 40 (2020) (08), 1160-1168, https://doi.org/10.3973/j.issn.2096-4498.2020.08.008. (in Chinese)

[6]. Z. Lu, K. Shi, A novel VMD-LHPO-KELM machine learning-based TBM boring parameter prediction. Earth Sci. Inform. 16 (2023), 2925-2938, https://doi.org/10.1007/s12145-023-01043-2.

[7]. Q. Zhang, Y. Zhu, R. Ma, C. Du, S. Du, K. Shao, Q. Li, Prediction Method of TBM Tunneling Parameters Based on PSO-Bi-LSTM Model. Front. Earth Sci. 10 (2022), https://doi.org/10.3389/feart.2022.854807.

[8]. T. Fu, T. Zhang, X. Song, A Novel Hybrid Transfer Learning Framework for Dynamic Cutterhead Torque Prediction of the Tunnel Boring Machine. Energies 15 (2022) (8), 2907, https://doi.org/10.3390/en15082907.

[9]. H. Wang, J. Wang, Y. Zhao, H. Xu, Tunneling parameters optimization based on multi-objective differential evolution algorithm. Soft Comput. 25 (2021), 3637-3656, https://doi.org/10.1007/s00500-020-05392-8.

[10]. K. Guo, L. Zhang, Data-driven optimization for mitigating tunnel-induced damages. Appl. Soft Comput. 115 (2022), 108128, https://doi.org/10.1016/j.asoc.2021.108128.

[11]. W. Liu, A. Li, C. Liu, Multi-objective optimization control for tunnel boring machine performance improvement under uncertainty. Automat. Constr. 139 (2022), 104310, https://doi.org/10.1016/j.autcon.2022.104310.

[12]. H. Wu, J. Chang, G. Li, D. Zhang, H. Huang, Prediction of Driving Posture and Optimization of Construction Parameters for Shield Based on Support Vector Machine. Tunn. Constr. 41 (2021) (S1), 11-18, https://doi.org/10.3973/j.issn.2096-4498.2021.S1.002. (in Chinese)

[13]. C. Zhou, L. Ding, Y. Zhou, H. Zhang, M.J. Skibniewsk, Hybrid Support Vector Machine Optimization Model for Prediction of Energy Consumption of Cutter Head Drives in Shield Tunneling. J. Comput. Civ. Eng. 33 (2019) 3, https://doi.org/10.1061/(ASCE)CP.1943-5487.0000833.

[14]. T. Yang, T. Wen, X. Huang, B. Liu, H. Shi, S. Liu, X. Peng, G. Sheng, Predicting Model of Dual-Mode Shield Tunneling Parameters in Complex Ground Using Recurrent Neural Networks and Multiple Optimization Algorithms. Appl. Sci. 14 (2024) (2), 581, https://doi.org/10.3390/app14020581.

[15]. G. Huang, Q. Zhu, C.K. Siew, Extreme learning machine: Theory and applications. Neurocomputing 70 (2006) (1-3), 489-501, https://doi.org/10.1016/j.neucom.2005.12.126.

[16]. R.M. Adnan, R.R. Mostafa, O. Kisi, Z.M. Yaseen, S. Shahid, M. Zounemat-Kermani, Improving streamflow prediction using a new hybrid ELM model combined with hybrid particle swarm optimization and grey wolf optimization. Knowl.-Based Syst. 230 (2021),107379, https://doi.org/10.1016/j.knosys.2021.107379.

[17]. C.C. Fab, Y. Zheng, Y. Wen, M. Sun, Classification and prediction of deformed steel and concrete bond-slip failure modes based on SSA-ELM model. Structures 57 (2023), 105131, https://doi.org/10.1016/j.istruc.2023.105131.

[18]. J. Xue, B. Shen, A novel swarm intelligence optimization approach: sparrow search algorithm. Syst. Sci. Control Eng. 8 (2020) (1), 22-34, https://doi.org/10.1080/21642583.2019.1708830.

[19]. Y. Yue, L. Cao, D. Lu, Z. Hu, M. Xu, S. Wang, B. Li, H. Ding, Review and empirical analysis of sparrow search algorithm. Artif. Intell. Rev. 56 (2023),10867-10919, https://doi.org/10.1007/s10462-023-10435-1.

[20]. J. Li, P. Li, D. Guo, X. Li, Z. Chen, Advanced prediction of tunnel boring machine performance based on big data. Geosci. Front. 12 (2021) (1), 331-338, https://doi.org/10.1016/j.gsf.2020.02.011.

Proceeding of the 10th International Conference on Innovative Production and Construction (IPC 2024), Perth, Australia, July 11-12, 2024

Toward a High-Performance and Secure Digital Twin Framework Using Enhanced Blockchain Technology

Xingyu Tao[1], Cong Huang[1], Chengliang Zheng[2], Moumita Das[1], Yuqing Xu[1], Jack C.P. Cheng[1]

1. Department of Civil and Environmental Engineering, The Hong Kong University of Science and Technology, Hong Kong 999077, China.
2. School of Cyber Science and Engineering, Wuhan University, Wuhan, China.

ABSTRACT: Digital twin (DT) technology has been increasingly adopted throughout the lifecycle of a construction project, especially in the facility management of buildings or infrastructures. However, most current DT systems rely on a centralized database, suffering from two cybersecurity vulnerabilities, data manipulation and overwriting, resulting in data traceability, integrity, and authenticity loss. Integrating blockchain with DT is a promising solution to safeguard DT data security. One gap is that the current blockchain has limited capacity to process high-speed and large-volume data (e.g., IoT, GIS, or BIM data) from the DT system, hindering the blockchain implementation. This paper aims to propose an optimized blockchain architecture to facilitate a high-performance and secure DT framework. The contributions lie in two aspects: (1) an event sourcing (ES)-blockchain integrated architecture will be developed to build a novel "data buffer" between the blockchain and DT system. (2) An integrity-checking smart contract algorithm is proposed to sign and verify data authenticity during information exchange. The framework is validated in a DT system for facility management. Results show that compared with the existing blockchain, the optimized blockchain with a buffer layer remains similar in throughput while reducing latency by up to 90%, improving blockchain workability in DT.

KEYWORDS: blockchain, digital twin, facility management, smart contract, event sourcing

1 INTRODUCTION

The construction industry is witnessing a transformative shift with the implementation of digital twin (DT) technology. A DT is a virtual representation of a physical asset or system that enables real-time monitoring, analysis, and simulation [1]. Digital twins offer immense potential for improving project planning, design, construction, and maintenance processes in the construction sector. By integrating data from various sources, including Building Information Modelling (BIM) and Internet of Things (IoT) devices, digital twins provide a comprehensive and dynamic understanding of a construction project's lifecycle. Especially, DT has been validated to improve the building operation phase during the facility management (FM), as it reflects the current asset condition and can be continuously updated with data from its physical counterpart [2]. Also, Digital twins can create simulations and predict future behavior, streamline collaboration, and optimize operations.

However, most current DTs rely on a single and centralized database, suffering two data security vulnerabilities: overwriting and data manipulation [3]. The risk of overwriting is particularly alarming as it involves new data supplanting historical records, erasing their traceability and accountability. This loss of historical insight can be irreversible, undermining the DT's role in providing a reliable chronological data narrative crucial for audits and informed decision-making. Moreover, the centralized nature of DT makes them vulnerable to hacking and manipulation, which can lead to the loss of data integrity and availability. Hackers can exploit vulnerabilities in the digital twin's network infrastructure, software, or devices to gain unauthorized access and manipulate critical data. Such attacks can compromise the DT's representation accuracy, leading to erroneous decisions and potentially catastrophic consequences in the physical construction environment [1].

Blockchain is a viable means of mitigating cybersecurity concerns in the construction sector's DT. As a distributed, unalterable record-keeping technology, blockchain brings significant benefits that bolster the security and veracity of DT [4]. Its resistance to tampering and inherent transparency establishes a reliable and verifiable data environment[5]. By distributing data across nodes, blockchain technology dispels the risks associated with a centralized point of failure and thwarts unauthorized data alterations. The ability to monitor and audit DT modifications instills a heightened level of integrity and responsibility [6].Moreover, combining blockchain with digital twins can promote secure data exchange and collaborative efforts, preserving confidentiality and security. Using smart contracts—self-executing contractual states stored on the blockchain—secure and definitive interactions among construction participants can be ensured [7]. Instances of blockchain's successful application to digital twins in construction have pointed out the advantages of blockchain for safeguarding digital twin data security and trust [8].

Yet, a significant challenge lies in the processing capacity of current blockchain frameworks. Conventional blockchains face transactional performance limitations, which could become problematic with the substantial data output from DTs, particularly when innumerable IoT devices continuously transmit data. For digital twins to accurately reflect and inform in construction, real-time data handling and analysis in a blockchain are imperative. The scalability issues of blockchain might impede the fluid fusion of digital twins and blockchain, potentially causing delays and reduced efficiency in data updates and validations within the digital twin system.

Therefore, this paper aims to propose a high-performance blockchain to tackle the mentioned problem. Two contributions of this paper are: (1) an event sourcing (ES)-blockchain integrated architecture will be developed to build a novel "data buffer" between the blockchain and DT system. (2) An integrity-checking smart contract algorithm is proposed to sign and verify data authenticity during information exchange.

2 METHOD

2.1 High-performance and secure digital twin (HPSDT) framework

Figure 1 shows the HPSDT framework integrating blockchain and event-sourcing (ES) technologies. ES is a design pattern and distributed database where application state changes are stored as events rather than just the final state [9]. This method not only provides a complete history of state transformations but also allows the reconstruction of past states. Its compatibility with blockchain is rooted in using immutable, append-only logs. Incorporating ES into the blockchain can significantly improve the latter's performance by easing data congestion. This enhancement is achieved by recording incremental changes as events, reducing the data volume processed in each block. As a result, blockchain systems can enjoy improved latency and throughput. By adopting ES principles, blockchain benefits from more efficient data management. This integration facilitates parallel processing of events across multiple nodes, enhancing scalability and responsiveness. Therefore, blockchain architectures that implement Event Sourcing are better equipped to handle high transaction volumes and provide real-time data processing capabilities, which are essential for DTs [10].

The foundational concept of the HPSDT framework is "Asynchronous data exchange." This indicates that information from the DT will not be directly transferred to the blockchain ledger. Specifically, the HPSDT enhances blockchain performance through a tri-layered model. The first layer is the "active layer," where the framework initially senses data from the DT platform. At this stage, ES collaborates with two additional technologies—Actor and Command and Query Responsibility Segregation (CQRS) [11]—to allocate space for the new data storage within the ES database. The second layer is the "buffer layer," ES's distributed databases function as a buffer between DT data and the blockchain ledger. Within this layer, two key processes occur: (1) DT data, characterized by high speed and volume, are sequentially placed into the ES database; (2) the DT data are packaged into discrete events, which serve as the basic information units within a blockchain. The "buffer layer" then pushes these events to the "blockchain layer" (the third layer) at regular intervals. This method ensures that all DT data are securely stored within the blockchain.

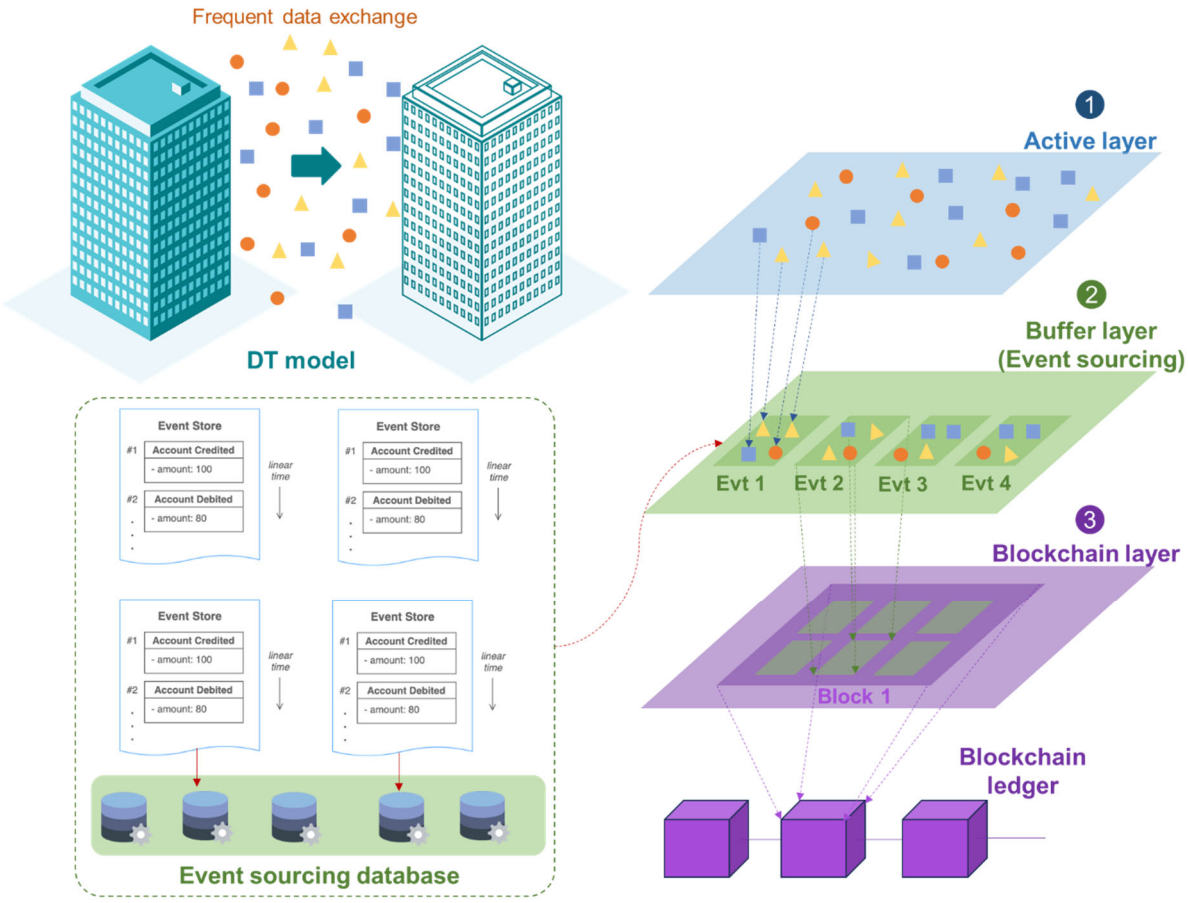

Figure 1. HPSDT framework

2.2 Integrity-checking smart contract (ICSC) algorithm

Smart contracts (SCs) are automated agreements embedded in blockchain code that execute actions when predefined conditions are met. They eliminate intermediaries by enforcing terms directly within the blockchain's immutable and transparent ledger. Once deployed, they cannot be altered, ensuring reliability. SCs trigger transactions automatically, providing a secure method for parties to transact directly with each other. This innovation streamlines processes, reduces costs, and enhances trust in digital operations, propelling various applications from financial exchanges to automated supply chain management.

Previous works on SC development in the construction industry primarily focused on data sharing, payment, and querying mechanisms. However, in the realm of blockchain-DT integration, where data is temporarily stored in an ES database before being recorded on the blockchain, there is a risk of data manipulation during this "buffer" process. A new SC algorithm, named the Integrity-Checking Smart Contract (ICSC), has been developed, as shown in Figure 2.

Figure 2(a) outlines the workflow of how the ICSC ensures the immutability of data transfer from the DT to the ES buffer and finally to the blockchain ledger through three phases. The first phase involves signing (steps 1-4 in Figure 2(a)). As DT data reaches the active layer, the

ICSC is invoked to generate a tamper-proof signature, forming immutable events. The second phase is asynchronous data storage, wherein the ICSC uploads these events to the blockchain (step 5 in Figure 2(a)), leading to the third phase, verification. Before the events are permanently added to the blockchain ledger, the ICSC verifies whether the signature matches the one from the first phase, thus ensuring the data has not been altered during the asynchronous period. Figure 2(b) presents a detailed algorithm for the verification phase.

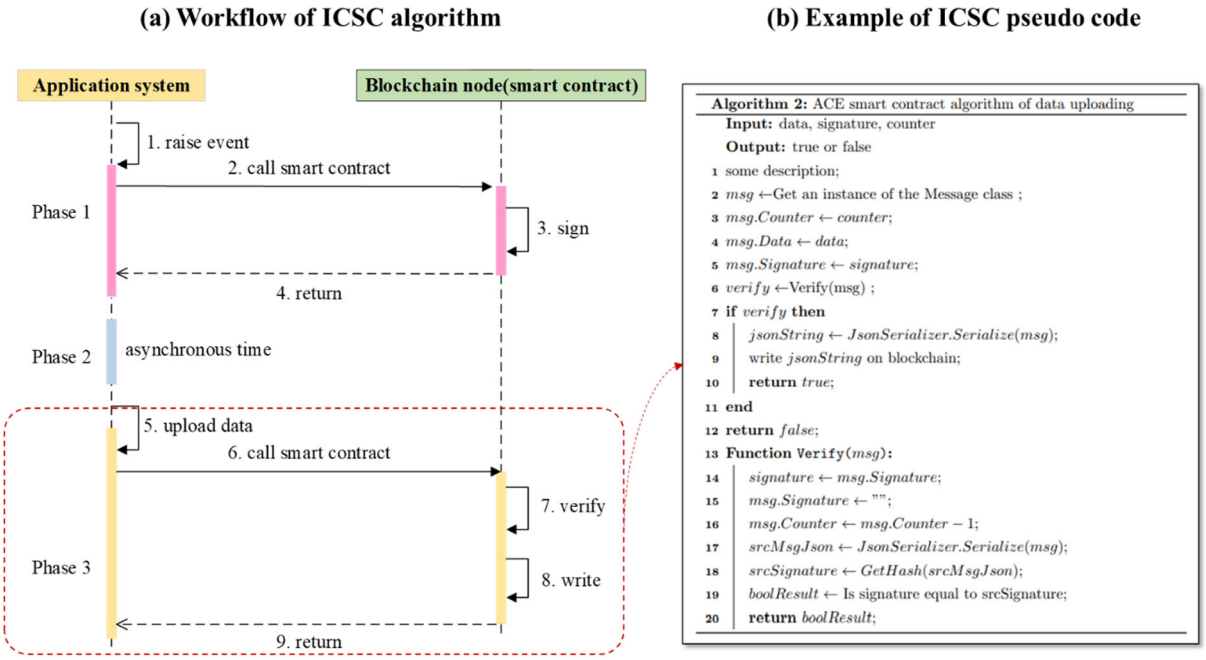

Figure 2. ICSC algorithm

3 PROOF OF CONCEPT

The proposed HPSDT framework has been deployed in a DT project for facility management. The framework utilizes blockchain technology to store various types of IoT data from DT, such as equipment status, indoor air quality (IAQ) data, and maintenance operation records, as illustrated in Figure 3(a). The primary metric used to evaluate the effectiveness of the framework is latency. Within the context of blockchain, latency is the duration required to confirm and record a transaction on the blockchain. This metric is crucial as it influences the speed of transactions and the system's overall throughput, affecting how swiftly operations are executed, and data is rendered immutable—both are essential for an optimal user experience and system efficiency. An open-source blockchain platform, Hyperledger Fabric (HF), was chosen as the underlying blockchain technology for the DT system. Hyperledger Fabric's permissioned network architecture offers improved privacy and scalability, making it more suitable for managing construction data than other platforms like Bitcoin and Ethereum. This preference is due to its ability to provide heightened control over sensitive information and support for complex business contracts.

A comparative study was carried out between the traditional "DT-blockchain" integration and the proposed "DT-buffer-blockchain" integration, represented by the HPSDT framework, as

depicted in Figure 3(b). The results, shown in Figure 3(c), indicate that the HPSDT framework can significantly enhance DT system performance by reducing latency by at least 85% and sometimes up to 90%.

Figure 3. Validation of HPSDT framework

4 CONCLUSION

This paper bridges the gap in enhancing blockchain performance for its integration with digital twin (DT) technology in the construction industry. The introduction of an event sourcing (ES)-aided blockchain architecture and an accompanying integrity-checking smart contract algorithm address the limitations of current blockchain systems. This optimized framework effectively manages high-speed and large-volume DT data, ensuring data integrity and significantly reducing latency by up to 90%. As a result, the study lays the groundwork for a more robust and efficient application of blockchain in securing DT systems, particularly in the realm of facility management. One limitation is some incompatible data formats between DT systems and blockchain. An openBIM-based data adaptor will be developed in the future to streamline this integration, facilitating a fully compatible and secure data exchange.

REFERENCES

[1]. D. Lee, S.H. Lee, N. Masoud, M.S. Krishnan, V.C. Li, Integrated digital twin and blockchain framework to support accountable information sharing in construction projects, Automation in Construction, 127, (2021), p. 103688. https://doi.org/10.1016/j.autcon.2021.103688

[2]. C. Boje, A. Guerriero, S. Kubicki, Y.J.A.i.c. Rezgui, Towards a semantic Construction Digital Twin: Directions for future research, 114, (2020), p. 103179

[3]. E.A. Parn, D. Edwards, Cyber threats confronting the digital built environment, Engineering, Construction and Architectural Management, 26, (2), (2019), pp. 245-266. https://doi.org/10.1108/ECAM-03-2018-0101

[4]. X. Tao, M. Das, Y. Liu, J.C.P. Cheng, Distributed common data environment using blockchain and Interplanetary File System for secure BIM-based collaborative design, Automation in Construction, 130, (2021), p. 103851. https://doi.org/10.1016/j.autcon.2021.103851

[5]. M. Das, X. Tao, J.C.P. Cheng, BIM security: A critical review and recommendations using encryption strategy and blockchain, Automation in Construction, 126, (2021), p. 103682. https://doi.org/10.1016/j.autcon.2021.103682

[6]. B. Teisserenc, S. Sepasgozar, Project Data Categorization, Adoption Factors, and Non-Functional Requirements for Blockchain Based Digital Twins in the Construction Industry 4.0, Buildings, Vol. 11, 2021. https://doi.org/10.3390/buildings11120626

[7]. X. Tao, M. Das, C. Zheng, Y. Liu, P.K.-Y. Wong, Y. Xu, H. Liu, X. Gong, J.C.P. Cheng, Enhancing BIM security in emergency construction projects using lightweight blockchain-as-a-service, Automation in Construction, 150, (2023), p. 104846. https://doi.org/10.1016/j.autcon.2023.104846

[8]. Y. Celik, I. Petri, Y. Rezgui, Leveraging BIM and Blockchain for Digital Twins, 2021 IEEE International Conference on Engineering, Technology and Innovation (ICE/ITMC), 2021, pp. 1-10. 10.1109/ICE/ITMC52061.2021.9570246

[9]. M. Overeem, M. Spoor, S. Jansen, The dark side of event sourcing: Managing data conversion, 2017 IEEE 24th International Conference on Software Analysis, Evolution and Reengineering (SANER), 2017, pp. 193-204. 10.1109/SANER.2017.7884621

[10]. Y. Zhong, W. Li, J. Wang, Using Event Sourcing and CQRS to Build a High Performance Point Trading System, Proceedings of the 2019 5th International Conference on E-Business and Applications, Association for Computing Machinery, Bangkok, Thailand, 2019, pp. 16–19. 10.1145/3317614.3317632. https://doi.org/10.1145/3317614.3317632

[11]. M. Slabinoha, S. Melnychuk, V. Kropyvnytska, B. Pashkovskyi, Comparative Analysis of Using Event Sourcing Approach in Web Application Based on the LAMP Stack, in: S. Shakya, G. Papakostas, K.A. Kamel (Eds.), Mobile Computing and Sustainable Informatics, Springer Nature Singapore, Singapore, 2023, pp. 257-269

Proceeding of the 10th International Conference on Innovative Production and Construction (IPC 2024), Perth, Australia, July 11-12, 2024

Adaptive Rescheduling Framework for Prefabricated Production under Dynamic Environment

Hui Lu*, Yuqing Bian and Danrui Chang

School of Economics and Management, China University of Geosciences, Wuhan, China 430074
* Corresponding author (luhui@cug.edu.cn)

ABSTRACT: In project practice, the production of prefabricated components is usually faced with uncertainties and interference. Some of these unexpected disturbances, called recessive disturbances (such as processing time changes), may interfere with the prefabricated production in the form of accumulated delay and eventually lead to the failure of the original schedule. It is difficult for managers to perceive the presence of recessive disturbances in time, and to evaluate their impact on the original schedule and make a decision on rescheduling. Thus, this study proposes a rescheduling decision mechanism for recessive disturbances in prefabricated production, aiming to achieve adaptive production rescheduling. Firstly, by analyzing the impact of recessive disturbances on prefabricated production, basic models under different rescheduling methods are established to facilitate the construction of rescheduling decision mechanisms. Secondly, the production feature vector representing the production status is developed to quantify the impact of recessive disturbances, and a large number of feasible experimental data sample are obtained through simulation experiments. Thirdly, an adaptive rescheduling decision mechanism based on random forest algorithm is constructed by analyzing the characteristics of data samples, which can intelligently address when to reschedule and which rescheduling method to apply. Finally, the implementation procedure of the proposed rescheduling decision mechanism is verified by a real case. The results show that the proposed approach can deal with recessive disturbances efficiently and timely.

KEYWORDS: Prefabricated production, Recessive disturbances, Rescheduling decision.

1 INTRODUCTION

The production scheduling management of prefabricated components (PCs) plays an important role in the development of prefabricated buildings. By optimizing the production scheduling of PCs, we can reduce costs, improve production efficiency, and ensure the timely delivery of components. However, the prefabrication production system usually encounters many uncertainties and disturbances, making it more difficult to plan effective PC production scheduling (Wang et al., 2018). According to the different degrees of influence on production, disturbances can be divided into two primary types: dominant disturbances and recessive disturbances (Zheng et al., 2019). Dominant disturbances will directly affect the initial schedule and lead to inevitable rescheduling (e.g., demand changes, urgent inserts, machine

failures). Unlike dominant disturbances, recessive disturbances are often hidden in the production process and are not easy to detect. Meanwhile, recessive disturbances may not have an immediate effect on production scheduling but their continuous accumulation can shut down the original schedule and require rescheduling (e.g., processing time variation). In this paper, we study the adjustment and optimization method of production schedule in the case of recessive disturbance to achieve adaptive production rescheduling. The goal of this research is to propose the evaluation index to quantify the impact of recessive disturbances and build an adaptive rescheduling decision mechanism based on machine learning method to achieve the purpose of responding to disturbances efficiently and quickly. In the practice of project management, this study can provide enlightenment for the disturbance response practice of prefabricated production scheduling optimization, including how to quantify the impact of disturbance and select the best rescheduling mode according to the degree of disturbance. In general, it provides scientific guidance for project management practice, helps to effectively respond to production disturbances and ensure the effective implementation of production schedules.

2 PROBLEM DESCRIPTION AND MOTIVATION

2.1 Problem Description

In precast construction, the components are prefabricated in precast factories before they are transported to construction sites for assembly. Generally, the project manager submits the demand information to the precast factory regarding type, quantity, and due dates. The precast factory then develops a production schedule based on the demand information to achieve just-in-time (JIT) delivery in a low-cost manner. To achieve high productivity and large-scale production, multiple production lines are employed in the precast factories, and each production line consists of six workstations dedicated to the six primary processes (Ma et al., 2018): 1) mold assembling; 2) rebars and embedded parts setting; 3) casting; 4) curing; 5) mold stripping; 6) finishing/repairing.

Precast components of multiple types are produced according to the original schedule. It is worth noting that the actual prefabrication production usually encounters various disturbances which may affect the implementation of the original schedule. As one of the disturbances, recessive disturbances will not shut down the original schedule immediately but gradually impair the schedule and ultimately necessitate inevitable rescheduling. Since it is difficult for decision-makers to accurately evaluate the impact of recessive disturbances on the original schedule, they cannot address such disturbance promptly and effectively, ultimately resulting in immeasurable losses. Thus, it is necessary to propose a method to quantify the impact of recessive disturbances, so that timely decisions can be made based on the quantitative results to determine whether the original schedule needs to be rearranged to reduce disturbance influence and resume production.

In addition, there is usually only one rescheduling method which is most suitable for a specific production environment with recessive disturbances. It means that the production system should select the better one to repair or update the original production plan in the production process. To promote the understanding of rescheduling methods, relevant definitions are given as following: i) partial rescheduling (PR) is a partial adjustment of the original production plan, which maintains the original production plan as much as possible. ii) Total rescheduling (TR) is the rescheduling of all remaining unprocessed jobs to generate a new production schedule. Therefore, for the precast scheduling problem under recessive disturbances, how to quantify the impact of recessive disturbance, decide when to reschedule and adaptively select the optimal rescheduling method to repair schedule according to the production status is a very challenging research.

2.2 Motivation

The solution proposed in this paper is mainly motivated by the following two considerations:

Firstly, the basic models under different rescheduling methods are constructed (BM-I, BM-II, and BM-III) to facilitate the construction of rescheduling decision mechanism. These three models represent different schedule control options under recessive disturbances. Among them, BM-I indicates that the current disturbances do not have a significant impact and do not need to be rescheduled yet; BM-II indicates that the disturbances have already affected the schedule and need to be locally rescheduled; and BM-III indicates that the disturbances have significantly affected the schedule and need to be globally rescheduled. Meanwhile, these basic models will then be used for data sample generation and adaptive rescheduling decision making.

Secondly, an adaptive rescheduling decision mechanism based on random forest is constructed to realize adaptive production rescheduling. In order to achieve that goal, a production feature vector representing the real-time production status is developed to quantitatively evaluate the impact of recessive disturbances, and a large number of feasible production data samples through simulation experiments is obtained. Then by analyzing the characteristics of data samples, a rescheduling decision mechanism based on random forest is constructed to intelligently decide when to reschedule and which rescheduling method to apply.

3 OVERVIEW OF ADAPTIVE RESCHEDULING FRAMEWORK

In the actual prefabrication production, the managers mainly deal with the recessive disturbance and resume production based on human experience. This method not only has low decision efficiency, but also with the increase of the number of workshops and the complexity of production process, it is difficult to accurately evaluate the impact of recessive disturbances on the original schedule and determine whether to rescheduled or not. Therefore, it becomes challenging to ensure quality and stability when solving such scheduling problems.

Furthermore, as the level of workshop informatization continues to improve, an increasing amount of production data can be captured. These datasets encompass a wealth of scheduling knowledge, which is difficult to find only by manual processing. Machine learning method can effectively mine the useful information of huge and redundant data, making it suitable for addressing predictive classification problems associated with high-dimensional workshop production data. Therefore, we will use random forest algorithm (RF) to build an adaptive rescheduling decision mechanism, aiming at addressing when to reschedule and which rescheduling method to apply. Fig. 1 shows the framework of the rescheduling decision mechanism, which mainly includes the following parts:

Firstly, a large number of production data samples about recessive disturbances are acquired through simulation experiments to train the model of rescheduling decision mechanism. The data sample information includes the production feature vector describing the production status and the corresponding optimal rescheduling method.

Secondly, by learning the characteristics of data samples, an adaptive rescheduling decision mechanism based on random forest (RF-ARDM) is constructed to realize the one-to-one mapping between the real-time production status and the optimal rescheduling method, so as to achieve adaptive production rescheduling.

Finally, the adaptive rescheduling decision mechanism is implemented to verify its effectiveness. The specific implementation procedures are as follows: (1) The initial production schedule is generated based on mathematical model and optimization algorithm, and subsequently executed; (2) By comparing the real time production data with the initial production schedule, the production feature vectors representing real-time production status are calculated; (3) At the completion time of each batch processing (i.e. rescheduling decision time), the adaptive rescheduling decision mechanism is initiated to assess the impact of recessive disturbances on the production schedule, and subsequently select an appropriate rescheduling method for updating or rectifying the original schedule based on the evaluation results.

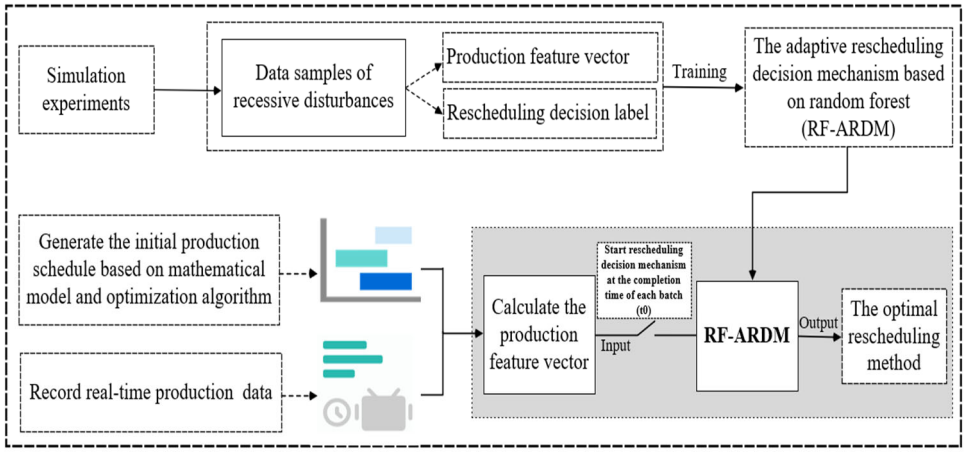

Fig.1. Overview of the rescheduling framework

3.1 Data Samples Acquisition

Considering that there are too few data samples about the recessive disturbance in the actual production to train the RF-ARDM. In addition, previous rescheduling decisions mainly based on human experience, so they could not be collected as data labels. Thus, we will use simulation experiments to generate a large number of data samples for learning and testing. The procedure of data samples acquisition is shown in Fig. 2, the collected sample data primarily comprises production status data under various recessive disturbance scenarios and corresponding rescheduling decision label.

1) Generate processing data. Recessive disturbance mainly affects the execution of the original schedule in the form of "processing time change". Thus, we introduce two types of random variables to change the processing time, so as to generate a large number of production data to simulate the recessive disturbance. The two random variables include: the number of disrupted batches and the degree of disturbance.

2) Determine the production feature vector. The original production schedule is generated using the mathematical model and genetic algorithm, which is then compared with the actual production process to calculate the production feature vector. The production feature vector is used to describe the production state at the rescheduling decision-making time. In this paper, we consider evaluating the production state from multiple perspectives, including the job processing state before rescheduling, the degree of disturbance, the total production cost, and the total completion time

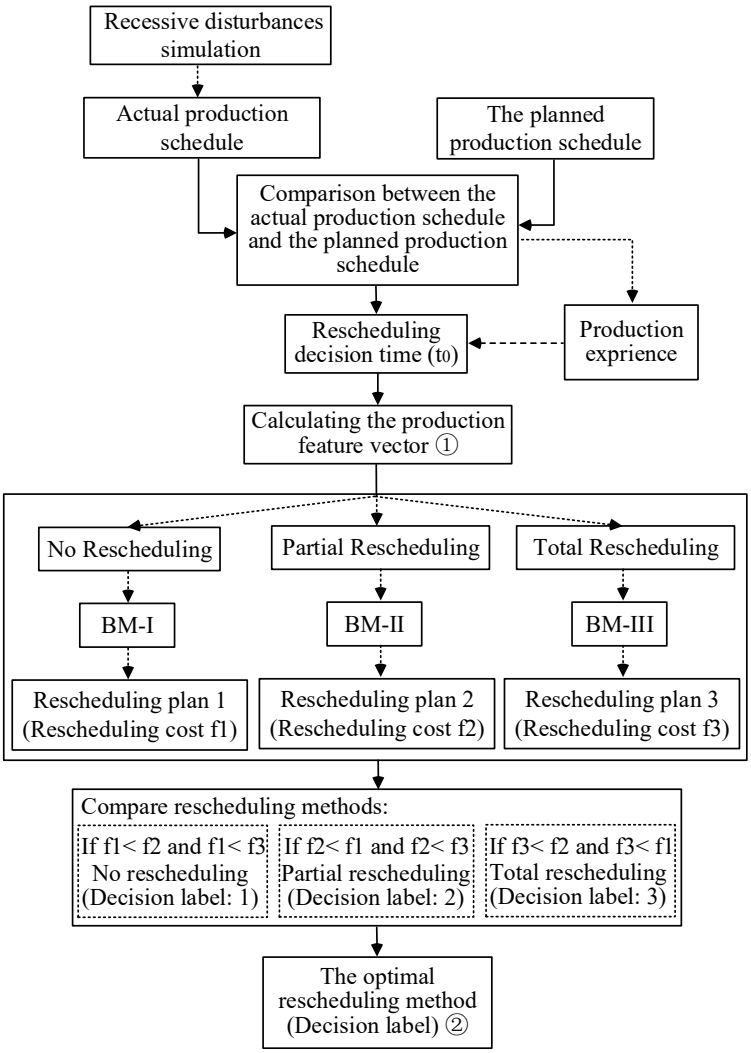

Fig. 2. The procedure of data samples acquisition

3.2 Rescheduling Decision Based on Random Forest

Random forest algorithm is an integrated model composed of multiple decision trees, which belongs to a typical machine learning algorithm (Hutengs and Vohland, 2016). A random forest is constructed by generating multiple decision trees through boot-strap method, and obtains the final decision based on the voting principle of decision trees (Yuan et al., 2020). Due to its strong anti-interference, anti-overfitting and generalization ability, the random forest algorithm can effectively address large-scale high-dimensional datasets and achieve high accuracy. Therefore, this paper uses random forest algorithm to build the rescheduling decision.

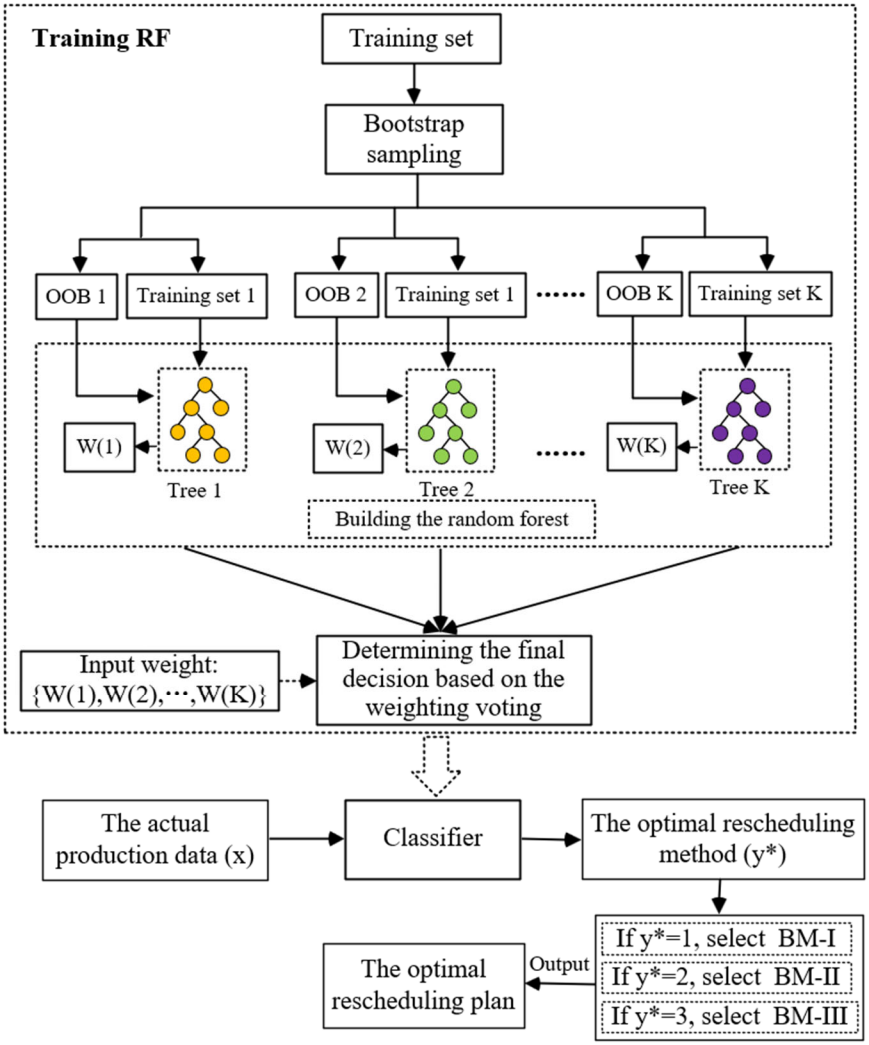

Fig. 3. The procedure of RF-ARDM

4 CASE STUDY

In order to verify the effectiveness and feasibility of our methods, date form a subway construction project was used. In this project, each segment comprises six segment blocks, and the segments will be produced in a prefabricated plant with two production lines (L_1 and L_2), each with a maximum capacity (L) of 12. The production information is shown in Table 3. The segments to be produced encompass the 1.5m standard ring, 1.5m left turn ring, 1.5m right turn ring, 1.2m standard ring, 1.2m left turn ring, and 1.2m right turn ring respectively, and these segment types are denoted by numbers from 1 to 6 for simplicity.

To validate the effectiveness of the adaptive rescheduling decision mechanism based on random forest (RF-ARDM), this subsection conducts comparative tests on 100 groups of randomly selected actual production data under recessive disturbances. The prediction performance of RF-ARDM was verified by comparing the actual result (i.e., the optimal rescheduling method calculated based on basic models) and the prediction result based on RF-ARDM, as shown in Table 1 and Fig. 4. The research results demonstrate that the rescheduling decision mechanism proposed in this paper can achieve good results in practical application, which is helpful to deal with various recessive disturbance scenarios efficiently, timely and accurately.

Table 1 Verifying the effectiveness of RF-ARDM based on instances

Instance No.	Production feature vector	Prediction result	Actual result
1	(0.792, 1.241, 0.008, 0.017, 6, 7, 8, 3, 5, 9, 38, 0.013, 0.042)	1	1
2	(6.856, 0.955, 0.033, 0.006, 9, 8, 17, 5, 6, 12, 57, 0.039, 0.268)	1	1
3	(−0.990, 0.545, −0.008, 0.006, 6, 7, 10, 3, 6, 11, 43, 0.005, −0.016)	1	1
4	(3.629, 2.781, 0.025, 0.022, 6, 7, 12, 5, 6, 12, 48, 0.023, 0.174)	**2**	**1**
…	……	…	…
30	(3.804, 12.600, 0.017, 0.067, 9, 8, 20, 5, 6, 12, 60, 0.084, 0.390)	2	2
31	(12.315, 3.886, 0.075,0.028, 7, 8, 13, 5, 6, 12, 51, 0.089, 0.544)	2	2
…	……	…	…
98	(3.220, 1.309, 0.917, 0.044, 2, 6, 3, 3, 2, 7, 23, 0.045, 0.132)	3	3
99	(1.346, 4.609, 0.017, 0.072, 6, 7, 7, 3, 3, 9, 35, 0.052, 0.127)	3	3
100	(7.939, 6.182, 0. −58, 0.056, 6, 7, 11, 4, 6, 12, 46, 0.060, 0.416)	**2**	**3**

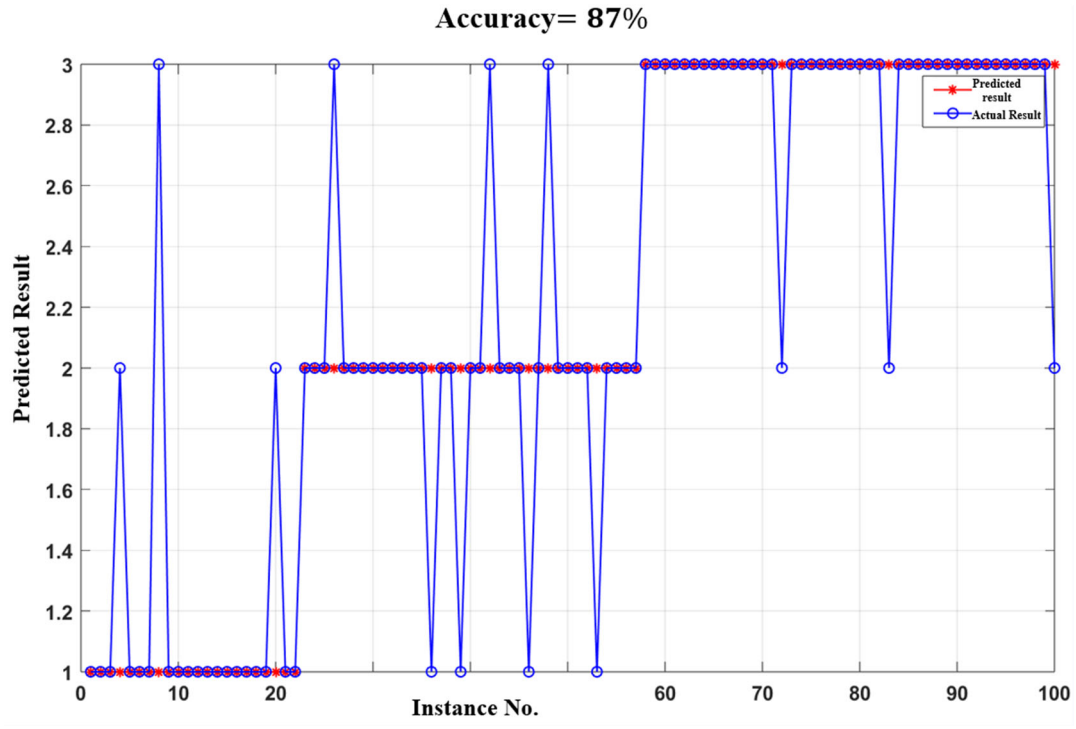

Fig. 4. Comparison of Actual and Predicted Results

5 CONCLUSION

Considering the recessive disturbances in the prefabrication production, it is difficult for decision-makers to accurately evaluate its impact on the schedule and timely decide whether

to repair or update the original schedule. Therefore, this study establishes an adaptive rescheduling decision-making mechanism to help precast factories improve their ability to deal with production disturbances and ensure production stability. In order to enhance the applicability of the model, we introduce the concept of batch production into the prefabricated production process and build the basic model (BM-I, BM-II, and BM-III) under different rescheduling modes. These models reflect the implementation effect of various rescheduling methods in mathematical form and lay the foundation for constructing an adaptive rescheduling decision mechanism. Secondly, we determine the production feature vector to quantify the impact of recessive disturbances, and obtain a large number of data samples with decision labels through simulation experiments, which provides a low-cost method to generate rescheduling decision samples when massive samples cannot be obtained. Then, by learning the characteristics of data samples, we build an adaptive rescheduling decision mechanism based on random forest (RF-ARDM) to adaptively decide when and how to reschedule according to the real-time production status, which offers a fresh research perspective for intelligent production scheduling and interference response of prefabricated production. The proposed mechanism can greatly improve the efficiency of rescheduling decision-making, enhance the ability of the precast factories to deal with production disturbances, and ensure the stable implementation of production.

There are some limitations and shortcomings in this paper, which can serve as future research directions. Firstly, with the continuous development of machine learning methods, future research can endeavor to employ more efficient algorithms to improve the prediction accuracy of the rescheduling decision mechanism. Secondly, this paper solely focuses on a single recessive disturbance scenario. However, disturbances often occur concurrently in practical production; for example, dominant disturbances such as demand changes and machine failures may coincide with recessive disturbances. Henceforth, future research should consider how to conduct production scheduling when confronted with multiple simultaneous disturbances.

REFERENCES

[1]. Z. Wang, H. Hu, and J. Gong, "Simulation based multiple disturbances evaluation in the precast supply chain for improved disturbance prevention," J. Clean Prod., vol. 177, pp. 232-244, Mar 2018.

[2]. P. Zheng, J. Wang, J. Zhang, C. Yang, and Yongqiao Jin, "An adaptive CGAN/IRF-based rescheduling strategy for aircraft parts remanufacturing system under dynamic environment," Robot. Comput.-Integr. Manuf., vol. 58, pp. 230-238, Apr 2019.

[3]. Z. L. Ma, Z. T. Yang, S. L. Liu, and S. Wu, "Optimized rescheduling of multiple production lines for flowshop production of reinforced precast concrete components," Autom. Constr., vol. 95, pp. 86-97, Nov 2018.

[4]. C. Hutengs and M. Vohland, "Downscaling land surface temperatures at regional scales with random forest regression," Remote Sens. Environ., vol. 178, pp. 127-141, Jun 2016.

[5]. D. Yuan, J. Huang, X. Yang, J. R. Cui, and Ieee, "Improved random forest classification approach based on hybrid clustering selection," Chin. Aut. Congr., pp. 1559-1563, Nov 2020.

Proceeding of the 10th International Conference on Innovative Production and Construction (IPC 2024), Perth, Australia, July 11-12, 2024

Applications of LLMs in Construction: Case Studies in China

Liang Ma[1,2], Xinyu Zhao[1,2], Chengke Wu[3*], Yuanjun Guo[3], Zhile Yang[3], Qinge Xiao[3], Hanping Guo[4]

1. School of Management, Shanghai University, Shanghai 200444, China
2. Institute of Regional and Urban Development, Shanghai University, Shanghai 200444, China
3. Shenzhen Institute of Advanced Technology, Chinese Academy of Sciences, Shenzhen, Guangdong, 518055, China
4. Shenzhen Tianhua Architectural Design Institute, Shenzhen, 518038, China

ABSTRACT: Large Language Models (LLMs) have been applied in intelligent question answering of housing and construction knowledge, design assistance, analysis and decision-making. This paper uses a combination of literature research and case analysis. Firstly, this paper conducts a literature analysis, sorts out the development process of LLMs, and introduces the related technologies of LLMs. Secondly, nine application cases of LLMs in China are analyzed, and the technology, function and application scenarios are discussed. Through case analysis, this paper finds that LLMs are only initially applied to the upstream and downstream industry chain and the whole life cycle of buildings. At present, the vast majority of LLMs applications are simple question answering and the generation of building plane, elevation, and interior effect drawings. LLMs are not yet integrated with the workflows of construction management (safety, cost, schedule, quality, etc.). Meanwhile, most LLMs applications directly apply the cloud model API without local training. As such, the security of data and the illusion of LLMs also restrict the development of the domain LLMs. Based on the current application status of LLMs in the construction industry, it can be improved in the following five aspects in the future: (1) Expand the dataset. (2) Combined with the construction management workflow. (3) Combined with IFC. (4) Provide personalized services. (5) Optimize model performance.

KEYWORDS: LLMs, construction industry, case studies

1 INTRODUCTION

The Fourth Industrial Revolution (4IR) has brought rapid technological changes to the world [1]. Information technologies under 4IR have triggered changes in many industries to meet the growing global market demands and improve the efficiency of workflows [2,3]. On the other hand, although the construction sector currently contributes about 13% to global GDP, productivity growth has only increased by 1% per year over the past two decades [4,5]. In addition, the industry is facing numerous challenges such as delays, health and safety, cost overruns, and other issues [6]. One way to address the issues is to adopt artificial intelligence (AI) techniques. For example, AI has been employed in cost forecasting, delay forecasting, building design energy forecasting, worker activity recognition, construction site safety, cash

flow forecasting, structural health monitoring, resource allocation and optimization, predictive maintenance, and decision making [7].

In recent years, the development of Conversational AI(CAI) has improved significantly [6], which deals with the application of NLP and enable computers to understand and interact with humans in an intuitive manner using natural language [8]. In the construction industry, most existing Conversational AI tools are based on traditional NLP methods, which require time to process and label data. Moreover, most tools require expertise to use, thereby restricting their usefulness and practicality.

LLMs are neural networks with large parameters that are trained using self-supervised learning and semi-supervised learning on large datasets. These LLMs have improved NLP and shifted direction away from training with labeled data for defined objectives. The Generative Pre-trained Transformer (GPT) model comes from OpenAI's decoder structure, which has gained significant attention, especially when GPT-3.5 was released in 2022. Due to the excessive large training dataset and parameters, the GPT model achieves few-shot (provide contexts and examples in the prompts), zero-shot (no example is provided in the prompt) learning capabilities [9].

In the construction industry, although LLMs have the potential to overcome existing challenges of AI applications by saving data collection and labelling time and lowering the requirements of using AI [6]. The industry lacks a systematic analysis of current LLMs applications. Thus, this paper analyzes nine application cases of LLMs in Chinse construction domain and shed light on challenges and future opportunities. China is selected as it witnesses the fast adoption of over 200 domain-specific LLMs, making it a suitable subject of such case studies; 2) China is the largest construction contractor in the world, indicating excessive potential and value of implementing AI techniques like LLMs.

2 LLMs

LLMs are pre-trained language models based on self-supervised learning of large-scale unlabeled data, which have strong general ability and can adapt to and complete multi-scene tasks[10,11]. Currently, popular LLMs are: GPT-4 (1.8 trillion parameters), GPT-3 (175 billion parameters), BERT (of which BERT-large has 340 million parameters), ERNIE (of which ERNIE 3.0 has 260 billion parameters), etc. In 2017, Google proposed Transformer [12,13]. Since then, OpenAI and Google have proposed GPT [14] and BERT [15], respectively, based on Transformer. GPT uses the decoder part of Transformer, which uses a one-way prediction mode from front to back. BERT, on the other hand, employs the encoder portion of the Transformer, using the bidirectional prediction model from above and below [16]. In 2023, Meta released the LLaMA model series[17], which further optimized the Transformer model architecture and trained the models with more sufficient data, achieving good performance. Since then, many researchers have continuously carried out local optimization based on LLaMA model, such as Baichuan, Yi, Mistral, Qwen, etc. [16].

In China, LLMs have been implemented in many industries and have been widely distributed and applied. In the financial industry, LLMs are used in scenarios such as intelligent customer

service and pre-sales assistants to improve the efficiency and quality of services. In the medical industry, LLMs are used in scenarios such as medical document generation and intelligent medical question answering. In addition, LLMs are also applied in architecture, education, office and other fields.

3 TECHNOLOGIES RELATED TO LLMS

3.1 Prompt Engineering

Prompt Engineering is an important concept in the field of Natural Language Processing (NLP), which refers to a fragment of text or sentence that is used to trigger and guide LLMs to generate a specific output. Prompt can be a word, a phrase, a question, or a complete sentence, and they can be used to guide the model to generate a specific response, text, summary, or other output. Currently, the main use of LLMs is prompt to ask the LLMs to perform a specific task. The key of Prompt Engineering is how to design effective prompt. This involves choosing the right vocabulary, grammatical structure, contextual information, instructions, etc. to ensure that the model understands and responds to the prompt correctly. With the continuous development and deepening of prompt technology in the field of NLP, the traditional prompt has gradually evolved into chain-of-thoughts and chain-of-tree.

3.2 Reinforcement Learning from Human Feedback

Reinforcement Learning from Human Feedback (RLHF) refers to the introduction of human annotators into the learning process of LLMs to train reward models aligned with human preferences, and then effectively guide the training of LLMs. The model can better follow the user's intention and generate content in line with user preferences. RLHF consists of the following steps: (1) Train Supervised policy model. (2) Train the reward model. (3) Use proximal policy optimization for reinforcement learning.

3.3 LLMs-based Autonomous Agent

LLMs-based Autonomous Agent refers to the agent technology that uses LLMs as the core brain to plan, make decisions and execute complex tasks. LLMs-based Autonomous Agent is divided into four main modules: Profiling Module、Memory Module、Planning Module、Action Module[18].The profiling module aims to indicate the profiles of the agent roles, which are usually written into the prompt to influence the LLMs behaviors. The memory module plays a very important role in the agent architecture design. It stores information perceived from the environment and leverages the recorded memories to facilitate future actions. The memory module can help the agent to accumulate experiences, self-evolve, and behave in a more consistent, reasonable, and effective manner. The planning module aims to empower the agents with such human capability, which is expected to make the agent behave more reasonably, powerfully, and reliably. The action module is responsible for translating the agent’s decisions into specific outcomes. [18].

3.4 Retrieval Augmented Generation

Retrieval Augmented Generation (RAG) is a powerful natural language processing model that combines retrieval and generation methods. The principle of RAG technique can be divided into the following steps: Firstly, according to the input question, the information related to the question is retrieved in the large-scale corpus. Secondly, the retrieved information was understood and processed, and the generative model was used to enhance the information to improve the accuracy and completeness of the information. Finally, the generative model is used to integrate the processed information into a complete answer and output [19]. RAG combines the strengths of language models and information retrieval techniques. When the model needs to generate text or answer a question, it first retrieves relevant information from a large collection of documents and then uses this retrieved information to guide the generation of the text. This combination improves the quality and accuracy of the prediction. In addition, since the RAG model combines retrieval and generation stages, it can reduce the occurrence of model illusion problem to a certain extent.

4 CASE ANALYSIS

This paper introduces the application of LLMs in the construction industry through the following nine cases.

Table 1: Application cases of LLMs in the construction industry

Case	Technology	Function	Application scenarios
Construction-GPT	RAG, Semi-supervised fine-tuning, value alignment	Dialogue on technical data of construction engineering	The whole life cycle of the building
Zhuo Ling	RAG,AI drawing review technology	Intelligent Interaction between LLMs and Engineering Drawings	The whole life cycle of the building
Gouli AI	RAG、knowledge graph	Intelligent Q&A	engineering
TeleChat	Knowledge graph reinforcement, multi round knowledge memory and reinforcement, RAG	Intelligent Q&A, assisted design, analytical decision-making	Architectural design and urban safe operation
IQbots	RAG, Intelligent agent	Support developers to create robots with zero code, low cost, and high quality	The whole life cycle of the building
XKool AI Cloud	RAG, SD1.5	Text or images generate renderings, Online model training	Architectural design
DvArch	SD 1.5	Text or images generate renderings	Architecture, landscape, urban, interior design, etc.
ArchitectureRealmix	SD 1.5	Text or images generate renderings	Architecture, landscape, urban, interior design, etc.
SiKong	RAG, LLaMA, Alpaca fine-tunes LLMs	Architectural assistant design, drawing guidance, comprehensive scoring, full life cycle prediction	The whole life cycle of the building

4.1 LLMs of Architectural Questions

4.1.1 Construction-GPT

Construction-GPT is the first 10-billion-character knowledge-enhanced dialog large language model in China's construction industry independently developed by the Construction Artificial Intelligence Research Laboratory of Shanghai Construction Fourth Construction Group. Construction-GPT contains four main functions: intelligent Q&A of specifications and standards, intelligent search of detailed drawings of engineering atlases, intelligent query of internal control technical documents, and intelligent construction of private knowledge base. The adoption of data throughput acceleration technology improves the inference speed of Construction-GPT model, and it only takes 5~10 seconds to answer the test without network delay. In addition, Construction-GPT also alleviate illusion of general LLMs, minimizing fabricated answers.

4.1.2 Zhuo Ling

Zhuo Ling can be used to understand, answer and manipulate various construction field data such as drawings, models and specifications. At the same time, Zhuo Ling can accurately understand the industry terminology and user intentions, to achieve industry-leading intelligent interaction. Unlike traditional data retrieval, which can only do one-time keyword searches within a certain range in isolation, Zhuo Ling can understand the user's intent through multiple rounds of dialog, rather than relying on the latest query statement, thus greatly improving the efficiency of the user's access to information. In addition, Zhuo Ling can improve communication quality by mining the user's hidden intent based on the current interaction context, rather than relying only on interrogative statements.

4.1.3 Gouli AI

Gouli AI converts construction industry knowledge such as national norms, national standard atlases, local standards, design drawings, engineering models, documentation, etc., into a knowledge graph for intuitive interaction. The platform provides not only a library of specifications, but also a think tank of experts to provide users with authoritative interpretations and real-time correlations. Gouli realizes the functions of precise query of knowledge, voice Q&A, expert answer, intelligent recommendation, and decision-making support, so as to serve the whole life cycle of planning, design, review, and operation and maintenance. The main novelty of this product is to enhance RAG using knowledge graph by allowing tracing the typology of information.

4.1.4 TeleChat

TeleChat can efficiently process and analyze a large amount of construction industry data, thus helping industry decision makers better understand market trends, optimize design solutions, and improve construction efficiency. In addition, the model is able to predict the life of a building and the need for maintenance and renewal by analyzing its structure, materials and use. However, TeleChat does not provide testing entry; based on the current capabilities of general LLMs, which are still not professional at tasks like prediction and classification, the authors believe that the functionalities of TeleChat are not realized by the LLMs itself, instead, the LLMs are responsible for understanding the user input, and then employ local small models to carry out the task, such as using a Bi-directional long-short term

memory (Bi-LSTM) model to predict building life and using a tunned optimizer that improves design or layout.

4.1.5 IQbots

IQbots is a one-stop industry intelligent dialog platform based on AI technology and the knowledge base of the construction industry, providing intelligent dialog services and integrating robot creation, configuration and operation. Users can quickly create their own proprietary robots with zero code using IQbots without having to master complex AI technology. Meanwhile, IQbots provides access terminals for robots, where users can make inquiries, including intelligent dialog, associative prompts, popular questions and other functions to help users quickly locate the answers they want. IQbots is the only architectural LLMs that applies agents, which are AI-centric systems that can autonomously perceive their environment, make decisions, and perform actions. But IQbots agents are just custom chatbots and not intended to integrate with customer workflows.

4.2 LLMs of Architectural Drawing

At present, LLMs has been applied to architectural design, and there are about a dozen products that generate design drawings based on LLMs, but all of them directly call SD or MID JOURNEY API and do not train local image large model.

4.2.1 XKool AI Cloud

XKool AI Cloud uses SaaS technology to deploy its products in the cloud, and users access the software and hardware services in the cloud by purchasing IDs. Meanwhile, XKool AI Cloud provides functional modules such as Inspiration Square, Inspiration Creation, Model Bazaar, Model Training, AI Toolbox, etc., which allow users to generate concept maps based on text or images, and share and use high-quality AI models. Finally, XKool AI Cloud can perform AI-assisted creation according to text or pictures, generate the same design drawing, and provide online model training.

4.2.2 DvArch

DvArch (Multi-Prompt Architecture Tuned Model) is a powerful model that is particularly suitable for the field of architecture and interior design. This model can generate realistic building appearance, and can also generate interior decoration layout. Architects can use the model to generate 3D rendered images of the exterior and interior Spaces of the building to more intuitively demonstrate design concepts and assist in the communication and decision-making process with clients. Interior designers can use the model to quickly generate different styles of interior decoration layout and material rendering, thereby helping clients better understand the design scheme, and compare and choose between multiple schemes.

4.2.3 ArchitectureRealmix

ArchitectureRealmix is suitable for the vast majority of architectural, landscape, urban and interior design scenarios. This model was released by author laizhende at civitai, based on

SD1.5, with a total model volume of 3.95G. On civitai, the total number of downloads of the model reached 23K and the total number of user likes was 2.1K, showing its wide recognition and popularity as an excellent architectural drawing model.

Fig.2: ArchitectureRealMix line drawings and renderings

4.2.4 SiKong

SiKong has a wide range of applications in the field of architectural planning. As one of LLMs based on Chinese construction industry knowledge, it learns the construction industry knowledge data, so that the language model has the ability to judge information and integrate information like a professional architect. Specifically, SiKong can provide intelligent assistance in architectural design to help designers quickly generate compliant architectural designs. At the same time, it can also be used in architectural planning, landscape design, interior design and other scenarios, providing comprehensive support from concept to detail. Although SiKong can provide aided design and fine-tune the model based on LLaMA, the model size of SiKong is small (only 7B), which restricts the promotion of SiKong.

5 GAPS, OPPORTUNITIES AND FUTURE WORK

5.1 Gaps of current application

Although LLMs have been used in the construction industry, its application is very limited. At present, the vast majority of LLMs applications are simple question answering and the generation of building plane elevation and interior effect drawings. This is the simplest and most straightforward way to use LLMs and is not yet integrated with the workflows of construction management (safety, cost, schedule, quality, etc.). At the same time, most LLMs applications do not train locally, but directly apply the cloud model API. This is due to the lack of high-quality datasets for fine-tuning in the construction industry and the lack of computing resources. Even if the model is trained locally, there are at most 100B model levels, which limits its performance.

In addition, in LLMs applications, building models contain a large amount of sensitive data and information, such as design details and cost estimates. How to ensure the security and privacy protection of data is an important challenge. Also, the cost of interoperability in the construction industry is huge [20], and the different software and digital tools used have different formats, which makes seamless interoperability difficult. Due to the lack of unified data format, the conversion and sharing of LLMs between different software becomes difficult, which may lead to hindered project cooperation and communication, affecting work efficiency.

Finally, despite improvements in NLP in LLMs, models are prone to hallucinations (giving untruthful voices and plausible information), which reduces system performance and user expectations [21]. When generating a building plan or analyzing data, the model selects the most likely option based on probability. This selection process can introduce randomness and sometimes cause the model to generate "illusions" that do not match the facts. The false

information generated by the illusion of large language model may affect the quality of the project, and even threaten the life and health of the staff.

5.2 Opportunities and future work

At present, LLMs have been initially applied to the construction sector. It can provide intelligent design management and design review solutions to upstream enterprises, and can provide construction solutions combined with assembly type to downstream supply chain enterprises. In addition, LLMs have also been initially applied to the whole life cycle of buildings.

In the investment preparation stage, LLMs can be used by analyzing historical data and current market trends. In the design stage, the architect can use the model to generate 3D rendered images of the building's exterior and interior Spaces to more intuitively present the design concept and assist in the communication and decision-making process with the client. In the construction stage, engineers can use LLMs to ask for project data, such as searching for "What is the total floor area of this project?". LLMs can intelligently identify project information, quickly response with data and drawings. In addition, engineers can also use LLMs to retrieve technical data, such as: construction management data, engineering quality control data, safety and functional inspection data, and engineering quality acceptance data. In the product sales stage, real estate developers and agents can use LLMs to produce high-quality promotional pictures that show the appearance, apartment type and interior decoration effect of the property and attract the attention of potential buyers. In the operation and maintenance phase, LLMs can analyze the data generated by the building, such as equipment logs, sensor data, etc., and combine natural language processing techniques to perform a simple analysis of possible faults.

Based on the current application status of LLMs in the construction industry, it can be improved in the following five aspects in the future: (1) Enlarge the dataset. At present, some LLMs (Construction-GPT, Gouli AI, etc.) have transformed the Construction industry knowledge such as national specifications, documents and expert experience into computer program language through artificial intelligence technology. In the future, LLMs can also make full use of two types of data resources. The first is the industry examination. A variety of engineering test questions at home and abroad have naturally formed the form of question and answer pairs. The multiple choice questions can also provide positive and negative examples at the same time, which is very suitable for large model training. Second, the public construction industry related legal documents (judgments, rulings, etc.). The construction industry involves a large number of claims and construction disputes, and these case documents are open, compared with the standard specification, the number is larger, and more suitable for actual production, which can be used as a supplement to the standard specification.

(2) Combined with the building management workflow. We propose to focus on the core PDCA process of construction management, starting from the management dimensions of safety, cost, schedule, quality, and sort out the points that can be automated to reduce

repetitive work, and then use agents for automation. Agents understand the job requirements, automatically plan the function execution and the data needed to perform it, and then directly output the results, enabling the coupling of large model capabilities and workflows.

(3) Combined with IFC. IFC is the basis of BIM, and BIM is a characteristic model of the construction industry, which is not available in other industries. We suggest that the training and application of large models should be combined with BIM, and the training process can combine IFC data. IFC is a data format in the form of code, which is more formatted and standardized than natural language, with minimal ambiguity. In the future, IFC files can be generated based on natural language, so as to realize natural language driven BIM modeling. One possible way of training is to consider the IFC data between two related components of the BIM model (such as the wall and the window on the wall). These IFC data are also naturally related, and we know that at the time of modeling, there is the wall before the window, so the order relationship is also determined. Therefore, IFC data can be used to fine-tune LLMs by referring to the training method of Transformer models (known upstream corpus or code, predicted downstream corpus or code).

(4) Provide personalized service. Because LLMs cannot provide privatized data services, the privacy of engineering management cannot be guaranteed, which leads to its low application degree. At present, some LLMs try to establish private knowledge base and build personal exclusive intelligent knowledge system. For example, the Construction-GPT research and development team has independently developed a multi-modal data analysis algorithm. Technicians only need to upload files with one click, and Construction-GPT can automatically parse 24 kinds of documents, drawings, and audio format files, establish a personal exclusive knowledge space, and create a personal exclusive intelligent knowledge retrieval system.

(5) The model performance was optimized to reduce the errors caused by LLMs illusion. Knowledge traceability is an effective method to reduce the illusion of LLMs, which can make the generated technical solutions more reliable. At present, some architectural language models support knowledge traceability. For example, the TeleChat can associate questions with reference sources through various traceability methods, making the generated answers more reliable. In addition, Construction-GPT can also achieve answer traceability.

6 CONCLUSIONS

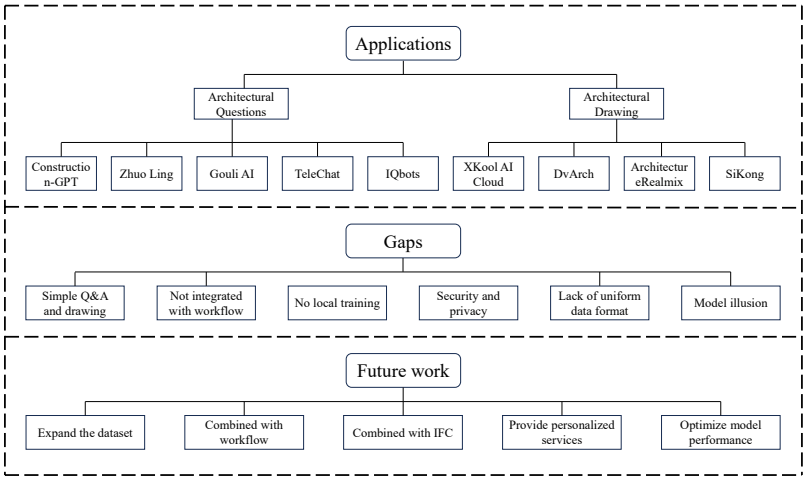

This paper conducts an in-depth analysis of the application of LLMs in the construction industry through specific cases. Firstly, through literature analysis, the development process of large language model is sorted out, and the related technologies of large language model are introduced. Secondly, nine application cases of language models such as Construction-GPT are deeply analyzed, and the technology, function and application scenarios of the models are discussed. Through case analysis, this paper finds that LLMs have been initially applied to the upstream and downstream industry chain and the whole life cycle of buildings, but its application degree is very limited. At present, the vast majority of LLMs applications are simple question answering and the generation of building plane elevation and interior effect drawings. Not integrated with construction management workflows (safety, cost, schedule, quality, etc.). At the same time, most LLMs applications do not perform local training, but directly apply the cloud model API. Even if the model is trained locally, the model size is small. In addition, the security of data and the illusion of LLMs also restrict the development of LLMs.

Fig.1: Applications of LLMs in construction

Based on the current application status of LLMs in the construction industry, it can be improved in the following five aspects in the future: (1) Enlarge the dataset. In addition to the standard, specification and other corpus, we can also make full use of two types of data resources. One is the industry examination, the other is the public construction industry related legal documents (judgments, rulings, etc.). (2) Combined with the building management workflow. We suggest aiming at the core PDCA process of construction management, starting from the management dimensions of safety, cost, schedule, quality, etc., to sort out the points that can be automated to reduce repetitive work, and then use agents for automation, so as to realize the coupling of large model capabilities and workflows. (3) Combined with IFC. IFC is the basis of BIM, and BIM is a characteristic model of the construction industry, which is not available in other industries. We suggest that the training and application of large models should be combined with BIM, and the training process can combine IFC data. (4) Provide personalized services to ensure the privacy of engineering management. (5) Optimize model performance, such as using knowledge traceability technology to reduce errors caused by LLMs illusion.

REFERENCES

[1]. Kazaz, A., & Acıkara, T. (2015). Comparison of labor productivity perspectives of project managers and craft workers in Turkish construction industry. Procedia Computer Science, 64, 491-496.

[2]. Kumar, K., Zindani, D., & Davim, J. P. (2019). Industry 4.0: developments towards the fourth industrial revolution. Cham, Switzerland: Springer.

[3]. Leviäkangas, P., Paik, S. M., & Moon, S. (2017). Keeping up with the pace of digitization: The case of the Australian construction industry. Technology in Society, 50, 33-43.

[4]. Egan, J., 1998. Rethinking Construction: Report of the Construction Task Force on the Scope for Improving the Quality and Efficiency of UK Construction. Department of the Environment & R. (DETR). T. a. t. https://constructingexcellence.org.uk/wp-content/uploads/2014/10/rethinking_construction_report.pdf.

[5]. Ribeirinho, M. J., Mischke, J., Strube, G., Sjödin, E., Blanco, J. L., Palter, R., ... & Andersson, T. (2020). The next normal in construction: How disruption is reshaping the world's largest ecosystem. McKinsey & Company.

[6]. Saka, A., Taiwo, R., Saka, N., Salami, B. A., Ajayi, S., Akande, K., & Kazemi, H. (2023). GPT models in construction industry: Opportunities, limitations, and a use case validation. Developments in the Built Environment, 100300.

[7]. Abioye, S. O., Oyedele, L. O., Akanbi, L., Ajayi, A., Delgado, J. M. D., Bilal, M., ... & Ahmed, A. (2021). Artificial intelligence in the construction industry: A review of present status, opportunities and future challenges. Journal of Building Engineering, 44, 103299.

[8]. Kulkarni, P., Mahabaleshwarkar, A., Kulkarni, M., Sirsikar, N., & Gadgil, K. (2019, September). Conversational AI: An overview of methodologies, applications & future scope. In 2019 5th International conference on computing, communication, control and automation (ICCUBEA) (pp. 1-7). IEEE.

[9]. Wei, J., Wang, X., Schuurmans, D., Bosma, M., **a, F., Chi, E., ... & Zhou, D. (2022). Chain-of-thought prompting elicits reasoning in LLMs. Advances in neural information processing systems, 35, 24824-24837.

[10]. Bender, E. M., Gebru, T., McMillan-Major, A., & Shmitchell, S. (2021, March). On the dangers of stochastic parrots: Can language models be too big? In Proceedings of the 2021 ACM conference on fairness, accountability, and transparency (pp. 610-623).

[11]. Hu Kaibao, Gao Li. Foreign Language Development in the Context of Large Language Models: Problems and prospects. Foreign Language World, 2024,(2):7-12.

[12]. Vaswani, A., Shazeer, N., Parmar, N., Uszkoreit, J., Jones, L., Gomez, A. N., ... & Polosukhin, I. (2017). Attention is all you need. Advances in neural information processing systems, 30.

[13]. Hochreiter, S., & Schmidhuber, J. (1997). Long short-term memory. Neural computation, 9(8), 1735-1780.

[14]. Radford, A., Narasimhan, K., Salimans, T., & Sutskever, I. (2018). Improving language understanding by generative pre-training.

[15]. Devlin, J., Chang, M. W., Lee, K., & Toutanova, K. (2018). Bert: Pre-training of deep bidirectional transformers for language understanding. arxiv preprint arxiv:1810.04805.

[16]. Han Bingtao, Liu Tao. Key Technology and Application of Large Model [J/OL]. Zte Technologies. https://link.cnki.net/urlid/34.1228.TN.20240418.1324.004

[17]. Touvron, H., Lavril, T., Izacard, G., Martinet, X., Lachaux, M. A., Lacroix, T., ... & Lample, G. (2023). Llama: Open and efficient foundation language models. arxiv preprint arxiv:2302.13971.

[18]. Wang, L., Ma, C., Feng, X., Zhang, Z., Yang, H., Zhang, J., ... & Wen, J. (2024). A survey on large language model based autonomous agents. Frontiers of Computer Science, 18(6), 1-26.

[19]. Zhou Yang, CAI Pei-han, DONG Zhen-jiang. Big Model Knowledge Management System [J/OL]. Zte Technologies. https://link.cnki.net/urlid/34.1228.TN.20240422.1818.002.

[20]. Ji, Z., Lee, N., Frieske, R., Yu, T., Su, D., Xu, Y., Ishii, E., Bang, Y.J., Madotto, A., Fung, P., 2023. Survey of hallucination in Natural Language generation. ACM Comput. Surv. 55 (12), 1–38. https://doi.org/10.1145/3571730.

[21]. Shehzad, H.M.F., Ibrahim, R.B., Yusof, A.F., Khaidzir, K.A.M., Iqbal, M., Razzaq, S., 2021. The role of interoperability dimensions in building information modelling. Comput. Ind. 129 https://doi.org/10.1016/j.compind.2021.103444.

Proceeding of the 10th International Conference on Innovative Production and Construction (IPC 2024), Perth, Australia, July 11-12, 2024

From Digital Model to Digital Twin in Tunnel Construction

Hannah Salzgeber, Melanie Ernst, Matthias Flora

Unit of Construction Management and Tunnelling (iBT), University of Innsbruck, Innsbruck, Austria

ABSTRACT: This paper takes a further step on the digitalisation path in tunnelling by implementing the concept of the digital twin and examining its potential at the three levels of real-world integration: digital model, digital shadow, digital twin. It evaluates the current implementation of Tunnel Information Modelling (TIM) and its adoption in the infrastructure sector. The importance of structured and real-time data synchronization through technologies such as IoT and Big Data is emphasised. It explores advancements from tunnel model to shadow to twin (DT), emphasising the importance of structured and data real-time synchronisation through technologies like IoT and Big Data. A comprehensive literature review highlights both technical and non-technical barriers to the implementation of DT. Continuous improvement of DT, supported by advancements in data acquisition and analytical methods, is expected to significantly enhance tunnel construction. As a main focus, this paper provides a framework for a centralised and comprehensive platform for all levels of tunnel twin development, leveraging Autodesk Platform Services (APS). It concludes with a vision for the future, advocating for a strategic approach to digital transformation in tunnelling that leverages technological innovations for sustainable development and societal benefits.

KEYWORDS: BIM; TIM; tunnel twin; digitalisation; tunnelling

1. INTRODUCTION

The construction industry is undergoing a digital revolution, with Building Information Modelling (BIM) leading the way. Tunnel Information Modelling (TIM), an extension of BIM, is increasingly embraced for its capacity to handle the vast data generated in tunnel construction, despite facing hurdles such as inconsistent standards and legal complexities surrounding data ownership and large file sizes.

At the outset of this paper, the current landscape, practices, and research in TIM are examined, followed by an investigation into the principles and guidelines governing its implementation. It then delves into the concept, definition, and progression of digital tunnel twins, highlighting their potential to revolutionise tunnel construction through real-time data synchronisation and structured data management, with a particular focus on the tunnel twin's distinctive challenges and opportunities.

Subsequently, the paper outlines a comprehensive methodology for integrating all levels of real-time data synchronisation, from tunnel model to twin, within a unified platform, exemplified by the use of Autodesk Platform Services (APS), stressing the importance of

structured data environments for enhancing data processing and management beyond the digital model. Furthermore, it consolidates the University of Innsbruck's research efforts and TIM model approaches into a cohesive environment, paving the way for the next step, the sensor data incorporation and model advancement elevating the TIM model into the tunnel shadow.

The initial achievement of a functional tunnel shadow is viewed as a crucial step towards the full utilisation of a tunnel twin, emphasising the transformative potential of digital twins in actively influencing real-world models through actuator control. Their versatility is explored not only in post-construction phases to influence a real-world entity but also in pre-construction stages through “mocked” twins, facilitating pre-emptive optimisations. Through practical applications and examples, the broad benefits of digital twins are examined, underlining the necessity of holistic approaches for maximal efficacy. Additionally, the pivotal role of seamless integration across systems and data sources in realising the full potential of digital twins is discussed, addressing challenges and presenting examples such as the realisation in APS.

Finally, the paper discusses the rapid advancement of artificial intelligence (AI), particularly in machine learning, computer vision, and natural language processing. Due to the consistent processing and interpretation of real-time data and the need for coordinated data structures in both technologies, the conjunction of digital twinning and AI is the logical consequence for efficient and intelligent data management. To fully harness AI's capabilities, ensuring a substantial amount of high-quality data is imperative, as AI models heavily rely on the quality of their training data. Consequently, the generation of robust data structures and high-quality tunnel models and tunnel shadows is deemed essential for maximizing the efficacy of AI applications and to further achieve a functional tunnel twin.

1.1 Tunnel Information Modelling - TIM

Building Information Modelling (BIM), as a clear trend of digitalisation within the construction industry, is rapidly becoming widely adopted. While a few years ago, its use was limited, especially in infrastructure construction, its importance has become indispensable for many. The growing use of various terms such as Infrastructure Building Information Modelling (I-BIM, InfraBIM), Infrastructure Information Modelling (IIM), Civil Information Modelling (CIM), Mining Information Modelling (MIM, MiningBIM), and Tunnel Information Modelling (TIM or TunnellingBIM) in recent articles and journals reflects the increasing recognition and significance of the adoption of the BIM-Method into the infrastructure field. Despite the proliferation of new terms, they all lead to the same conclusion: the use of the established BIM method within their respective disciplines [1], [2], [3], [4].

Globally, both clients and contractors are increasingly adopting BIM to tackle diverse challenges, such as the construction industry's low productivity index. Particularly in public and governmental construction projects, there is a growing demand for BIM to manage the

vast amounts of data which is being produced and has to effectively be managed over many years. Experts agree that exchanging digital models created with BIM using internationally recognised open standards like Industry Foundation Classes (IFC), Extensible Markup Language (XML) or other shareable formats offers numerous benefits for effective data management in the future [4].

As BIM becomes increasingly important in infrastructure construction, it's evident that Tunnel Information Modelling (TIM) has the least number of BIM-related scientific publications compared to other structural sectors. Despite TIM's lower profile in the industry, tunnel construction is widely acknowledged as particularly well-suited for BIM implementation due to the significant amount of structured data it produces and therefore it being one of the most closely monitored linear infrastructures. The substantial data generated throughout the various project phases links TIM to contemporary topics like the Internet of Things (IoT), Big Data, and API/Web platforms [5], [6], [7].

Given the complexity of infrastructure projects, which often involve multiple interacting disciplines, free form geometry and many information sources it is crucial to establish a coordinated workflow and ensure data compatibility to optimise information flow for interoperability. For this, some challenges like insufficient standards and unresolved legal issues in terms of data access, data ownership and use still remain obstacles for full and thorough implementation. Currently, a shortage of necessary BIM skills among project participants and stakeholders to fully launch and utilise the real potential of the method is identified. Extensive training, common goals and strategies as well as joint workshops are essential to bring participants to a common level of understanding and collaborative project implementation and realisation [8], [9], [10].

1.1.1 Current practice and research

Since Tunnel Information Modelling (TIM) is more and more demanded especially by European clients in the infrastructure sector, the German Committee for Underground Construction (DAUB) has issued recommendations for the application of Building Information Modelling (BIM) specifically for underground structures. These guidelines create an initial framework, particularly laying a focus on creating a common understanding of the method and all its new terms as well as laying the foundations for the implementation of ground models and tunnel structures. The recommendation comprises several parts, the first two explaining the basic concepts, defining standardised terms for object-specific elements in tunnel construction and their associated information, and outlining general processes related to data structure, information exchange, management, and provision. The third part focuses on ground modelling, while parts four and five address the tunnel structure, its modelling, and the creation of a model-based bill of quantities [11]. Similar recommendations and research efforts are being undertaken across the entire DACH region (Germany, Austria, Switzerland), contributing to a robust body of knowledge in this field. These guidelines and studies from DAUB and other institutions are crucial for advancing BIM practices nationally as well as

internationally, providing a comprehensive approach to managing complex underground construction projects.

Inspired by BIM practices, infrastructure projects also employ various specialised and partial models to capture the project using digital building models. In the context of Tunnel Information Modelling (TIM), the endowed professorship at the University of Innsbruck has defined three essential models to organise the overall representation of a tunnel project: the ground model, the structural model, and the site model, refer to Figure 4. This approach aligns with the DAUB recommendations and current practices and enhances the ability to manage and visualise the intricate details of tunnel construction projects effectively [12].

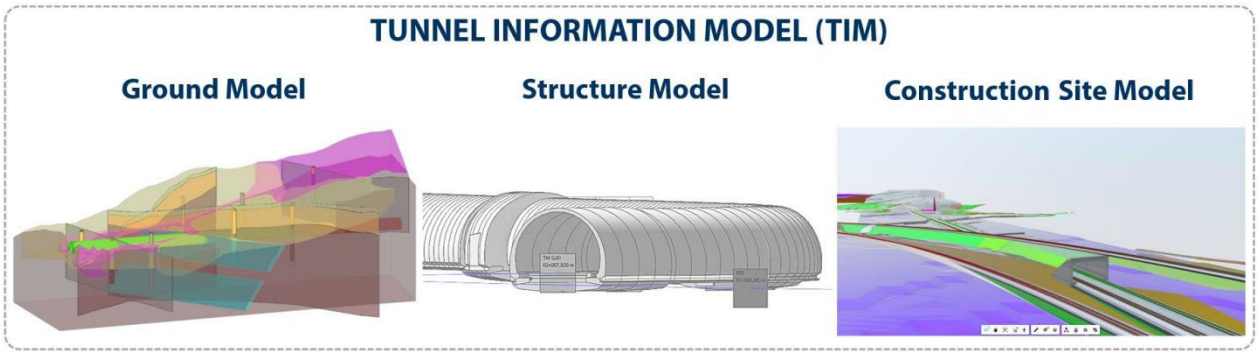

Figure 4: Defined partial models by the University of Innsbruck [4]

1.1.2 Current principles and standards

A 2021 international study analysed global BIM standards, finding that the USA and the United Kingdom lead in their development, while other countries adapt these standards to their needs. Some countries, including China and Germany, already implemented quite a few standards, however, lack specific project planning guidelines. The study emphasises the importance to create project-specific frameworks and documentation guidelines for project success. Despite the USA having numerous BIM specific standards, their state-level organisation leads to fragmentation and increased efforts. Effective BIM application requires coordinated standards to enhance efficiency. Overall, BIM standards in most countries are still in early development stages, preventing uniform implementation and underscoring the need for more comprehensive guidelines [13].

A key international standard for BIM widely used in practice is the ISO 19650 series. It sets out principles and requirements for managing information models, covering concepts, principles, and processes of information management, including security aspects across its lifecycle. Aligned with British (UK 1192 standards) and American standards, it incorporates the same principles and requirements as the UK BIM Framework. The term "Level of Information Need" (LOIN) was introduced in ISO 19650-1 to define minimum information requirements in digital building models [14], [15].

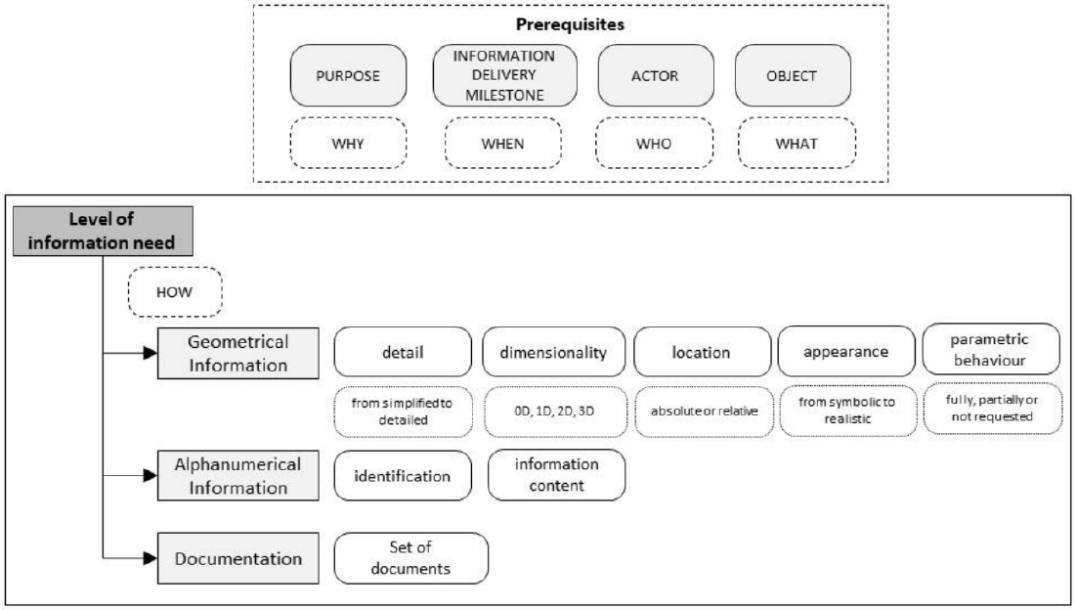

Figure 5: Level of Information Need according to EN17412 [16]

The European standard EN 17412 outlines the LOIN and its methodology, defining the extent and detail of information exchange. LOIN encompasses geometric, alphanumeric, and/or documentary information, with a primary focus on establishing machine-readable requirements, particularly for geometric data, that has up to now been primarily described through graphics. Figure 5 illustrates the structured framework of LOIN as envisioned by the EN standard [16].

Given the overarching objective of structuring various data types—geometric, alphanumeric, and document lists—into machine-readable formats, the LOIN emerges as a cornerstone for organising databases. This framework may involve to establish a crucial connection between geometry and databases via a unique identifier, thereby obviating the necessity of inputting all generated data into modelling software. Especially, current practices of creating dummy objects to solely represent information with no geometrical or visual benefit may be abolished if a database may be linked over identifiers or cross-references. Moreover, defining the LOIN across different models and potentially even twins can profoundly impact to establish a universal comprehension of the geometrical and alphanumeric intricacies within models. While defining the LOIN marks a significant stride towards standardization, its practical implementation is yet to be realised.

In today's standards landscape, most of the guidelines and standards are primarily concerned with broadly applicable aspects of information management or are deliberately formulated in a neutral way to accommodate different sectors. Therefore, in the field of Tunnel Information Modelling (TIM), there is still a lack of specific standards that are explicitly tailored to the infrastructure needs of tunnel construction. Currently, some clients are opting to develop their own guidelines based on pilot projects for project- and company-specific implementation of BIM in infrastructure construction. This is either to enhance existing normative standards or

to fill gaps. This latter approach, however, risks creating potential future interface complications, particularly on larger projects, and may once again result in an unmanageable data mess.

1.2 The definition of Digital Twin

The term "digital twin" is attracting a great deal of attention in various industries in the field of digitalisation. Coined by Dr Michael Grieves in 2002, its initial association with product lifecycle management was aimed at enhancing physical systems through the inclusion of a parallel virtual system containing a comprehensive set of data that mirrored its real-world counterpart. Over time, the concept has undergone a significant evolution and has found application in a variety of forms and contexts. [17].

Originally, the term applied only to the digital representation of a product/process/asset. In the construction industry, for example, a digital building model created by BIM was often equated with a 'digital twin'. In recent years, however, the potential of a digital twin as extension of BIM has been recognised beyond its original scope. The search for a single, cross-industry definition has proven to be challenging due to differences in technological advances and industry requirements, resulting in a wide range of interpretations. Nevertheless, the most recent definitions tend to emphasise one core principle: that a digital twin maintains a bi-directional flow of data with its virtual representation and its physical counterpart [18], [19].

In view of the unique challenges and objectives of the construction industry, it is imperative to clarify and differentiate the fundamental concepts of digital model, digital twin and intermediate stages. Therefore, three key concepts for these stages are introduced by Flora et al., each reflecting different degrees of integration between tangible and virtual entities [18], [20] :

- **Digital Model:** A digital model represents a virtual depiction of the real object, with data being linked manually between the two entities.
- **Digital Shadow:** In the case of the digital shadow, an automated linkage is established for communication and data transmission from the real object to its virtual counterpart (e.g. sensors).
- **Digital Twin:** The digital twin goes a step further by not only integrating an automated link but to also enable bidirectional data transmission, allowing for continuous synchronisation between the real and virtual objects and to actually steer or carry out task through the virtual model in the real entity.

These terms, each playing a unique role at different stages of a structure’s lifecycle, are essential building blocks for accurately representing construction projects at different levels of integrity. These differences in link dynamics are illustrated in Figure 6.

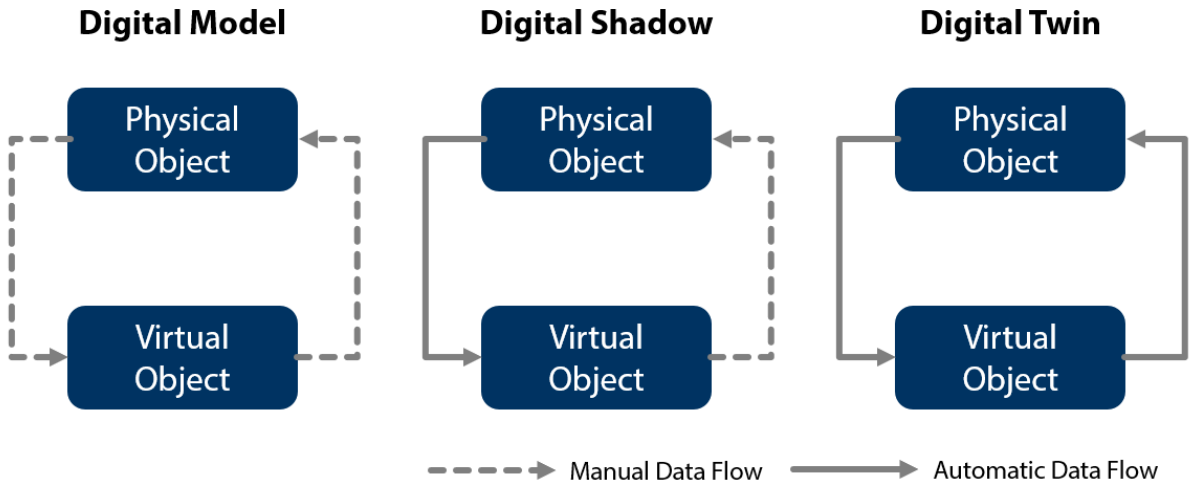

Figure 6: Distinction between Digital Model, Digital Shadow, and Digital Twin [20]

According to current developments and the defined definitions and stages above, a comprehensive Digital Twin in construction relies on integrating three key elements: the real object, a virtual data model and their integration in a shared data environment. This dynamic synergy not only ensures an accurate digital representation of the construction project, but also facilitates the creation of a responsive monitoring and control framework that is able to take advantage of real-time data inputs, see Figure 7.

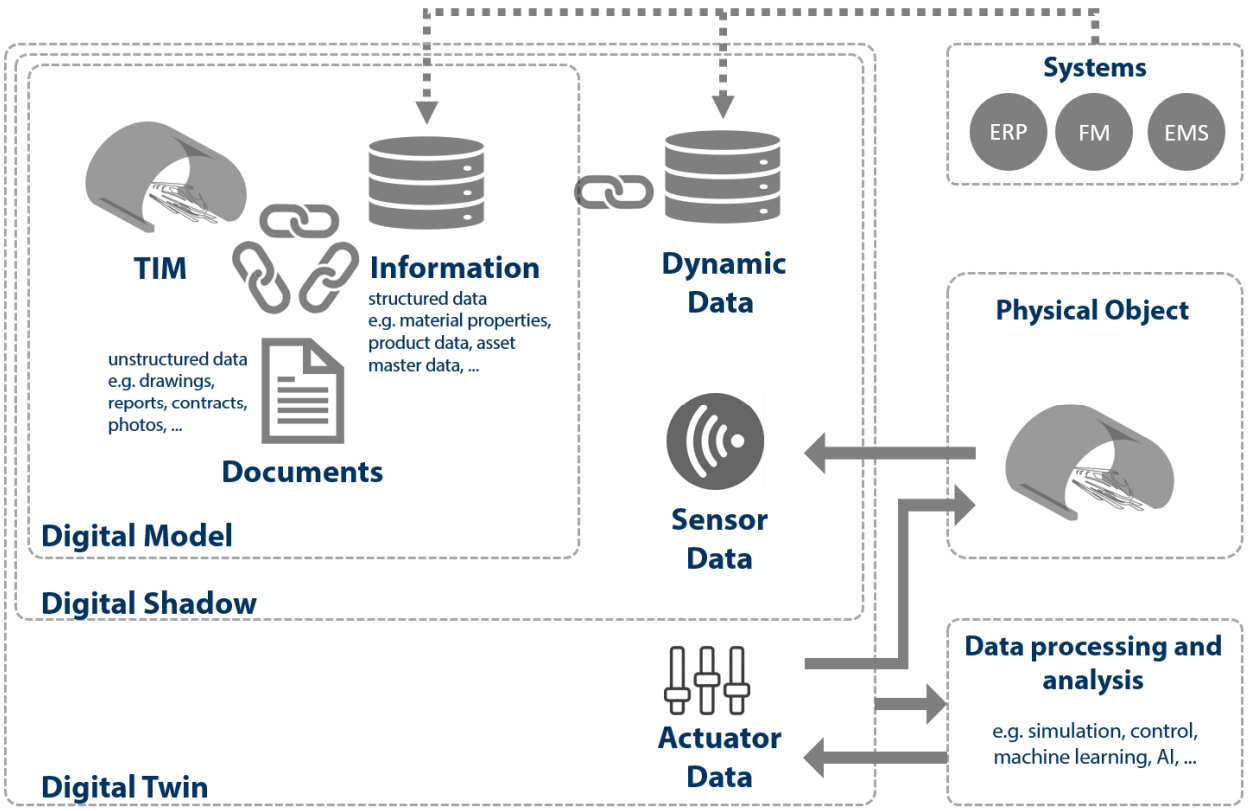

Figure 7: Structure of a digital twin with associated data sources [20]

1.3The Tunnel Twin

As of today, the Digital Twin (DT) technology in tunnelling reflects a growing sophistication in its application, emphasising its potential to significantly enhance tunnel construction processes. The use of digital twins in tunnel construction not only promises more efficient operational processes but can also offer significant advantages during the execution as well as the operational phase. A deliberate definition of goals and use cases sets the framework for the scope of the real and virtual space to eventually realise a true tunnel twin. These goals and use cases critically determine which components, subdivisions, systems, data and integration methodologies are incorporated into the tunnel twin, ensuring a comprehensive and coherent digital representation that aligns with the specified requirements and objectives.

A comprehensive literature review by Li et al., published in February 2024, revealed that although the concept of digital twins (DT) was introduced in 2003, it only began to receive significant attention in the tunnel industry starting in 2019. Current research primarily focuses on general technologies such as conceptual frameworks and modelling methods, with a particular emphasis on the operation and maintenance phase. Further, often simple geometrical representations are already considered as a DT. As per the definition of the three levels of integrity of the DT in chapter 0, for tunnelling the main components could be seen as follows: the physical entities e.g., geology, machinery or structure, the connection of data for the digital shadow is realised through sensors, data processing and transmission, and the virtual digital model may be created using the TIM method and therefore geometric, semantic, and analytical models [21].

Achieving a fully realistic DT for tunnelling is challenging due to inherent uncertainties in data and physical mechanisms. The technology must account for these uncertainties and continuously update the virtual model based on new data. Effective implementation of DTs requires multi-scale, self-learning, interoperable, and extensible systems to adapt to the dynamic nature of tunnel construction. Additionally, there are significant technical and non-technical barriers, including issues related to data quality, security, economic investments, and collaborative management practices that need to be addressed for successful DT adoption. The continuous improvement of DT models, supported by advances in data acquisition technologies and analytical methods, is expected to further enhance the safety, efficiency, and quality of tunnel construction. Ongoing research aims to refine these models to better integrate traditional construction methods and address complex geological and structural challenges effectively [21].

To understand the varying integrity levels of digital twins in tunnel construction, their application potential, and the ways to overcome associated challenges, we need to closely examine the three stages Digital Model, Digital Shadow, Digital Twin in detail. This examination will lay the groundwork for creating a fully functional tunnel twin.

2. A POSSIBLE PATH TO THE TUNNEL TWIN

An application of digital twins in tunnel construction offers numerous advantages spanning the entire life cycle of the tunnel project. As previously described, the use case determines the informational and functional content of a digital twin, thereby also defining whether it is a digital shadow or a true digital twin. Furthermore, a comprehensive digital twin can be composed of various discipline-specific, sub-, or partial twins. By aggregating these, a holistic digital twin may be formed. Therefore, individual partial twins can be generated for one or more use cases and can also be utilized independently.

A few possible examples may be but are not limited to:

- Enhanced Decision-Making and Automation
- Early Fault Detection
- Improved Operation Efficiency
- Sustainability Optimization
- Smart Operational Management

With the increasing importance of digitalisation in the construction industry, there are more and more options for creating a digital twin. Prime examples of possible platforms are Tandem and Autodesk Platform Services (APS), both products from the Autodesk Group [22][23]. Another notable solution is Microsoft Azure Digital Twins, which is a Platform-as-a-Service that allows the creation of a digital twin based on digital models [24].
The focus in the following sections is on APS, as it allows the creation of extensions that can be tailored to individual use cases.
APS is a cloud development platform that consists of a set of APIs with which it is possible to implement, visualise, and automate various workflows.
The basic core of APS makes it possible to upload and visualise a digital model. Not only are data formats from Autodesk itself supported, but also a variety of other standards, including open standards, such as IFC.
With the various APIs offered in APS, it is also possible to link several models together and extract, modify, and manipulate information from the model. This gives one the possibility to extract information from sensors, such as the ID, and create a link to a database where the sensor data is stored. The values of these sensors can then be visualised in the application. APS can be used to create dashboards but also heat maps, for example, illustrating the temperature in the tunnel and on the machine and whether a component, e.g. ventilation, is running and at which capacity[23].

Similar to BIM, the consistent use of a digital twin throughout the life cycle is advantageous and more economical, as the implementation of a digital twin requires a certain amount of effort, which is spread over the individual phases or use cases when used consistently. The structuring of the data or division of the sub-twins according to use cases is also like the BIM approach. This is the only way to ensure that the required data is available in the required scope and quality for further processing [4].

2.1. Digital Tunnel Model

The digital model, as the first step towards the DT and its virtual entity, is not a single model but rather a coordination of multiple partial and discipline-specific models, creating a shared project environment. Research by the University of Innsbruck highlights that this coordination or master model includes at least three defined partial models: the construction site, the structure, and the ground model, all developed using the TIM method. The exact number of independently created models is determined on a project-by-project basis and can consider factors such as the number of stakeholders as well as location and time dependencies.

Currently, pilot projects often embed all alphanumeric information directly into native objects within various modelling software. A new approach involves extracting only the necessary alphanumeric data, such as geometrical outputs or material specifications, defined in the modelling software. In addition, geometrical objects are linked to a centralised database with a unique identifier. This allows each element to be enriched with additional information outside of the modelling software, preventing the software and exported files from being overloaded with data and resulting in smaller file sizes. As seen in Figure 8, in a shared project environment, in this example APS, all models will be coordinated and visualised through a viewer and dashboards, where the link between databases and geometry can be accessed and utilised.

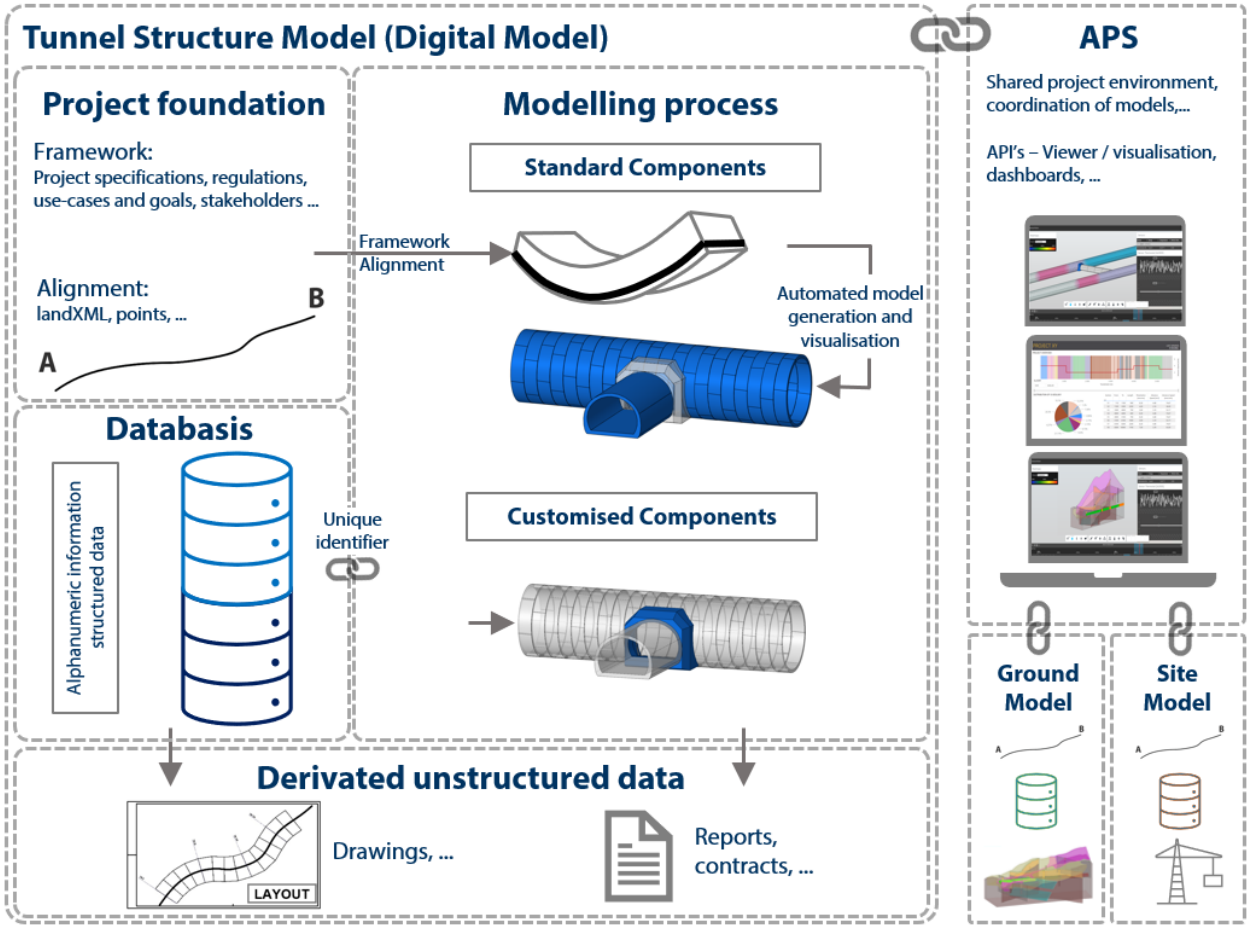

Figure 8: The digital model, its link to databases and coordination within APS

Additional structured data from database-driven management systems, including ERP (Enterprise Resource Planning), FM (Facility Management), and EMS (Energy Management System), serving as immutable master data, as well as unstructured data in the form of documents such as plans or reports, may be linked to or derived from a Digital Model and the databases. This represents a static as well as dynamic state and provides a robust foundation for time-specific analyses, such as periodic cost tracking, time calculations, or calculation of quantities.

The significance of a well-structured database in this context cannot be overstated. Linking objects and elements with minimal information to the information rich database forms the foundational building block for all subsequent assumptions, calculations, and eventually AI evaluations. This integration also enables the simulation of variant studies, scenarios, and other analyses. When used as the basis for workflows, processes, calculations, and simulations across various projects and stakeholders, a shared and reusable structure becomes indispensable to keep workflows and data flows running. Embracing this innovative approach allows stakeholders to harness a comprehensive digital model which ensures the resilience and efficacy of project management, decision making, and execution.

2.2. Digital Tunnel Shadow

The development of digital shadows or twins can take place at different levels of complexity, depending on the definition of the use cases and the resulting requirements for the data models. The extension of the digital model into a digital shadow, through an automated data flow from the real object and its virtual counterpart, requires the integration of systems that produce dynamic data. This dynamic data can originate from sensors, processed data, or machine data. Integration into the digital shadow requires structured data and a link to the digital model. The data models can be linked at the component level, spatial level (e.g., via tunnel meters or coordinates), and/or temporal level. In terms of real-time monitoring of the built environment, it is currently possible to collect data from construction sites or tunnel operations using IoT technologies such as Wi-Fi, WSN, 5G, LP-WAN, and surveillance cameras [20],[4],[25].

As well as the digital model, the digital shadow can also be created using APS by linking (real-time) data from the real world and the digital model. APS allows the real-time data to be visualised in the model, for example through dashboards and the highlighting of certain structure elements [23]. One example of this is a tunnel boring machine (TBM). The TBM utilises GPS integration to measure its current location and registers important parameters for each advance. This allows for precise tracking of how much distance the TBM has driven over a specific period, see Figure 9. Dashboards can be used to view this registered parameter history, such as penetration, revolutions per minute, thrust force, etc. and this information can then be plotted as interacting graphs in the virtual model in the APS. It is important, that the link from the sensors in the real object to the virtual environment is automated and live. Only

then, live evaluations may be possible and time sensitive decisions may be made manually. The plotting of these graphs of the live data must also be readily available, for example to the machine operator in the operator cabin. Only then the live tracking of the data launches its full potential.

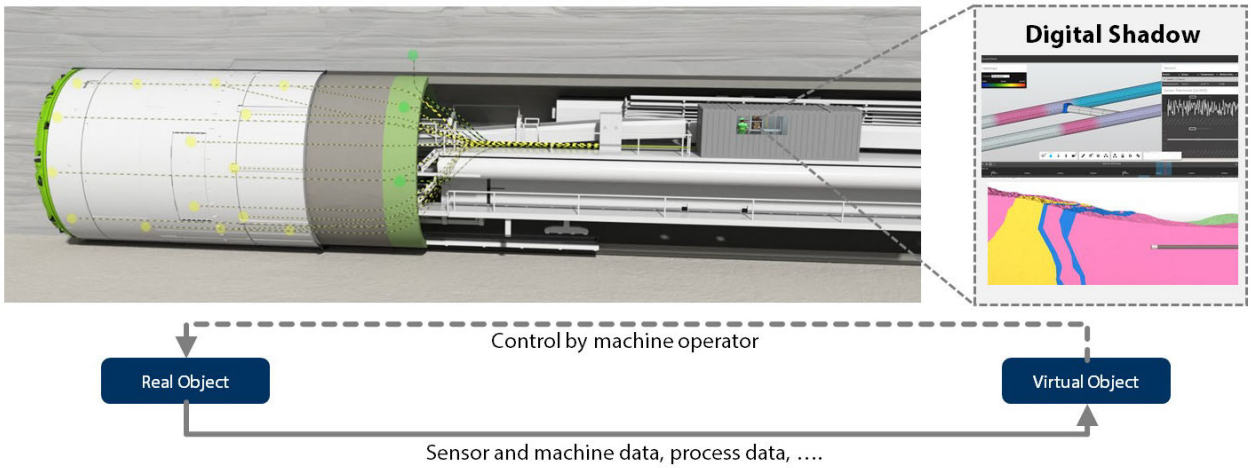

Figure 9: Digital Shadow of a tunnel boring machine [4]

In addition to visualisations and analyses of real-time data, the values can further be used to generate forecasts, such as a final project completion date. By linking geological information with sensor data from the TBM, automated calculations can predict based on already achieved performance how far the TBM will travel within a specific time frame. The forecast can then be repeatedly updated with the latest values of the machine. This workflow is especially interesting when comparing the tender and target data, as discussed in a paper by Exenberger et. al [26]. This comparison helps identify when and why delays occurred. It also allows for analysis of which aspects of human interaction led to improved performance, thereby enhancing overall efficiency in the future.

It is important to emphasise here that the structure of the information to be linked, e.g., the structure of the sensor information, in this case, the ID, should be consistent. For example, the name of the parameter must be the same in all models so that an automatic link can be made, and the manual steps can be reduced. These requirements for uniform naming, structuring, and data specifications can be effectively defined through the LOIN.

2.3. Digital Tunnel Twin

A digital twin can be realised when the digital shadow influences the real model by controlling actuators.

Using the example of sensors from the previous chapter, sensor data and potentially additional real-time information from other systems can be processed to lead to automated decisions, which can be translated into control commands. These control commands, represented as actuator data in the digital twin can be set and will influence the real tunnel.

However, a digital twin can not only be used from the construction phase onwards but also before construction of the real model has even started. A so-called mocked digital twin is created, which carries out various simulations using fictitious sensor data. One example of this is the monitoring of the air quality during a traffic jam or an accident in the tunnel and possible actions and their effects on the situation. This makes it possible to check which changes should and must be made to the design in order to achieve an optimised model [4].

In practical applications, especially in the operational phase, the application possibilities of a digital twin in tunnel construction are wide-ranging. Given the various use cases, the greatest added value is achieved through a holistic approach. This requires comprehensive aggregation or networking of all partial twins. It is also conceivable and desirable that aspects and software from the planning simulation are integrated into the control system. An application example is the control of a tunnel ventilation system that uses sensors to measure the air quality in a tunnel and then sends automatic control commands to the system. This is also covered by a conventional system, so the added value must again lie in a predictive control system that, for example, integrates data from weather reports or similar data sources. Furthermore, the traffic flow could also be analysed using image recognition software and integrated into the control software. This example is intended to show that only the linking of different systems, different data, and their joint analysis will bring benefits [4].
A specific illustration of this concept can be seen in APS, which is a prime example of how a functional, minimal digital twin can be created with relatively small effort. Once a virtual model has been created and sensor data has been linked to it, all that remains to be done is to install a control element, both in the virtual and real environment. Again, an example of this may be the ventilation system: if the measured pollution is too high, the ventilation can be switched on - manually or automatically. In APS, the sensor data is displayed as heat maps and as soon as a threshold is exceeded, i.e., the user, in this case, the operating company, can be prompted to take action. Of course, this process could be carried out automatically, but in some use cases, human interaction is recommended or even required due to the safety-critical nature.
In Figure 9 below, this process is displayed. The first step is to create a digital model, which can be imported into the APS application, indicated in blue. The next step is to link the model to real data to create a digital shadow: sensor data is sent to a database, such as InfluxDB, and is then processed on our custom server. The processed sensor data can then be visualised in our frontend.

To create the digital twin, action calculations are performed based on measurements and predictions. These actions can either be executed automatically or, for now, displayed in the frontend so that the user still must make the final decision.

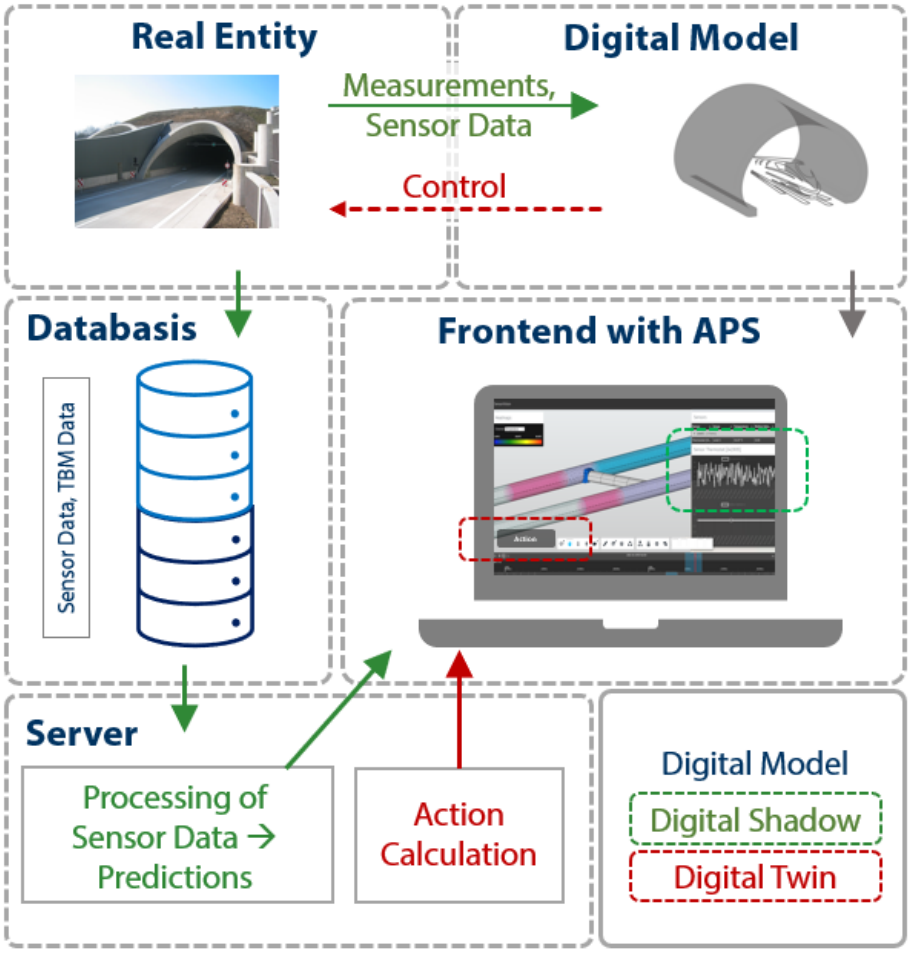

Figure 10: Process Overview using APS

For these systems to optimally function, a fundamental prerequisite for the digital twin is digital consistency. Without seamless integration of all relevant systems, sensors, and data sources, the twin cannot develop its full potential. The main challenge here is to integrate existing systems into the digitalisation process, whether in the sense of inventory tunnels, which are to be digitally recorded and prepared for the digital twin, or existing FM or ERP systems, which were not designed for such integration from the outset [4].

3. FURTHER POSSIBILITIES AND EMERGING TECHNOLOGIES

The development of artificial intelligence (AI) is rapidly progressing and is increasingly becoming important in research as AI makes it possible to understand, simplify, or even automate many processes [27]. Therefore, the Unit of Construction Management and Tunnelling (iBT) at the University of Innsbruck is progressively focusing on this topic. The possibilities are vast, with common fields including machine learning, computer vision, and natural language processing (NLP).

Computer vision and NLP refer to the automatic analysis and interpretation of images or language respectively [27]. In tunnel construction, for example, computer vision can be used

particularly well in tunnelling to categorise the types of rock and adapt the tunnel boring machine processes accordingly to what types are being encountered and further to possibly identify the need of further deposit or processing of the rock [28]. NLP could be particularly helpful in documentation. For example, processes on the construction site could be documented verbally. These are then converted into text and summarised so that progress can be documented more easily. Later, depending on the current progress, a list of tasks can be created.
ML uses statistical techniques to learn from existing data. With the help of ML, data can be clustered and correlations between various parameters can be determined. In general, machine learning (ML) makes it possible to analyse data and create a better understanding of correlations. However, it is also possible to go further and use this data and calculated correlations to create intelligent forecasts and run through scenarios [27].

Many researchers are currently working hard to simplify or automate various use cases in tunnelling with the help of artificial intelligence [25],[29][27][29]. Based on a review of almost one hundred papers, the focus is on the following areas [31]:

- Rock and Soil characterisation
- Construction optimisation with a focus on risk assessment and safety management
- Construction performance TBM:
    - Design and operation of TBM,
    - Performance prediction models, and
    - Fault detection
- Construction performance non TBM:
    - Optimisation and decision-making,
    - Tunnel stability and
    - Excavation

In order to achieve high-quality and meaningful results, the first step must be to collect data, as the AI learns based on so-called training data. To realise the full potential of an AI, a very large amount of high-quality data is required. After all, an AI is only as good as its training data. In addition, it is important to process and annotate the data carefully to ensure that the AI delivers precise and reliable results.
If you have too little data, you may run into the problem that different scenarios are not covered, and the AI then does not know how to react and act in this situation. There is also the problem of overfitting. If too little data is provided, it is more difficult to recognise a scheme and correlations. As a result, the AI model often only focuses on irrelevant parameters and performs sensationally well with training data, but is unreliable with real/new data [27].

The iBT work area is addressing this issue: we want to ensure structure and functioning data model to subsequently develop truly useful AI applications. Currently, a lot of data is kept in file formats like Excel, often unstructured and inconsistent, as everyone uses different names and structures, which makes the process considerably more difficult and not saleable at all.

Therefore, the initial focus is on the quality of the data in order to be able to create high-quality AI models. This is already working well in some areas, but there is still considerable room for improvement. Therefore, our current task is to ensure the quality of the data to maximise the potential of artificial intelligence in the future.

4. CONCLUSION

Tunnelling is well on the way to digitalisation, as shown by the number of publications and the significant progress made in research and business.

In this paper, we have primarily focused on the concepts of the digital model, digital shadow, and digital twin. A digital model represents a physical model, whereby the linking of the real and digital models is done completely manually. In contrast, digital shadow automates this link, allowing real-time data flow from the real model to its digital counterpart. With a digital twin, the data exchange is bidirectional, meaning information from the virtual model flows to the physical model and vice versa. Actions are carried out on the real model via the digital shadow.

In order to successfully implement the digital transformation in tunnelling with the existing structures, a forward-looking approach is necessary. This is presented in the form of a vision which, from the authors' point of view, describes an evolutionary rather than revolutionary path of transformation through technological innovations. The current challenges in the construction industry, its economic framework conditions, and social change must be considered. It is crucial to utilise digital innovations in a targeted and profitable manner in order to prevent them from becoming an end in themselves. As other sectors are already demonstrating, digital twins will be an integral part of the life cycle of buildings in the future and contribute to the digitalisation of the construction industry with the aim of sustainable development.

Despite all the digital possibilities, such as data analyses and artificial intelligence, those involved in the construction industry must ensure that technological developments and the resulting structures benefit society and individuals without creating new risks. In order to implement the digital transformation in tunnelling in an orderly manner, it is advantageous for those responsible to evaluate digital innovations impartially and analyse their benefits. This is the only way to utilise the upcoming changes as an opportunity.

REFERENCE

[1]. J. Salmi, R. Heikkilä, and M. Hyytinen, TUNNELLING & MINING INFORMATION MODELLING; A DIGITAL ENVIRONMENT FOR NEXT GENERATION MINING. 2023.

[2]. A. Fakhimi and J. Majrouhi Sardroud, “Civil Information Modeling Transformation Framework in Oil, Gas and Petrochemical Construction Industry,” Archives of Computational Methods in Engineering, vol. 30, no. 6, pp. 3559–3583, Jul. 2023, doi: 10.1007/s11831-023-09917-w.

[3]. F. Abbondati, S. A. Biancardo, S. Palazzo, F. S. Capaldo, and N. Viscione, “I-BIM for existing airport infrastructures,” Transportation Research Procedia, vol. 45, pp. 596–603, 2020, doi: 10.1016/j.trpro.2020.03.052.

[4]. M. Flora, G. Fröch, H. Salzgeber, and L. Schneiderbauer, Beton-Kalender 2025. Ernst und Sohn, 2024.

[5]. R. Sacks, I. Brilakis, E. Pikas, H. S. Xie, and M. Girolami, "Construction with digital twin information systems," Data-Centric Engineering, vol. 1, p. e14, Nov. 2020, doi: 10.1017/dce.2020.16.

[6]. A. Salzano, M. Intignano, C. Mottola, S. A. Biancardo, M. Nicolella, and G. Dell'Acqua, "Systematic Literature Review of Open Infrastructure BIM," Buildings, vol. 13, no. 7, p. 1593, Jun. 2023, doi: 10.3390/buildings13071593.

[7]. J. J. Cepa, R. M. Pavón, M. G. Alberti, A. Ciccone, and D. Asprone, "A Review on the Implementation of the BIM Methodology in the Operation Maintenance and Transport Infrastructure," Applied Sciences, vol. 13, no. 5, p. 3176, Mar. 2023, doi: 10.3390/app13053176.

[8]. P. Matějka, "The importance of a transport infrastructure construction for the implementation of BIM," an international scientific conference, pp. 1805–6784, 2014, Accessed: May 22, 2024. [Online]. Available: www.fce.vutbr.cz/ekr/PBE

[9]. A. Ciccone, S. Stasio, D. Asprone, A. Salzano, and M. Nicolella, "Application of openBIM for the Management of Existing Railway Infrastructure: Case Study of the Cancello–Benevento Railway Line," Sustainability, vol. 14, no. 4, p. 2283, Feb. 2022, doi: 10.3390/su14042283.

[10]. S. Kurwi, P. Demian, and T. M. Hassan, "Integrating BIM and GIS in railway projects: A critical review," in Proceeding of the 33rd Annual ARCOM Conference, 2017.

[11]. German Tunnelling Committee (DAUB), "BIM (Building Information Modeling)," Recommendations of DAUB. Accessed: May 22, 2024. [Online]. Available: https://www.daub-ita.de/en/publikationen/empfehlungen/

[12]. M. Flora, T. Weiser, P. Zech, A. Fontana, A. Ruepp, and K. Bergmeister, "Mehrwerte im maschinellen Tunnelvortrieb durch intelligente Systeme," Geomechanics and Tunnelling, vol. 14, no. 5, pp. 592–599, Oct. 2021, doi: 10.1002/geot.202100047.

[13]. A. Ganah and G. Lea, "A GLOBAL ANALYSIS OF BIM STANDARDS ACROSS THE GLOBE: A CRITICAL REVIEW," Journal of Project Management Practice, vol. 1, pp. 52–60, Jul. 2021, doi: 10.22452/jpmp.vol1no1.4.

[14]. M. Y. Ibrahim and D. A. Al-Kazzaz, "A comparative analysis of BIM standards and guidelines between UK and USA," J Phys Conf Ser, vol. 1973, no. 1, p. 012176, Aug. 2021, doi: 10.1088/1742-6596/1973/1/012176.

[15]. X. Pan, A. Mateen Khan, S. M. Eldin, F. Aslam, S. Kashif Ur Rehman, and M. Jameel, "BIM adoption in sustainability, energy modelling and implementing using ISO 19650: A review," Ain Shams Engineering Journal, vol. 15, no. 1, p. 102252, Jan. 2024, doi: 10.1016/j.asej.2023.102252.

[16]. Austrian Standards International, Bauwerksinformationsmodellierung - Informationsbedarfstiefe. 2021.

[17]. M. Grieves and J. Vickers, "Digital Twin: Mitigating Unpredictable, Undesirable Emergent Behavior in Complex Systems," in Transdisciplinary Perspectives on Complex Systems, Cham: Springer International Publishing, 2017, pp. 85–113. doi: 10.1007/978-3-319-38756-7_4.

[18]. W. Kritzinger, M. Karner, G. Traar, J. Henjes, and W. Sihn, "Digital Twin in manufacturing: A categorical literature review and classification," IFAC-PapersOnLine, vol. 51, no. 11, pp. 1016–1022, 2018, doi: 10.1016/j.ifacol.2018.08.474.

[19]. M. Liu, S. Fang, H. Dong, and C. Xu, "Review of digital twin about concepts, technologies, and industrial applications," J Manuf Syst, vol. 58, pp. 346–361, Jan. 2021, doi: 10.1016/j.jmsy.2020.06.017.

[20]. M. Flora, L. Schneiderbauer, and G. Fröch, "Von BIM zum Digitalen Zwilling – Möglichkeiten der Umsetzung," in STUVA-Tagung 2023 - Internationales Forum für Tunnel und Infrastruktur: 8. bis 10. November 2023, 2023, pp. 360–365.

[21]. T. Li, X. Li, Y. Rui, J. Ling, S. Zhao, and H. Zhu, "Digital twin for intelligent tunnel construction," Autom Constr, vol. 158, p. 105210, Feb. 2024, doi: 10.1016/J.AUTCON.2023.105210.

[22]. A. Ghosh, "Unleashing the full potential of digital twins with Autodesk Tandem." Accessed: May 24, 2024. [Online]. Available: https://blogs.autodesk.com/autodesk-life/inside-autodesk/digital-twin/

[23]. S. Chand and G. Busecan, "Autodesk Platform Services Documentation." Accessed: May 24, 2024. [Online]. Available: https://blogs.autodesk.com/autodesk-life/inside-autodesk/digital-twin/

[24]. Bailey Anderson, "Was ist Azure Digital Twins?" Accessed: May 31, 2024. [Online]. Available: https://learn.microsoft.com/de-de/azure/digital-twins/overview

[25]. C. do B. C. S. Alvarenga, M. T. P. De Aguilar, R. do B. C. Sales, and R. B. Caldas, "Digital twins a digital transformation for management of the construction industry," CONTRIBUCIONES A LAS CIENCIAS SOCIALES, vol. 17, no. 2, p. e4250, Feb. 2024, doi: 10.55905/revconv.17n.2-036.

[26]. H. Exenberger, I. Massimo-Kaiser, H. Salzgeber, P. Kompolschek, F. Heil, and M. Flora, "Concept for Tunnel Information Modelling based work-preview and documentation during construction at Tunnel Angath," 15th ISRM Congress 2023 & 72nd Geomechanics Colloquium. Schubert & Kluckner (eds.) © ÖGG, 2023.

[27]. A. Géron, Hands-on machine learning with Scikit-Learn, Keras, and TensorFlow. O'Reilly Media, Inc, 2022.

[28]. T. Marcher, G. Erharter, and P. Unterlass, "Capabilities and Challenges Using Machine Learning in Tunnelling," in Theory and Practice of Tunnel Engineering, IntechOpen, 2022. doi: 10.5772/intechopen.97695.

[29]. A. Mahmoodzadeh, M. Mohammadi, A. Daraei, H. Farid Hama Ali, A. Ismail Abdullah, and N. Kameran Al-Salihi, "Forecasting tunnel geology, construction time and costs using machine learning methods," Neural Comput Appl, vol. 33, no. 1, pp. 321–348, Jan. 2021, doi: 10.1007/s00521-020-05006-2.

[30]. A. Baghbani, H. Baghbani, and K. Kiany, "Utilizing Artificial Intelligence and Finite Element Method to Simulate the Effects of New Tunnels on Existing Tunnel Deformation," Journal of Computational and Cognitive Engineering, Aug. 2022, doi: 10.47852/bonviewJCCE2202307.

[31]. L. Liu, Z. Song, and X. Li, "Artificial intelligence in tunnel construction: A comprehensive review of hotspots and frontier topics," Geohazard Mechanics, vol. 2, no. 1, pp. 1–12, Mar. 2024, doi: 10.1016/j.ghm.2023.11.004.

Proceeding of the 10th International Conference on Innovative Production and Construction (IPC 2024), Perth, Australia, July 11-12, 2024

Multi-Reference Images Based on AI Identification to Complete Automatic Assembly Fasteners by Robot

Wen-Yang Chang, Michael Leandro Hartono, Chia-Jung Lin

1. National Formosa University, Department of Mechanical and Computer-Aided Engineering, Taiwan
2. National Formosa University, Smart Machinery and Intelligent Manufacturing Research Center, Taiwan
3. Mosa safety system corporation, Taiwan

ABSTRACT: The implementation of screwdrivers in assembling components stands as a foundational process in various production industries. Presently, the automated assembly technology integrates robotic arms alongside screwdrivers to autonomously fasten parts according to predefined positions. This research employs a robust image processing with convolution-based object detection algorithm aimed at accurately guiding the placement of a robotic arm equipped with a screwdriver. A 6-DoF robot arm with a webcam and an intelligent automatic screwdriver are integrated. To minimize error, this paper assesses and discusses the detection accuracy of the custom trained YOLOv5 object detection models by evaluating the F1-scores and the confusion matrices of the trained models in this study. According to the trained models in this study, the highest F1-Score obtained is 100% at 0.672 confidence rate. This model has a True-Positive (TP) score of 100% and 93% for the True-Negative (TN) score. Additionally, this study also discusses and compares the assembling performance of the screwdriver robot arm system developed by relying on both "Preset Positions" and "AI Detection Positions" for the screw hole position. From trials, the AI object detection algorithm applied to the screw driving robot arm system shows a significant enhancement to the system's capabilities in accurately classifying and recognizing screws, screw holes, and their respective positions throughout the assembly process, which provides more flexibility to the system for fastening screws compared to relying on the preset positions.

KEYWORDS: multi-reference images, CNN, confusion matrix, F1-score, fasten

INTRODUCTION

As the ongoing industrial revolution, often referred to as Industry 4.0, continues to evolve, the focus now revolves around digitizing robots through the integration of IoT systems and AI technologies. Within this Industry 4.0 landscape, the development of AI or machine learning (ML) models has expanded significantly, particularly due to their applicability in daily life. The realm of AI and machine learning encompasses various systems, including those dedicated to object detection. Specifically, ma-chine
learning models designed for object detection exhibit numerous variations and ver-sions, such as YOLO, ResNet, R-CNN, Fast R-CNN, among others. These different models and their performances will be explored in the subsequent discussion, drawing insights from past

research articles published in this domain. For innovations of automated screw driving robot arm, Ling [1] delves into the development of a screw
fastening robot arm that integrates a KUKA 6-DoF robot arm with a manual slotted screwdriver in which it is equipped with a torque sensor. Pitipong [2] conducted research focused on developing an automated screw fastening 4-DoF robot arm utilizing visual serving for the screwing process. Ruiya [4] has devel-oped an automated screw removal robot arm system utilizing a collaborative robot arm known for its heightened sensitivity to the surrounding environment. Alireza [5] conducted research on developing a nut unfastening robot integrated with a robotic surface exploration system. This study employed the FRANKA EMIKA Panda 7-DoF collaborative robot arm, equipped with a parallel jaw gripper end effector, and incor-porated a LOGITECH camera positioned within the working area. For machine learning models for screws and holes detection, Giovanni [6] focused on comparing
the performance of two object detection models and a binary classifi-cation (BC) model in identifying screws and screw holes on a laptop's PCB and chas-sis. Ibrahim [7] uses color camera attached to a 4 degreeof-freedom robot arm to reconstruct a 3D model with holes. This research utilizes Canny edge detector and LIME algorithm to both detect the edge of the object as well as reducing the noise from the Canny processed images. Zhihui [8] applied deep learning algorithm with CNN model to detect screws and screw holes on a phone's PCB for disassembly and assembly. This
research utilizes UR5 6-DoF collaborative robot integrated with two color cameras for scanning. Wanhao [10] researched on detecting screws and screw holes on mobile phones motherboard PCB by applying the semantic segmentation model.

CONCLUSIONS

With the system developed in this study, as the system performance is tested and compared in both preset positions and AI object detection condition to identify the screw hole positions, the number of fail trials which the system relies on the preset positions of the screw hole is at approximately 17%, which are mostly caused by the misalignment of the screw in the pickup process. On the other hand, as the system relies on the AI object detection to identify the screw holes with all the fail trials hap-pens on the process of fastening the last screw hole with the other 3 screw holes has been fastened. This is due to the fluctuation of the bounding box pre-diction size on the last screw holes, in which it is caused by the lack of illumination or lighting on the working area and the overshadowing of the other three assembled screw on work piece.

REFERENCES

[1]. L. Tang and Y.-B. Jia, "Robotic fastening with a manual screwdriver," 2023 IEEE International Conference on Robotics and Automation (ICRA), 2023. doi:10.1109/icra48891.2023.10161139

[2]. S. Pitipong, P. Pornjit, and P. Watcharin, "An automated fourdof robot screw fastening using Visual Servo," 2010 IEEE/SICE International Symposium on System Integration, Oct. 2010. doi:10.1109/sii.2010.5708355

[3]. R. Li et al., "Unfastening of hexagonal headed screws by a collaborative robot," IEEE Transactions on Automation Science and Engineering, vol. 17, pp. 1–14, Jan. 2020. doi:10.1109/tase.2019.2958712

[4]. Rastegarpanah, A., Ner, R., Stolkin, R., & Marturi, N. (2021). Nut unfastening by robotic surface exploration. Robotics, 10(3), 107. https://doi.org/10.3390/robotics10030107

[5]. G. Burresi et al., "Image-based defect detection in assembly line with Machine Learning," 2021 10th Mediterranean Conference on Embedded Computing (MECO), 2021. doi:10.1109/meco52532.2021.9460291

[6]. Baykal, I. C. (2018). Inspection of screw holes on machine parts using Robot Vision. 2018 International Conference on Artificial Intelligence and Data Processing (IDAP). https://doi.org/10.1109/idap.2018.8620904

[7]. Z. Deng, D. Guan, Y. Qiao, and C. Zhuang, "Tiny screw and screw hole detection for Automated Maintenance Processes,"2022 IEEE International Conference on Mechatronics and Automation (ICMA), 2022. doi:10.1109/icma54519.2022.9855990

[8]. W. Niu, H. Wang, and C. Zhuang, "Detection for tiny screw and screw hole by semantic segmentation model," 2023 9th International Conference on Mechatronics and Robotics Engineering (ICMRE), 2023. doi:10.1109/icmre56789.2023.10106576

Automatic Inspection Strategy for Underground Utilities Based on BIM

Zihan Yang, Jiangpeng Shu, Liang Zhao and Yong Bai

Zhejiang University College of Civil Engineering and Architecture, Hangzhou 310058, China

ABSTRACT: In response to the low level of automation in underground utilities infrastructure and high frequency of inspection needs, this article integrates underground utilities BIM with various automation algorithms, achieving a fully automated end-to-end planning process from the underground utilities to the inspection path. Firstly, a BIM information automatic extraction and modification algorithm based on geometric computation and graph theory was developed, which allows researchers to obtain and modify information related to inspections, such as utilities locations and obstacle dimensions.; Based on the obtained information, an automatic inspection strategy based on Chinese Postman Problem (CPP) has been developed. Finally, a Dynamo prototype was introduced to integrate all automation algorithms, minimizing manual intervention and achieving full process automation. The proposed method was validated in two existing BIM models of underground utilities, and the experimental results showed that the proposed method can automatically extract information from different section types of utilities models and calculate the shortest full coverage inspection path in the order of milliseconds.

KEYWORDS: underground utilities; building information model (BIM); inspection; path planning

1 INTRODUCTION

In recent years, with the rapid development of urbanization, underground utilities have emerged as one of the most prominent infrastructural elements[1][2]. Serving as a crucial component of urban underground planning and construction, these utilities integrate various pipelines such as water supply, gas, and electricity, delivering essential energy resources to countless households. As of 2021, the total length of China's urban underground comprehensive utilities has reached 6,706.95 kilometers. However, such large-scale and rapidly developing infrastructure construction has also brought about some challenges. The internal pipelines and walls within the underground utilities are gradually aging, potentially leading to various defects such as cracks and leaks[3]. To ensure the safety and sustainability of urban operations, regular and frequent inspections and maintenance of the underground utilities are essential[4]. Currently, the detection of underground utilities still relies predominantly on traditional manual methods, which are inefficient and pose safety risks. Thus, there have been research and experimental developments on track robots in confined environments[5][6]. These robots can follow predetermined tracks to perform various functions, automatically monitor spatial environments and equipment operations, and carry out tasks such as data collection[7][8]. However, these robots are severely constrained in their autonomy and must operate within limited ranges. Therefore, it is essential to develop autonomous

detection strategies and autonomous mobile robots for effective underground utilities inspections.

New technologies such as autonomous mobile robots and LiDAR have provided fresh opportunities for the intelligent inspection of underground utilities. Utilizing wheeled mobile robots equipped with sensors allows for comprehensive coverage inspection within the utilities, replacing manual operations[9][10]. The LiDAR mounted on the robot enables three-dimensional scanning, rapidly creating a digital twin model of the utility structure. Using algorithms to compare the digital model with the design model, the LiDAR can identify the location and severity of various defects such as cracks, collapses, and leaks within the utility[11]. As a digital tool, Building Information Modeling (BIM) has become the core technology for smart buildings. Many scholars have applied BIM to the full life-cycle management of buildings, with major application stages including the following: (1) Construction Phase: Comparing the construction site conditions with the designed BIM model to indicate differences in construction progress and plans[12], and automatically planning construction routes based on construction site conditions[13][14], (2) Operation and Maintenance Phase: Aligning actual damage information with the designed BIM model to create a visual and easily manageable damage information model[15][16], and making reasonable plans for indoor navigation paths using BIM information[17][18]. Currently, the application of BIM models for the management and visualization of above-ground buildings is relatively mature. However, there is limited research on the application of BIM technology in the underground utility environment.

This paper provides a detailed exposition of our work in developing an automated inspection method for underground utilities based on Building Information Modeling (BIM). The framework is designed for the full automation of inspections in underground utilities environments using mobile robots equipped with laser radar. The entire process can be automated and controlled through the development of Dynamo built-in in the Autodesk Revit 2024 software[19]. This advanced automation technology not only enhances the efficiency of underground utilities inspections but also ensures the accuracy and comprehensiveness of inspections. An innovative solution for underground utilities management is presented, providing robust support for the sustainable development of urban infrastructure.

2 METHOD

Figure 1 illustrates the proposed automatic inspection strategy for underground utilities based on Building Information Modeling (BIM). The process is divided into three main parts: utilities information extraction, modification based on initial information, and generation of inspection paths. Firstly, location information such as pipelines and utilities centerlines from existing BIM model are automatically extracted. Secondly, in order to prevent robots from getting too close to the pipeline and colliding with its supporting structure (the buttresses), the extracted centerline of the pipeline is offset based on the positions of the pipeline centerline and the pipe buttresses. The offset centerline is then segmented at specified intervals, extracting unordered path points, ensuring that the robot ultimately remains in the central position between the pipeline buttresses and the wall on one side away from the pipeline during inspection. Subsequently, utilizing the Chinese Postman Problem (CPP) planning

algorithm, the unordered coordinates on the offset utilities centerline are planned to form an ordered sequence of coordinate points. This coordinate sequence serves as the final reference for navigation information. Finally, the entire proposed information extraction-navigation planning process is implemented in Dynamo, achieving fully automated point-to-point planning from the utilities BIM model to the inspection path.

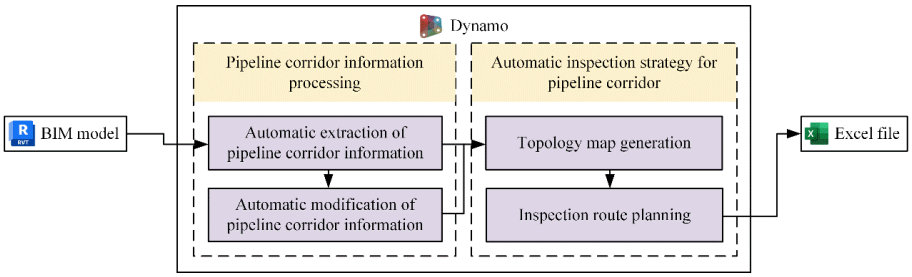

Figure 1. Workflow diagram of the BIM-based automated inspection strategy for underground utilities.

2.1 Geometric information extraction and modification

This section outlines the steps for extracting necessary information based on the original BIM model of the utilities.The process primarily focuses on extracting the following types of location information:

- Utilities branch centerline position: Basic position for robot navigation in the map.
- Intersection center point position of utilities: Basic position for robot navigation in the map.
- Pipeline centerline position: Basic information about obstacles and reference for offsetting utilities centerline.
- Pipeline radius: Basic information about obstacles.

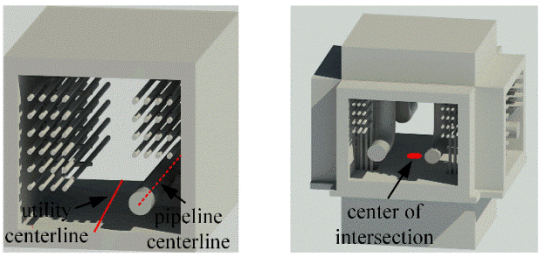

Figure 2. Schematic diagram of pipeline centerline, utility centerline and center of intersection, (a) pipeline centerline and utility centerline, (b) center of intersection.

After extracting all the pipeline centerlines, utilities centerlines, intersection positions, and geometric dimensions of buttresses, basic processing should be applied to the extracted information.The first step is to register pipeline centerlines with the utilities centerlines, meaning to identify multiple pipeline segments corresponding to the utilities segments and establish a correspondence relationship between their centerlines. The center points of all lines are selected for registering the lists. Using the utilities centerlines as a reference, the pipeline centerline list is registered and sorted. Firstly, the center point of each utilities centerline and pipeline centerline is calculated. Secondly, using the utilities center point as a

reference, the two closest center points from all pipeline center points are sequentially identified. These two center points correspond to the pipelines closest to the segment of the utilities (one on each side). By repeating the above steps, we establish a correspondence relationship for each segment of utilities, pipeline 1 and pipeline 2.

The second step involves modifying the position of the utilities centerline based on the pipeline's positional information. The ideal navigation position should be in the middle of the two nearest pipelines, meaning the utilities centerline should be appropriately offset based on the positions of the pipelines. The concept of automatic offsetting algorithm for utility centerlines is illustrated in the Figure 3. The direction of offsetting is determined by a vector starting from the utilities center point to the center point of the farther pipeline, and the offset distance can be calculated using the Eq.(1):

$$distance = \left|(d_1 - r_1) - (d_2 - r_2)\right| / 2 \tag{1}$$

Where d_1 and d_2 represent the projections onto the XY plane of the distances from the utilities center point to the center points of pipeline 1 and pipeline 2 respectively, and r_1 and r_2 are the radii of pipeline 1 and pipeline 2.

Using the offset vector (providing directional information) and the offset distance (providing distance information), we can now offset the initial utilities centerline. After all the utilities paths following the offset are obtained, they are discretized at certain intervals (the interval depends on the method used for damage data collection; for example, smaller intervals are needed for photographic methods, while relatively larger intervals can be used for LiDAR scanning). This gives us a set of inspection waypoints along the utilities branches. By adding the coordinates of all intersection points of the utilities into the set, we obtain a preliminary set of inspection positions that the robotic vehicle should maintain.

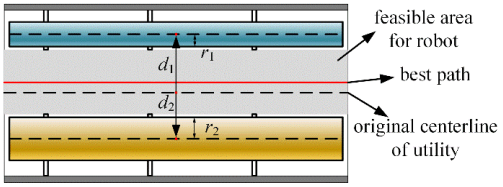

Figure 3. Schematic diagram of robot feasible area and offsetting process.

2.2 Automatic inspection strategy

In this section, the obtained unordered coordinate point information will be automatically formatted and transformed into a map data format that is more suitable for specific scene requirements and is required by path planning algorithms. We will start by taking the coordinate points from the branches and intersections of the pipeline, converting all extracted unordered path points into the format of topological maps. The final output should consist of two lists, named the final points list and the final points' relationships list, respectively describing all the points that need to be planned and the relationships between adjacent points.

- For each branch of the utilities: As shown in Figure 4 (a), let the n^{th} branch in the pipeline utilities be denoted as B_n, with a total of m pre-planned coordinate points on the

route, represented as B_{n1}, ..., B_{nm}. Since in the offset pipeline centerlines list, although there is no sequential relationship between the lines, all points extracted on each route are arranged in order. Therefore, for the R_n branch, the two points adjacent on this line can be written in pairs (B_{ni}, B_{ni+1}) (i+1<m). The relationship between all points on the remaining lines is also formed according to this method. At this point, the points and relationships on each utilities branch have been obtained, but adjacent branches are still independent of each other due to the lack of intersection connections.

- For utilities intersections: As shown in Figure 4(b), the center point of the n^{th} utilities intersection is denoted as I_n. Search for all points among the points of all branches that are within a certain distance from I_n. Connect these points to I_n, forming multiple points relationships.

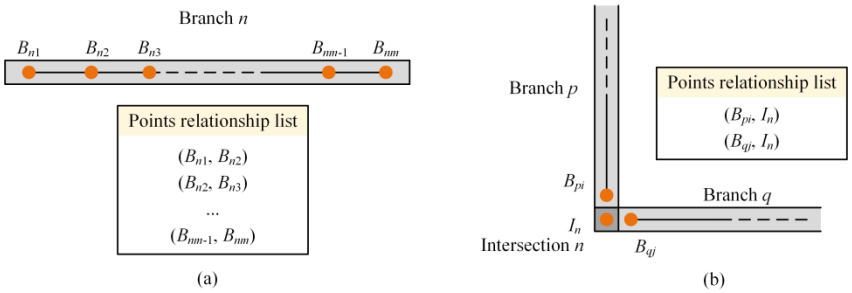

Figure 4. Diagram of relationships, (a) the relationships for each branch of the utilities, (b) the relationships for intersections.

Then, the underground pipeline utilities inspection problem is abstracted into the Chinese Postman Problem (CPP). CPP is a graph theory algorithm aimed at finding an optimal circuit where each edge in the graph is traversed at least once. The main purpose of the CPP algorithm based on the underground pipeline utilities environment is to achieve automatic inspection of the pipeline utilities. In this paper, the CPP algorithm based on the underground utilities' environments can be simplified into the following process: (1) calculate the degree of each point. Determine the degree of each point in the final points list, i.e., the number of relationships or pairs each point has, (2) use the minimum weight matching method, convert the original non-Euler graph containing multiple odd points into a Euler graph, (3) use the Fleury algorithm to solve the Euler circuit. Through the CPP algorithm based on the underground utilities environment, the final points list and final points' relationships list will result in an ordered list of coordinate points, providing the real location information for robot navigation.

2.3 Dynamo framework

A Dynamo framework is developed to integrate all the processes mentioned above, achieving end-to-end output from BIM model to ordered coordinate points. The developed framework consists of four parts: (1) Extraction of basic utilities information, (2) Modification of basic utilities information, (3) Generation of and topological map (4) Path planning algorithm and results output. The entire Dynamo framework integrates multiple automation algorithms, maximizing the reduction of manual intervention while considering the randomness in

modelling, and achieving the functionality of fully automatic information extraction from BIM models to path output.

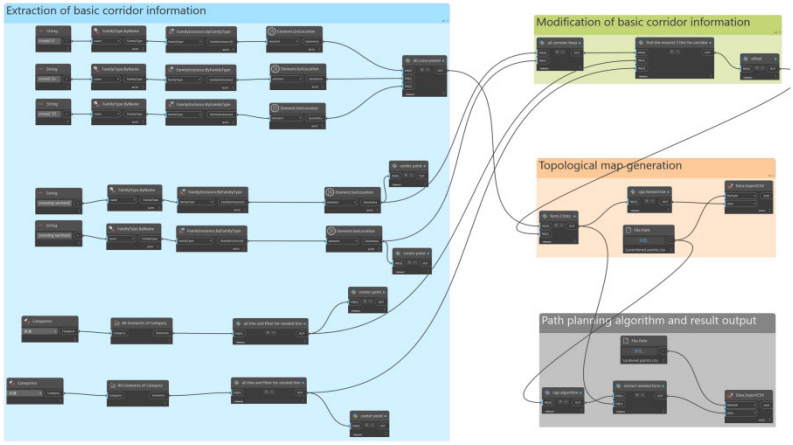

Figure 5. Dynamo prototype of proposed framework.

2.4 Results of two existing utilities BIM models

Two existing underground utilities from different cities were selected, named Utility 1# and Utility 2#, along with their corresponding BIM models. We first extracted the necessary location and obstacle information for two utilities, and calculated the locations that need to be inspected. By using the CPP algorithm that conforms to the characteristics of the utilities, the shortest full coverage inspection path for each underground utility was found, as shown in Figure 6. The robot started from the monitor center of each utility, performed inspections on each branch, and then returned to the monitor center.

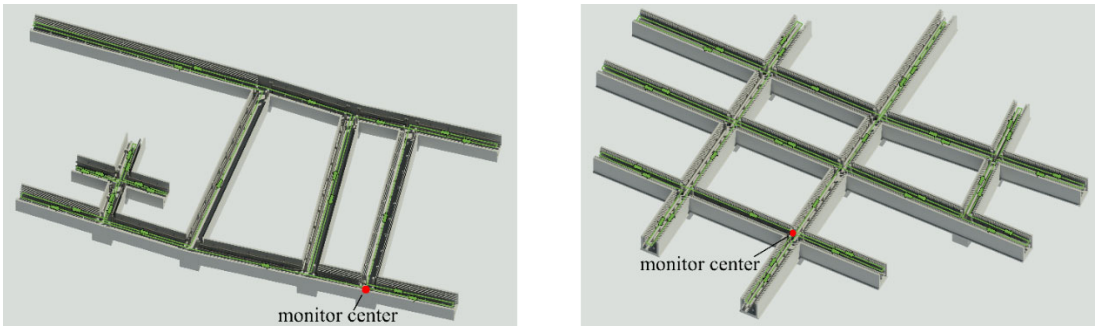

Figure 6. Planned inspection route, (a) Utility 1#, (b) Utility 2#.

To validate the effectiveness of the proposed inspection algorithm, two topological maps from BIM models were analyzed using three algorithms: the CPP algorithm, traditional Depth-First Search (DFS), and a refined DFS with random optimizations. The performance of these algorithms on the maps, Utility 1# and Utility 2#, was compared in terms of path length, computation time, and execution time.

For the smaller Utility 2#, all three algorithms achieved 100% coverage. However, the DFS algorithm resulted in a path exactly twice the length of the utility, indicating a 100% repetition rate, which was unacceptable. Both the CPP algorithm and refined DFS generated shorter paths of about 410.01 meters with a 55.65% repetition rate. Similar trends were

observed for the larger Utility 1#, where DFS produced a path of 838.97 meters, while CPP and refined DFS provided paths of 718.92 meters with a 71.38% repetition rate.

Table 1. The total path length, coverage rate and repetition rate for two utilities.

	Number of edges	Algorithm	Total path length	Coverage rate	Repetition rate
Utility 1#	97	**CPP**	718.89m	100%	71.38%
		DFS	838.97m	100%	100%
		refined DFS(t = 80)	718.92m	100%	71.38%
	Number of edges	**Algorithm**	**Total path length**	**Coverage rate**	**Repetition rate**
Utility 2#	66	**CPP**	410.01m	100%	55.64%
		DFS	526.87m	100%	100%
		refined DFS(t = 30)	410.03m	100%	55.65%

In terms of computation time, DFS was the fastest, taking 3ms for Utility 1# and 2ms for Utility 2#. The CPP algorithm took 24ms and 23ms, respectively. Refined DFS showed variability depending on the number of random search executions(t). For Utility 2#, fewer executions were needed to find the shortest path. However, for Utility 1#, the refined DFS required more executions, leading to a significant increase in computation time, reaching 1272ms after 80 executions, which can be seen from Figure 7.

The execution time in the ROS system showed that both CPP and refined DFS could find the shortest path, with execution times around 6000 seconds for Utility 1# (CPP: 6035.98s, refined DFS: 6069.23s) and around 4000 seconds for Utility 2# (CPP: 3927.50s, refined DFS: 4011.16s). The DFS algorithm had much longer execution times of 7253.44s for Utility 1# and 5041.79s for Utility 2#, making it significantly less efficient.

Overall, while all three algorithms achieved full coverage path planning, their effectiveness varied greatly. Traditional DFS, though quick in computation, resulted in excessively long paths and high execution times. Refined DFS improved path length but at the cost of increased computation time with larger maps. The CPP algorithm demonstrated the best balance, providing the shortest paths with stable and relatively short computation times, making it the most efficient and reliable choice among the three.

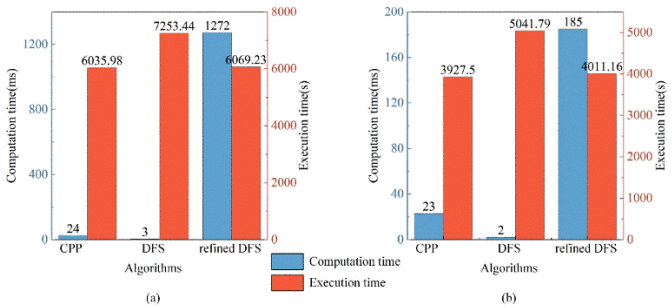

Figure 7. The computation and execution time for Utility 1# and Utility 2#, (a) Utility 1#, (b) Utility 2#.

3 CONCLUSION

This paper proposes an end-to-end automatic planning method from underground utility BIM models to inspection routes. Firstly, this method can extract the necessary information such as positions of utilities and pipelines inside for path planning of different BIM models. Then further modifications are performed to basic information and path planning method that are suitable for the pipeline corridor environment is applied to find the optimal inspection path. The effectiveness of proposed method is validated using two existing utility BIM models. The conclusions of this study are as follows: (1) in response to the widespread application of BIM models during the construction and maintenance phases of underground utilities, an automated algorithm for extracting utilities information is developed, which can automatically extract the position and obstacle information inside the utilities containing pipes of different types and cross-sectional areas, and modify the basic information for robot inspection tasks, effectively utilizing the rich information resources of BIM, (2) addressing the high inspection frequency requirements and complex, hazardous environments of utilities, an automatic inspection strategy based on the specific environmental characteristics of the utilities is proposed. This strategy can achieve full coverage detection of underground utilities, ensuring that each branch is passed through with the shortest total distance. Experimental results show that this detection strategy can calculate the shortest full coverage detection path in milliseconds, (3) in order to reduce the need for manual intervention in BIM information extraction and inspection processes, Dynamo is introduced. The developed Dynamo framework integrates the algorithms for automatic information extraction and optimal inspection path planning mentioned above, achieving end-to-end planning from the BIM model to the optimal inspection path.

REFERENCES

[1]. HAN B J, JIANG Y S, WANG Z, et al, 2021. Analysis of the Risk Path of the Pipeline Corridor Based on System Dynamics[J/OL]. Shock and Vibration, 2021: 1-13. DOI:10.1155/2021/5529642.

[2]. GE F, XU X, 2019. Research report on the Utility Tunnel Engineering based on BIM technology[J/OL]. Journal of Physics: Conference Series, 1176: 042028. DOI:10.1088/1742-6596/1176/4/042028.

[3]. DANG L M, WANG H, LI Y, et al, 2022. Automatic tunnel lining crack evaluation and measurement using deep learning[J/OL]. Tunnelling and Underground Space Technology, 124: 104472. DOI:10.1016/j.tust.2022.104472.

[4]. LU Z, ZHU F, SHI L, et al, 2019. Automatic seepage detection in cable tunnels using infrared thermography[J/OL]. Measurement Science and Technology, 30(11): 115902. DOI:10.1088/1361-6501/ab30d9.

[5]. DONG L, CHEN N, LIANG J, et al, 2023. A review of indoor-orbital electrical inspection robots in substations[J/OL]. Industrial Robot, 50(2): 337-352. DOI:10.1108/IR-06-2022-0162.

[6]. FANG S J, 2022. Simulation analysis of indoor orbital inspection robot based on Gazebo[C/OL]//TAN G, CEN F. INTERNATIONAL CONFERENCE ON INTELLIGENT TRAFFIC SYSTEMS AND SMART CITY (ITSSC 2021): Volume 12165. Bellingham: Spie-Int Soc Optical Engineering: 121651V[2024-01-26]. DOI:10.1117/12.2628608.

[7]. ZHANG C, CHEN S, ZHAO L, et al, 2021. Fpga-based linear detection algorithm of an underground inspection robot[J/OL]. Algorithms, 14(10). DOI:10.3390/a14100284.

[8]. XIAO Y, YAN Y, YU Y, et al, 2022. Research on pose adaptive correction method of indoor rail mounted inspection robot in GIS Substation[J/OL]. Energy Reports, 8: 696-705. DOI:10.1016/j.egyr.2022.03.155.

[9]. AZPÚRUA H, REZENDE A, POTJE G, et al, 2021. Towards Semi-autonomous Robotic Inspection and Mapping in Confined Spaces with the EspeleoRobô[J/OL]. Journal of Intelligent & Robotic Systems, 101(4): 69. DOI:10.1007/s10846-021-01321-5.

[10]. CID A, NAZARIO M, SATHLER M, et al, 2020. A Simulated Environment for the Development and Validation of an Inspection Robot for Confined Spaces[C/OL]//2020 Latin American Robotics Symposium (LARS), 2020 Brazilian Symposium on Robotics (SBR) and 2020 Workshop on Robotics in Education (WRE). Natal, Brazil: IEEE: 1-6[2023-06-18]. DOI:10.1109/LARS/SBR/WRE51543.2020.9307007.

[11]. BOSCHÉ F, AHMED M, TURKAN Y, et al, 2015. The value of integrating Scan-to-BIM and Scan-vs-BIM techniques for construction monitoring using laser scanning and BIM: The case of cylindrical MEP components[J/OL]. Automation in Construction, 49: 201-213. DOI:10.1016/j.autcon.2014.05.014.

[12]. IBRAHIMKHIL M H, SHEN X, BARATI K, et al, 2023. Dynamic Progress Monitoring of Masonry Construction through Mobile SLAM Mapping and As-Built Modeling[J/OL]. Buildings, 13(4): 930. DOI:10.3390/buildings13040930.

[13]. GAO Y, MENG J, SHU J, et al, 2022. BIM-based task and motion planning prototype for robotic assembly of COVID-19 hospitalisation light weight structures[J/OL]. Automation in Construction, 140: 104370. DOI:10.1016/j.autcon.2022.104370.

[14]. GAO Y, SHU J, XIAO W, et al, 2023. Polyhedron-bounded collision checks for robotic assembly of structural components[J/OL]. Automation in Construction, 152: 104904. DOI:10.1016/j.autcon.2023.104904.

[15]. CHOI M, KIM S, KIM S, 2024. Semi-automated visualization method for visual inspection of buildings on BIM using 3D point cloud[J/OL]. Journal of Building Engineering, 81. DOI:10.1016/j.jobe.2023.108017.

[16]. ZHANG C, WANG F, ZOU Y, et al, 2023. Automated UAV image-to-BIM registration for building façade inspection using improved generalised Hough transform[J/OL]. Automation in Construction, 153. DOI:10.1016/j.autcon.2023.104957.

[17]. HAMIEH A, BEN MAKHLOUF A, LOUHICHI B, et al, 2020. A BIM-based method to plan indoor paths[J/OL]. Automation in Construction, 113: 103120. DOI:10.1016/j.autcon.2020.103120.

[18]. CHEN Z, WANG H, CHEN K, et al, 2024. Improved coverage path planning for indoor robots based on BIM and robotic configurations[J/OL]. Automation in Construction, 158: 105160. DOI:10.1016/j.autcon.2023.105160.

[19]. Autodesk, 2024. https://help.autodesk.com/view/RVT/2024/ENU/. April 19, 2023.

Proceeding of the 10th International Conference on Innovative Production and Construction (IPC 2024), Perth, Australia, July 11-12, 2024

Automatic Classification for Construction Waste Using Deep Learning Models Based on Feature Fusion

Yiqun Zhang[1], Kunpeng Jing[2], Shaoli Wang[1] and Honglei Xu[1]

1. School of Electrical Engineering, Computing and Mathematical Sciences
Curtin University, Perth, WA, 6845, Australia
2. School of Economics and Management, Yanshan University, Qinhuangdao, 066004, China

ABSTRACT: With the rapid development of the construction industry, the classification and recycling of construction waste have become particularly important to decrease construction waste disposal in landfills. Traditional disposal methods rely on inefficient and costly manual classification. This paper proposes a deep learning model based on feature fusion to automatically classify construction waste images, to improve the accuracy and efficiency of classification. We adopt two deep neural network models and enhance their recognition ability for construction waste images through their feature fusion. Feature fusion is achieved through a customized fusion layer that combines the feature outputs of two networks and classifies them through a fully connected layer. Experimental results show that the fusion model has higher accuracy and robustness than the single model in the classification task of construction waste. We also explore the impact of different data augmentation techniques on model performance. The proposed method improves automation and intelligence capabilities for construction waste classification.
KEYWORDS: construction waste classification; deep learning; feature fusion; neural networks

1. INTRODUCTION

In recent years, deep learning has been widely applied in garbage classification to improve classification efficiency and accuracy. Meanwhile, in the field of construction waste management, deep learning provides an effective automation solution that helps optimize traditional waste disposal methods. Deep learning models, especially convolutional neural networks (CNNs), have been successfully applied to the classification of solid waste. These models are capable of processing and analyzing large amounts of image data, automatically identifying and classifying various waste materials. For example, Simonyan and Zisserman[2] demonstrated the powerful ability of convolutional neural networks in image recognition through the VGG-19 model. In addition, Szegedy et al. [3] introduced a balance between depth and width through Google Net to improve model performance. He et al. [4] further explored the possibility of improving recognition accuracy by increasing network depth. The research by Abdul et al. [5] focuses on using these deep learning models to effectively identify and classify construction waste, promoting the development of intelligent construction waste management. These studies indicate that deep learning models based on feature fusion can not

only improve the accuracy of construction waste classification but also enhance the model's ability to distinguish different types of waste.

Feature fusion is one of the key strategies to improve model performance. By combining features from different sources, the model can recognize subtle differences in images, thereby more accurately classifying various types of construction waste. Feature fusion not only enhances the performance of the model but also helps to handle more complex classification problems [6]. Cai et al. [7] proposed a method based on multi-scale feature fusion, which was applied to RGB and hyperspectral images, significantly improving the classification accuracy of transparent PET bottles. In addition, Ashary et al. [8] applied the entropy-based feature fusion method to the YOLO-v7 model, enhancing the robustness of the model by evaluating and selecting features with low entropy values for fusion. Mungoli [9] proposed adaptive feature fusion technology that utilizes meta-learning components to optimize feature combinations to adapt to specific tasks or scenarios, improving the model's generalization ability. Yu et al. [10] further combined the original RGB stream and local binary pattern encoding stream to effectively improve the accuracy of aviation scene classification.

In summary, the application of deep learning models through feature fusion in construction waste classification not only improves construction waste classification but also provides substantial support for environmental protection and resource recovery. This paper integrates the powerful functions of different deep learning models to achieve efficient and accurate classification of construction waste, demonstrating higher accuracy and processing capabilities than traditional methods. In addition, by adopting a feature fusion strategy, this study not only improves the generalization ability of the classification model but also provides solutions for dealing with complex practical scenarios.

2. METHOD

2.1 GoogLeNet model

GoogLeNet is a convolutional neural network that was introduced by Szegedy et al. in 2014. [11] This model significantly advanced the state of the art for large-scale image recognition challenges, specifically the ImageNet competition, by utilizing an innovative architecture known as the Inception module. The Inception module is designed to optimize local sparse structures within convolutional networks using a combination of variously sized filters within each block, which allows the model to efficiently use computing resources and manage computational costs.The GoogLeNet architecture is characterized by its deep and complex structure, comprising 22 layers. Unlike typical deep networks, which might use increasingly large convolutions, GoogLeNet employs multiple smaller, more efficient convolutional filters to cover different areas of the input space. This architecture helps in handling the immense variety of image information more effectively, thus enhancing the network's ability to detect and classify a wide range of objects with greater accuracy .

2.2 VGG-19 model

The VGG-19 model was developed by Simonyan and Zisserman in 2014. It is a deep learning model based on convolutional neural networks and has shown outstanding performance in the field of image recognition. The model consists of 19 trainable layers, of which 16 are

convolutional layers and 3 are fully connected layers [12].The main feature of VGG-19 is that its convolutional layers all use small convolutional kernels of the same size (3x3), which can capture local features of the image and maintain a reasonable number of parameters. In addition, it uses ReLU activation functions between convolutional layers to introduce nonlinearity, enabling the model to learn more complex image patterns. The VGG-19 model also adopts a stacked convolutional layer design, followed by a maximum pooling layer every two to three convolutional layers, which helps to gradually reduce the spatial size, thereby reducing the overall number of parameters and increasing the model's abstraction ability. This layered and pooled structural design makes VGG-19 very effective in depth feature extraction, especially when dealing with images with complex textures, shapes, and sizes.

2.3 GoogLeNet and VGG-19 feature fusion network

In this article, the goal of improving classification accuracy is achieved by integrating the features of Google Net and VGG-19 model. Therefore, the front ends of the two models are considered as feature extractors. The features extracted by GoogLeNet and VGG1-9 during the feature extraction process are

$$f_g = G(I) \tag{1}$$

$$f_v = V(I) \tag{2}$$

where *G* and *V* represent the forward propagation process of GoogLeNet and VGG-19 models, and *I* represents the input image.

In the process of feature fusion between Google Net and VGG19 models, image features are not simply pieced together. We have established an attention mechanism layer at this stage, which can more effectively extract useful features. The feature attention processing of Google Net and VGG19 models are as follows

$$f_g' = \text{sigmoid}\left(W_{g2} \cdot \text{ReLU}\left(W_{g1} \cdot f_g\right)\right) \odot f_g \tag{3}$$

$$f_v' = \text{sigmoid}\left(W_{v2} \cdot \text{ReLU}(W_{v1} \cdot f_v)\right) \odot f_v \tag{4}$$

where W_{g1}, W_{g2}, W_{v1} and W_{v2} are learning parameters.

The process of feature fusion is shown in the following formula

$$f = \text{ReLU}\left(W_f \cdot \left[f_g'; f_v'\right]\right) \tag{5}$$

where $\left[f_g'; f_v'\right]$ represents concatenation of features, W_f is the fusion stage weight matrix classification output as

$$y = W_c \cdot f \tag{6}$$

where W_c is classification stage matrix.

After calculating the classification output, we obtain the loss function

$$L\left(y, \hat{y}\right) = -\sum_{c=1}^{C} \hat{y}_c \log(y_c) \tag{7}$$

where $\hat{y}$ is true label's one-hot encoding, y is the probability distribution output by the model, C is the number of classes.

For the processing of the loss function as formula (7), this article adopts stochastic gradient descent for parameter optimization

$$\theta_{t+1} = \theta_t - \eta \nabla_\theta L(\theta) \tag{8}$$

where θ represents the model parameter, η is the learning rate, and $\nabla_\theta L$ is the gradient of the loss function L with respect to θ.

The above is the process of integrating the features of two models in one iteration until the maximum number of iterations is met, and the entire training process ends. As shown in Figure 1, we designed a hybrid deep learning framework by combining the characteristics of GoogLeNet and VGG-19 model. In this framework, the front end of each model serves as a feature extractor, and its output is then merged and processed through a custom fusion layer. In addition, by introducing an attention layer in the fusion stage, the model's ability to capture subtle features is enhanced, thereby improving the accuracy of classification.

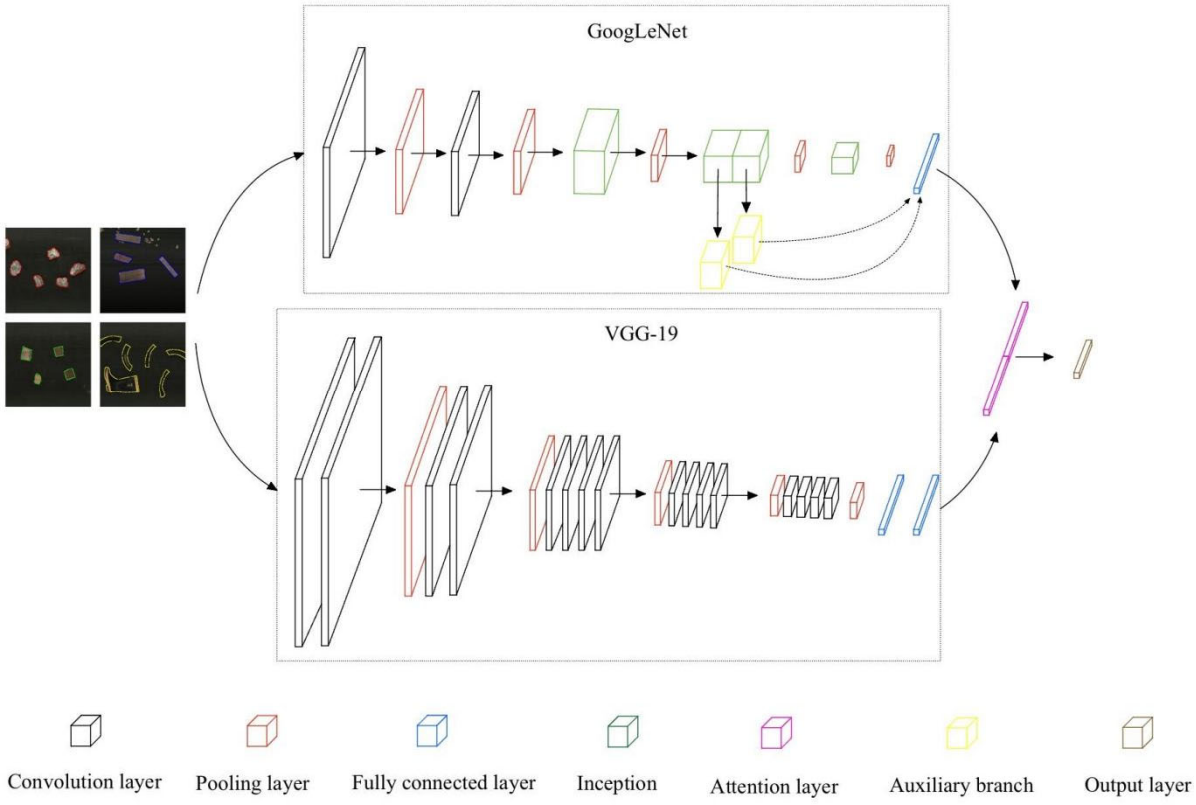

Figure 1: Schematic diagram of GoogLeNet and VGG-19 model structure and feature fusion

3. EXPERIMENTS AND RESULTS

The dataset used in this article includes four common types of construction solid waste, with a total of 298 samples: 95 bricks, 60 concrete, 79 wood, and 64 rubber [13]. 80% of the data are used as training data, and 20% of the data is used as testing data. The experiment results are shown in Table 1.

Table 1: Experiment results

	Bricks	Concrete	Wood	Rubber	Total accuracy
GoogLeNet	85.12%	94.64%	79.05%	92.48%	89.95%
VGG19	90.38%	85.71%	86.89%	96.57	92.12%
GoogLeNet and VGG19	92.86%	91.07%	88.52	98.10%	94.56%

According to the experimental results, the network model that integrates the features of Google Net and VGG-19 has higher feature accuracy. When comparing the classification accuracy of each category, we can find that with the support of the attention mechanism layer, the classification probability of each category has been improved, indicating that the addition of attention mechanism helps the model to better fuse features and select the correct features for learning.

4. CONCLUSION

This paper proposes an automated construction waste image classification method using cutting-edge feature fusion techniques and deep learning models. The proposed approach outperforms traditional manual methods and single-model approaches in terms of accuracy and efficiency by integrating the capabilities of GoogLeNet and VGG-19 with an attention mechanism layer. The combination of these models' features improves classification performance and shows resilience with a variety of waste materials. Furthermore, the investigation of diverse data augmentation tactics highlights the method's flexibility to diverse environmental settings, thereby augmenting its pragmatic usefulness in waste management scenarios. The combination of deep learning and feature fusion has the potential to transform the classification of construction waste and pave the way for improved automation, ecological sustainability, and resource recovery in the construction sector.

REFERENCES

[1]. Anjum, Mohd, M. Sarosh Umar, and Sana Shahab. "Systematic literature review of deep learning models in solid waste management." In AIP Conference Proceedings, vol. 2494, no. 1. AIP Publishing, 2022.

[2]. Simonyan, Karen, and Andrew Zisserman. "Very deep convolutional networks for large-scale image recognition." arXiv preprint arXiv:1409.1556 (2014).

[3]. Szegedy, Christian, Wei Liu, Yangqing Jia, Pierre Sermanet, Scott Reed, Dragomir Anguelov, Dumitru Erhan, Vincent Vanhoucke, and Andrew Rabinovich. "Going deeper with convolutions." In Proceedings of the IEEE conference on computer vision and pattern recognition, pp. 1-9. 2015.

[4]. He, Kaiming, Xiangyu Zhang, Shaoqing Ren, and Jian Sun. "Deep residual learning for image recognition." In Proceedings of the IEEE conference on computer vision and pattern recognition, pp. 770-778. 2016.Huang, G., Liu, Z., Van Der Maaten, L., & Weinberger, K. Q. (2017). Densely Connected Convolutional Networks. Proceedings of the IEEE conference on computer vision and pattern recognition.

[5]. Abdu, Haruna, and Mohd Halim Mohd Noor. "A survey on waste detection and classification using deep learning." IEEE Access 10 (2022): 128151-128165.

[6]. Choi, Janghee, Byeongju Lim, and Youngjun Yoo. "Advancing Plastic Waste Classification and Recycling Efficiency: Integrating Image Sensors and Deep Learning Algorithms." Applied Sciences 13, no. 18 (2023): 10224.

[7]. Cai, Zhenxing, Jianhong Yang, Huaiying Fang, Tianchen Ji, Yangyang Hu, and Xin Wang. "Research on Waste Plastics Classification Method Based on Multi-Scale Feature Fusion." Sensors 22, no. 20 (2022): 7974.

[8]. Ashary, Ehab Bahaudien, Sahar Jambi, Rehab B. Ashari, and Mahmoud Ragab. "Entropy Based Feature Fusion Using Deep Learning forWaste Object Detection and ClassificationModel." Computer Systems Science & Engineering 47, no. 3 (2023).

[9]. Mungoli, Neelesh. "Adaptive Feature Fusion: Enhancing Generalization in Deep Learning Models." arXiv preprint arXiv:2304.03290 (2023).

[10]. Yu, Yunlong, and Fuxian Liu. "Dense connectivity based two-stream deep feature fusion framework for aerial scene classification." Remote Sensing 10, no. 7 (2018): 1158.

[11]. Szegedy, Christian, Wei Liu, Yangqing Jia, Pierre Sermanet, Scott Reed, Dragomir Anguelov, Dumitru Erhan, Vincent Vanhoucke, and Andrew Rabinovich. "Going deeper with convolutions." In Proceedings of the IEEE conference on computer vision and pattern recognition, pp. 1-9. 2015.

[12]. Simonyan, Karen, and Andrew Zisserman. "Very deep convolutional networks for large-scale image recognition." arXiv preprint arXiv:1409.1556 (2014).

[13]. Ji, Tianchen, Jiantao Li, Huaiying Fang, RenCheng Zhang, Jianhong Yang, and Lulu Fan. "Rapid dataset generation methods for stacked construction solid waste based on machine vision and deep learning." Plos one 19, no. 1 (2024): e0296666.

Exploring The Interplay of Bottom-Up and Top-Down Attention in Hazard Perception: Insights from Electroencephalogram and Eye-Tracking Methods

Zhe Zhang[1], Brian H.W. Guo[2], Zhenan Feng[3], Yang Miang Goh[4]

1. Civil and Natural Resources Engineering, University of Canterbury, New Zealand. Email: zhe.zhang@pg.canterbury.ac.nz
2. Civil and Natural Resources Engineering, University of Canterbury, New Zealand. Email: brian.guo@canterbury.ac.nz
3. School of Built Environment, Massey University, New Zealand. Email: z.feng1@massey.ac.nz
4. Department of Built Environment, National University of Singapore, Singapore. Email: bdggym@nus.edu.sg

ABSTRACT: The construction industry remains one of the most hazardous industries. This study investigates the interplay between bottom-up (stimulus-driven) and top-down (goal-directed) attentional mechanisms in hazard perception within immersive virtual reality (VR) environments. Twenty students participated in the experiment, performing forklift operating and bricklaying tasks while exposed to various hazards. Eye-tracking and electroencephalogram (EEG) data were collected to measure attention. Results indicated that augmented aversive stimuli significantly increased both the count and duration of fixations on hazards and triggered a higher amplitude in the P200 component of the event-related potential (ERP). Moreover, the interplay of bottom-up and top-down attention resulted in improved hazard perception performance, as well as increased amplitude in the P1, N1, P300, and P3b components of the ERP. This research highlights the importance of integrating both attentional mechanisms in safety training and design, suggesting improvements in safety training by incorporating proactive attentional interplay strategies, enhancing Safety in Design (SID) with reactive and anticipatory design, and developing adaptive attention-based human-machine interactions.

KEYWORDS: bottom-up attention; top-down attention; hazard perception; eye tracking; electroencephalogram

1 INTRODUCTION

The significant number of fatalities within the construction industry highlights its status as one of the most hazardous industries. A significant number of these accidents can be partly attributed to failures in hazard perception [1]. To enhance hazard perception, it is crucial to understand the mechanisms of attention [2]. Bottom–up attention is determined by the salience of stimuli in the environment [3]. Top-down attention is defined as ‘the task-dependent

direction of cognitive and neural resources by the subject' [4], for instance, safety goals, efficiency goals, and quality targets. The dynamics of attention allocation, specifically the interplay between bottom-up (stimulus-driven) and top-down (goal-directed) mechanisms, collectively influence how individuals identify and respond to hazards. [5, 6]. Nevertheless, research focusing on the interplay between these two attention mechanisms and their influence on hazard perception remains limited.

Previous research has identified several brain regions related to bottom-up attention, including the primary visual cortex (V1), V2, V3, and V4; the inferior temporal (IT) cortex; the ventral part of the lateral prefrontal cortex (PFC); the middle temporal (MT) area; the medial superior temporal (MST) area; the posterior parietal cortex (PPC); and the dorsolateral part of the PFC (dlPFC) [7]. Regarding top-down attention, the prefrontal cortex (PFC) [8] and the temporoparietal junction (TPJ) [9] were identified as related brain regions.

Technological advancements have facilitated construction safety research in a digitalization-based manner. Specifically, immersive virtual reality (VR) technology has the capability to simulate immersive and interactive hazardous construction site scenarios in a way that is both controlled and immersive [10-12]. Jameson [13] applied the concept of information fusion to identify hidden patterns within multiple data sources. The use of information fusion to integrate eye-tracking and EEG data for a deeper understanding of the interplay between bottom-up and top-down attentional processes remains insufficiently explored.

This research aims to understand how bottom-up attentional processes and their interplay with top-down attention influence hazard perception in immersive VR environments. Specifically, the research seeks to answer the following questions: (1) How do augmented aversive stimuli affect the bottom-up attentional processes and hazard perception? (2) How does the combination of augmented aversive stimuli and safety goals influence the interplay between bottom-up and top-down attentional processes and hazard perception?

2 METHOD

This research employed a VR-based experiment to address the research questions. Twenty students from the University of Canterbury were recruited. Ethical approval was granted by the University of Canterbury's Human Research Ethics Committee (Ref: HREC 2023/73/LR-PS). Consent forms were obtained from each participant before the experiment.

The experiment utilizes several advanced equipment. Participants engaged with a construction site simulation via an HTC VIVE Focus 3 headset. This advanced VR device enables a per-eye resolution of 2448 x 2448 pixels, a refresh rate of 90 Hz, and a 120-degree field of view. Additionally, eye movements were tracked using an eye-tracking add-on for the VIVE Focus 3. This device captured gaze data at a frequency of 120 Hz with an accuracy ranging from 0.5° to 1.1°. It enabled tracking of gaze origin and gaze direction, timestamped with millisecond accuracy. The study employed the EMOTIV EPOC Flex Gel Sensor Kit for EEG data collection, which features 32 channels and a reference electrode positioned according to the 10-10 international system. EEG signals were captured at a rate of 128 samples per second (SPS) using a sequential sampling method. This advanced immersive solution to data collection and environmental design enriched the participants' immersive interactions with

virtual hazards and provided valuable insights into attentional processes and hazard perception.

The project employed Unity 2021.3.27f1 to create an interactive virtual construction site. Within this immersive virtual environment, participants were tasked with two primary activities: transporting brick containers by forklift and bricklaying. To examine hazard perception, the simulation was designed with four hazards: (1) the forklift posing a collision risk with workers and materials, (2) the possibility of lifting objects detaching from the load carried by the tower crane, (3) the risk of exposure to live electrical wiring, and (4) the approaching of the tower crane load to scaffolding, which could induce scaffold collapse.

To examine how bottom-up attentional processes and their interplay with top-down attention influence hazard perception, the experiment was structured into three stages: Stage A (No safety goals and no augmented aversive stimuli), which included two tasks and eight hazards; Stage B (No safety goals and augmented aversive stimuli), which introduced early warning laser systems to highlight hazard zones and enhance bottom-up attention; and Stage C (Safety goals and augmented aversive stimuli), which added a safety goal before the tasks in addition to the early warning laser systems to assess the combined effect of top-down and bottom-up attention on hazard perception. Upon arrival, participants went through a brief training session to familiarize themselves with the VR equipment and the two tasks. Following a general goal toolbox meeting that only provided information to complete the two tasks, participants proceeded to stage A. Next, a toolbox meeting with a production goal was held to avoid emphasizing safety, followed by stage B. Finally, the safety goal was emphasized in the toolbox meeting before stage C. Each stage lasted six minutes, with rest periods provided between stages.

The analysis of eye-tracking data concentrated on identifying the fixation count and the total fixation duration on hazards, with a higher number of fixations and longer durations indicating heightened bottom-up attentional engagement. Additionally, EEG data were analyzed using event-related potential (ERP) analysis to identify patterns of brain activity associated with shifts in bottom-up and top-down attention. This was accomplished by employing EEGLAB v2024.0 and ERPLAB v10.11 toolbox in MATLAB R2024a [14, 15].

3 RESULTS

As shown in Figure 11, the analysis of bottom-up attention-related eye-tracking data on hazards suggested an increasing trend in both fixation count and duration across stages A, B, and C. When comparing stages A and B, the introduction of augmented aversive stimuli significantly enhanced both fixation count and duration on hazards, suggesting a more significant hazard perception influenced by bottom-up processes. Furthermore, when comparing stages A, B and C, the interplay of bottom-up and top-down attention led to increased fixation count and duration compared to situations with augmented aversive stimuli alone or without augmented aversive stimuli, indicating a more strategic allocation of attention on hazards driven by interplay between bottom-up and top-down processes.

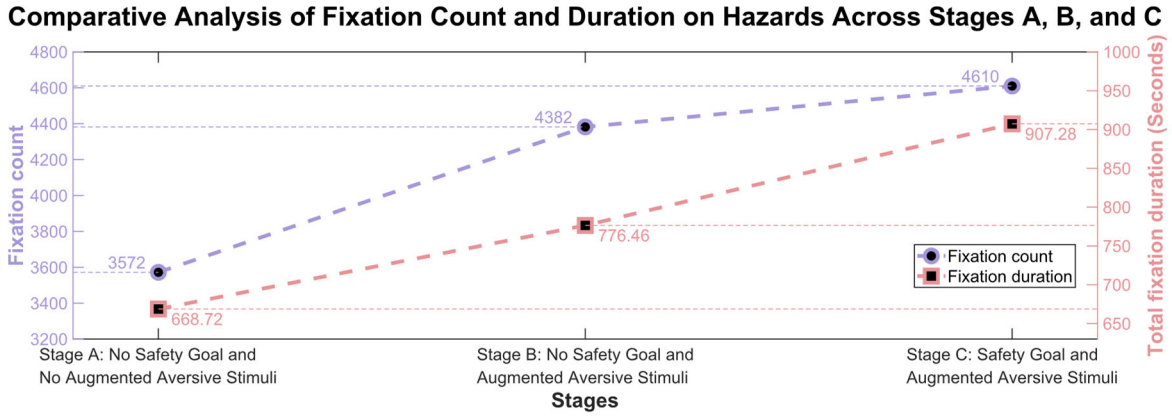

Figure 11 Comparative Analysis of Fixation Count and Duration on Hazards Across Stages A, B, and C

The EEG data provided insights into the neuropsychological mechanisms of attention during hazard perception. Figure 12 provides cross participants averaged ERP waveforms on stages A and B. The P200 component appears between 150 and 250 milliseconds (ms) after a stimulus and was identified as related to bottom-up attention. In stage B, the P200 component showed higher amplitude compared to stage A, suggesting that the augmented aversive stimuli in stage B triggered a stronger attention response, aligning the findings from the eye-tracking data in Figure 11.

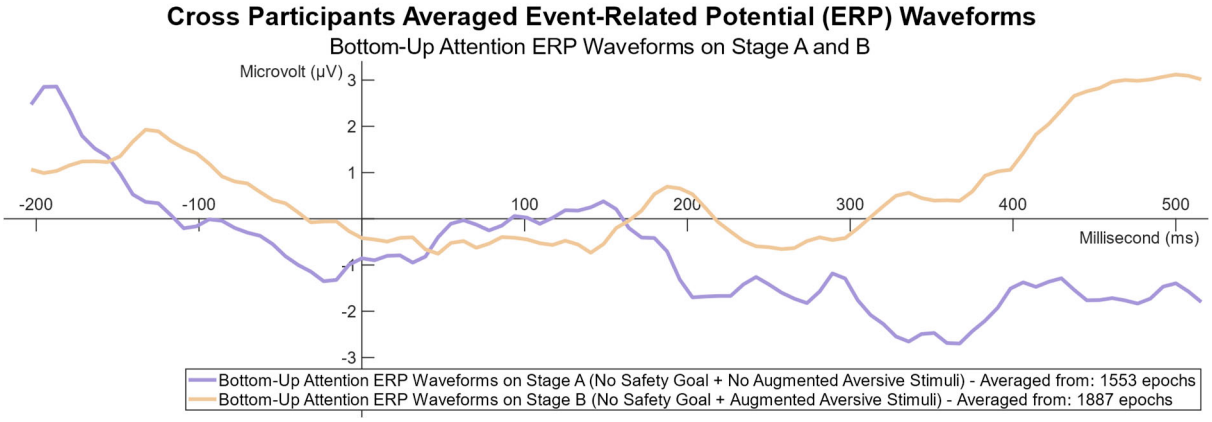

Figure 12 Cross Participants Averaged Event-Related Potential (ERP) Waveforms - Bottom-Up Attention ERP Waveforms on Stage A and B

Figure 13 illustrates bottom-up and top-down attention interplay ERP waveform on stage C. Four ERP components associated with top-down attention were investigated: P1, N1, P300, and P3b. The P1, a positive deflection, emerges approximately 100ms post-stimulus. Following this, the N1, a negative deflection, typically peaks between 150 and 200ms. Subsequently, the P300, another positive deflection, occurs around 300ms after stimulus presentation. The P3b, a subset of the P300, manifests as a positive-going potential within the 310–380 millisecond range. In stage C, all these ERP components can be observed. This indicates that the interplay of bottom-up and top-down attentional mechanisms triggered a stronger attentional response.

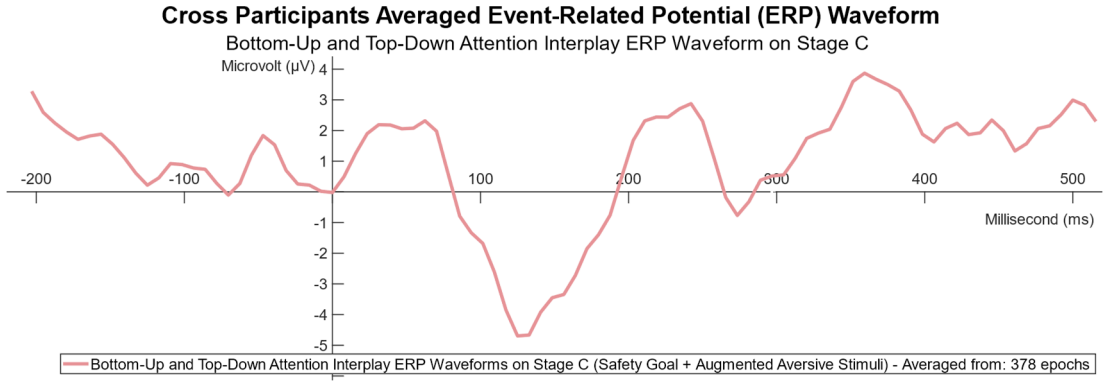

Figure 13 Cross Participants Averaged Event-Related Potential (ERP) Waveform-Bottom-Up and Top-Down Attention Interplay ERP Waveform on Stage C

Figure 14, Figure 15 and Figure 16 present ERP scalp maps at 0ms, 100ms, 200ms, 300ms, 400ms, and 500ms for stage A, B and C, respectively, to compare the spatial distribution of amplitudes in ERP components. At 200ms post stimuli, Figure 15 shows higher positive amplitudes at C3, C4, F3, F4, F7, F8, O1, O2, Oz, P3, P4, PO10, PO9, T7, and T8, compared to Figure 14. These areas are associated with bottom-up attention [7]. At 100ms, 200ms, 300ms, and 400ms post stimuli, Figure 16 demonstrated negative or positive amplitudes at F3, F4, F7, F8, P3, and P4 corresponding to P1, N1, P300, and P3b ERP components. This indicates that the interplay of bottom-up and top-down attention leads to higher amplitude in ERP components than bottom-up attention alone.

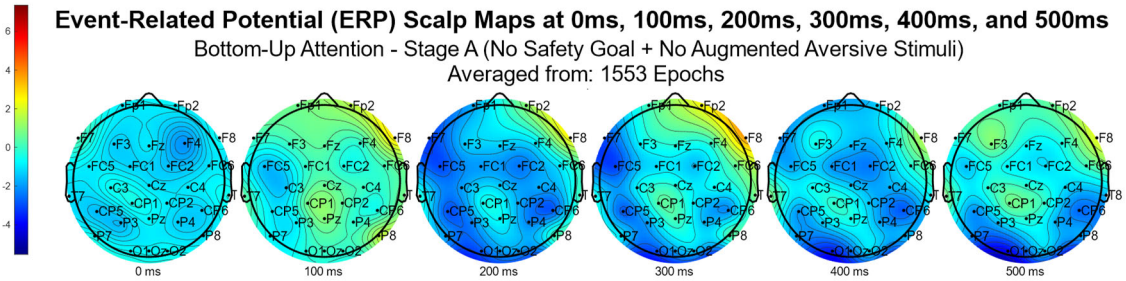

Figure 14 Stage A (No Safety Goal + No Augmented Aversive Stimuli) Event-Related Potential

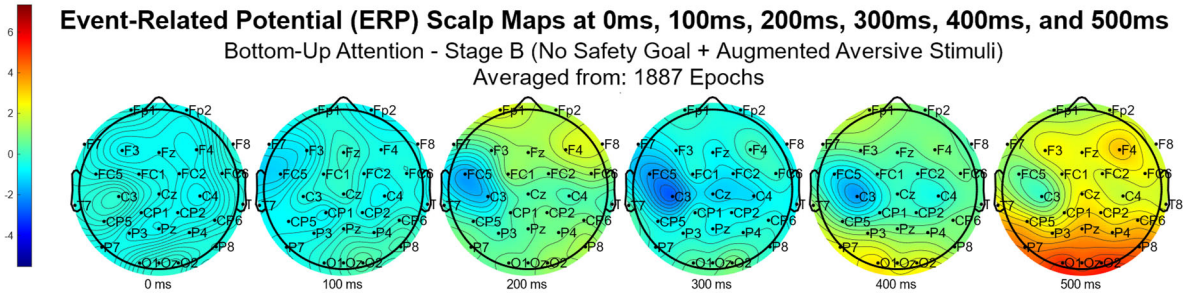

(ERP) Scalp Maps

Figure 15 Stage B (No Safety Goal + Augmented Aversive Stimuli) Event-Related Potential (ERP) Scalp Maps

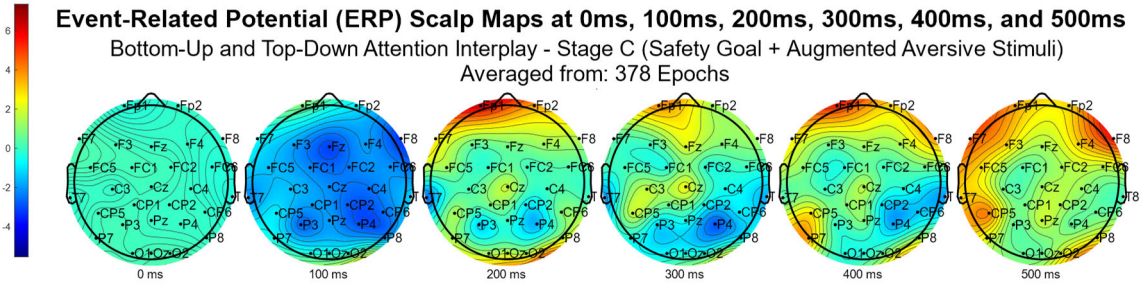

Figure 16 Stage C (Safety Goal + Augmented Aversive Stimuli) Event-Related Potential (ERP) Scalp Maps

The results of this study demonstrate that both bottom-up and top-down attentional processes play critical roles in hazard perception. The interplay between bottom-up and top-down attentional processes results in superior hazard perception performance compared to situations with augmented aversive stimuli alone or in their absence.

4 Discussion and conclusion

Attention, a gatekeeper of information, operates through an interplay of bottom-up and top-down processes, playing a pivotal role in hazard perception. Bottom-up attention, driven by sensory cues, reflexively informs workers of immediate hazards, while top-down attention, shaped by training and experience, enables the strategic perception of hazards.

The findings highlight three contributions: improving safety training by introducing proactive attentional interplay strategies, enhancing Safety in Design (SID) by integrating reactive and anticipatory design, and providing insights into adaptive attention-based human-machine interactions. One limitation of the study is the use of simulated virtual environments, which may not fully capture the complex and dynamic nature of hazards present in the real life.

In conclusion, the present study offers a deeper understanding of attentional mechanisms in hazard perception, specifically of the interplay between bottom-up and top-down processes. The findings offer valuable insights for the SID and safety training programs, emphasizing the need to develop attentional control strategies. By integrating advanced neurophysiological and eye-tracking techniques, the study provides a promising framework for future research and practical applications. Future research could investigate how various hazards, as well as factors like SA, mental workload, fatigue, and long-term memory, affect attentional processes and hazard perception.

REFERENCES

[1]. Y. Han, Z. Yin, J. Zhang, R. Jin, and T. Yang, "Eye-Tracking Experimental Study Investigating the Influence Factors of Construction Safety Hazard Recognition," in Journal of Construction Engineering and Management vol. 146, ed: American Society of Civil Engineers, 2020.

[2]. K. Mrkva, J. C. Cole, and L. Van Boven, "Attention increases environmental risk perception," (in English), Journal of experimental psychology. General, vol. 150, no. 1, pp. 83-102, 2021, doi: 10.1037/xge0000772.

[3]. J. Theeuwes, "Top–down and bottom–up control of visual selection," (in English), Acta psychologica, vol. 135, no. 2, pp. 77-99, 2010, doi: 10.1016/j.actpsy.2010.02.006.

[4]. C. D. Jennings, "Attention and perceptual organization," (in English), Philos. Stud., Article vol. 172, no. 5, pp. 1265-1278, 2015, doi: 10.1007/s11098-014-0348-2.

[5]. M. Corbetta and G. L. Shulman, "Control of goal-directed and stimulus-driven attention in the brain," (in English), Nat. Rev. Neurosci., Article vol. 3, no. 3, pp. 201-215, 2002, doi: 10.1038/nrn755.

[6]. B. H. W. Guo, Y. M. Goh, and K. Le Xin Wong, "A system dynamics view of a behavior-based safety program in the construction industry," (in English), Safety science, vol. 104, pp. 202-215, 2018, doi: 10.1016/j.ssci.2018.01.014.

[7]. F. Katsuki and C. Constantinidis, "Bottom-Up and Top-Down Attention:Different Processes and Overlapping Neural Systems," The Neuroscientist, vol. 20, no. 5, pp. 509-521, 2014, doi: 10.1177/1073858413514136.

[8]. A. Gazzaley and A. C. Nobre, "Top-down modulation: Bridging selective attention and working memory," (in English), Trends Cogn. Sci., Review vol. 16, no. 2, pp. 129-135, 2012, doi: 10.1016/j.tics.2011.11.014.

[9]. A. B. Chica, P. Bartolomeo, and J. Lupiáñez, "Two cognitive and neural systems for endogenous and exogenous spatial attention," Behavioural Brain Research, vol. 237, pp. 107-123, 2013/01/15/ 2013, doi: https://doi.org/10.1016/j.bbr.2012.09.027.

[10]. Z. Feng, V. A. González, R. Amor, R. Lovreglio, and G. Cabrera-Guerrero, "Immersive virtual reality serious games for evacuation training and research: A systematic literature review," Computers & Education, vol. 127, pp. 252-266, 2018/12/01/ 2018, doi: https://doi.org/10.1016/j.compedu.2018.09.002.

[11]. Z. Zhang et al., "Digital technology enhanced situation awareness for construction safety: Systematic review and future research directions," Safety Science, vol. 167, p. 106280, 2023/11/01/ 2023, doi: https://doi.org/10.1016/j.ssci.2023.106280.

[12]. Y. Han, J. Yang, Y. Diao, R. Jin, B. Guo, and Z. Adamu, "Process and Outcome-based Evaluation between Virtual Reality-driven and Traditional Construction Safety Training," (in English), Advanced Engineering Informatics, vol. 52, 2022, doi: 10.1016/j.aei.2022.101634.

[13]. S. M. Jameson, "Architectures for Distributed Information Fusion To Support Situation Awareness on the Digital Battlefield," 2002.

[14]. A. Delorme and S. Makeig, "EEGLAB: an open source toolbox for analysis of single-trial EEG dynamics including independent component analysis," (in eng), J Neurosci Methods, vol. 134, no. 1, pp. 9-21, Mar 15 2004, doi: 10.1016/j.jneumeth.2003.10.009.

[15]. J. Lopez-Calderon and S. J. Luck, "ERPLAB: an open-source toolbox for the analysis of event-related potentials," (in English), Front. Human Neurosci., Technology Report vol. 8, 2014-April-14 2014, doi: 10.3389/fnhum.2014.00213.

Investigation of Quality Monitoring System for 3D Printing Concrete

Hongyu Zhao[1,2], Hamad AI Jassmi[3], Liu Xianda[1], Junbo Sun[4], Xinglong Xu[1], Zimo Li[1], Haicheng Li[5] , and Xiangyu Wang[1*]

1. School of Civil Engineering and Architecture, East China Jiaotong University, China
2. School of Civil Engineering, Chongqing University, Chongqing 400045, China
3. Emirates Center for Mobility Research, United Arab Emirates University, AL Ain 15551, UAE
4. Institute for Smart City of Chongqing University In Liyang, Chongqing University, Jiangsu 213300, China
5. Faculty of Construction and Environment, Hong Kong Polytechnic University, Hong Kong

[*]Corresponding author: Xiangyu Wang, E-mail address: Xiangyu.Wang@curtin.edu.au

ABSTRACT: This study introduced a real-time and highly accurate defect detection and measurement system for 3D concrete printing (3DCP) using deep learning (DL) and computer vision (CV) techniques. A range of improvement methods were applied in YOLOv7, showing better capacities of accuracy and speed for detecting defects in 3DCP than current cutting-edge detectors such as YOLOv8. Notably, the virtual high-fidelity data were produced by DL based data augmentation strategy and their effects were assessed. Replacing real data as the training dataset, the generated virtual data were used in the models to improve measurement accuracy. Applying the proposed method, comprehensive insights into 3DCP defects were obtained. Consequently, the relationship formula between defect frequency and printer parameters was investigated by the proposed method, guiding operators in effectively controlling printer parameters and preventing breakpoint defects during the printing process.
KEYWORDS: 3D concrete printing, real-time monitor, automatic system, deep learning, data augmentation.

1 INTRODUCTION

Additive manufacturing replaces traditional building methods yielding substantial reductions of 60% waste production, 50%-70% construction time, and 50%-80% labor expenses[1, 2]. Despite its potential, 3D printed concrete exhibits various defects such as breakpoints, voids, and pits[3, 4]. These issues arise from the concrete's lack of framework, rapid drying, hydration characteristics, and the inconsistent printing process, all of which negatively impact the mechanical properties of printed components[5, 6]. Addressing these challenges requires continuous monitoring of abnormalities and real-time adjustments to printing parameters and material conditions[7, 8]. Nevertheless, traditional monitoring techniques for large-scale 3DCP have been costly, inaccurate, offline, time-consuming, and insufficient [9, 10]. Consequently, there is an increasing demand for innovative and automated monitoring and control technologies.

The automated optical monitoring methods in 3DCP are categorized as non-algorithm-driven and CV-based monitors. Non-algorithm-driven methods rely on printing nozzle height and position, enhancing precision despite overlooking filament width anomalies[11, 12]. CV-based monitors driven by artificial intelligence(AI) algorithms renovate interlayer line, width, and height detection in 3DCP[13, 14]. Current defect detection methods in 3DCP lack timeliness and accuracy, struggling to handle monitoring complexities. However, DL algorithms like YOLO exhibit robustness and efficiency in identifying defects in cast concrete manufacturing processes[15, 16]. Notably, training data volume significantly impacts model accuracy in DL settings. To tackle limited training data, generative adversarial networks like StyleGAN3 are utilized to generate virtual images.

A 3DCP-YOLO model integrating dual DL techniques with CNN and GAN is proposed in order to provide a highly accurate and real-time defect detector of 3DCP with a restricted dataset[17, 18]. Our contribution is summed up as follows: (1) Multiple data augmentation strategies are proposed to address challenges with limited data volume; (2) Real-time automatic defect monitoring and measurement are introduced by presenting a method based on a 3DCP-YOLO model designed to detect printing breakpoint defects; (3) Several refinements were implemented to improve the accuracy and speed for the YOLOv7 algorithm; (4) Analysis of defect size and frequency is conducted, which reveals the connection between printer settings and defect generation to improve printing control during construction.

2 METHOD

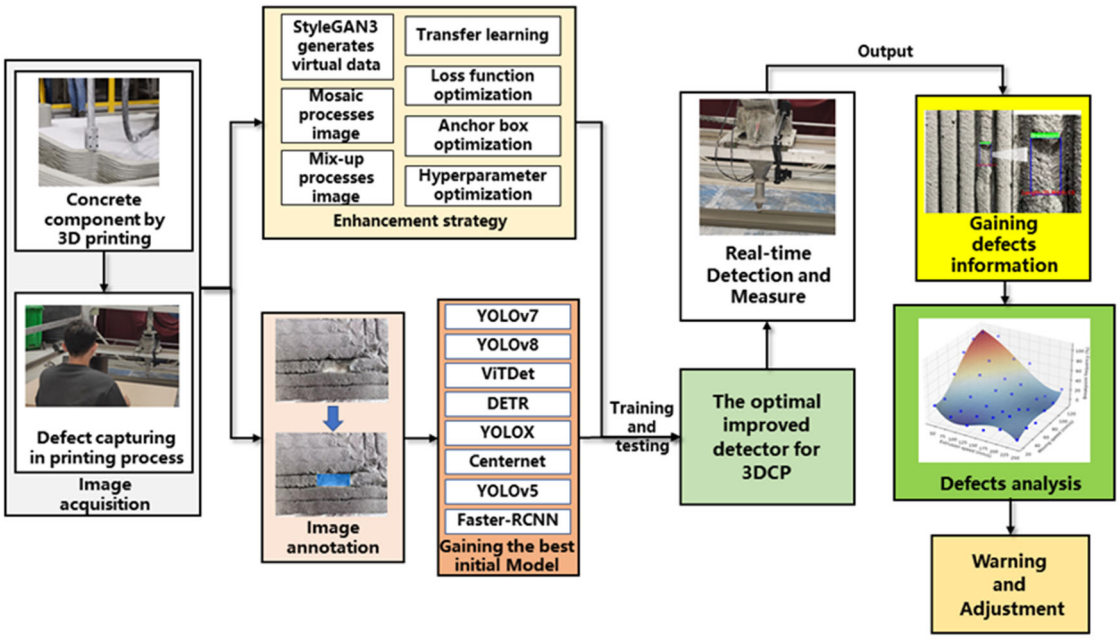

Figure 1. Flow diagram of the research.

Figure 1 illustrates the detailed research process. Following image collection during the 3DCP process, the initial data exhibiting defects and manually annotated material flaws was selected. To choose the best baseline model, various cutting-edge detection algorithms using the annotated data were trained and then their results were comprehensively compared.

Meanwhile, the initial images were used as a basis to produce more data via various data augmentation techniques. Subsequently, the augmented data into the optimal baseline model were integrated, enhancing the defect detector for 3DCP. This integration involved transfer learning, hyperparameter evolution, anchor box optimization, and optimized loss functions. Employing this top-performing detector facilitates real-time defect detection and measurement during the 3DCP process, thereby furnishing insights into defect dimensions. Utilizing this information, an investigation into the correlation between defect frequencies and printer parameters is conducted, yielding strategic printer parameter adjustments. Finally, this study introduces real-time alerts and printer parameter modifications in response to defects and anomalies detected during the printing process.

2.1 Setup for Image Acquisition

In this experiment, image acquisition parameters were configured as follows: A 51x39 cm shooting scope was obtained by adjusting the distance between the lens and the printed layer to 30 cm. In addition, a 4 mm industrial lens combined with a 90-frame industrial camera (HIKVISION MV-CS060-10GM) with a resolution of 2048 x 1536 pixels, yielding an approximate ratio of 0.25 mm per pixel between actual distances and pictures. The materials' extrusion speed was varied between 40 and 240 mm/s in increments of 40 mm/s. Similarly, the nozzle's movement speed was changed in 20 mm/s increments, spanning from 20 to 120 mm/s. This process yielded a total of 36 unique printer parameter combinations. For each combination, 100 printing processes were conducted. Consequently, 1300 images during the whole 3DCP construction efforts were captured. Among these photographs were 300 negative samples, which were normal printing shots devoid of any breakpoint flaws, and 1240 cases of breakpoint faults.

2.2. Data Augmentation

In this study, the image processing methods called mosaic (0.9 initial value of hyperparameter) and mix-up (0.3 initial value of hyperparameter) were applied to supply training samples. The mosaic method randomly crops four images and merges them into one combined image, while the mix-up method fuses two images into a new one using a fusion ratio of γ, as described in Equations (1) and (2).To generate sufficient training data for the detector, StyleGAN3 was utilized, incorporating a CNN-based discriminator and a generator with a mapping network and style-control modules, as depicted in Figure 2. To develop an optimal data-generator model, 1000 images with breakpoint defects were used in StyleGAN3 to train 400 kilo-images (k-img). Moreover, the training device used in this study were Intel(R) Core (TM) i9-13900FK CPU@3.00 GHz, RAM 128 GB, NVIDIA GeForce RTX 6000 48G, and the training environment was Pytorch. As a result, the virtual 512×512 pixel photos with verisimilitude breakpoint defects of various shapes, sizes, and quantities, were generated to train the models.

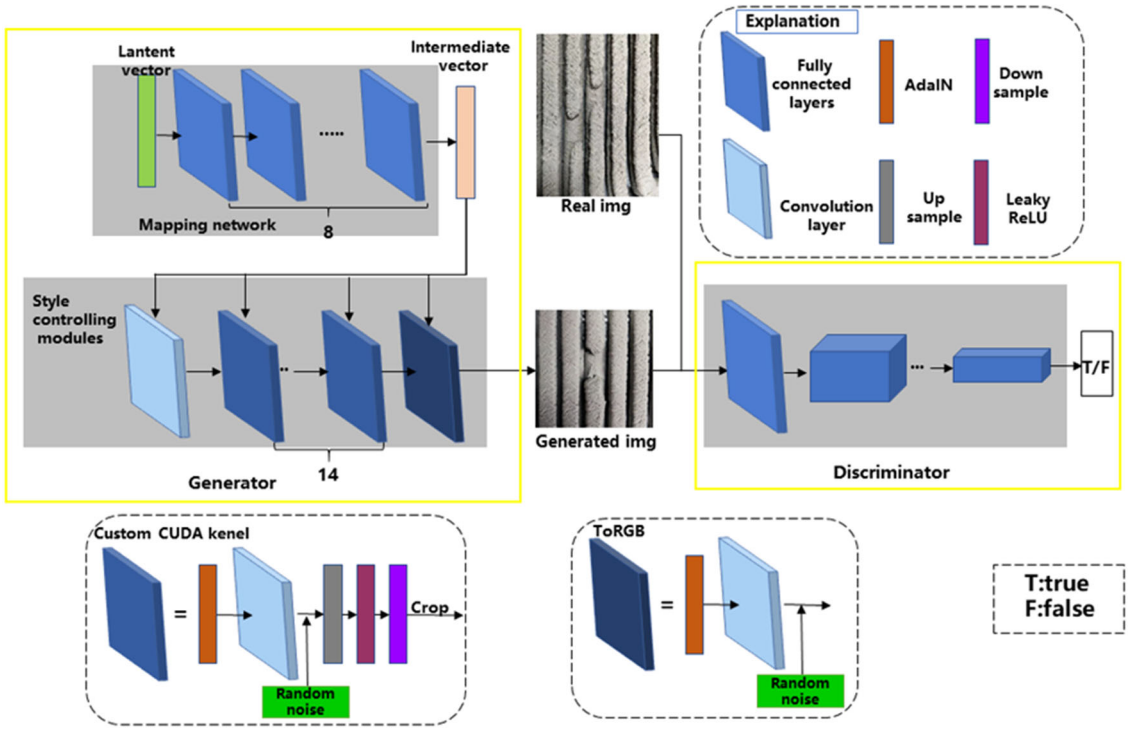

Figure 2. 3DCP defect data augmentation model applying StyleGAN 3.

$$\mathbf{FI} = \boldsymbol{\omega} * \mathbf{IA} + (\mathbf{1} - \boldsymbol{\omega}) * \mathbf{IB} \quad (1)$$

$$\boldsymbol{FL} = \boldsymbol{\omega} * \mathbf{LA} + (\mathbf{1} - \boldsymbol{\omega}) * \mathbf{LB} \quad (2)$$

where FI is the fused image vector, IA is the raw vector of image A, IB is the raw vector of image B, FL is fused one-hot label encodings, LA is the raw one-hot label encoding of image A, LB is the raw one-hot label encoding of image B, and $\boldsymbol{\omega}$ is a random value between 0 and 1.

2.3 Detector Optimization

The YOLO v7 algorithm segments images into grid cells, utilizing anchor boxes to predict bounding boxes and their associated probability scores for each class and selecting the class with the highest probability. Meanwhile, the parameters of the bounding box, the confidence score C, and object class O were predicted by the model. The relationship between the confidence score (C) and the probabilities P ($Class_i$|Object), P_r (Object), and IoU (intersection over union), as shown in Equation (3) and Equation (4).

$$\boldsymbol{C = P(Class_i|Object) * P_r(Object) * IOU_{pred}^{truth}} \quad (3)$$

$$\boldsymbol{IOU_{pred}^{truth} = \frac{|A \cap B|}{|A \cup B|}} \quad (4)$$

Note: P ($Class_i$|Object) represents conditional probability of a class. P_r (Object) = 1 if the bounding box contains objects in the grid cell; otherwise, Pr (Object) = 0. A represents ground truth bounding box and B represents predicted bounding box.

The initial images were resized to 640x640 pixels before input into the YOLO v7 model, resulting in three layers of feature maps with different sizes and outputting predicted results.

The overall framework of the YOLO v7 model is presented in Figure 3. Transfer learning techniques and the pre-trained weights from Microsoft were employed in this research to expedite the training process and improve the model's capabilities.

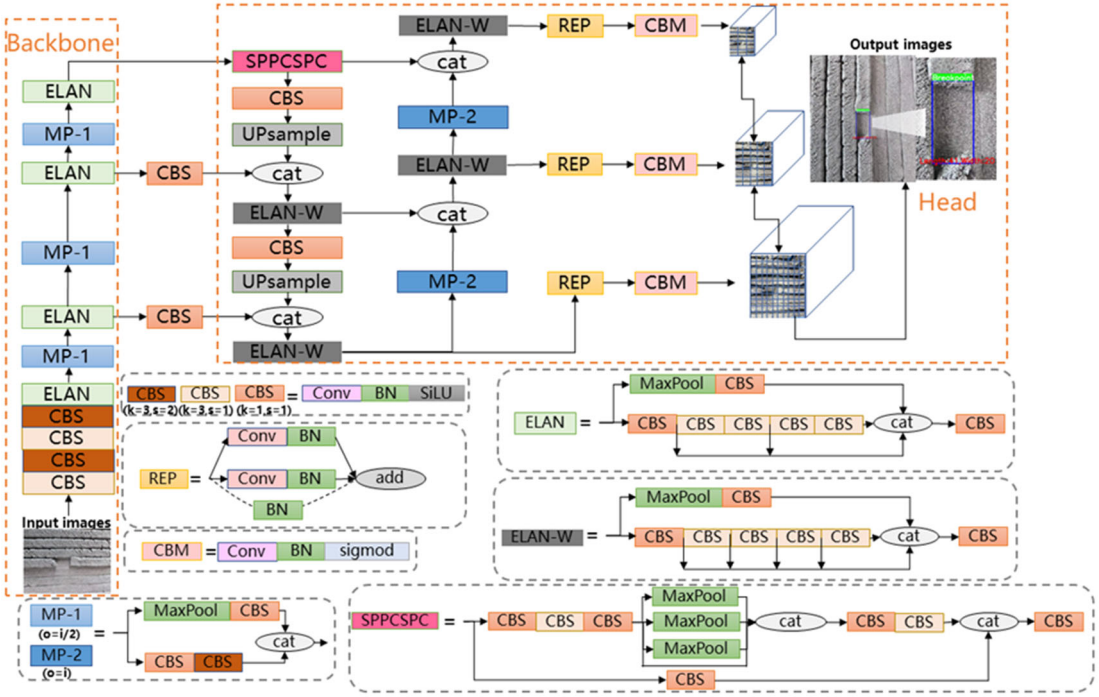

Figure 3. The overall framework of the YOLO v7 model.

YOLOv7 model's initial loss function is the CIoU loss function, as shown in Equation (5). This method neglects the complete loss of both length and width, leading to a deviation between regressing targets and computed results of the bounding box size. To address this issue, this study applied the EIoU loss function, as shown in Equation (6), which directly integrates the elements of bounding box loss to improve regression accuracy.

$$L_{CIoU} = 1 - IoU_{(A,B)} + \frac{p^2(b,b^{gt})}{(h^c)^2+(w^c)^2} + \frac{4}{\pi^2}(arctan\frac{w^{gt}}{h^{gt}} - arctan\frac{w}{h})^2 \quad (5)$$

$$L_{EIoU} = L_{IoU} + L_{centre} + L_{width} + L_{Length}$$

$$= 1 - IoU_{(A,B)} + \frac{p^2(b,b^{gt})}{c^2} + \frac{p^2(w,w^{gt})}{C_w^2} + \frac{p^2(h,h^{gt})}{C_h^2} \quad (6)$$

Denotes: IoU loss (L_{IoU}), central point loss (L_{centre}), width loss (L_{width}), and length loss (L_{Length})

This study employed the k-means++ clustering algorithm to optimize the anchor box size. By inputting data from 1000 real bounding boxes into the algorithm, initial cluster centers were randomly selected to calculate the shortest distance d (x_i) between each sample point and the existing centers, as illustrated in Equation (7). Subsequently, a set of k cluster centers was determined using a roulette method until the shortest distance reached a threshold, as illustrated in Equation (8). Thereby, the optimum 9 various-size anchor boxes (83.0×40.9 pixels, 61.5×64.1 pixels, 90.5×72.7 pixels, 78.8×106.5 pixels, 85.5×140.0 pixels,

126.3×100.9 pixels, 103.8×193.6 pixels, 259.6×102.0 pixels, 128.8×294.4 pixels) were obtained when the input size of images were 640×640 pixels.

$$\boldsymbol{d(x_i) = min_{j\in[1,2,\ldots,n]} \left\| x_i - c_j \right\|_2^2} \tag{7}$$

$$\boldsymbol{p(x_i) = \frac{d(x_i)}{\sum_{j=1}^{n} d(x_j)}} \tag{8}$$

where x_i represents i-th sample point and c_j represents j-th cluster centre.

This study utilized a genetic algorithm-based method for hyperparameter optimization. The model's hyperparameters, employing the stochastic gradient descent (SGD) optimizer, underwent 300 variations and 300 epochs of training. As a result, optimal hyperparameter results were attained within the specified period including 0.0067 initial learning rate, 0.938 SGD momentum, 0.00073 optimizer weight decay, 0.35 IoU training threshold, 0.9 mosaic, and 0.3 mix-up.

2.5 Polynomial Regression

The adoption of polynomial regression obtains the linear regression model to determine the relationship between breakpoint frequency and printer parameters, resulting in a transparent and interpretable model, as presented in Equations (9) [19].

$$BF = \beta_0 + \sum_{i=1}^{n} \beta_i S_i + \varepsilon \tag{9}$$

where BF was breakpoint frequency, β_0 was a constant and β_i were regression coefficients, vector S_i represented the printer parameters (the extrusion speed of materials and the moving speed of the nozzle).

The elastic net combines L1 (Lasso) and L2 (Ridge) regularization to enhance the model's generalization and simplification, as well as its ability to adapt to multicollinearity in the regression model, as illustrated in Equation (10) [20].

$$\hat{\mu} = min_{\mu} \left(\sum_{i=1}^{n} \left(y_i - \mu_0 - \sum_{j=1}^{p} x_j \mu_j \right)^2 + \lambda_1 \sum_{j=1}^{p} \mu_j^2 + \lambda_2 \sum_{j=1}^{p} |\mu_j| \right) \tag{10}$$

where $\hat{\mu}$ represented a set of μ, min_{μ} was the parameter on the minimum with μ, p was the number of data, y was the value of the dependent variable, x represented the value of the independent variables, λ_1 and λ_2 represented the complexity parameters for minimizing the validation error.

3 CONCLUSION

A multiple DL algorithms based method for real-time quality monitoring of printed concrete was presented in this study. The proposed method involved the utilization of an initial YOLOv7 model architecture, which was determined by a competition of various cutting-edge detectors. Furthermore, the StyleGAN3 and image processing strategies were employed to generate virtual images, expanding the training dataset. As a result,

comprehensive and precise information for breakpoint anomalies was obtained by 3DCP-YOLO through the application of multiple improvement strategies, enabling high accuracy for 3DCP defect detection despite a limited data volume. Finally, the warning was prompted to the operator, enabling them to timely repair the defects and revise the printer parameters.The key conclusions drawn from this study include:

1. For detecting 3DCP defects, the enhancement strategies were adopted, resulting in YOLOv7's improvement performances on mAP50 by 0.031, mAP50-95 by 0.119, and a 25% reduction in the training period.

2. The 3DCP-YOLO exhibited superior performance, significantly overcoming the YOLOv8 in 3DCP breakpoint detection, with mAP50 increase by 0.048, mAP50-95 increase by 0.141, and faster speed.

3. The optimal model for StyleGAN3 was achieved by training approximately 350 k-img. Based on this training weight, the FID value of generated virtual data was 101, which was close to real data. These high-quality virtual data replacing real data in detectors' training processes improved measuring accuracy and reduced model training period because of a larger capacity dataset.

4. The 3DCP-YOLO was used in the monitoring process to achieve 100% defect detection of printed concretes. The relative errors of 3% for length and 3.2% for width were acquired to measure breakpoint sizes. This demonstrated that the high accuracy was achieved by the 3DCP-YOLO.

5. A predictive formula was discovered, establishing the correlation between the frequency of breakpoint occurrence and printer settings. This formula revealed that coordinately improving material extrusion speed and reducing nozzle movement speed could prevent defects during the printing process.

6. The comprehensive, accurate, and lucid information on the breakpoint anomalies was obtained by the proposed method, timely facilitating operators to adjust printer parameters and repair defects during the printing process.

REFERENCES

[1]. Zhang, J., et al., *A review of the current progress and application of 3D printed concrete.* Composites Part A: Applied Science and Manufacturing, 2019. **125**: p. 105533.

[2]. Bos, F., et al., *Additive manufacturing of concrete in construction: potentials and challenges of 3D concrete printing.* Virtual and physical prototyping, 2016. **11**(3): p. 209-225.

[3]. Kaliyavaradhan, S.K., et al., *Test methods for 3D printable concrete.* Automation in Construction, 2022. **142**: p. 104529.

[4]. Sun, J., et al., *Fresh and mechanical behaviour of developed fibre-reinforced lightweight engineered cementitious composites for 3D concrete printing containing hollow glass microspheres.* Ceramics International, 2021.

[5]. Yang, L., et al., *Nozzle criteria for enhancing extrudability, buildability and interlayer bonding in 3D printing concrete.* Automation in Construction, 2023. **146**: p. 104671.

[6]. Sun, J., et al., *Mechanical enhancement for EMW-absorbing cementitious material using 3D concrete printing.* Journal of Building Engineering, 2021: p. 102763.

[7]. Wangler, T., et al., *Digital concrete: a review.* Cement and Concrete Research, 2019. **123**: p. 105780.

[8]. Alanazi, N., et al., *The Theory of Critical Distances to assess the effect of cracks/manufacturing defects on the static strength of 3D-printed concrete.* Engineering Fracture Mechanics, 2022. **269**: p. 108563.

[9]. Khan, M.S., F. Sanchez, and H. Zhou, *3-D printing of concrete: Beyond horizons.* Cement and Concrete Research, 2020. **133**: p. 106070.

[10]. Siddika, A., et al., *3D-printed concrete: Applications, performance, and challenges.* Journal of Sustainable Cement-Based Materials, 2020. **9**(3): p. 127-164.

[11]. Wolfs, R.J., et al., *A real-time height measurement and feedback system for 3D concrete printing*, in *High Tech Concrete: Where Technology and Engineering Meet*. 2018, Springer. p. 2474-2483.

[12]. Lindemann, H., et al. *Development of a shotcrete 3D-printing (SC3DP) technology for additive manufacturing of reinforced freeform concrete structures*. in *RILEM International Conference on Concrete and Digital Fabrication*. 2018. Springer.

[13]. Mechtcherine, V., et al., *A roadmap for quality control of hardening and hardened printed concrete.* Cement and Concrete Research, 2022. **157**: p. 106800.

[14]. Senthilnathan, S. and B. Raphael, *Using Computer Vision for Monitoring the Quality of 3D-Printed Concrete Structures.* Sustainability, 2022. **14**(23): p. 15682.

[15]. Cui, X., et al., *Deep learning for intelligent identification of concrete wind-erosion damage.* Automation in Construction, 2022. **141**: p. 104427.

[16]. Tan, Y., et al., *Automatic detection of sewer defects based on improved you only look once algorithm.* Automation in Construction, 2021. **131**: p. 103912.

[17]. Hao, Z., C. Lu, and Z. Li, *Highly accurate and automatic semantic segmentation of multiple cracks in engineered cementitious composites (ECC) under dual pre-modification deep-learning strategy.* Cement and Concrete Research, 2023. **165**: p. 107066.

[18]. Davtalab, O., et al., *Automated inspection in robotic additive manufacturing using deep learning for layer deformation detection.* Journal of Intelligent Manufacturing, 2022. **33**(3): p. 771-784.

[19]. Amruthamol, N., et al., *Bayesian learning approach to foresee compressive strength of concrete.* Materials Today: Proceedings, 2023.

[20]. Zhang, X., M.Z. Akber, and W. Zheng, *Predicting the slump of industrially produced concrete using machine learning: A multiclass classification approach.* Journal of Building Engineering, 2022. **58**: p. 104997.

Proceeding of the 10th International Conference on Innovative Production and Construction (IPC 2024), Perth, Australia, July 11-12, 2024

Performance Assessment of Public Transport Networks: An AHP-ANP Approach

Gang Lin[1,2], Hamad AI Jassmi[3], Honglei Xu[2], Yiqun Zhang[2], Shaoli Wang[2], Zimo Li[1], Haicheng Li[4], Xiangyu Wang[1]

1. School of Civil Engineering and Architecture, East China Jiaotong University, China
2. School of Electrical Engineering, Computation and Mathematical Sciences, Curtin University, Kent Street, Perth, 6102, WA, Australia
3. Emirates Center for Mobility Research, United Arab Emirates University, AL Ain 15551, UAE
4. Faculty of Construction and Environment, Hong Kong Polytechnic University, Hong Kong

ABSTRACT: Multi-criteria decision-making (MCDM) methods have been extensively employed by researchers in the public transport (PT) sector. While many studies utilize a single MCDM method, employing multiple MCDM methods can achieve more robust results. Furthermore, integrated MCDM methods have the potential to address the weaknesses and limitations inherent in single MCDM method. In this study, we address the limitations of single MCDM methods by integrating the analytic hierarchy process (AHP) with the analytic network process (ANP) to evaluate public transport networks performance. Based on the established public transport criteria matrix AHP model, we identify interdependencies among criteria. The AHP-ANP method is then applied to assess public transport networks in three case study cities in Australia. The sensitivity analysis conducted on both the AHP and integrated AHP-ANP approaches highlights the influence of criteria interdependency. This research contributes to mitigating the limitations of AHP method and applies AHP-ANP model to provide decision-makers with insights to enhance PT network performance and achieve smart PT network management.

KEYWORDS: smart public transport performance management; integrated AHP-ANP methods; MCDM; sensitivity analysis.

1. INTRODUCTION

Public transport (PT) is an active travel and sustainable transport mode that promoting sustainable development. As highlighted by UN-Habitat in *sustainable transport, sustainable development interagency report*, promoting sustainable PT development is curial for governments to achieve *the Paris Climate Change Agreement* and *the 2030 agenda for sustainable development*. This report suggests the governments to strengthen sustainable PT transport management and planning. The development of sustainable PT entails a multifaceted process characterized by the need to balance multiple criteria. The comprehensive multiple criteria assessment of PT network provides the governments with information about future improvements. Consequently, conducting an analysis of PT network performance from diverse perspectives becomes imperative. Multi-Criteria Decision Making (MCDM) methods are frequently employed for analysing PT performance.

Despite the availability of numerous MCDM methods, no single method is universally applicable across all decision-making scenarios (Mulliner et al., 2016; Ye et al., 2022). Enhanced decision-making outcomes can be achieved by employing multiple methods to tackle the same problem (Lee & Chang, 2018). Such integration enables the utilization of the respective strengths of each method, while simultaneously mitigating their inherent limitations (Kabir et al., 2014). Therefore, this study systematically reviews previous research on Multi-Criteria Decision Making (MCDM) methods in public transport (PT) performance. It further integrates and develops MCDM methods to address the limitations associated with single method approaches in evaluating PT network performance.

1.2 Multiple-criteria decision-making in PT performance

The MCDM methods are the comprehensive tool that combine qualitative and quantitative aspects to evaluate complex problems and support decision-makers (DMs) in making conclusive decisions (Khan & Ali, 2020). MCDM tools and applications have been used in numerous studies in the past to tackle a variety of area-specific problems, including, but not limited to, sustainability, material, environment, production management, construction and project management, energy, quality management, GIS, safety and risk management, technology and information management, manufacturing systems, operation research and soft computing, strategic management, tourism management, and supply chain management (Behzadian et al., 2010; Velasquez & Hester, 2013; Mardani et al., 2015; Kheybari et al., 2020). The main purpose of the MCDM tools is to rank, select, sort and evaluate alternatives or criteria (Behzadian et al., 2010; Mardani et al., 2015; Kheybari et al., 2020).

In the area of PT issues, MCDM methodologies are increasingly being used. According to Camargo Pérez et al. (2015), 58 different MCDM techniques have been used in the context of PT systems between 1982 and 2014, which ultimately led to the realisation that MCDM techniques have become a highly effective tool for assessing and making decisions pertaining to projects in PT systems in recent decades. As a result, MCDM has emerged as a crucial decision-making method that authorities, academics, and researchers use to assess how satisfied customers are with PT systems (Nassereddine & Eskandari, 2017).

AHP, and DEA are the two main MCDM techniques for evaluating the effectiveness of PT networks (Barnum et al., 2007; Holmgren, 2013; Boujelbene & Derbel, 2015). Beside AHP and DEA, there are also another four MCDM methods for evaluating and weighting PT network performance considered: PROMETHEE, TOPSIS, ANP, and ELECTRE (Brans & Vincke, 1985; Olson, 2004; Saaty, 2004; Bojković et al., 2010; Greco et al., 2016; Nassereddine & Eskandari, 2017; Zhang et al., 2018; Lin et al., 2023). We arrived at the details of the six MCDM methods listed in Table 1 by referring to references related to assessing and weighting PT network performance.

Table 1: List of MCDM methods in evaluating and weighting PT network performance

Reference	Specific area	Weighting method
Cyril et al. (2019)	Assess the PT performance in quality, effectiveness, efficiency, and economic aspects.	AHP
Sheth et al. (2007)	Measure the PT service from the users, societal, and service	DEA

	providers perspectives.	
Lin et al. (2023)	Measure the transit-oriented development performance degree within a zone.	ANP
Nassereddine and Eskandari (2017)	Evaluate the PT service quality in different PT modes.	PROMETHEE
Zhang et al. (2018)	Evaluate the PT priority implementation based on overall development level, infrastructure construction, PT service level, and policy support.	TOPSIS
Bojković et al. (2010)	Assess transport sustainability at a macro level in terms of economic, environmental, and social aspects.	ELECTRE

However, each MCDM method has its own limitations. DEA, used to evaluate the efficiency of decision-making units (DMUs), handles multiple inputs and outputs without explicitly specifying relationships among performance criteria (Farrell, 1957; Charnes et al., 1978; Sheth et al., 2007; Izadikhah et al., 2021). However, DEA struggles with imprecise data, assuming precise knowledge for all variables (Velasquez & Hester, 2013; Izadikhah et al., 2021). Most DEA application in PT consider the efficiency of PT network performance.

PROMETHEE, an outranking technique, ranks and selects among conflicting criteria but lacks a clear methodology for assigning weights, potentially resulting in negative weighting results (Brans & Vincke, 1985; Behzadian et al., 2010; Velasquez & Hester, 2013; Nassereddine & Eskandari, 2017). PROMETHEE lacks a clear criterion weighting method.

TOPSIS identifies alternatives closest to the ideal solution, relying on Euclidean distance, which ignores attribute correlations and faces challenges in attribute weighting and maintaining judgment consistency as the number of attributes increases (Olson, 2004; Velasquez & Hester, 2013; Zhang et al., 2018).

ELECTRE, similar to PROMETHEE, relies on decision-makers to determine criteria weights, and its outranking method impedes the direct identification of strengths and weaknesses within alternatives, complicating result and impact verification (Bojković et al., 2010; Greco et al., 2016; Konidari & Mavrakis, 2007). For TOPSIS and ELECTRE, the weighting process does not contain a consistency test. Therefore, these four methods are not suitable on the evaluating and weighting PT network performance context.

Due to the inputs and outputs of the MCDM methods, AHP and ANP are introduced to manage the PT criteria evaluation and ranking. Previous studies often use AHP and ANP to evaluate and weight the PT performance criteria. The details are introduced as follow.

1.2.1 Analytic hierarchy process model

The AHP model is a technique for MCDM that enables DMs to deal with complex problems involving a variety of subjective and conflicting criteria (Saaty, 1994; Boujelbene & Derbel, 2015). The AHP breaks down the problem into different levels and provides a prioritised framework of choices, ranking them from most to least preferred (Jain et al., 2014). Level

objectives are established using pairwise comparisons, and weights are given to each criterion. Pairwise comparisons are used to create the factors at each level, which calls for determining the relative weights of two criteria or sub-criteria (Jain et al., 2014).

Furthermore, AHP allows DMs to handle complex issues involving multiple conflicts and subjective criteria. In terms of PT, stakeholders are concerned with both direct and indirect effects (Daraio et al., 2016), and AHP addresses the financial benefit, the quality and effectiveness of the PT service, the foundational infrastructure of PT, and the degree of sustainable development. Given these areas of application, the AHP model can assist governments in more effectively monitoring and enhancing the performance of PT networks.

Despite its frequent use, AHP has been criticised for inconsistencies between criteria and ranking reversal, which can, however, be managed by testing consistency during calculations and limiting the number of criteria (Konidari & Mavrakis, 2007; Velasquez & Hester, 2013). One other issue though is the need for AHP to consider setting criteria before calculation to handle interdependence among them (Velasquez & Hester, 2013).

1.2.2 Analytic network process model

ANP is a more generalized model of AHP, catering to the interdependency among criteria within a hierarchical structure due to criteria interactivity (Saaty, 2004). In terms of merits, the model establishes a network structure where criteria, sub-criteria, and alternatives interact, allowing comprehensive communication and feedback among all network elements, and enabling interconnection between nodes (clusters) (Saaty, 2004; Kheybari et al., 2020). While ANP significantly encompasses relationships, it is not without limitations, including the necessity for exhaustive brainstorming sessions in attribute identification, the time-intensive nature of data acquisition, the higher computational requirements compared to AHP process, and the neglect of subjectivity in comparisons (Yellepeddi et al., 2006).

Although AHP and ANP can manage to evaluate and weight PT network performance criteria, ANP needs to spend more time for data acquisition and calculations. ANP is used to handle criteria interdependence, compared with AHP (Velasquez & Hester, 2013).

In conclusion, this section has provided a detailed consideration of current MCDM methods in PT network performance. The current research applies singe MCDM method to attain performance reports and criteria weights. Each MCDM method contains limitations. As mentioned before, the limitation can be managed by utilising multiple methods. Limited studies consider the interrelationship among PT network performance criteria, and the criteria hierarchy and network at the same time. To mitigate the limitations, this research applies AHP-ANP approach to evaluate PT network performance.

Compared with mentioned research, the contribution of this paper is outlined as follows: 1. The interrelationship among PT network criteria are identified. 2. The AHP-ANP model framework is developed to assess the PT network performance. 3. The comparative analysis of the proposed method and PTCM-AHP methods are examined through three case studies.

In the next section, the framework of the proposed AHP-ANP framework to evaluate PT network performance is introduced in section 2. Section 3 describes the details of case study areas. Section 4 analyses and discusses the results of three cities, and section 5 concludes the research and discusses the research limitations and future directions.

2. METHODOLOGY AND METHOD

In this paper, the PT network performance criteria hierarchy structure is established refer to Lin et al. (2024). The evaluation framework is included 4 levels criteria which are basic PT infrastructure level, PT service level, economic benefit level, and sustainable development level (Lin et al., 2021; Lin et al., 2022; Lin et al., 2024). The details of the subcriteria are identified in Lin et al. 2021. As can be seen from Figure 1, the hierarchy structure involves 15 subcriteira.

By applying AHP-ANP approach, the Figure 2 shows the interdependence occurs among criteria and subcriteira. Based on the city planning policies and strategies, we identified the interdependency among the subcriteria. Refer to Figure 2, basic PT infrastructure level is influenced by PT service level and sustainable development level criteria, and has the interdependencies exists among criteria and subcriteria. PT service level is affected by Basic PT infrastructure level criteria. Hence, the weighting results of subcriteria in basic PT infrastructure level and PT service level are calculated in ANP process. The subcriteria include PT network ratio, PT coverage ratio, Harbour-type bus stop setting ratio, PT priority lane setting ratio, PT on-time ratio, peak hours intersection blocking rate, and PT land area per capita. Once the AHP-ANP model structure for evaluating PT network performance is established. And the criteria interdependency is identified. In criteria weighting process, we calculate the test the criteria weighting results. The details of weighting process are displayed as follows.

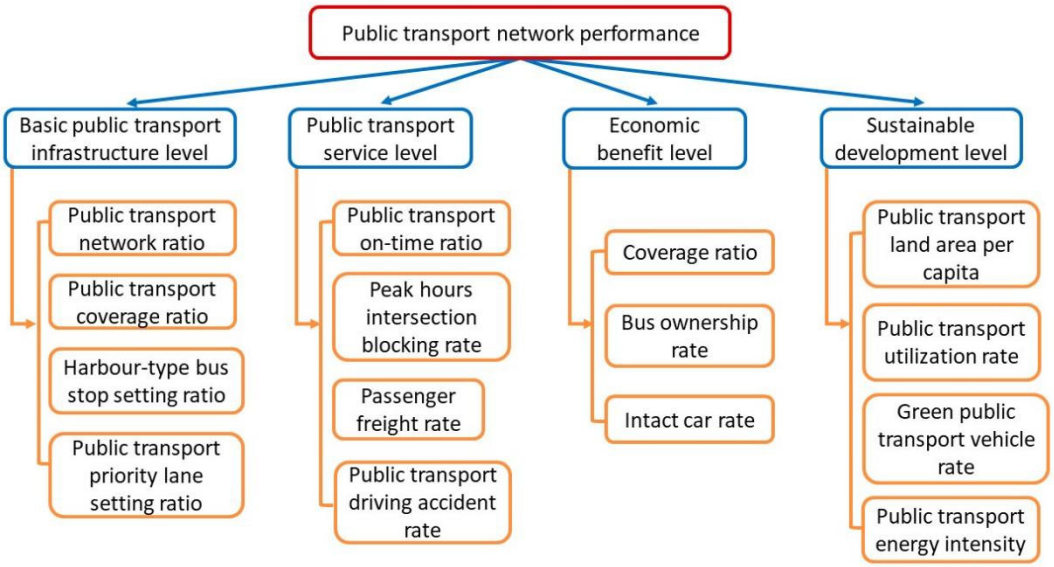

Figure 1: Public transport network performance criteria hierarchy stucture (Lin et al., 2024)

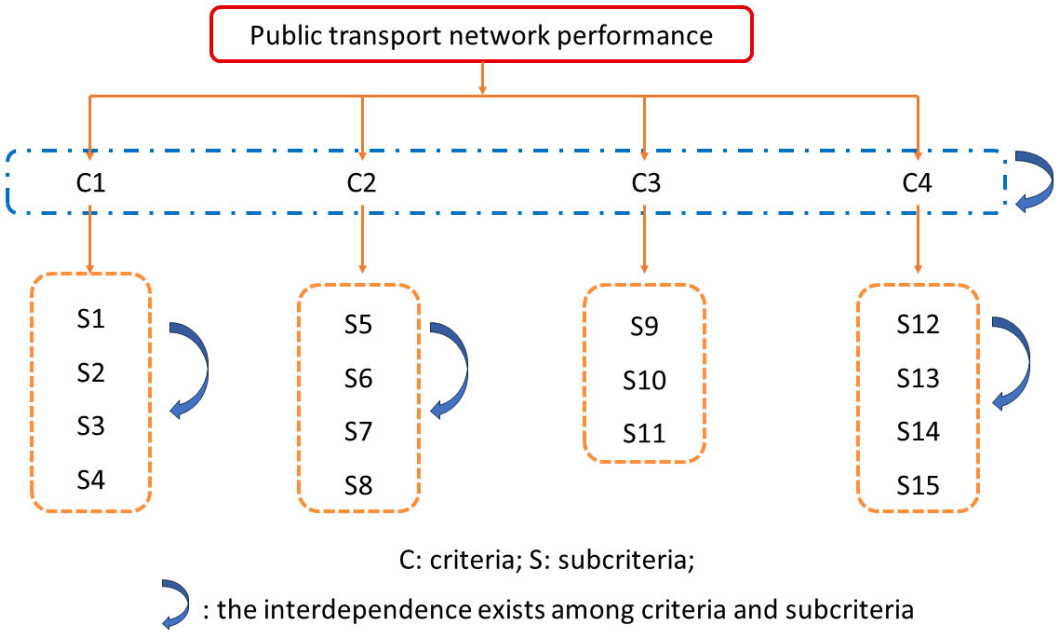

Figure 2: AHP-ANP model criteria structure

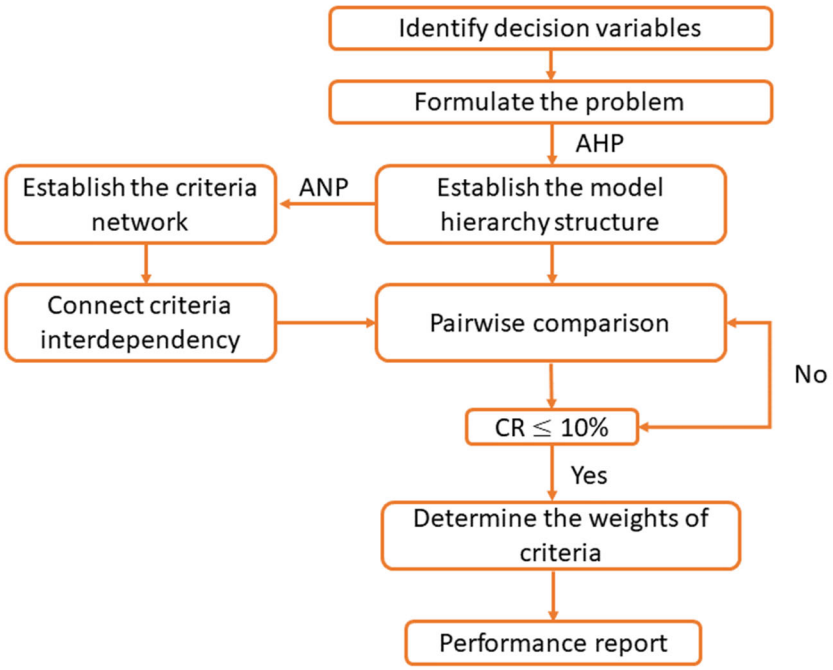

Figure 3: AHP-ANP model framework

3.1 AHP-ANP process

The decision variables of the proposed AHP-ANP model can be found in Lin et al. (2021). The criteria are chosen from PT evaluation indices and assessments, and the details of selected criteria are demonstrated in Lin et al. (2021). After setting the PT network

evaluation model criteria and subcriteria to consider the criteria interdependence, the related subcriteria is amend the hierarchical structure into the network. As can be seen from Figure 3, the details of the AHP-ANP model for evaluating PT network performance is contained in three processes.

Process 1: Developing AHP model structure to evaluate PT netowrk performance.

In AHP process, the AHP software is used to determine the criteria and subcriteria weights and calculates the consistency ratio for criteria hierarchy structure. There are 3 steps includes in the AHP process.

Step 1. Selecting and identifying decision variables.

As mentioned before, the criteria are selected from existing PT performance evaluation indices and assessments which are the *Evaluation Index System of Public Transportation City Assessment* (Ministry of Transport, 2014), the *Code for Transport Planning on Urban Road GB50220-1995* (Ministry of Construction, 1995), the *Passenger Transport Services for Bus/Trolleybus GB/T22484-2008* (Ministry of Housing and Urban-Rural Development, 2018), *GBT 22484-2016,* the *Passenger Transport Services Specifications for Urban Bus/Trolleybus* (Ministry of Transport, 2016), and the *Urban Road Traffic Management Evaluation Index System* (2012 edition) (Ministry of Transport, 2012). The selected criteria details are presented in Appendix A1.

Step 2. Establishing criteria and subcriteria hierarchy AHP model structure.

Based on the selected subcriteria, the model structure is divided into 4 levels. The PT network performance criteria hierarchy structure is shown in Figure 1 (Lin et al., 2024).

Step 3. Calculating the criteria and subcriteria weights.

Following the establishment of the hierarchical model structure for public transport network performance criteria, AHP model is utilized to assign weights to criteria and subcriteria through pairwise comparison, ranging from 1 to 9 (Saaty, 1994). The matrices for pairwise comparison of criteria and subcriteria are derived by reviewing the planning policies and strategies of the case study areas.

Finally, the consistency ratio (CR) for each matrix is determined. In instances where CR exceeds 10%, it necessitates a repetition of the pairwise comparison process for criteria until CR is $\leq 10\%$.

Process 2: Developing ANP model for the criteria and subcriteria.

In ANP process, the interdependencies among criteria and subcriteria are identified. Subsequently, the SupDecisions software is employed to compute the weights of the subcriteria. The process contains 3 steps.

Step 1. Identifying the interdependence exists among the criteria and subcriteria.

The interdependencies among the criteria and subcriteria, and pairwise comparison matrix are identified through a review of relevant planning policies and strategies. Saaty's 1-9 scale is utilized in the ANP framework (Saaty, 2004). Subsequently, the subcriteria supermatrix is employed to ascertain the weights of the subcriteria.

Step 2. Calculating the subcriteria weights.

Utilizing the SupDecisions software, the supermatrix for the supcriteria S1-S6 is established. If the CR of judgments for the supermatrix falls below 10%, the comparison is deemed

internally coherent. However, if the comparison process exhibits inconsistency, it necessitates repetition.

Step 3. Determining the AHP-ANP criteria and subcriteria weights.

Last, the criteria and subcriteria weights are determined by AHP-ANP model results. The subcritera S1-S6, and S12 weights are identified in limit super-matrix via ANP model. According to the AHP and ANP criteria and subcriteria weighting results, the model adjusts the subcriteria weights.

Process 3: Calculating case study areas PT network performance score.

Last but not least, the case study areas PT network performance score can be calculated based on AHP-ANP model criteria weights results and level grade for all subcriteria (refer to Table A1).

To validate the proposed AHP-ANP PT network performance evaluation model, the model is applied in three cities in Australia. The details of cities are demonstrated in the next section.

3. Case study

(**a**) (**b**) (**c**)

Figure 3: (a) City boundary of Stonnington; (b) city boundary of Bayswater; (c) city boundary of Cockburn [24].

This study applies AHP-ANP model to evaluate the PT network performance in three Australian study areas: the City of Stonnington, the City of Bayswater, and the City of Cockburn. Furthermore, this study also conducts comparative analysis with public transport criteria matrix (PTCM)-AHP model to validate the effectiveness of the model.

Bayswater and Stonnington are suburbs located near the Perth and Melbourne Central Business Districts, respectively, while Cockburn is situated in the southern part of Perth. These cities primarily rely on trains and buses as the main modes of public transport. The population densities of Bayswater, Cockburn, and Stonnington are 19.94 persons per hectare, 6.98 persons per hectare, and 46.27 persons per hectare, respectively. These cities are primarily designated for residential purposes. Further details of the case studies can be found in Lin et al. (2021). The locations of these three cities are depicted in Figure 3.

4. Results and discussion

In this section, the AHP-ANP PT network performance results are identified. To reveal the difference of criteria weighting results, the sensitive analysis between AHP-ANP model and PTCM-AHP model results is conducted.

4.1 AHP-ANP application

As indicated in section 3, both AHP-ANP and PTCM-AHP models contains the same criteria and subcriteria, the structure and calculation process are different. The AHP process structure and results are identified in Lin et al. (2021). The criteria weights distribution of PT criteria matrix is presented in Table B1.

In ANP process, Table 2 is the unweighted subcriteira supermatrix for subcriteria in basic PT infrastructure level, PT service level and sustainable development level. The unweighted subcriteria supermatrix is conducted by pairwise comparisons as shown in Table 2. The unweighted supermatrix is given by reviewing the current city strategies and plans. The zero value in the matrix is shown that there is no impact involved between the subcriteria.

The generation of the limit supermatrix is achieved by computing the limiting power of the weighted supermatrix. Referring to Table 3, the subcriteria priorities is the weights of the seven subcriteria. The global weight of the seven subcriteria is obtained by multiplying the basic PT infrastructure level and PT service level weights.

Table 2: Unweighted subcriteria supermatrix

	Public transport network ratio	Public transport coverage ratio	Harbor type bus stop setting ratio	Public transportation priority lane setting ratio	Public transport on-time rate	Intersection blocking rate during peak hours	Public transport land area per capita
Public transport Network ratio	1	1	3	2	3	3	2
Public transport coverage ratio	1	1	3	2	2	2	2
Harbor type bus stop setting ratio	1/3	1/3	1	1/2	1/2	0	0

Public transportation priority lane setting ratio	1/2	1/2	2	1	3	0	0
Public transport on-time rate	1/3	1/2	2	1/2	1	2	0
Intersection blocking rate during peak hours	1/3	1/3	0	0	1/2	1	0
Public transport land area per capita	1/2	1/2	0	0	0	0	1

Table 3: Subcriteria priorities (Limit supermatrix)

	S1	S2	S3	S4	S5	S6	S12	CR
Weigt	25	22	7	17	10	8	11	2.11%

4.2 Sensitive analysis

Based on the AHP-ANP model results, the interdependency among the subcriteria are identified, and the adjust subcriteria weights of AHP-ANP model is demonstrated in Table 4 and 5. The global weight of criteria and ranking results of AHP-ANP and PTCM-AHP models are shown in Table 6.

Referring to Tables 4 and 6, the global weight (GW) of PT network ratio (S1) increases to 14.6%, exhibiting a difference of 0.3% compared to the PTCM-AHP result.

Moreover, the ranking results from AHP-ANP highlight the distinction between PT coverage ratio (S2) and S1. The weight of S2 declines to 12.7% with 11.19% difference rate (refer to Figure 4). Furthermore, the AHP-ANP model weight result of habor type bus stop setting ratio (S3) stands at 4.1%, reflecting a reduction of 0.4%. In contrast, the ranking of PT priority lane setting ratio (S4) has shifted from 5th to 3rd place. Referring to Figure 4, this change is accompanied by a notable increase in its global weight, with a difference rate of 24.05%.

Table 5 demonstrates that the ranking of PT on-time rate (S5) retains its 7th place, despite a decrease in weight to 6.1% compared to the weight of S5 in PTCM-AHP model. The GW of intersection blocking rate during peak hours (S6) increases to 5% with a growth of 0.4%. Besides the ranking results of S1-S6 mentioned earlier, Table 6 also illustrates the differences in subcriteria ranking without any changes in GW for coverage rate (S9), bus ownership rate (S10), green PT vehicle rate (S14), and PT energy intensity (S15).

Table 4: AHP-ANP model subcriteria weights for basic public transport infrastructure level

Criteria	LW (%)	GW (%)	Difference (%)
S1: Public transport network ratio	35	14.6	0.3
S2: Public transport coverage ratio	31	12.7	-0.6
S3: Harbor type bus stop setting ratio	10	4.1	-0.4
S4: Public transportation priority lane setting ratio	24	9.8	1.9

Table 5: AHP-ANP model subcriteria weights for public transport service level

Criteria	LW (%)	GW (%)	Difference (%)
S5: Public transport on-time rate	32	6.1	-0.4
S6: Intersection blocking rate during peak hours	26	5	0.4
S7: Passenger freight rate	28	5.3	-
S8: Public transport driving accident rate	14	2.6	-

Table 6: AHP-ANP criteria Ranking results

Criteria	AHP-ANP		PTCM-AHP	
	Ranking	GW	Ranking	GW
S1	**1**	**14.6**	**1**	**14.3**
S2	**2**	**12.7**	**1**	**14.3**
S3	**12**	**4.1**	**11**	**4.5**
S4	**3**	**9.8**	**5**	**7.9**
S5	7	6.1	7	6.5
S6	**9**	**5**	**10**	**4.6**
S7	8	5.3	8	5.3
S8	14	2.6	14	2.6
S9	**10**	**4.8**	**9**	**4.8**
S10	**11**	**4.3**	**12**	**4.3**

S11	15	1.9	15	1.9
S12	6	7.8	6	7.8
S13	13	3.2	13	3.2
S14	**4**	**9**	**3**	**9**
S15	**4**	**9**	**3**	**9**

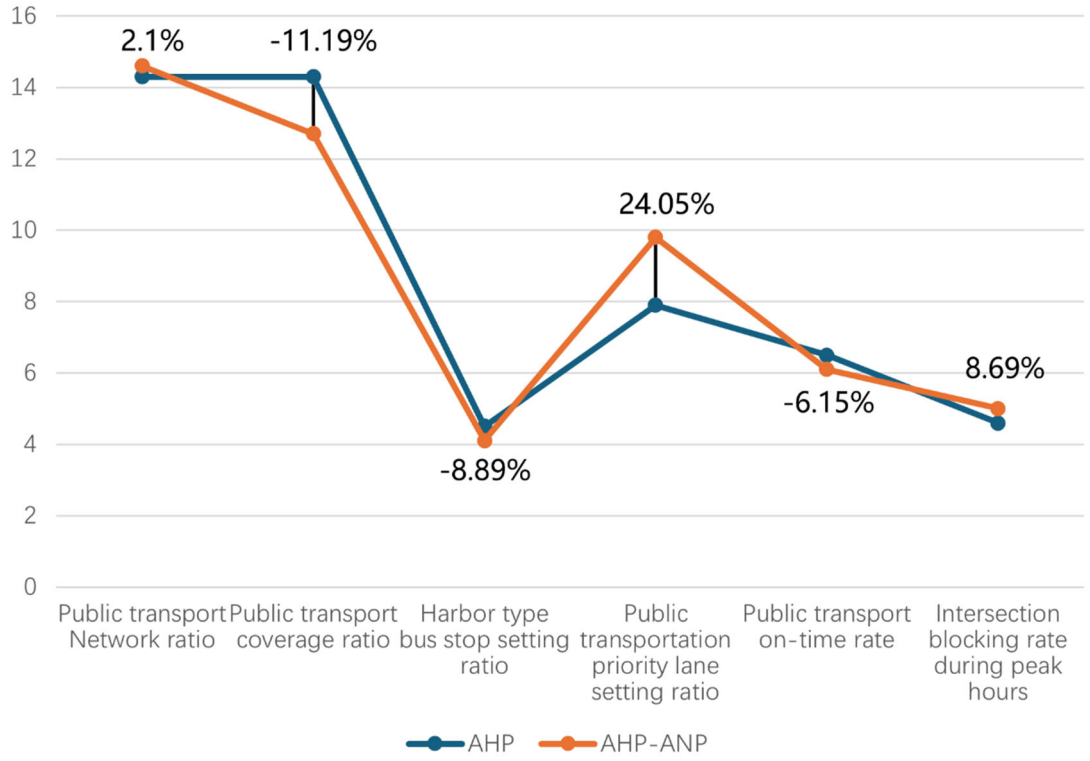

Figure 4: AHP and AHP/ANP subcriteria model weighting results difference rate

Table 7 presents the AHP-ANP model city scores for Bayswater, Cockburn, and Stonnington. The PTCM-AHP model results for these three cities are detailed in Lin et al. (2021). Bayswater's PT network achieves a score of 61.82, indicating a reduction of 2.7% difference rate compared to the PTCM-AHP results. Cockburn's performance decreases to 65.19, with a difference rate of 2.1%. Stonnington's city score improves to 84.43, reflecting a difference rate of 2.4% compared to the PTCM-AHP result.

To sum up, the above discussion clearly reveals the difference on subcriteria weights obtained by AHP-ANP and PTCM-AHP model. The fluctuations in relative weights and city scores between the two models elucidate the impact of interdependencies among criteria and subcriteria on their weighting and city score outcomes. Through comparison, the integrated AHP-ANP model offers a methodology to simulate the interrelationships among PT network performance criteria. The criteria weights calculated by the AHP-ANP model reveal a higher degree of differentiation compared to the PTCM-AHP results, thereby assisting decision-makers in understanding the significance of criteria for enhancing PT network performance.

Table 7: AHP-ANP model case study city score

Criteria		GW		
		Bayswater	**Cockburn**	**Stonnington**
C1: Basic public transport infrastructure level	S1: Public transport network ratio	3.09	3.37	13.25
	S2: Public transport coverage ratio	9.34	10.27	12.7
	S3: Harbor-type bus stop setting ratio	2.7	1.51	3.19
	S4: Public transportation priority lane setting ratio	0	0.19	8.89
C2: Public transport service level	S5: Public transport on-time rate	5.12	5.12	4.68
	S6: Intersection blocking rate during peak hours	0	3.16	4.72
	S7: Passenger freight rate	5.3	5.3	5.3
	S8: Public transport driving accident rate	2.01	2.01	0.76
C3: Economic benefit level	S9: Coverage rate	3.34	3.34	3.86
	S10: Bus ownership rate	1	1	1.06
	S11: Intact car rate	1.9	1.9	1.9
C4: Sustainable development level	S12: Public transport land area per capita	7.8	7.8	6.62
	S13: Public transport utilization rate	2.99	2.99	3
	S14: Green public transport vehicle rate	9	9	9
	S15: Public transport energy intensity	8.23	8.23	5.5
	Total	61.82	65.19	84.43
	Difference rate	-2.7%	-2.1%	2.4%

5. CONCLUSION

The proposed AHP-ANP model makes significant contributions to the evaluation of PT network performance from both practical and methodological perspectives. It addresses limitations inherent in previous PTCM-AHP models by incorporating AHP-ANP frameworks to account for the interdependencies among criteria and subcriteria, thereby enabling a comprehensive assessment of PT network performance. The validity of the AHP-ANP model is demonstrated and verified through three case studies conducted in Australia. This novel model not only facilitates the evaluation of PT network performance within cities but also serves as a valuable tool for government entities in formulating PT network plans and strategies. The results clarify the priorities for PT network improvement based on the importance of criteria.

Based on the results of this research, three case studies show the following recommendations when utilizing the AHP-ANP model. It is recommended that adjustments be made to the criteria selection and AHP-ANP structure framework to align with the specific requirements

of local governments. Moreover, the incorporation of additional criteria and subcriteria warrants careful consideration, with a particular focus on reviewing the interdependencies among criteria.

Nonetheless, the limitations of this research should mitigate and manage in the future work. While we have generalized the criteria weights and ranked the PT network performance of cities based on existing local planning policies and strategies in Australia, future studies should engage experts or consider a broader selection of planning policies and strategies from diverse geographical areas to validate the research findings in a global context.

REFERENCES

[1]. Barnum, D. T., McNeil, S., & Hart, J. (2007). Comparing the efficiency of public transportation subunits using data envelopment analysis. *Journal of Public Transportation*, *10*(2), 1-16. https://doi.org/10.5038/2375-0901.10.2.1

[2]. Behzadian, M., Kazemzadeh, R. B., Albadvi, A., & Aghdasi, M. (2010). PROMETHEE: A comprehensive literature review on methodologies and applications. *European Journal of Operational research*, *200*(1), 198-215. https://doi.org/10.1016/j.ejor.2009.01.021

[3]. Bojković, N., Anić, I., & Pejčić-Tarle, S. (2010). One solution for cross-country transport-sustainability evaluation using a modified ELECTRE method. *Ecological Economics*, *69*(5), 1176-1186. https://doi.org/10.1016/j.ecolecon.2010.01.006

[4]. Boujelbene, Y., & Derbel, A. (2015). The performance analysis of public transport operators in Tunisia using AHP method. *Procedia Computer Science*, *73*, 498-508. https://doi.org/10.1016/j.procs.2015.12.039

[5]. Brans, J. P., & Vincke, P. (1985). Note—A Preference Ranking Organisation Method: (The PROMETHEE Method for Multiple Criteria Decision-Making). *Management Science*, *31*(6), 647-656. https://doi.org/10.1287/mnsc.31.6.647

[6]. Camargo Pérez, J., Carrillo, M. H., & Montoya-Torres, J. R. (2015). Multi-criteria approaches for urban passenger transport systems: A literature review. *Annals of Operations Research*, *226*, 69-87. DOI 10.1007/s10479-014-1681-8

[7]. Charnes, A., Cooper, W. W., & Rhodes, E. (1978). Measuring the efficiency of decision making units. *European Journal of Operational Research*, *2*(6), 429-444. https://doi.org/10.1016/0377-2217(78)90138-8

[8]. Cyril, A., Mulangi, R. H., & George, V. (2019). Performance optimization of public transport using integrated AHP–GP methodology. *Urban Rail Transit*, *5*(2), 133-144. https://doi.org/10.1007/s40864-019-0103-2

[9]. Daraio, C., Diana, M., Di Costa, F., Leporelli, C., Matteucci, G., & Nastasi, A. (2016). Efficiency and effectiveness in the urban public transport sector: A critical review with directions for future research. *European Journal of Operational Research*, *248*(1), 1-20. https://doi.org/10.1016/j.ejor.2015.05.059

[10]. Farrell, M. J. (1957). The measurement of productive efficiency. *Journal of the Royal Statistical Society Series A: Statistics in Society*, *120*(3), 253-281. https://doi.org/10.2307/2343100

[11]. Greco, S., Figueira, J., & Ehrgott, M. (2016). *Multiple criteria decision analysis*. New York: springer.

[12]. Holmgren, J. (2013). The efficiency of public transport operations–An evaluation using stochastic frontier analysis. *Research in Transportation Economics*, *39*(1), 50-57. https://doi.org/10.1016/j.retrec.2012.05.023

[13]. Izadikhah, M., Azadi, M., Toloo, M., & Hussain, F. K. (2021). Sustainably resilient supply chains evaluation in public transport: A fuzzy chance-constrained two-stage DEA approach. *Applied soft computing*, *113*, 107879. https://doi.org/10.1016/j.asoc.2021.107879

[14]. Jain, S., Aggarwal, P., Kumar, P., Singhal, S., & Sharma, P. (2014). Identifying public preferences using multi-criteria decision making for assessing the shift of urban commuters from private to public transport: A case study of Delhi. *Transportation Research Part F: Traffic Psychology and Behaviour*, *24*, 60-70. https://doi.org/10.1016/j.trf.2014.03.007

[15]. Kabir, G., Sadiq, R., & Tesfamariam, S. (2014). A review of multi-criteria decision-making methods for infrastructure management. *Structure and infrastructure engineering*, *10*(9), 1176-1210. https://doi.org/10.1080/15732479.2013.795978

[16]. Khan, A. U., & Ali, Y. (2020). Analytical hierarchy process (AHP) and analytic network process methods and their applications: a twenty year review from 2000-2019: AHP & ANP techniques and their applications: Twenty years review from 2000 to 2019. *International Journal of the Analytic Hierarchy Process*, *12*(3). https://doi.org/10.13033/ijahp.v12i3.822

[17]. Kheybari, S., Rezaie, F. M., & Farazmand, H. (2020). Analytic network process: An overview of applications. *Applied mathematics and Computation*, *367*, 124780. https://doi.org/10.1016/j.amc.2019.124780

[18]. Konidari, P., & Mavrakis, D. (2007). A multi-criteria evaluation method for climate change mitigation policy instruments. *Energy Policy*, *35*(12), 6235-6257. https://doi.org/10.1016/j.enpol.2007.07.007

[19]. Lee, H. C., & Chang, C. T. (2018). Comparative analysis of MCDM methods for ranking renewable energy sources in Taiwan. *Renewable and sustainable energy reviews*, *92*, 883-896. https://doi.org/10.1016/j.rser.2018.05.007

[20]. Lin, G., Wang, S., Lin, C., Bu, L., & Xu, H. (2021). Evaluating performance of public transport networks by using public transport criteria matrix analytic hierarchy process models—Case study of Stonnington, Bayswater, and Cockburn public transport network. *Sustainability*, *13*(12), 6949. https://doi.org/10.3390/su13126949

[21]. Lin, G., Xu, H., Wang, S., Lin, C., & Huang, C. (2022). Performance optimisation of public transport networks using AHP-dependent multi-aspiration-level goal programming. *Energies*, *15*(17), 6479. https://doi.org/10.3390/en15176479

[22]. Lin, G., Xu, H., Wang, S., Lin, C., Zhang, F., & Zhu, J. (2024). Navigating Uncertainty: A Framework for Optimising Public Transport Networks' Performance. *Sustainability*, *16*(3), 1325. https://doi.org/10.3390/su16031325

[23]. Lin, J. J., Lin, T. Y., Kadali, B. R., & Subbarao, S. S. (2023). Zone-based TOD evaluation considering interdependences among criteria and zones. *Transport Policy*, *133*, 108-119. https://doi.org/10.1016/j.tranpol.2023.01.011

[24]. Mardani, A., Jusoh, A., Nor, K., Khalifah, Z., Zakwan, N., & Valipour, A. (2015). Multiple criteria decision-making techniques and their applications–a review of the literature from 2000 to 2014. *Economic research-Ekonomska istraživanja*, *28*(1), 516-571. https://doi.org/10.1080/1331677X.2015.1075139

[25]. Ministry of Construction. (1995). *Code for transport planning on urban road GB50220-1995*.

[26]. Ministry of Transport. (2012). *Urban road traffic management evaluation index system 2012 edition*.

[27]. Ministry of Transport. (2014). *Evaluation index system of public transportation city assessment*.

[28]. Ministry of Transport. (2016). *GBT 22484-2016 Passenger transport services specifications for urban bus/trolley bus*.

[29]. Ministry of Housing and Urban-Rural Development. (2018). *Passenger transport services for bus/trolleybus GB/T22484-2008.*

[30]. Mulliner, E., Malys, N., & Maliene, V. (2016). Comparative analysis of MCDM methods for the assessment of sustainable housing affordability. *Omega*, *59*, 146-156. https://doi.org/10.1016/j.omega.2015.05.013

[31]. Nassereddine, M., & Eskandari, H. (2017). An integrated MCDM approach to evaluate public transportation systems in Tehran. *Transportation Research Part A: Policy and Practice*, *106*, 427-439. https://doi.org/10.1016/j.tra.2017.10.013

[32]. Olson, D. L. (2004). Comparison of weights in TOPSIS models. *Mathematical and Computer Modelling*, *40*(7-8), 721-727. https://doi.org/10.1016/j.mcm.2004.10.003

[33]. Saaty, T. L. (1994). Highlights and critical points in the theory and application of the analytic hierarchy process. *European Journal of Operational Research*, *74*(3), 426-447. https://doi.org/10.1016/0377-2217(94)90222-4

[34]. Saaty, T. L. (2004). Fundamentals of the analytic network process—Dependence and feedback in decision-making with a single network. *Journal of Systems science and Systems engineering*, *13*, 129-157. https://doi.org/10.1007/s11518-006-0158-y

[35]. Sheth, C., Triantis, K., & Teodorović, D. (2007). Performance evaluation of bus routes: A provider and passenger perspective. *Transportation Research Part E: Logistics and Transportation Review*, *43*(4), 453-478. https://doi.org/10.1016/j.tre.2005.09.010

[36]. Velasquez, M., & Hester, P. T. (2013). An analysis of multi-criteria decision making methods. *International Journal of Operations Research*, 2013, *10*, 56–66. https://api.semanticscholar.org/CorpusID:6891121

[37]. Yellepeddi, S., Liles, D. H., & Rajagopalan, S. (2006). An Analytical Network Process (ANP) approach for the development of a reverse supply chain performance index in consumer electronics industry. *Faculty of the Graduate School of the University of Texas at Arlington in Partial Fulfillment of the Requirements for the Degree of Doctor of Philosophy*, *The University of Texas at Arlington*, *26*. https://pomsmeetings.org/ConfProceedings/004/PAPERS/004-0069.pdf

[38]. Ye, F., Chen, Y., Li, L., Li, Y., & Yin, Y. (2022). Multi-criteria decision-making models for smart city ranking: Evidence from the Pearl River Delta region, China. *Cities*, *128*, 103793. https://doi.org/10.1016/j.cities.2022.103793

[39]. Zhang, X., Zhang, Q., Sun, T., Zou, Y., & Chen, H. (2018). Evaluation of urban public transport priority performance based on the improved TOPSIS method: A case study of Wuhan. *Sustainable cities and society*, *43*, 357-365. https://doi.org/10.1016/j.scs.2018.08.013

Appendix A

Table A1: Level grade for all sub-criteria (Lin et al., 2021)

	Level Grade	Level A	Level B	Level C	Level D	Level E
Public transport network ratio (unit: %)	Index value interval	[60, 70]	[55, 60)	[50, 55)	[0, 50)	—
	Score interval	[90, 100]	[75, 90)	[60, 75)	[0, 60)	—
Public transport coverage ratio (unit: %)	Index value interval	≥55	[50, 55)	[45, 50)	[35, 45)	<35
	Score interval	[90, 100]	[80, 90)	[70, 80)	[60, 70)	[0, 60)
Harbor-type bus stop setting ratio (unit: %)	Index value interval	[35, 100)	[25, 35)	[15, 25)	[0, 15)	—
	Score interval	[90, 100]	[75, 90)	[60, 75)	[0, 60)	—
Public transport priority lane setting ratio (unit: %)	Index value interval	≥ 25	[20, 25)	[15, 20)	[10, 15)	[0, 10)
	Score interval	[90, 100]	[80, 90)	[70, 80)	[60, 70)	[0, 60)
Public transport on-time rate (unit: %)	Index value interval	[95, 100]	[85, 95)	[70, 85)	[0, 70)	—
	Score interval	[90, 100]	[75, 90)	[60, 75)	[0, 60)	—
Peak hours intersection blocking rate (unit: %)	Index value interval	[0, 2]	(2, 5]	(5, 8]	(8, 11]	>11
	Score interval	[90, 100]	[80, 90)	[70, 80)	[60, 70)	[0, 60)
Passenger freight rate (unit: %)	Index value interval	<3.5	[3.5, 4.5)	[4.5, 5.5)	[5.5, 6.5)	≥6.5
	Score interval	[90, 100]	[80, 90)	[70, 80)	[60, 70)	[0, 60)
Public transport driving accident rate (unit: times /million kilometres)	Index value interval	[0, 1.5]	[1.5, 2)	[2, 2.5)	[2.5, 3)	>3
	Score interval	[90, 100]	[80, 90)	[70, 80)	[60, 70)	[0, 60)
Coverage rate (unit: %)	Index value interval	>150	(100, 150]	= 100	[50, 100)	<50
	Score interval	[90, 100]	[80, 90)	[70, 80)	[60, 70)	[0, 60)
Bus ownership rate (unit: car/10,000)	Index value interval	[20, 25]	[19, 20)	[18, 19)	[0, 18)	—
	Score interval	[90, 100]	[75, 90)	[60, 75)	[0, 60)	—

Intact car rate (unit: %)	Index value interval	≥ 92	[88, 92)	[84, 88)	[80, 84)	<80
	Score interval	[90, 100]	[80, 90)	[70, 80)	[60, 70)	[0, 60)
Public transport land area per capita (unit: m2/person)	Index value interval	≥11	[8, 11)	[6, 8)	[4, 6)	<4
	Score interval	[90, 100]	[80, 90)	[70, 80)	[60, 70)	[0, 60)
Public transport utilisation rate (unit: %)	Index value interval	[0.17, 2)	[0.14, 0.17)	[0.11, 0.14)	[0.08, 0.11)	<0.08
	Score interval	[90, 100]	[80, 90)	[70, 80)	[60, 70)	[0, 60)
Green Public transport vehicle rate (unit: %)	Index value interval	≥ 95	[95, 92)	[88, 92)	[85, 88)	<85
	Score interval	[90, 100]	[80, 90)	[70, 80)	[60, 70)	[0, 60)
Public transport energy intensity (unit: g standard coal/person-km)	Index value interval	[0, 30)	[30, 80)	[80, 130)	[130, 200)	—
	Score interval	[90, 100]	[75, 90)	[60, 75)	[0, 60)	—

Appendix B

Table B1: AHP criteria weights distribution matrix. (Lin et al., 2021)

Criteria	**LW (%)**	**GW (%)**
C1: Basic public transport infrastructure level: 41%		
S1: Public transport network ratio	35	14.3
S2: Public transport coverage ratio	35	14.3
S3: Harbor type bus stop setting ratio	11	4.5
S4: Public transportation priority lane setting ratio	19	7.9
C2: Public transport service level: 19%		
S5: Public transport on-time rate	34	6.5
S6: Intersection blocking rate during peak hours	24	4.6
S7: Passenger freight rate	28	5.3
S8: Public transport driving accident rate	14	2.6
C3: Economic benefit level: 11%		
S9: Coverage rate	44	4.8
S10: Bus ownership rate	39	4.3
S11: Intact car rate	17	1.9

C4: Sustainable development level: 29%		
S12: Public transport land area per capita	27	7.8
S13: Public transport utilization rate	11	3.2
S14: Green public transport vehicle rate	31	9
S15: Public transport energy intensity	31	9

Proceeding of the 10th International Conference on Innovative Production and Construction (IPC 2024), Perth, Australia, July 11-12, 2024

Ddim Sampling for Generative Aibim, A Faster Intelligent Structural Design Framework

Zhili He, Yu-Hsing Wang

Department of Civil and Environmental Engineering,
The Hong Kong University of Science and Technology, HKSAR, China

ABSTRACT: Generative AIBIM, a successful structural design pipeline, has proven its ability to intelligently generate high-quality, diverse, and creative shear wall designs that are tailored to specific physical conditions. However, the current module of Generative AIBIM that generates designs, known as the physics-based conditional diffusion model (PCDM), necessitates 1000 iterations for each generation due to its reliance on the denoising diffusion probabilistic model (DDPM) sampling process. This leads to a time-consuming and computationally demanding generation process. To address this issue, this study introduces the denoising diffusion implicit model (DDIM), an accelerated generation method that replaces the DDPM sampling process in PCDM. While the original DDIM was designed for DDPM and the optimization process of PCDM differs from that of DDPM, this paper designs "DDIM sampling for PCDM," which modifies the original DDIM formulations to adapt to the optimization process of PCDM. Experimental results demonstrate that DDIM sampling for PCDM can accelerate the generation process of the original PCDM by a factor of 100 while maintaining the same visual quality in the generated results. This study effectively showcases the effectiveness of DDIM sampling for PCDM in expediting intelligent structural design. Furthermore, this paper reorganizes the contents of DDIM, focusing on the practical usage of DDIM. This change is particularly meaningful for researchers who may not possess a strong background in machine learning theory but are interested in utilizing the tool effectively.

KEYWORDS: deep learning; computer vision; generative AI; diffusion model

1 INTRODUCTION

Within the entire lifecycle of building projects, the structural design of buildings stands as a paramount and indispensable task. The accelerated pace of global urbanization has resulted in an ever-increasing demand for efficient and effective structural designs [1]. Presently, these designs are exclusively carried out by skilled structural engineers. However, this manual approach exhibits two distinct characteristics. Firstly, it heavily relies on vast structural knowledge and design expertise. Secondly, structural designs necessitate multiple iterations for refinement. Consequently, the process of structural design is time-consuming [2], labour-intensive, and inefficient [3], posing challenges in meeting the current demands [4]. Hence, there exists an urgent need for an innovative and intelligent design paradigm to address these challenges and alleviate the aforementioned issues faced by practitioners.

In the present era, rapidly evolving and widely followed AI technologies have ushered in revolutionary solutions across various industries [5],[6]. The data-driven paradigm of AI [7] possesses two remarkable attributes: (1) AI models possess virtually limitless memory capacity, enabling them to retain and represent vast amounts of data characteristics. Notably, models such as ChatGPT and GPT-4 can effectively encapsulate the entirety of human knowledge; (2) AI models operate with automation and efficiency [8], rendering their inference time nearly negligible when compared to human counterparts. Consequently, AI emerges as a natural fit for structural design tasks, and the exploration of effective utilization of AI in designing structures has become a prominent area of research.

Given the vast diversity in forms and layouts of buildings, current research efforts in the field primarily focus on the intelligent design of high-rise residential buildings utilizing shear wall systems [1]-[4]. This emphasis is primarily driven by two key factors: First, high-rise residential buildings constitute a substantial proportion of the overall building landscape, with design and construction demands continuously on the rise. Second, the layout of such buildings tends to exhibit a relatively regular pattern, often characterized by rectangular rooms and walls. This inherent regularity simplifies the design process for AI systems, making it more amenable to intelligent design applications.

Initially, the studies on intelligent design utilizing AI primarily employed regression-based methods. For instance, Pizarro et al. [9],[10] utilized multi-layer perceptrons (MLPs) and convolutional neural networks (CNNs) to regress shear wall structure layouts. Zhao et al. [3],[11] introduced graph neural networks (GNNs) to regress the graph representation of shear wall layouts. However, regression-based methods suffer from inherent drawbacks: First, they often lack diversity in their generated outputs [1]. Second, the results obtained from regression-based models do not consistently align with human perception, leading to visibly lower quality predictions [12]. Lastly, these methods tend to produce results with fewer high-fidelity details [13]. In contrast, deep generative models (DGMs), a novel AI framework, offer a promising alternative. DGMs can generate more intricate, diverse, and perceptually plausible images when compared to regression-based models [12],[13].

Consequently, researchers have recently turned their attention towards integrating DGMs into intelligent design methodologies. Among these DGMs, two notable ones are generative adversarial networks (GANs) [14] and the more recent diffusion models (DMs) [15],[16]. Liao et al. [2] were the first to extend the application of GANs to intelligent shear wall design, proposing StructGAN [2] along with a series of variants such as StructGAN-PHY [4] and StructGAN-AE [17]. However, GANs exhibit two inherent limitations: (1) training instability and oscillation, and (2) failure to explore and cover the entire distribution of training data [18], often getting trapped in specific modes of data distribution [19]. These characteristics hinder the visual quality of the generated results from StructGAN and its variants. For instance, many designed walls fail to meet the fundamental design requirements of having horizontal or vertical boundaries and of having clear enough design drawings [1]. On the other hand, diffusion models (DMs), particularly the denoising diffusion probabilistic model (DDPM) [16], have garnered substantial attention in recent years due to their enhanced stability and superior generation capabilities. DMs have demonstrated remarkable performance not only in image

synthesis but also in various downstream computer vision tasks such as deblurring [12], super-resolution [13], and denoising [20]. Moreover, DMs have found successful applications in influential commercial AI products like DALL·E [1] and Stable Diffusion [2] for image generation, as well as Sora[3] for video generation. Building upon these advancements, He et al. [1] propose Generative AIBIM, an automatic and intelligent structural design pipeline. In this framework, they introduce a novel physics-based conditional diffusion model (PCDM) for the intelligent generation of structural design drawings. Experimental results demonstrate that PCDM surpasses all GAN-based models, not only in quantitative evaluations but also in terms of visual quality and image details. Additionally, PCDM accommodates diverse and creative design requirements tailored to specific physical conditions, such as building heights and earthquake intensities.

Nevertheless, it is crucial to acknowledge a significant drawback of DDPM: its sampling process demands a substantial number of iterations to generate high-quality samples [21]. Since PCDM's sampling process is built upon that of DDPM, it inherits the same limitation. In their work [1], He et al. mention that PCDM requires 1000 iterations to complete a single generation, which is exceedingly time-consuming and resource-intensive. This becomes challenging when there is a need to generate multiple structural designs. To address this critical flaw in DDPM, Song et al. [21] propose the denoising diffusion implicit model (DDIM). DDIM effectively reduces the length of sampling chains while ensuring the generation of high-quality results. In fact, Song et al. [21] demonstrate that DDIM can accelerate the generation process of DDPM by a remarkable factor of 10 to 100 times.

Consequently, this study incorporates DDIM into Generative AIBIM to explore its potential for expediting the generation of structural design drawings. First, the original DDIM paper [21] primarily focuses on theoretical coherence, which may prove challenging for researchers without a strong background in machine learning and probability theory. As civil engineers, our primary concern lies in the practical utilization of the tool rather than delving into intricate mathematical theories. Therefore, this paper reorganizes the contents of DDIM, emphasizing its practical application and omitting the more obscure theoretical aspects, as presented in Subsection 2.2. Second, the original DDIM formulation is specifically designed for DDPM and cannot be directly applied to PCDM due to the differing optimization processes involved. Consequently, this study modifies the formulations to ensure their integration with PCDM, resulting in a modified version of DDIM known as "DDIM sampling for PCDM," as elucidated in Subsection 2.3. The experimental results, presented in Section 3, demonstrate that DDIM can accelerate the generation process of PCDM by a factor of 100 while maintaining the same level of generation quality. DDIM sampling for PCDM has been integrated into the code of Generative AIBIM, which is publicly available at https://github.com/hzlbbfrog/Generative-BIM.

2 METHOD

[1] https://openai.com/index/dall-e-3/
[2] https://stability.ai/
[3] https://openai.com/index/sora/

2.1 Generative AIBIM

In their seminal work [1], He et al. integrate Building Information Modeling (BIM) with the intelligent design of shear walls, presenting an innovative Generative AIBIM pipeline for structural design. This pipeline not only expands the application range of BIM but also complements the existing methodologies for intelligent design that are confined to CAD drawings. The Generative AIBIM framework encompasses four stages: (1) Stage I: from BIM models to architectural design drawings; (2) Stage II: intelligent structural design based on generative AI; (3) Stage III: from structural design drawings to BIM models; and (4) Stage IV: BIM-integrated applications. It is worth noting that Stage II stands as the pivotal component of this framework. In this stage, He et al. [1] devise a two-stage generation framework, drawing inspiration from the human drawing process. Their algorithm initially generates line drawings based on input canvases in Stage 1. In Stage 2, the line drawings are subsequently colored into structural design drawings (refer to Fig. 3 in [1] for enhanced comprehension). In the two-stage generation framework, Stage 1 is the core part, where He et al. [1] propose PCDM for generating line drawings based on DDPM. PCDM includes three distinct processes: the forward diffusion process, the reverse denoising process (also known as the sampling process), and the optimization process. These processes are summarized as follows:

In the forward diffusion process, PCDM injects Gaussian noise $\boldsymbol{\epsilon} \in \mathbb{R}^D$ step-by-step through a T-step Markov chain:

$$q(\mathbf{x}_t|\mathbf{x}_{t-1}) \triangleq \mathcal{N}\left(\mathbf{x}_t; \sqrt{1-\beta_t}\mathbf{x}_{t-1}, \beta_t \mathbf{I}_D\right), \tag{1}$$

where D denotes the dimension of a line drawing, $t \in \{1,2,\dots,T\}$ is the time step, $\mathbf{x}_t$ means the noise sample, and clearly, $\mathbf{x}_0$ is the clean sample, namely, a canvas. $\mathbf{I}_D$ denotes the identity matrix. β_t is the noise schedule and is defined by the following formulation:

$$\beta_t = 1 - \frac{\bar{\alpha}_t}{\bar{\alpha}_{t-1}}, \tag{2}$$

where $\bar{\alpha}_t$ is a cosine function and $\beta_t \in (0,1)$ for $\forall t$. Furthermore, we can obtain $\mathbf{x}_t$ through a single sampling for arbitrary t:

$$\mathbf{x}_t \sim q(\mathbf{x}_t|\mathbf{x}_0) = \mathcal{N}\left(\mathbf{x}_t; \sqrt{\bar{\alpha}_t}\mathbf{x}_0, (1-\bar{\alpha}_t)\mathbf{I}_D\right). \tag{3}$$

By the reparameterization trick, we can derive the formulation of $\mathbf{x}_t$:

$$\mathbf{x}_t = \sqrt{\bar{\alpha}_t}\mathbf{x}_0 + \sqrt{1-\bar{\alpha}_t}\boldsymbol{\epsilon}. \tag{4}$$

where $\boldsymbol{\epsilon} \sim \mathcal{N}(0, \mathbf{I}_D)$.

In the reverse denoising process, PCDM wants to regenerate clean samples $\hat{\mathbf{x}}_0$ from $\mathbf{x}_T$ and to make $\hat{\mathbf{x}}_0$ follow the real data distribution. First, we need to determine $\mathbf{x}_T$. Based on Eq. (3), clearly, when T is a large number, approximately, $\mathbf{x}_T \sim \mathcal{N}(0, \mathbf{I}_D)$. Thus, we can start from $\hat{\mathbf{x}}_T \sim \mathcal{N}(0, \mathbf{I}_D)$ and the difference between the distributions of $\mathbf{x}_T$ and $\hat{\mathbf{x}}_T$ can be

considered negligible. In PCDM, T is set to 1000. Further, we can formulate $q(\mathbf{x}_{t-1}|\mathbf{x}_t, \mathbf{x}_0)$:

$$q(\mathbf{x}_{t-1}|\mathbf{x}_t, \mathbf{x}_0) = \mathcal{N}\left(\mathbf{x}_{t-1}; \tilde{\boldsymbol{\mu}}_t(\mathbf{x}_t, \mathbf{x}_0), \tilde{\boldsymbol{\Sigma}}_t\right), \tag{5}$$

where

$$\tilde{\boldsymbol{\mu}}_t(\mathbf{x}_t, \mathbf{x}_0) = \frac{\sqrt{1-\beta_t}(1-\bar{\alpha}_{t-1})}{1-\bar{\alpha}_t}\mathbf{x}_t + \frac{\sqrt{\bar{\alpha}_{t-1}}\beta_t}{1-\bar{\alpha}_t}\mathbf{x}_0, \tag{6}$$

and

$$\tilde{\boldsymbol{\Sigma}}_t = \tilde{\beta}_t \mathbf{I}_D, \tilde{\beta}_t = \frac{1-\bar{\alpha}_{t-1}}{1-\bar{\alpha}_t}\beta_t. \tag{7}$$

In the reverse denoising process, PCDM uses a transition distribution $p_{\boldsymbol{\theta}}(\mathbf{x}_{t-1}|\mathbf{x}_t, \mathbf{y}, d)$ to substitute $q(\mathbf{x}_{t-1}|\mathbf{x}_t, \mathbf{x}_0)$ and follows DDPM to run a reverse Markov chain to sample data from $t = T$ to $t = 1$ to obtain the ultimate generation result $\hat{\mathbf{x}}_0$ based on the distribution $p_{\boldsymbol{\theta}}(\mathbf{x}_{t-1}|\mathbf{x}_t, \mathbf{y}, d)$. The schematic diagrams of the forward and reverse processes are shown in Fig. 1. Clearly, PCDM needs $T = 1000$ iterations to finish one generation.

The goal of the optimization process is to efficiently model $p_{\boldsymbol{\theta}}(\mathbf{x}_{t-1}|\mathbf{x}_t, \mathbf{y}, d)$ to make it approximate $q(\mathbf{x}_{t-1}|\mathbf{x}_t, \mathbf{x}_0)$. First, $p_{\boldsymbol{\theta}}(\mathbf{x}_{t-1}|\mathbf{x}_t, \mathbf{y}, d)$ is also defined as a Gaussian distribution:

$$p_{\boldsymbol{\theta}}(\mathbf{x}_{t-1}|\mathbf{x}_t, \mathbf{y}, d) \triangleq \mathcal{N}\left(\mathbf{x}_{t-1}; \boldsymbol{\mu}_{\boldsymbol{\theta}}(\mathbf{x}_t, t, \mathbf{y}, d), \boldsymbol{\Sigma}_{\boldsymbol{\theta}}(\mathbf{x}_t, t, \mathbf{y}, d)\right), \tag{8}$$

For simplicity, $\boldsymbol{\Sigma}_{\boldsymbol{\theta}}$ is set to $\tilde{\boldsymbol{\Sigma}}_t$. Then, the question is simplified into "how to model $\boldsymbol{\mu}_{\boldsymbol{\theta}}$ to make it close to $\tilde{\boldsymbol{\mu}}_t$. DDPM first combines Eq. (4) and Eq. (6) to eliminate $\mathbf{x}_0$:

$$\tilde{\boldsymbol{\mu}}_t = \frac{1}{\sqrt{1-\beta_t}}\left(\mathbf{x}_t - \frac{\beta_t}{\sqrt{1-\bar{\alpha}_t}}\boldsymbol{\epsilon}\right). \tag{9}$$

Then, it builds a neural network $\hat{\boldsymbol{\epsilon}} = \boldsymbol{\epsilon}_{\boldsymbol{\theta}}(\mathbf{x}_t, t, \mathbf{y}, d)$ to approximate $\boldsymbol{\epsilon}$, and $\boldsymbol{\mu}_{\boldsymbol{\theta}}$ can be defined as

$$\boldsymbol{\mu}_{\boldsymbol{\theta}} = \frac{1}{\sqrt{1-\beta_t}}\left(\mathbf{x}_t - \frac{\beta_t}{\sqrt{1-\bar{\alpha}_t}}\hat{\boldsymbol{\epsilon}}\right). \tag{10}$$

PCDM proposes another solution. It first divides $\mathbf{x}_0$ into two parts: shear walls $\mathbf{s}_0$ and infill walls $\mathbf{y}$. Then, a neural network is constructed to approximate $\mathbf{s}_0$: $\hat{\mathbf{s}}_0^t = f_{\boldsymbol{\theta}}(\mathbf{x}_t, t, \mathbf{y}, d)$, so, $\hat{\mathbf{x}}_0^t = f_{\boldsymbol{\theta}}(\mathbf{x}_t, t, \mathbf{y}, d) + \mathbf{y}$. Next, plug $\hat{\mathbf{x}}_0^t$ into Eq. (6) to model $\boldsymbol{\mu}_{\boldsymbol{\theta}}$:

$$\boldsymbol{\mu}_{\boldsymbol{\theta}} = \frac{\sqrt{1-\beta_t}(1-\bar{\alpha}_{t-1})}{1-\bar{\alpha}_t}\mathbf{x}_t + \frac{\sqrt{\bar{\alpha}_{t-1}}\beta_t}{1-\bar{\alpha}_t}\hat{\mathbf{x}}_0^t, \tag{11}$$

As for the neural network, PCDM introduces an innovative attention block that includes a self-attention block [22] and a parallel cross-attention block, along with an adaptive Instance Normalization block to facilitate the fusion of data from different domains.

2.2 DDIM Sampling

As elucidated in Subsection 2.1, the original PCDM follows the sampling process of DDPM, necessitating T iterations to obtain $\hat{\mathbf{x}}_0$, and T is a large number to ensure that the distribution of $\mathbf{x}_T$ close to $\mathcal{N}(0, \mathbf{I}_D)$ (T is set to 1000 in PCDM). Then, DDIM is proposed to expedite the generation process of DDPM by shortening sampling chains.

First of all, following the optimization process of DDPM, the prediction object of the neural network is still noise: $\hat{\boldsymbol{\epsilon}} = \boldsymbol{\epsilon}_{\boldsymbol{\theta}}(\mathbf{x}_t, t)$. Then, the core idea of DDIM is that if we have a subset of the original time steps $\{1,2,\dots,T\}$: $\tau = \{\tau_1, \tau_2, \dots, \tau_S\}$, where $\tau_1 < \tau_2 < \cdots < \tau_S \in [1, T]$, and S denotes the total time step of the sub-sequence. Clearly, $S < T$. Further, if the ultimate sample generated by the sub-sequence, $\hat{\mathbf{x}}_0$, has the same quality as the data sampled along $\{1,2,\dots,T\}$, we only need to consider the sampling along the sub-sequence, and the number of iterations is reduced to N from T. Thus, generation efficiency is increased. DDIM proves that by modifying the sampling rule, different sub-sequences are equivalent to the original $\{1,2,\dots,T\}$ and can be adopted as the sampling chain. The implementation details of the new rule are introduced as follows:

The same as DDPM, we still start from the end of data and sample $\hat{\mathbf{x}}_{\tau_S}$ from $\mathcal{N}(0, \mathbf{I}_D)$. τ_S still should be a large number, and τ_S is set to T for simplicity. Similarly, τ_1 is always set to 1. Based on mathematical induction, if we can define the transformation regulations from $\mathbf{x}_{\tau_i}$ to $\mathbf{x}_{\tau_{i-1}}$, we can achieve the sampling along the new chain τ. First, for different elements in τ, DDIM defines a variable variance hyperparameters σ:

$$\sigma_{\tau_i}(\eta) = \eta \sqrt{\frac{1-\bar{\alpha}_{\tau_{i-1}}}{1-\bar{\alpha}_{\tau_i}}} \sqrt{1-\frac{\bar{\alpha}_{\tau_i}}{\bar{\alpha}_{\tau_{i-1}}}}, \tag{12}$$

where i is the index of τ, and $\eta \geq 0$ is a controllable hyperparameter. Based on the above equation, we can define the direction pointing to $\mathbf{x}_{\tau_i}$:

$$\mathbf{x}_{\tau_i}^d = \sqrt{1-\bar{\alpha}_{\tau_{i-1}}-\sigma_{\tau_i}^2} \cdot \boldsymbol{\epsilon}_{\boldsymbol{\theta}}(\mathbf{x}_{\tau_i}, \tau_i), \tag{13}$$

where $\mathbf{x}_{\tau_i}^d$ denotes the direction pointing to $\mathbf{x}_{\tau_i}$. Recall Eq. (4), we have derived the formulation of $\mathbf{x}_t$. Since we have known $\mathbf{x}_{\tau_i}$ and $\boldsymbol{\epsilon}_{\boldsymbol{\theta}}(\mathbf{x}_{\tau_i}, \tau_i)$, we can represent $\mathbf{x}_0$ by $\mathbf{x}_{\tau_i}$ and $\boldsymbol{\epsilon}_{\boldsymbol{\theta}}(\mathbf{x}_{\tau_i}, \tau_i)$, and this representation is the prediction of $\mathbf{x}_0$ at $t = \tau_i$:

$$\hat{\mathbf{x}}_0^{\tau_i} = \frac{\mathbf{x}_{\tau_i} - \sqrt{1-\bar{\alpha}_{\tau_i}}\boldsymbol{\epsilon}_{\boldsymbol{\theta}}(\mathbf{x}_{\tau_i}, \tau_i)}{\sqrt{\bar{\alpha}_{\tau_i}}}, \tag{14}$$

where, $\hat{\mathbf{x}}_0^{\tau_i}$ is the prediction of $\mathbf{x}_0$. Combining Eqs. (13) and (14), we can formulate $\mathbf{x}_{\tau_{i-1}}$:

$$\mathbf{x}_{\tau_{i-1}} = \sqrt{\bar{\alpha}_{\tau_{i-1}}}\hat{\mathbf{x}}_0^{\tau_i} + \mathbf{x}_{\tau_i}^d + \sigma_{\tau_i}\boldsymbol{\epsilon}_{\tau_i}$$

$$= \sqrt{\bar{\alpha}_{\tau_{i-1}}}\left(\frac{\mathbf{x}_{\tau_i} - \sqrt{1-\bar{\alpha}_{\tau_i}}\boldsymbol{\epsilon}_{\boldsymbol{\theta}}(\mathbf{x}_{\tau_i}, \tau_i)}{\sqrt{\bar{\alpha}_{\tau_i}}}\right) + \sqrt{1-\bar{\alpha}_{\tau_{i-1}} - \sigma_{\tau_i}^2}\cdot\boldsymbol{\epsilon}_{\boldsymbol{\theta}}(\mathbf{x}_{\tau_i}, \tau_i) + \sigma_{\tau_i}\boldsymbol{\epsilon}_{\tau_i}, \quad (15)$$

where $\boldsymbol{\epsilon}_{\tau_i}$ follows a standard normal distribution: $\boldsymbol{\epsilon}_{\tau_i}\sim\mathcal{N}(0,\mathbf{I})$. This is equivalent to Eq. (12) in [21]. It is important to note that in DDIM sampling, η is set to 0, resulting in $\sigma_{\tau_i} = 0$, and DDIM sampling is transferred into DDPM sampling if η is assigned a value of 1 [21]. Then, we can notice that the DDIM sampling process is deterministic in comparison to DDPM sampling. The above content is the new sampling rule, and we omit the theoretical part, specifically, the proof of equivalence between sub-sequences and the original sequence $\{1,2,\dots,T\}$.

2.3 DDIM sampling for PCDM

The original DDIM is designed for DDPM, and in the optimization process of DDPM, the prediction of the neural network is noise $\boldsymbol{\epsilon}_{\boldsymbol{\theta}}$. While in the optimization process of PCDM, the prediction is shear walls $\hat{\mathbf{s}}_0^t = f_{\boldsymbol{\theta}}(\mathbf{x}_t, t, \mathbf{y}, d)$, we need to make modifications to the original DDIM sampling formulations. As shown in Fig. 1, the modified DDIM sampling process is named DDIM sampling for PCDM, which is detailed as follows:

First, we can directly obtain the prediction of $\mathbf{x}_0$ at $t = \tau_i$, which is different from Eq. (14):

$$\hat{\mathbf{x}}_0^{\tau_i} = f_{\boldsymbol{\theta}}(\mathbf{x}_{\tau_i}, \tau_i, \mathbf{y}, d) + \mathbf{y}. \quad (16)$$

Plugging the above equation into Eq. (14), we can formulate $\boldsymbol{\epsilon}_{\boldsymbol{\theta}}$:

$$\boldsymbol{\epsilon}_{\boldsymbol{\theta}} = \frac{\mathbf{x}_{\tau_i} - \sqrt{\bar{\alpha}_{\tau_i}}\hat{\mathbf{x}}_0^{\tau_i}}{\sqrt{1-\bar{\alpha}_{\tau_i}}} = \frac{\mathbf{x}_{\tau_i} - \sqrt{\bar{\alpha}_{\tau_i}}(f_{\boldsymbol{\theta}}(\mathbf{x}_{\tau_i}, \tau_i, \mathbf{y}, d) + \mathbf{y})}{\sqrt{1-\bar{\alpha}_{\tau_i}}}. \quad (17)$$

The new direction pointing to $\mathbf{x}_{\tau_i}$ is

$$\mathbf{x}_{\tau_i}^d = \sqrt{1-\bar{\alpha}_{\tau_{i-1}} - \sigma_{\tau_i}^2}\boldsymbol{\epsilon}_{\boldsymbol{\theta}} = \sqrt{1-\bar{\alpha}_{\tau_{i-1}} - \sigma_{\tau_i}^2}\frac{\mathbf{x}_{\tau_i} - \sqrt{\bar{\alpha}_{\tau_i}}(f_{\boldsymbol{\theta}}(\mathbf{x}_{\tau_i}, \tau_i, \mathbf{y}, d) + \mathbf{y})}{\sqrt{1-\bar{\alpha}_{\tau_i}}}. \quad (18)$$

At this time, $\mathbf{x}_{\tau_{i-1}}$ is still equal to $\sqrt{\bar{\alpha}_{\tau_{i-1}}}\hat{\mathbf{x}}_0^{\tau_i} + \mathbf{x}_{\tau_i}^d + \sigma_{\tau_i}\boldsymbol{\epsilon}_{\tau_i}$, However, $\hat{\mathbf{x}}_0^{\tau_i}$ and $\mathbf{x}_{\tau_i}^d$ should be replaced with Eqs. (16) and (17), respectively.

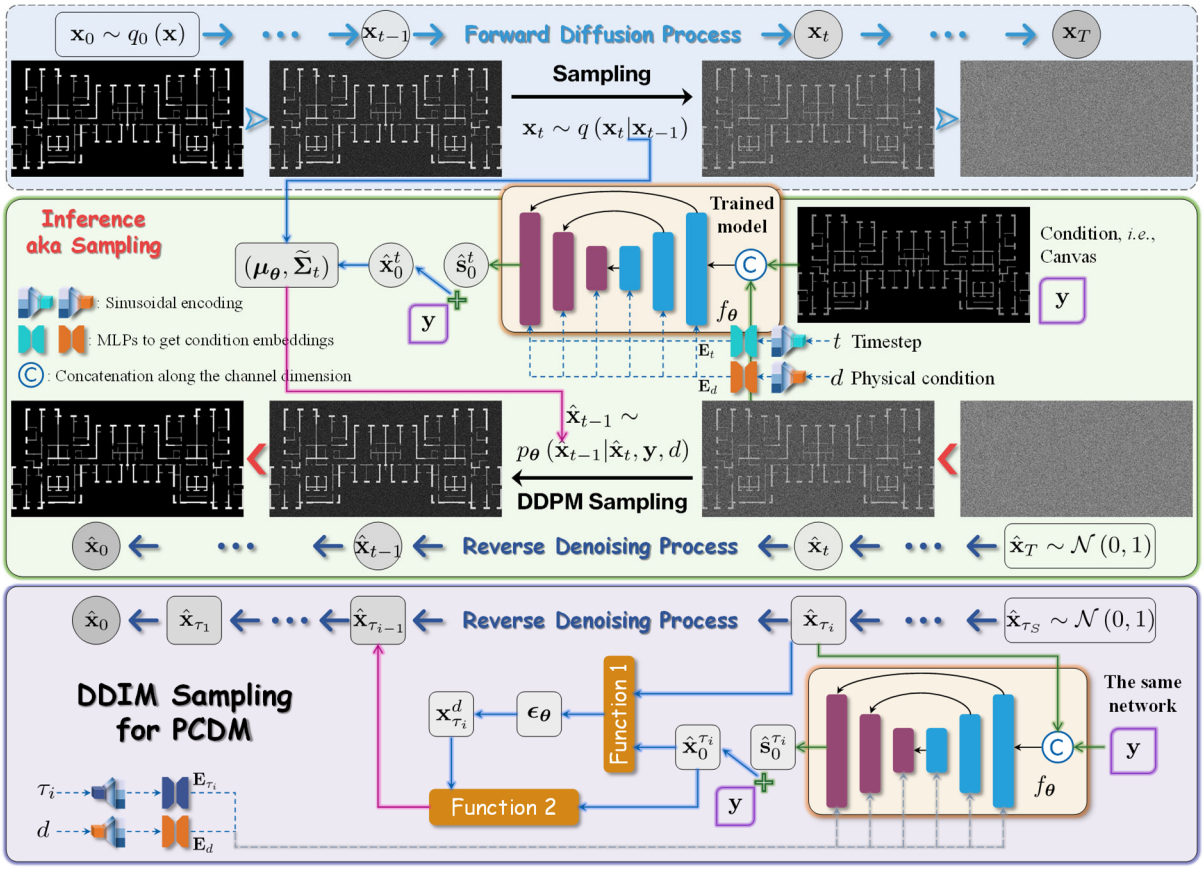

Fig. 1. Schematic diagram of the forward diffusion process and the reverse denoising processes.

3 EXPERIMENTS

3.1 Details of implementation

Dataset. The dataset used in this study is Modified-dataset proposed in [1] and can be publicly available at https://github.com/hzlbbfrog/Generative-BIM. This dataset consists of 700 training images and 24 images in the test set.

Inference environment. The hardware and software environments are the same with [1]. For example, the GPU is a Nvidia GeForce RTX 4090, and the version of PyTorch is 1.12.1.

Evaluation metrics. The Fréchet Inception Distance (FID) is adopted to evaluate the quality of the generated images following [1]. FID is consistent with human perception and is capable of quantitatively evaluating the visual quality of the generated samples.

3.2 Comparison of the generation results of PCDM and DDIM sampling for PCDM

Extensive experiments are conducted in this subsection to evaluate the effectiveness of DDIM sampling for PCDM, which stands as the central contribution of this study. Specifically, we employ the well-trained model in [1] and execute the reverse denoising process using both the original sampling method in PCDM (i.e., DDPM sampling) and DDIM sampling for PCDM outlined in Subsection 2.3. Additionally, to explore the generation efficiency, we consider four different lengths of sub-sequences in DDIM sampling: $S = 10$, $S = 20$, $S = 50$, and $S = 100$. Correspondingly, the generation speeds are approximately accelerated by 100×, 50×, 20×, and 10×, respectively (recall that the sequence length of PCDM is 1000). The FID

results, presented in Table 4, indicate that the FID values are remarkably close, with no discernible differences. Furthermore, the qualitative comparison results between the original PCDM and the proposed DDIM sampling for PCDM are depicted in Fig. 2. Evidently, the perceptual quality and details of the generated outputs are strikingly similar, making it arduous to distinguish which method is superior. The qualitative comparison aligns with the quantitative findings, leading us to draw the conclusion that DDIM sampling for PCDM can accelerate the reverse sampling process of the original PCDM by up to 100 times while maintaining the same level of visual quality. This shows the proposed DDIM sampling for PCDM is a practical solution to expedite intelligent structural design.

Table 4. Quantitative evaluation of the results obtained from different lengths of sampling sequences.

Length of sequence	10	20	50	100	1000 (i.e., PCDM)
FID ↓	15.03	14.22	14.90	14.39	14.94

Notes: (1) ↓ means for FID, the lower the value, the better. (2) Unlike [1], FIDs here are measured on the entire test set, namely, the combination of the three sub-datasets.

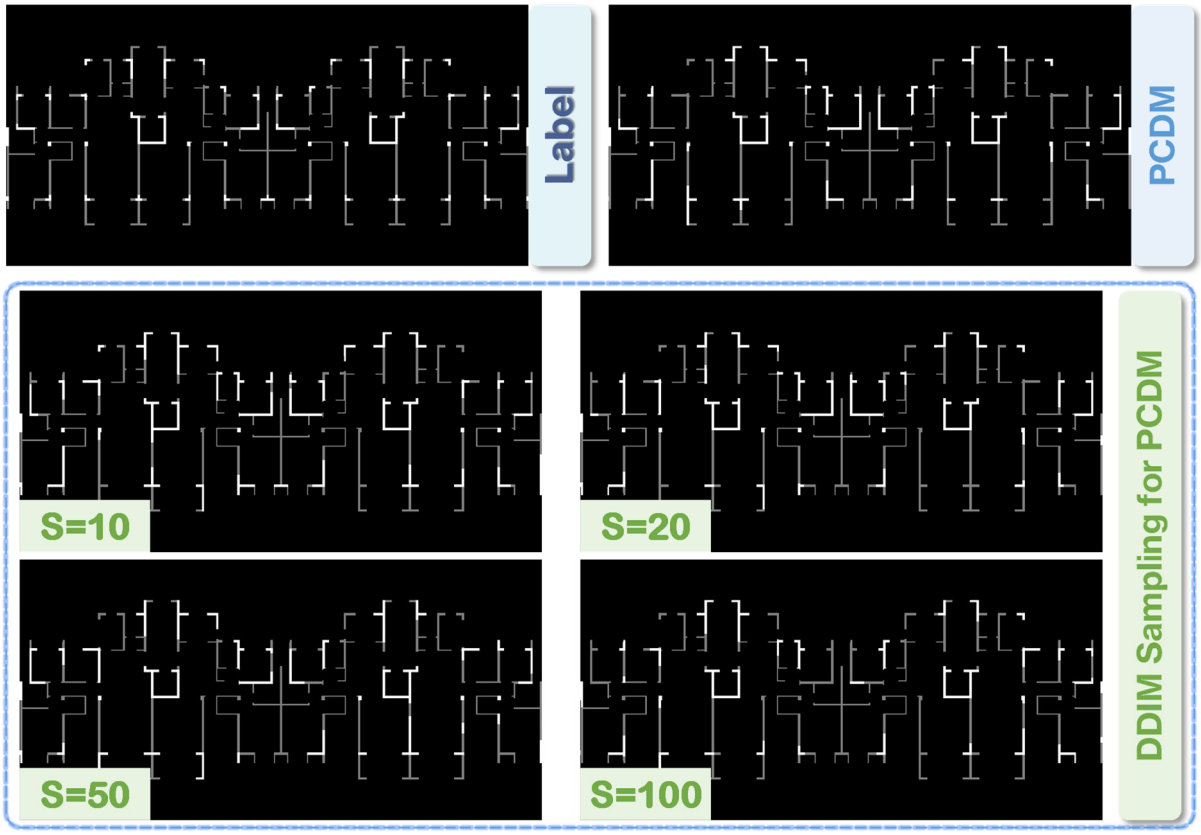

Fig. 2. Comparison of visualization results of labeling and the ones obtained from the original sampling method in PCDM and the proposed DDIM sampling for PCDM.

4 CONCLUSION

Generative AIBIM is a successful and intelligent framework for structural design, with its core module being PCDM, a novel physics-based conditional diffusion model capable of

generating high-quality shear wall designs that meet diverse physical conditions. However, PCDM needs 1000 iterations to generate each high-quality sample, hindered by the nature of the adopted DDPM sampling method, which is so time-consuming and requires substantial computing resources. To address this limitation, this study introduces DDIM into the Generative AIBIM framework to expedite the generation process. The key innovations of this research are as follows: First, this paper reorganizes the content of the original DDIM paper, emphasizing its practical usage and making it more accessible to researchers who may not possess an extensive background in machine learning. This change is particularly valuable for those who are primarily interested in utilizing the tool rather than delving into its theoretical intricacies. Second, this study presents DDIM sampling for PCDM, which is a modification of the original DDIM to suit its integration into PCDM. This adaptation is necessary as the original DDIM cannot be directly embedded into PCDM. Third, extensive experiments are conducted to validate the effectiveness of DDIM sampling for PCDM. The experimental results demonstrate that DDIM sampling for PCDM can accelerate the sampling process of PCDM by 100× while maintaining the same level of visual quality in the generated outputs. Overall, this study offers a successful implementation of DDIM within the Generative AIBIM pipeline and provides compelling evidence for the efficiency of DDIM sampling for PCDM in accelerating intelligent structural design.

REFERENCES

[1]. Z. He, Y.-H. Wang, J. Zhang, Generative structural design integrating BIM and diffusion model, arXiv: 2311.04052v1, https://arxiv.org/abs/2311.04052, 2023.

[2]. W. Liao, X. Lu, Y. Huang, Z. Zheng, Y. Lin, Automated structural design of shear wall residential buildings using generative adversarial networks, Automation in Construction. 132 (2021), 103931, https://doi.org/10.1016/j.autcon.2021.103931.

[3]. P. Zhao, W. Liao, Y. Huang, X. Lu, Intelligent design of shear wall layout based on graph neural networks, Advanced Engineering Informatics. 55 (2023), 101886, https://doi.org/10.1016/j.aei.2023.101886.

[4]. X. Lu, W. Liao, Y. Zhang, Y. Huang, Intelligent structural design of shear wall residence using physics-enhanced generative adversarial networks, Earthquake Engineering & Structural Dynamics, 51 (2022), pp. 1657-1676, https://doi.org/10.1002/eqe.3632.

[5]. Z. He, S. Jiang, J. Zhang, G. Wu, Automatic damage detection using anchor-free method and unmanned surface vessel, Automation in Construction. 133 (2022), 104017, https://doi.org/10.1016/j.autcon.2021.104017.

[6]. J.K. Chow, Z. Su, J. Wu, P.S. Tan, X. Mao, Y.-H. Wang, Anomaly detection of defects on concrete structures with the convolutional autoencoder, Advanced Engineering Informatics. 45 (2020), 101105, https://doi.org/10.1016/j.aei.2020.101105.

[7]. J.K. Chow, K.-f. Liu, P.S. Tan, Z. Su, J. Wu, Z. Li, Y.-H. Wang, Automated defect inspection of concrete structures, Automation in Construction. 132 (2021), 103959, https://doi.org/10.1016/j.autcon.2021.103959.

[8]. W. Chen, Z. He, J. Zhang, Online monitoring of crack dynamic development using attention-based deep networks, Automation in Construction. 154 (2023), 105022, https://doi.org/10.1016/j.autcon.2023.105022.

[9]. P.N. Pizarro, L.M. Massone, F.R. Rojas, R.O. Ruiz, Use of convolutional networks in the

conceptual structural design of shear wall buildings layout, Engineering Structures. 239 (2021), 112311, https://doi.org/10.1016/j.engstruct.2021.112311.

[10]. P.N. Pizarro, L.M. Massone, Structural design of reinforced concrete buildings based on deep neural networks, Engineering Structures. 241 (2021), 112377, https://doi.org/10.1016/j.engstruct.2021.112377.

[11]. P. Zhao, Y. Fei, Y. Huang, Y. Feng, W. Liao, X. Lu, Design-condition-informed shear wall layout design based on graph neural networks, Advanced Engineering Informatics. 58 (2023), 102190, https://doi.org/10.1016/j.aei.2023.102190.

[12]. J. Whang, M. Delbracio, H. Talebi, C. Saharia, A. G. Dimakis, P. Milanfar, Deblurring via stochastic refinement, in: 2022 IEEE/CVF Conference on Computer Vision and Pattern Recognition (CVPR), IEEE, New Orleans, LA, USA, 2022, pp. 16272-16282, https://doi.org/10.1109/CVPR52688.2022.01581.

[13]. C. Saharia, J. Ho, W. Chan, T. Salimans, D.J. Fleet, M. Norouzi, Image super-resolution via iterative refinement, IEEE Transactions on Pattern Analysis and Machine Intelligence. 45 (4) (2023), pp. 4713-4726, https://doi.org/10.1109/TPAMI.2022.3204461.

[14]. F. Ni, Z. He, S. Jiang, W. Wang, J. Zhang, A Generative adversarial learning strategy for enhanced lightweight crack delineation networks, Advanced Engineering Informatics, 52 (2022), 101575, https://doi.org/10.1016/j.aei.2022.101575.

[15]. J. Sohl-Dickstein, E. Weiss, N. Maheswaranathan, S. Ganguli, Deep unsupervised learning using nonequilibrium thermodynamics, in: 32nd International Conference on Machine Learning (ICML), PMLR, Lille, France, 2015, pp. 2256-2265, https://proceedings.mlr.press/v37/sohl-dickstein15.html.

[16]. J. Ho, A. Jain, P. Abbeel, Denoising diffusion probabilistic models, in: 34th International Conference on Neural Information Processing Systems (NeurIPS), ACM, Vancouver, BC, Canada, 2020, pp. 6840-6851, https://dl.acm.org/doi/abs/10.5555/3495724.3496298.

[17]. P. Zhao, W. Liao, Y. Huang, X. Lu, Intelligent design of shear wall layout based on attention-enhanced generative adversarial network, Engineering Structures. 274 (2023), 115170, https://doi.org/10.1016/j.engstruct.2022.115170.

[18]. L. Metz, B. Poole, D. Pfau, J. Sohl-Dickstein, Unrolled Generative Adversarial Networks, in: 2017 International Conference on Learning Representations (ICLR), Toulon, France, 2017, pp.1-25, https://openreview.net/forum?id=BydrOIcle.

[19]. A. Srivastava, L. Valkov, C. Russell, M.U. Gutmann, C. Sutton, VEEGAN: Reducing mode collapse in GANs using implicit variational learning, in: 2017 International Conference on Neural Information Processing Systems (NIPS), ACM, Long Beach, CA, USA, 2017, pp. 3310-3320, https://dl.acm.org/doi/10.5555/3294996.3295090.

[20]. Y. Wang, J. Yu, J. Zhang, Zero-shot image restoration using denoising diffusion null-space model, in: 2023 International Conference on Learning Representations (ICLR), Kigali Rwanda, 2023, pp. 1-31, https://openreview.net/forum?id=mRieQgMtNTQ.

[21]. J. Song, C. Meng, S. Ermon, Denoising diffusion implicit models, arXiv: 2010.02502v4, https://arxiv.org/abs/2010.02502, 2022 (accessed 20 May 2023).

[22]. Z. He, W. Chen, J. Zhang, Y.-H. Wang, Crack segmentation on steel structures using boundary guidance model, Automation in Construction. 162 (2024), 105354, https://doi.org/10.1016/j.autcon.2024.105354.

Proceeding of the 10th International Conference on Innovative Production and Construction (IPC 2024), Perth, Australia, July 11-12, 2024

Exploring the Influence Mechanism of Inclusiveness in Transportation Infrastructure System

Jinchan Liu, Chuan Chen, Wenting Zhan, Yubo Guo

Business School, Sichuan University, Chengdu, China

ABSTRACT: Transportation infrastructure system (TIS) play a pivotal role in shaping the socio-economic landscape of regions and nations. However, ensuring the inclusiveness within the TIS remains a critical challenge. This paper aims to explore the influence mechanism of inclusiveness of the TIS, elucidating its significance in fostering equitable development and social cohesion.

Drawing on the triple-bottom-line theory and characteristics of the TIS, this paper explores five distinct influencing areas, i.e., spatial, economic, social, environmental and institutional, regarding inclusiveness of the TIS. In line with systems thinking, the interrelationships among the influencing areas are explored. The empirical research was conducted through a questionnaire survey with 279 participants in China. Then, a confirmatory analysis was conducted to validate the interrelationships through structural equation modeling (SEM).

By unraveling the influence mechanism of inclusiveness in the TIS, this paper contributes to a deeper understanding of the complex interplay between infrastructure development, social equity, and sustainable urbanization. It offers valuable insights for policymakers, planners, transportation professionals, and community stakeholders to formulate strategies and interventions aimed at fostering inclusive transportation system that cater to the diverse needs of society while advancing the goals of equity and sustainability.

KEYWORD: inclusiveness; influence mechanism; transportation infrastructure system

Proceeding of the 10th International Conference on Innovative Production and Construction (IPC 2024), Perth, Australia, July 11-12, 2024

Drivers and Barriers for Digital Twin Application in Water Infrastructure: A Text Mining Approach

Yubo Guo[1], Xiaowei Luo[1], Jinchan Liu[2], Chuan Chen[2]

1. City University of Hong Kong
2. Sichuan University

ABSTRACT: Digital Twin (DT) has been gradually adopted in various industries, ranging from manufacturing to infrastructure. In the water industry, there is a tremendous need to apply DT to enhance the efficiency of constructing and operating water infrastructure, considering the significant benefits it offers. However, there is limited focus on the driving forces of DT in water infrastructure, and a knowledge gap remains regarding the barriers hindering its application. This study aims to address the research problem of identifying the factors that drive or hinder the adoption of DT in water infrastructure. To investigate these factors, a text mining approach was employed. Data was collected from two sources: academic publications and posts/comments related to DT applications on Zhihu, the largest Chinese question and answer (Q&A) social media platform dedicated to discussing professional knowledge. Initially, drivers and barriers were extracted from academic literature. Subsequently, sentiment analysis based on SnowNLP and the Latent Dirichlet Allocation (LDA) model was conducted to extract drivers and barriers from the opinions of practitioners expressed in Zhihu posts and comments. Finally, the Decision-making Trial and Evaluation Laboratory (DEMATEL) method was applied to evaluate the importance of these factors and identify critical drivers and barriers for DT application in water infrastructure. Through a comprehensive literature review and text mining, this research identified thirty-eight drivers and thirty barriers. This list was further refined to eleven critical drivers and eight barriers. The value of this study is in showcasing which of the multitude drivers and barriers should be prioritized in moving DT development of water infrastructure forward.

KEYWORD: drivers and barriers for digital twin application in water infrastructure: a text mining approach

Proceeding of the 10th International Conference on Innovative Production and Construction (IPC 2024), Perth, Australia, July 11-12, 2024

Developing an Accident-Enabled Virtual Reality Training System: A Digital Coach for Tower Crane Operators

Junyu Chen, Hung-Lin Chi, Haicheng Li,

Department of Building and Real Estate, The Hong Kong Polytechnic University, Hung Hom, Kowloon, Hong Kong SAR

ABSTRACT: Tower crane operation is the lifeline for controlling safety hazards and pursuing productivity gains in prefabricated construction. Despite the implementation of strict safety requirements and innovative technology advancements, catastrophic accidents attributed to human errors by tower crane operators have continued to be reported. As one primary accident prevention strategy, existing virtual reality (VR)-based safety training still fails to impart experienced tower crane operators' on-site safety and productivity concerns to novices. This study examined the potential of an accident-enabled VR training system for enhancing tower crane operation performance by bridging the gap between safety knowledge provided in existing VR-based safety training and safety implications emphasized by accident analysis efforts. The training system was built by embedding synthesized safety knowledge into a virtual construction site as the initial step: information from an authentic building project determining safety and productivity requirements for tower crane lifts was utilized to model the virtual training environment, whereas on-site safety constraints identified in association with potential crane failure modes based on previous accident investigations were extracted as training elements. Then, a roguelike-style role-playing game (RPG) design was adopted to replicate real-world accident causation by linking trainees' safety violations to specific accident consequences in the virtual environment, requiring them to restart the operational task until they identified hazards and took countermeasures to go through within a single attempt. For comparison, a conventional training mode was designed to provide trainees unlimited access to perform the training task with stepwise safety guidance, but without demonstrating accident consequences or requiring a start-over. The safety knowledge acquisition and operation skill development of trainees who had experienced different training modes were evaluated through a before-after experiment. Training feedback was gathered through a post-test questionnaire survey to identify the potential factors influencing trainees' experience concerning their perceptions of the VR training environment and cognitive loads for completing the training task. The findings reveal that the proposed accident-enabled VR training system reduced safety violations and improved the operation productivity of trainees, indicating that it can be utilized as a digital coach to help develop trainees' competence for navigating safety hazards and productivity pressure during real-world construction situations.

KEYWORD: digital coach; tower crane operator training; virtual reality; crane safety; accident analysis

Proceeding of the 10th International Conference on Innovative Production and Construction (IPC 2024), Perth, Australia, July 11-12, 2024

Enhancing Deep Reinforcement Learning with Neuro-evolution for Adaptive Mining Fleet Management

Xiaolei Xiang[1], Xiangyu Wang[2], Danqi Li[1], Quanxi Shao[3]

1. Curtin University
2. East China Jiao Tong University
3. CSIRO

ABSTRACT: Efficient fleet management is crucial for the productivity and profitability of open-pit mining operations. However, the complex and dynamic nature of mining environments presents significant challenges to traditional optimization methods. This paper explores the integration of neuro-evolution and deep reinforcement learning (DRL) techniques to address these challenges and develop adaptive optimization strategies for mine fleet management. We propose a novel approach that leverages neuro-evolution to optimize the architecture of deep neural networks in the DRL algorithm, enabling the automatic discovery of efficient network structures tailored to specific mining scenarios. The proposed framework is evaluated in a simulated open pit mine environment, and its performance is compared with conventional DRL algorithms and traditional dispatching heuristics. The findings highlight the potential benefits of combining neuro-evolution and DRL for developing more efficient and adaptive fleet management strategies in real-world mining operations. This research contributes to the growing body of work on the application of advanced AI techniques in the mining industry.

KEYWORD: artificial intellgence, deep reinforcement learning, neuro-evolution network, fleet management

Proceeding of the 10th International Conference on Innovative Production and Construction (IPC 2024), Perth, Australia, July 11-12, 2024

Dynamic Knowledge Graph-based Accident Causal Analysis and Warning: A Case Study of Bridge Foundation Construction

Juntong Zhang, Han Si, Xin Ruan

Department of Bridge Engineering, College of Civil Engineering, Tongji University, Shanghai, China

ABSTRACT: With the advancement of society, production systems have grown increasingly large and complex, accompanied by frequent occurrences of production accidents. To spare lives and properties from loss, it is crucial to conduct causal analysis and early warning for these accidents. Existing methods, however, were limited to single-dimensional network modeling and static analysis, struggling to address the complexity and variability of systems. In this study, we innovatively propose a dynamic knowledge graph-based approach for system hazard analysis and accident early warning. It is capable of representing the correlation between risks using heterogeneous graphs and modeling the potential accident paths in the system. Importantly, this method introduces the concept of label entities on top of general knowledge graphs, where event entities are attached to their corresponding labels. It efficiently calculates and reconstructs the topological structure according to spatial-temporal changes of the scenario, enabling the transition from static to dynamic in hazard analysis. Furthermore, a series of graph analysis metrics are proposed to evaluate the risk status of the system and to facilitate proactive warning and control strategies. Finally, the practicality and effectiveness of the proposed method are validated through a bridge foundation construction scenario.

KEYWORD: accident causal analysis; accident warning; dynamic knowledge graph; bridge construction

Proceeding of the 10th International Conference on Innovative Production and Construction (IPC 2024), Perth, Australia, July 11-12, 2024

Augumenting Construction Progress Tracking and Digital Information Modeling Utilizing Computer Vision and BIM

Wei Wei

Tongji University

ABSTRACT: Regular construction progress monitoring plays a pivotal role in effective project management. Despite the efficient application of non-invasive methods like computer vision in progress monitoring, existing challenges have limited progress recognition accuracy, such as partial feature occlusion. While BIM offers an integrated information platform that enhances project management efficiency, it is less commonly used in construction management compared to the design phase. To enable precise and efficient progress management, we have concentrated on automating progress tracking and information modeling across various complex construction scenarios, such as soil-foundation construction, structural construction, indoor construction, as well as mechanical and electrical installations. We aimed to precisely recognize construction elements leveraging advanced computer vision technology, taking into account the typical features and challenges inherent in complex construction scenarios. Furthermore, we have achieved progress information modeling in BIM utilizing the mechanisms of three-dimensional spatial mapping. This study not only promotes unmanned supervision but also offers a viable approach to digital twins in construction.

KEYWORD: BIM; computer vision; construction progress; deep learning

Proceeding of the 10th International Conference on Innovative Production and Construction (IPC 2024), Perth, Australia, July 11-12, 2024

The Unification of Design Calculation and Drawing of Foundation Pit Retaining Structure: One Model Multi-purpose Method

Qiwei Wan, YiQing Yang, Changjie Xu*, Xiangyu Wang, Wentao Hu, Zimo Li

East China Jiaotong University, China

ABSTRACT: As BIM (Building Information Modeling) integration gains momentum in underground engineering, the need for harmonizing BIM models with physical models is crucial, yet no mature standards currently exist to address the discrepancies between geometric and physical requirements across various domains. This study advances the IFC 4.3 standard to facilitate the integration of mechanical analysis and design drafting, introducing an innovative integrated design framework for braced pit support structures centered on deformation control. By extending IfcBracedPit and related structural objects, the research establishes a novel link between IFC and mechanical models alongside an optimization model for deformation-controlled mechanical design. It introduces drafting rules, especially key technologies for automatic reinforcement detailing. Demonstrated through a subway station construction in Hangzhou, Zhejiang, China, the proposed framework markedly outperforms existing tools in automation for deformation control design and reinforcement detailing. This contribution is pivotal for increasing the automation in pit design and holds potential for broad application in similar design domains to enhance efficiency and reduce workload.

KEYWORD: BIM (Building Information Modeling); IFC 4.3 standard; integrated design framework; deformation control; automation in design

Proceeding of the 10th International Conference on Innovative Production and Construction (IPC 2024), Perth, Australia, July 11-12, 2024

Performance Evaluation of In-Service Bridge Expansion Joints Using Transformer-Based Deep Learning Approaches

Dalei Wang, Yiqing Dong, Yue Pan

College of Civil Engineering, Tongji University

ABSTRACT: Bridge expansion joints (BEJs) are crucial structural components facilitating the accommodation of thermal movements and various loads. However, they are susceptible to deterioration and damage from factors such as fatigue, corrosion, impact, and environmental conditions, resulting in wear and structural damage. Over the past few decades, numerous approaches have been proposed for BEJ damage evaluation. This study introduces two methods leveraging Transformer-based deep learning models for BEJ status assessment. Firstly, a traffic load simulation model presented for high-fidelity modeling of traffic load on the bridge deck. Subsequently, through transient dynamic analysis of the bridge finite element model, wear damage of BEJs can be accurately evaluated. Secondly, a cascading voiceprint recognition method is developed for detecting structural damage in in-service BEJs. Vehicle impact sounds serve as input features, and our trained model demonstrates satisfactory performance in identifying BEJ faults. These methodologies offer valuable insights into intelligent inspection and monitoring of BEJs and other bridge components.

KETWORDS: bridge expansion joints; performance evaluation; fault detection; deep learning; transformer module

Proceeding of the 10th International Conference on Innovative Production and Construction (IPC 2024), Perth, Australia, July 11-12, 2024

Predictive Modelling of Road Deterioration Using Bayesian Belief Networks

Babitha Philip, Hamad AlJassmi

Emirates Center for Mobility Research, UAE University

ABSTRACT: The ability to predict road deterioration is the cornerstone for developing a reliable Pavement Management System (PMS) that optimizes pavement maintenance programs on the lights of main road distress parameters, such as cracking, rutting, deflection and International Roughness Index (IRI). The prediction of these inter-related parameters becomes increasingly important, especially when highway agency funds are confined. This paper presents the development of time-series Dynamic Bayesian Beleif Network models for road deterioration using big data from UAE for a collection of 3,272 road sections, representing a variety of 32 arterial, collector, freeway, and expressway roads in from 2013 to 2019.

KEYWORD: road distress parameters, uncertainty, Bayesian belief network, decision-making, pavement management system

Proceeding of the 10th International Conference on Innovative Production and Construction (IPC 2024), Perth, Australia, July 11-12, 2024

Fresh and Hardended Proporties of 3D-printed Mortar Containing Coral Sand

Di Wang

School of Civil Engineering and Architecture, East China Jiaotong University; School of Civil Engineering, Chongqing University

ABSTRACT: The island is far from the land, facing the extremely high cost of transporting construction materials. Besides, poor island living conditions lead to a shortage of construction workers. The 3D printing concrete technology provides a feasible method for island construction. This paper utilizes coral sand in the printing ink and analyses the fresh and hardened properties. Four mix proportions were designed with variable supplemental cementitious materials to improve the fresh and hardened properties. Besides, the interlocking structure between layers was also employed to further improve the weak surface bonding between layers. The effect of mix proportions, interlayer structure, and anisotropy was analyzed by the buildability, compressive strength, flexural tensile strength, and shear strength. Meanwhile, the digital image correlation (DIC) was employed to depict the strain and crack development process. The anisotropic mechanical strength reached the highest values when the content of silica fume and fly ash was 10% and 15% in the interlocking structure A. Fibres are more likely to agglomerate in the Y direction first attributed to the fibre orientation in 3D printing process and excessive fibre incorporation.

KEYWORD: 3D printing; coral sand; anisotropy; DIC; interlocking structure

Proceeding of the 10th International Conference on Innovative Production and Construction (IPC 2024), Perth, Australia, July 11-12, 2024

Graph-Based Multi-Action HVAC Control: A Hierarchical Reinforcement Learning Strategy

Yilong Jia, Jun Wang, Wenchi Shou

Deakin University, Western Sydney University, Australia

ABSTRACT: Efficient control of Heating, Ventilation, and Air Conditioning (HVAC) systems across multiple zones in buildings remains a significant challenge, particularly when addressing the complex task of simultaneously optimizing multiple control actions such as temperature and airflow. This paper introduces a novel approach that leverages Hierarchical Reinforcement Learning (HRL) combined with Graph Neural Networks (GNNs) to manage these multifaceted control requirements. Our method models the multi-zone system as a graph, where nodes represent individual zones and edges capture the interactions between them, allowing for the nuanced understanding of spatial dependencies necessary for effective multi-action control. GNNs are employed to process this graph structure, facilitating informed decision-making that accounts for the intricate dynamics of multi-zone environments. The HRL framework allows for task decomposition, enabling the concurrent optimization of diverse local control strategies within zones and the alignment with global system objectives. We present a two-level HRL architecture where the high-level policy orchestrates the selection and coordination of zone-specific sub-policies, each optimized for a distinct set of control actions, underpinned by GNN-derived insights. This multi-action control capability represents a significant advancement over traditional single-action HVAC control methods, offering improvements in both energy efficiency and thermal comfort.

KEYWORD: HVAC control, graph neural networks, reinforcement learning

Optimizing Mechanical Performance of 3D Printed Concrete with Interlayer Glass Fiber Mesh and Structural Adhesive Enhancement

Xinglong Xu, Zuxiang Lei*

School of Civil Engineering and Architecture, East China Jiaotong University, Nanchang, Jiangxi 330013, China

ABSTACT: Extrusion-based 3D printing of concrete entails a layered manufacturing process, resulting in weak interfaces between layers, thus significantly compromising the mechanical performance. To enhance the mechanical properties between layers, this study explores four methods of interface reinforcement (laying glass fiber mesh between each layer or every two layers of concrete, adding structural adhesive per layer, and a hybrid approach) to improve the mechanical performance and microstructure of concrete. The preparation of cement-based composite materials was optimized based on the comparison of 7-day mechanical strengths from six mixing ratios. XRD/SEM image analysis techniques were employed to analyze interface porosity structures and microstructural effects under different methods. Experimental results indicate that adding structural adhesive increases compressive and diagonal shear strength, while incorporating glass fiber mesh enhances flexural strength, with the hybrid approach showing the best performance. Concrete with added structural adhesive exhibits the highest increase in compressive strength by 33.3 % to 55.83 MPa and 24.0 % in diagonal shear strength, while flexural strength decreases by 27.3 %. Incorporating glass fibre mesh in each layer during the printing process increases the flexural strength by a maximum of 96.6 %. Microstructural analysis reveals enhanced interface adhesion with structural adhesive addition, while the addition of glass fiber mesh introduces numerous microcracks at the interface.

KEYWORD: 3D printed concrete; interface; microscopic properties; mechanical property

Proceeding of the 10th International Conference on Innovative Production and Construction (IPC 2024), Perth, Australia, July 11-12, 2024

Research on the Crater of Explosion in Calcareous Sand Foundation

Changchun Li[1,2], Xiangyu Wang[1], Yumin Chen[2], Yongze Song[1], Yufei Wang[1]

1. Curtin University
2. Hohai University

ABSTRACT: The problem of explosion in calcareous sand foundations is a research focus in the field of geotechnical engineering. The method of combining field tests and numerical simulation of Smooth Particle Hydrodynamic (SPH)- Finite Element (FE) coupling in the LS-DYNA software were used to research the type and size of the crater in calcareous sand foundation. The results indicate that when the scaled burial depth is less than 1.11 m/kg1/3, the crater is ejecta-type; when the scaled burial depth is in the range of 1.11~2.05 m/kg1/3, the crater is collapse-type crater; when the scaled burial depth is greater than 2.05 m/kg1/3, a concealed explosion phenomenon occurred. At the same scaled burial depth, the size of the crater in calcareous sand is larger than that of silica sand. An empirical prediction formula for the crater of the calcareous sand foundation was derived from the results of field tests and numerical simulations, which can provide theoretical reference for the explosion resistance design of calcareous sand foundations.

KEYWORD: crater; field test; SPH-FE; calcareous sand; explosion

Proceeding of the 10th International Conference on Innovative Production and Construction (IPC 2024), Perth, Australia, July 11-12, 2024

Enhancing Construction Efficiency through Automated Crane Cameras: A Novel Approach to Monitoring Concrete Pouring Process

Songbo Hu, Jun Wang, Yihai Fang

Western Sydney University

ABSTRACT: This paper presents a novel strategy that leverages a knowledge graph to augment Computer Vision (CV) capabilities in the context of monitoring concrete pouring processes using crane cameras. Traditional CV methods often struggle with obscured views and the complexity inherent in dynamic construction environments. Our proposed knowledge graph-enhanced CV approach introduces a relational understanding of the items involved, specifically tower cranes, workers, and material delivery systems, to better interpret complex activities that are harder to decode. By synthesising contextual information with object recognition, this method not only overcomes the limitations posed by incomplete data but also adapts to diverse behavioural patterns of cranes in real-time. Preliminary evaluations of this system in a live construction setting have shown its effectiveness in providing detailed insights into the progress of concrete pouring tasks, thereby enhancing operational safety and efficiency. The integration of a knowledge graph into CV reasoning marks a significant advance in the automated monitoring of construction activities, promising substantial improvements in both the accuracy and utility of observational data in complex environments. Furthermore, the adaptation of this strategy to include multi-modal data interpretation, such as crane movement, extends its application to a broader array of construction scenarios, thereby increasing its practical utility.

KEYWORD: knowledge graph, crane activity, construction efficiency, computer vision (CV)

Proceeding of the 10th International Conference on Innovative Production and Construction (IPC 2024), Perth, Australia, July 11-12, 2024

Research Hotspots and Trends in Smart City Construction in China: A Systematic Literature Review

Ziduan Zheng[1,2], Dora Marinova[1], Yuan Gao[2], Yongze Song[1]

1. Curtin University
2. ZhengZhou University

ABSTRACT: The smart city is undoubtedly a new concept and model that deeply integrates the new generation of information and communication technology with urban economic and social development to promote smart urban planning, construction, management, and services. This new model is now receiving great attention from the academic community. This study uses bibliometric methods and conducts a visual analysis of 760 CSSCI, SCI, EI, core journals, and CSCD source journal documents in the China National Knowledge Infrastructure Database (CNKI) based on the cite space research tool. To provide theoretical reference and practical significance for the development of smart cities.

KEYWORD: smart city construction；bibliometrics；systematic；china；visualization

Proceeding of the 10th International Conference on Innovative Production and Construction (IPC 2024), Perth, Australia, July 11-12, 2024

Research on The Mechanical and Electrical Conductivity Anisotropy of Electrically Conductive Cementitious Composite

Weichen Tang[1], Junbo Sun[2,3*], Yufei Wang[4], Zhaohui Chen[1,4]

1. School of Civil Engineering, Chongqing University, Chongqing, 400045, China
2. Institute for Smart City of Chongqing University in Liyang, Chongqing University, Jiangsu, 213300, China
3. School of Civil Engineering and Architecture, East China Jiao Tong University, Nanchang, 330013, China.
4. School of Design and Built Environment, Curtin University, Perth, WA 6102, Australia

ABSTRACT: Electrically conductive cementitious composites (ECCC) possess promising applications in roadway de-icing, radiant building heating, and structural health monitoring. However, conventional cast ECCC displayed finite fiber dispersion and orientation. 3D printing technology extrudes materials from the nozzle and builds up the shape layer-by-layer, effectively enhancing the conductive filler orientation phenomenon. Meanwhile, the directional printing process aligns the fillers differently in each direction which causes anisotropy in performance. In this paper, the anisotropy of mechanical properties and electrical conductivity in 3D-printed steel fiber-copper slag ECCC is investigated. Piezoelectric zirconium titanate (PZT) sensors were employed to gauge the 7-28day RMSD values revealing the mechanical strength development of 3D printed samples. The compressive and flexural strengths of the printed ECCC samples were enhanced by 20.15% and 72.72%, respectively. In addition, the conductive anisotropy experiment was also conducted through the four-pole methodology. In total, 270 ECCC samples of 10 types of mix ratios were prepared for mechanical tests and electrical resistance experiments. The C40F3 group exhibited comprehensive optimal results with compressive strength of 65.69MPa, flexural strength of 11.98MPa, and electrical resistance of 13.389 kΩ·cm. Lastly, the digital image correlation (DIC) method and scanning electron microscopy (SEM) were applied to evaluate the microphenomenon of fiber orientation.

KEYWORD: 3D printing technology; mechanical anisotropy; electrical conductivity anisotropy; electrically conductive cementitious composite.

Proceeding of the 10th International Conference on Innovative Production and Construction (IPC 2024), Perth, Australia, July 11-12, 2024

Using Vision and AI Techniques for Digital Twins Applications in Civil Engineering

Jun Li

Curtin University

ABSTRACT: This talk presents developing and using vision and AI techniques for digital twins applications in civil engineering structures. Vision and AI techniques are used to measure phsical displacements and create point clouds of structures. AI techniques are applied to improve the 3D displacement measurement and recontruction of depth information in point clouds more accurately.

KEYWORD: vision; deep learning; digital twin

Proceeding of the 10th International Conference on Innovative Production and Construction (IPC 2024), Perth, Australia, July 11-12, 2024

Intelligent Monitoring of The Long-Span Cable System Bridge Based on Machine Vision

Hao Zhu

CCCC Second Harbor Engineering Company Ltd.

ABSTRACT: This study focuses on cable shape dynamic monitoring、cable tension efficient measurement and vehicle load spatio-temporal distribution, by Integrating artificial intelligence and machine vision algorithms, the intelligent monitoring technology in long-span cable system bridge was innovated. A method of cable shape real-time dynamic monitoring based on machine vision was proposed, developed measurement equipment, realized dynamic measurement error within 3mm under strong wind conditions; A method of cable tension efficient measurement based on mobile phone video was proposed, a cable tension estimation APP was developed, compared with the cable force dynamic measuring instrument, the measurement efficiency is increased by 5 times; A visual recognition method of vehicle load spatio-temporal distribution in long-span bridge was presented, created a model of cross-view vehicle tracking based on information matching , the method was accurate about 91.23%。The above innovative technologies have been successfully applied to major bridge engineering projects such as the Lingdingyang Bridge, the Xianxin Road Yangtze River Crossing, and the Baijusi Yangtze River Bridge, significantly improved the intelligent monitoring level of the long-span cable system bridge.

KEYWORD: long-span cable system bridge; cable shape dynamic monitoring; cable tension efficient measurement; vehicle load spatio-temporal distribution; machine vision

Solar Energy Applications in Buildings and Urban Environment

Chengyang Liu, Rebecca Yang

RMIT University

ABSTRACT: This presentation will focus on applied research to enable the integration of solar energy in buildings and suburban. The presentation will cover three main research domains in the lab: (1) Building Integrated PV (BIPV): including the digitalisation process, safety, standardization, and the collaborative work in the International Energy Agency Photovoltaic Power Systems Programme, (2) Solar enabled community/industry decarbonization, by empowering them to generate their own energy and reduce their dependence on centralized power plants and distribution networks. This can lead to a more sustainable, resilient, and decentralized energy system that benefits both the environment and the local economy; and (3) Solar energy in urban scale, including the development of advanced modelling, simulation, and optimization tools to analyse the technical feasibility and economic viability of solar energy systems in urban areas.

KEYWORD: solar energy, building, urban

Proceeding of the 10th International Conference on Innovative Production and Construction (IPC 2024), Perth, Australia, July 11-12, 2024

Resource Optimisation in Construction Projects: Exploring Synergies between Artificial Intelligence and Building Information Modelling

Ali Alashwal

Western Sydney University

ABSTRACT: This research aims to explore the integration of Artificial Intelligence (AI) and Building Information Modelling (BIM) for effective resource optimisation in construction projects. The optimisation of resources in construction has several challenges such as time-cost trade-offs, resource overallocation, and resource allocation in a multi-project environment. These challenges can lead to several issues including unrealistic schedules, project delays, cost overruns, and human resource strain. By leveraging AI algorithms within the BIM framework, this study seeks to address resource allocation challenges, enhance decision-making, and improve overall project outcomes. The research intends to bridge the gap in the literature by providing a comprehensive understanding of how AI-integrated BIM can resolve resource optimisation issues. The contribution of this research lies in its potential to advance resource management practices, reduce project risks, and promote effective project execution.

KEYWORD: AI; BIM; resource management; construction

Development of Governmental Subsidy Policy for The Promotion of Prefabrication

Huiwen Wang, Wen Yi

Hong Kong Polytechnic University

ABSTRACT: Prefabrication is a sustainable construction approach that brings both social and environmental advantages over traditional all-in-situ construction. Currently, many governments are devoting great efforts to designing subsidy policies offered to contractors to increase the uptake of prefabrication. This study focuses on the governmental subsidy problem and establishes a bi-level programming model. First, the government at the upper level (i.e., leader of the bi-level model) decides the unit subsidy offered to the contractors that purchase prefabricated components (PCs) with the objective of maximizing the use of prefabrication. Then, the contractors at the lower level (i.e., followers of the bi-level model) decide whether to use PCs or cast-in-situ construction with the objective of minimizing the total project costs. A tailored algorithm is proposed to efficiently solve the model to optimality. Overall, the findings and their implications are expected to promote more sustainable construction operations.

KEYWORD: construction management; prefabricated components; subsidy design; bi-level relationship

Proceeding of the 10th International Conference on Innovative Production and Construction (IPC 2024), Perth, Australia, July 11-12, 2024

Optimizing Human-Robot Collaboration in Off-site Modular Structure Assembly Using Deep Reinforcement Learning

Yizhe Wang[1], Yihai Fang[1], Cong Zhang[2]

1. Department of Civil Engineering, Monash University
2. Nanyang Technological University

ABSTRCT: As modular structure assembly in off-site factories gains momentum, the controlled environment of these factories offers opportunities for employing advanced robotic systems, such as robotic arms and mobile robots. Yet, robots face challenges in completing complex construction tasks autonomously. This paper proposes a framework for human-robot collaboration for assembling modular structures, leveraging the unique capabilities of both entities. Within this framework, humans and robots operate collaboratively in spatially separated workspaces, maximizing productivity while ensuring safety. Building upon this collaborative model, the paper introduces a Deep Reinforcement Learning (DRL) based optimization method for task sequencing and allocation tailored to modular structure assembly. The proposed approach adapts the DRL algorithm that is traditionally employed in solving the Capacitated Vehicle Routing Problem (CVRP), to accommodate the unique demands of construction tasks. Furthermore, dependency factors are incorporated into the decoding process of the DRL model, enhancing its applicability to complex construction task dependencies. The outcomes of this research facilitate a more effective integration of robotic systems in construction, potentially improving efficiency and reducing operational costs.

KEYWORD: human-robot collaboration, off-site modular structure assembly; deep reinforcement learning; task sequencing and allocation

CELM-Based Carbon-Neutral City Definition and Assessment: A Novel Social-Ecological Driving Mechanism for Sustainable Urban Climate Mitigation

Baoming Yang*, Lingtong He, Xinghua Liu, Chuanfeng Han, Lingpeng Meng, Yi Jiao, Peizheng Xu

Cowin Institute, School of Economics and Management, Tongji University, Shanghai, China

ABSTRACT: The current trend of rapid urbanization is causing urban areas to warm up at a rate twice of global warming and therefore is crucial to the implementation of the 2030 Agenda for Sustainable Development. As the world is becoming increasingly urbanized, cities play a key role in achieving the climate goals of Paris Agreement. Many climate-change related city concepts have been introduced by academic research and policy discourse, such as carbon-neutral city, low-carbon city, negative carbon city, and zero carbon city, etc. In practice, however, many open questions remain on its criteria and assessment methods.

This study presents findings that provide a novel and elegant solution to address these issues. First, we propose a new model of Carbon Emission Liability Mechanism (CELM) that suggests a "consumer liability" (instead of "producer liability") of carbon emission and re-builds the accountability of various stakeholders (country, city, organization, individual, etc.). Second, we analyze range 1-3 of carbon emission liability in Green House Gas Protocol and give a precise definition of CELM based carbon-neutral city. We further propose a three-level assessment criterion in detail (i.e., carbon emission balanced city, relative carbon-neutral city, and real carbon-neutral city) with quantitative assessment methods and formulas. Third, we discuss related assessments in cities based on quantitative data analysis and practical experiences from ongoing work in China and Europe cities aiming at carbon neutrality. Finally, we discuss the relation, effect, and limitations of carbon-neutral city with global carbon neutrality given the liquidity of carbon dioxide.

The article aims to bridge gaps between research and practice, and discuss useful next steps for policy makers, including legislation, methods and tools that could support cities in their transition to carbon neutrality.

KEYWORD: Carbon Emission Liability Mechanism (CELM); carbon-neutral city; carbon-neutral city definition; carbon-neutral city assessment; sustainable urban development

Sustainability Assessment of 3D-Printed Ultra-High-Performance Concrete (UHPC) Modified

Bo Huang, Yutong Li, Jianqun Wang, Junbo Sun

Hunan University of Science and Technology, China

ABSTRACT: Ultra-high-performance concrete (UHPC) is an emerging construction material exhibiting excellent mechanical performance and durability. Antimony tailings (AT) as an industrial waste of environmental pollution was urgently required to be addressed in terms of its resource utilization. In addition, 3D printing technology widely applied in construction was utilized in this test. Therefore, this paper examines the sustainability and mechanical properties of UHPC incorporated with AT using 3D printing. Five different incorporating percentages (2.7%, 5.4%, 8.1%, 10.8%, and 13.5-wt%) of AT were used to examine the compressive and flexural properties. Experimental results showed that 10.8-wt% AT demonstrated the optimal compressive and flexural strength (135.5MPa and 21.8MPa, respectively). Additionally, the z-axis printing direction exhibited more excellent compressive performance than the x-axis and y-axis. The variation of cementitious composite microstructure affected by AT and printing method was elucidated via microscopic characterization like scanning electron microscopy (SEM), X-ray micro-computed tomography (X-CT), and X-ray diffraction (XRD). The increase in AT content from 2.7% to 13.5%, along with a decrease in pore volume from 5.8% to 2.02%, suggests AT can improve mixture density coupled with a reduction in pore structure. The UHPC combined with 10.8-wt% AT achieves better engineering characteristics as well as lower CO2 emissions for 3D-printed concrete practical construction.

KEYWORD: 3D-printed; UHPC; antimony tailing; mechanical properties; sustainability

Research on The Working and Mechanical Properties of Tannic Acid-Doped Green 3D Printed Mortar

Qian He, Tingting Zhang, Xue Wang

Yangzhou university

ABSTRACT: The setting time of 3D printing mortar to some extent does not meet the entire construction duration, which poses an obvious challenge to the initial working characteristics and mechanical properties of mortar. To address this issue, we propose an efficient, simple, and environmentally friendly method: the addition of tannic acid (TA) as a chemical enhances both the working performance and mechanical properties of cement mortar for printing. We investigated the impact of tannic acid (TA) under natural and water curing conditions on the working and mechanical properties of 3D printing mortar. After adding 0.5%TA, the final setting duration was changed from 195 min to 270 min. Constructability was assessed by printing 40 layers of vase specimens with a bottom diameter of 130mm, a top diameter of 90mm, and a height of 2300mm. A flexural and compressive mechanical tests were conducted at 14-day and 28-day intervals using a universal testing machine. Our findings showed a 10.45% improvement in compressive strength at 14 days, and a 5.66% increase at 28 days. Flexural strength increased by 27.58% on the 14-day, and by 25.33% the 28-day. The printing mortar also underwent analysis using the Cary 5000 UV-Vis-NIR absorption spectrometer. Notably, the spectrum revealed the lowest peak at 2213nm and the highest peak at 276nm. Especially, after adding 0.75%TA, the intensity of the peak at 1346nm increased. The FTIR spectra showed that no significant crystal structure variation was obtained for TA-treated mortar with strong cementitious characteristic. In conclusion, our study highlights the significant influence of TA on the working performance and mechanical properties of printing mortar, with implications for sustainability, industrial development, and the broad application of intelligent construction technology in 3D printing mortar.

KEYWORD: 3D printing mortar; mechanical property; tannic acid

Proceeding of the 10th International Conference on Innovative Production and Construction (IPC 2024), Perth, Australia, July 11-12, 2024

ChatBIM: Interactive Data Retrieval and Visualization from BIM

Jia-Rui Lin[1,2], Ke-Yin Chen[1], Peng Pan[1,2], Da-Peng Wu[3,2], Jian-Ping Zhang[1,2]

1. Department of Civil Engineering, Tsinghua University, Beijing 100084, China
2. Key Laboratory of Digital Construction and Digital Twin, Ministry of Housing and Urban-Rural Development, Beijing 100084, China
3. Beijing Yun Jian Xin Technology Co. Ltd., Beijing 100193, China

ABSTRACT: Building Information Modeling (BIM) has become a cornerstone technology for the digital transformation of the construction industry, facilitating multi-disciplinary data integration and sharing throughout the building life cycle. However, the increasing complexity of BIM systems and user interfaces has resulted in increased learning costs and reduced design and decision-making efficiency. To address this challenge, we propose to integrate our previous works as an interactive AI assistant, ChatBIM, which supports intelligent data retrieval and visualization through voice- or text-based interactions. Here we introduce our early attempt based on traditional Natural Language Processing (NLP) techniques and its improvement based on deep learning and Large Language Models (LLMs).

Our first attempt is developed a decade ago based on NLP. To understanding textual user input, NLP techniques including word segmentation, tagging, and syntactic analysis are utilized, to recognize key objects (e.g., beams, walls, etc.) by detecting noun phrases and their relations with dependency parsing. Then, International Framework for Dictionaries (IFD), which links concepts in different CAD systems are used to map recognized objects to data entities in Industry Foundations Classes (IFC). IFD is also further extended to include synonyms, alias, abbreviations of the same concept for better mapping accuracy. After that, database queries are generated based on graph pathing searching in IFC data scheme. Finally, executing the queries produces the required data of the users, and a few rule templates are predefined for the visualization of the retrieved data, for example, data series should be visualized in tables or charts, and building elements should be visualized in 3D view and colored according to their categories. Integrating all the steps together creates an AI assistant that could filter user concerned BIM objects and aggregates the properties (e.g., quantities, costs, construction progresses, etc.) of retrieved BIM objects for better decision-making.

With recent development of LLMs, we rebuilt the AI assistant based on a Domain-Specific LLM (DS-LLM). First of all, we further pretrained the DS-LLM by collecting plenty of domain documents and further fine-tuning an open-sourced foundation LLM. After that, user inputs in texts or voices could be understood via the developed DS-LLM with a higher accuracy than before. The key objects expressed in various words could be detected and linked with concepts in the data model, even if they are not in a standard form. Also, Retrieval Augmented Generation (RAG) is adopted to create a more natural response to the users.

With the above-mentioned approaches, a prototype software system as well as a prototype hardware called ChaoXi Screen are developed and verified in a few cases. Results show that the proposed method is easy to learn, and provides an intuitive way for the construction managers and decision makers. It would also be a promising way for future developing future human-computer interface in a new era for AI and metaverse.

KEYWORD: building information modeling; natural language processing; data retrieval; large language model, human-computer interaction

Proceeding of the 10th International Conference on Innovative Production and Construction (IPC 2024), Perth, Australia, July 11-12, 2024

Ecological Influence of Oasisization on Adjacent Regions

Xueyuan Zhang, Yongze Song, Ashraf Dewan

School of Design and the Built Environment, Curtin University, Bentley
Spatial Sciences Discipline, School of Earth and Planetary Sciences, Curtin University, Perth, WA 6102, Australia.

ABSTRACT: Sustainable development of oases plays an important role in reversing land degradation in arid region. However, it is unclear to what extent oasis change leads to ecological quality (EQ) degradation, especially in the peripheral/surrounding environment. To comprehensively evaluate the ecological effects of oasisization, this study developed a remote sensing ecological quality index based on nighttime light data to characterise spatio-temporal patterns and driving mechanism of EQ in different oasis type areas. The results show that oases area has increased by 37.44% in the past 22 years. The EQ of the core area was stable, but EQ declined in newly developed urban areas. The affect range of oasis on the adjacent regions EQ is 12km, and the expansion of the oasis is improved EQ of adjacent regions. The driving factors of EQ widely varied among different oasis areas. The vegetation index showed strong impacts on each oasis area. Human activities and soil moisture showed most significant explanatory power in the core area, but weak power is observed in the changed and peripheral areas. Climate factors had the strongest influence on the changed and peripheral areas. The findings have important implications for ecological protection of oases in arid regions.

KEYWORD: ecological quality; nighttime light data; remotely sensed ecological index; oasis peripheral area.

Proceeding of the 10th International Conference on Innovative Production and Construction (IPC 2024), Perth, Australia, July 11-12, 2024

Spatiotemporal Analysis on Material Stock and Environmental Impact of Residential Buildings: Towards a Circular Economy

Shengping Li

Curtin University, Perth, WA 6102, Australia

ABSTRACT: The building sector is material-intensive and responsible for embodied energy and greenhouse gas (GHG) emissions. Comprehensively analysing the evolution of material stocks (MSs) and associated environmental impacts in the building sector can support better decision-making on material management and energy conservation. However, there is a gap in the literature to evaluate the spatial patterns and dynamics of residential building stocks systematically and comprehensively. A simulation-based bottom-up approach is proposed to systematically analyse the spatiotemporal evolution of residential buildings' MSs and their environmental impacts at initial and replacement stages with a high resolution. Notably, the development of the material intensity dataset is essential for analysing MSs in the building sector. The proposed innovative approach links different building characteristic factors for developing a specific material intensity dataset. The proposed approach is demonstrated in Inner Melbourne, with more than 260,000 residential buildings. The results illustrate the spatially and temporally explicit MSs, embodied energy and GHG emissions in the case study area. The initial spatial maps visualise that large quantities of MSs, embodied energy and GHG emissions are located in areas with clusters of houses or high-rise apartments. The replacement maps can indicate the locations with large replacement material outflows where a cluster of historic buildings exist. The temporal analysis shows that the residential buildings' MSs in Inner Melbourne has increased by a factor of 9.6 over the past 120 years, reaching 27,488 kt in 2019. The growth rate has accelerated since 1990, particularly in areas (e.g. Melbourne CBD, Docklands, Southbank and South Yarra) with a large number of apartments have been built during this period. The high resolution of the results shows the benefits of the proposed simulation-based bottom-up approach compared to the traditional approach. This result is significant as it provides new insights for evidence-based decision-making on material management and energy conservation towards a more circular construction.

Author Index

(Sorted by first name of first author)